Analysis of a Very Low Tare Mass Wagon Concept for Intermodal Freight

by

Shah Sanjar Nafis Ahmad

A thesis submitted in partial fulfilment of the requirements for the degree of Doctor of Philosophy (Railway Engineering)

Central Queensland University

November 2017

Abstract

The empty weight or tare load of railway freight wagons is significant compared to the gross load (13-43% of the gross load) which not only reduces the possibility of carrying a higher payload but also increases the energy consumption per payload tonne hauled. One way to reduce the energy consumption per tonne payload is to reduce the tare load. One possibility of lowering the tare load is to reduce the number of components such as a bolster, sideframes, and axles. A two-axle wagon compared to a bogied wagon creates a possibility to reduce tare by up to 4-5t on a two-axle configuration. The fewer components on a two-axle wagon, however, result in inferior dynamic performance such as low critical hunting speed, poor curving ability, greater vehicle response to short irregularities etc, so, in spite of having low tare, the two-axle wagons are not as popular as the bogied wagons.

To take advantage of the lower tare mass of a two-axle wagon, a new concept wagon was conceptualised as a wagon with maximum axle load (~41 tonnes) and with enough load space to ensure a 80 tonne gross mass. The developed concept resulted in a wagon with a deck length of ~19.8m that allows carrying three 20', or a 20' and a 40', or a 65' container. The axle spacing (13.8m), overhang length (3m), tare mass (8t) and gross mass (80t) of the developed concept wagon is considerably different to the normal two-axle wagon. The challenge then was to design a suspension that would pass dynamics and roadworthiness tests.

It was reasoned that as the developed concept wagon was a new and radical concept, a more rigorous test approach to dynamic testing should be added to the normal tests and acceptance parameters in railway standards. A more rigorous test approach was developed which included consideration of test track defect lengths based on bogie centre distance (BCD) and resonance conditions for the cyclic track defects. The consideration of resonance condition requires developing equivalent amplitudes of track defects corresponding to the wavelengths in the track which are multiples of bogie centre distance for the cyclic bounce, pitch and roll track defects.

Using the more rigorous testing regime an innovative axle suspension was developed and refined to a design with three stages consisting of a conventional leaf spring, and the UIC link suspension in series with two multi-stage coil springs. It was also necessary to add longitudinal stiffness to improve axle yaw stability and hunting speed. The resulting design showed excellent stability with a critical speed of 204km/h and the multi-stage suspension allowed for negotiation of isolated lateral, vertical and long twist track defects as per AS7509 up to the defect band F of the ARTC track geometry standard. The short twist tests were however problematic. The resultant concept requires a smaller short twist track defect limit (8mm over 2m) than the defect band G of ARTC track geometry standard. The developed concept performed satisfactorily on track spectra up to FRA class 6 track.

Finally, the energy consumption of the developed wagon concept was evaluated and compared with similar capacity wagons such as RQTY, sgns60 and double stack container wagons in a train simulation. The energy saving ranged from 6 to 12% across various operating scenarios.

Acknowledgement

I would like to thank my supervisors Professor Colin Cole and Professor Maksym Spiryagin for their continuous support throughout the tough journey. I appreciate the time and experience Professor Colin Cole provided during the long and exhausting process of the research work. His passion for precise wording has been a life-long education for me and I appreciate every minute of it. Professor Maksym helped me a lot in understanding the simulation software 'Gensys' and also checked my modelling from time to time.

I acknowledge the financial support I received from the Central Queensland University and CRC for rail innovation. I am indebted to Tim McSweeney for his proof reading. It was a great privilege to have Tim to read my thesis as he has over 30 years of experience in the railway industry.

I am thankful to Dr. Yan Quan Sun for providing me a model of a three piece bogie which I used in my thesis. My sincere thanks to Ingemar Persson for helping me out with some of the complicated matters of the GENSYS simulation software. I want to acknowledge Dr. Per-Anders Jonsson for his work on UIC link suspension that was a great help for my thesis.

I appreciate the support of all the staff and students of Centre for Railway Engineering. They made my stay at the centre enjoyable. I also got different aspects of research in the centre which helped me a lot to get a better understanding of research overall.

I also thank the Bangladeshi community in Rockhampton that provided me an enjoyable social life and made my stay in Rockhampton more settling than I could have imagined.

I will always miss my grandmother Faridernessa Begum who was the key person to encourage higher study in our family. My father Dr. Shah Muhammad Shafiqullah has been the main motivator for all of my academic endeavour. My mother Rabeya Begum has supported me in everything new I have tried ever. My siblings- Salma, Asma, Adil, and Ghalib have always something cheerful around myself which helped me keep going.

Finally, I admire the effort and sacrifice my wife Rafia put into creating a pleasant environment in our family. Our son Afif and daughter Farzin came to us during the period of this difficult research work and has made life wonderful.

Acknowledgements:

Financial/Other Support (Thesis)

ACKNOWLEDGEMENT OF FINANCIAL SUPPORT

I gratefully acknowledge the funding received from CRC for Rail Innovation through the R3 Program which has supported this research.

ACKNOWLEDGEMENT OF SUPPORT PROVIDED BY THE AUSTRALIAN GOVERNMENT

This research higher degree candidature was supported by a Scholarship from the Australian Government's Research Training Program / Research Training Scheme. I gratefully acknowledge the financial support provided by the Australian Government.

Copyright Statement

Research Division

I, the undersigned author of the thesis, state that this thesis may be copied and distributed for private use and study, however, no chapter or materials of this thesis, in whole or in part, can be copied, cited or reprinted without the prior permission of the author and /or any reference fully acknowledged.

[redacted]

06/ 12/ 2017

…… ……

(Original signature of Candidate) Date

List of Publications

S. S. N. Ahmad, C. Cole, M. Spiryagin, and Y. Sun, "Integrated Methodology for Investigation of Wagon Design Concepts by Simulations," in *Proceedings of the ASME 2014 International Design Engineering Technical Conferences & Computers and Information in Engineering Conference*, Buffalo, USA, 2014.

S. S. N. Ahmad, C. Cole, M. Spiryagin, and Y. Sun, "Integrated Methodology For Investigation of Wagon Bogie Concepts by Simulation," in *ASME 2014 12th Biennial Conference on Engineering Systems Design and Analysis (ESDA2014)*, Copenhagen, Denmark, 2014.

M. Spiryagin, **S. S. N. Ahmad**, C. Cole, Y. Q. Sun, and T. McSweeney, "Wagon Multibody Model and Its Real-Time Application," in *New Trends in Mechanism and Machine Science*. vol. 24, P. Flores and F. Viadero, Eds., ed: Springer International Publishing, 2015, pp. 523-532.

M. Spiryagin, A. George, **S. S. N. Ahmad**, K. Rathakrishnan, Y. Q. Sun, and C. Cole, "Wagon model acceptance procedure using Australian standards," in *Conference on Railway Engineering*, Brisbane, 2012.

TABLE OF CONTENTS

Chapter 1
Introduction

1.1 Introduction

Increasing wagon capacity and improving productivity of the existing design have been considered important steps toward overall increase of efficiency in railway sectors around the world such as in the Europlan FP7 and FERRMED standards (FERRMED is an association formed in Brussels in 2004 to develop standards for freight rail in the European Union countries [1]) and wagon concept projects [2, 3]. Both of these projects aim to increase payload per wagon and per train in addition to facilitate efficient loading and unloading procedures.

The energy consumption of freight wagons is largely dependent on the mass of the rollingstock. Wagon tare weight or self-weight can be up to 13-43% of the gross load among the different freight wagons running all over the world [4-7]. The high tare load has two consequences- restriction on available payload capacity as track infrastructure is constrained on the tonne axle load (tal) requirement; and the cost of carrying tare mass that does not add to the profit of the freight transportation.

The energy consumption per tonne per trip can be worse when considering running empty wagons on the return path for bulk product heavy haul freight networks after unloading the product. The door to door delivery of intermodal freight transportation may require frequent loading and unloading situations which then carry the tare load only for a portion of the journey that doesn't add to the productivity. In addition to the cost of fuel, the current drive to reduce carbon emissions worldwide would encourage railway companies to adopt low energy consumption options.

The goal of achieving increased capacity with lower fuel costs can be obtained by increasing the size of the train and reducing the weight of both wagon body and running gear. Reducing the tare weight not only has challenges from the dynamics perspective, but modifications also need to ensure that the savings due to the lower tare are significant to convince any railway company to make changes in the current design of the rail system which has been self-optimised over the last 150 years. The situation of implementing a new design in the railway sector can become complicated when considering the rigorous interlinking between the different parts of the railway such as infrastructure, train operating companies, regulators etc. [8]. However, there is an obvious notion found in a case study among different train operating companies, rollingstock owners, Government and infrastructure operators that the opportunity exists for the reduction of mass of the current trains [9].

The improvement in capacity and efficiency is limited by the existing constraints in infrastructure such as the presence of tunnels and over-bridges with specified height and width on the network. The height of a wagon is subject to the approval of the rail network operator and the maximum length of the train can be determined based on the longitudinal train dynamics, traffic requirements, and length of the crossing loops of any network. The tare weight of a wagon depends on the material and design of the body structure and the weight of the running gear. The variation in the running gear depends on the number of axles/ bogies per wagon and weight of various suspension components used.

In addition to the constraints of the rail network, the market for a new concept wagon needs to be considered when commencing development. Some of the rail network systems carrying products such as coal or iron ore, where loading and unloading have usually come to an optimised stage, may not be inclined to implement a slight improvement in wagon design due to the high cost involved. However, the container wagon in an intermodal system has the potential for improvement due to the variation in the type of loading, the length of the journey, mixed freight and back-loading.

In considering wagon design, the rollingstock can generally be divided into bogied and bogieless wagons. The bogie improves curving behaviour, but requires additional elements such as two additional wheelsets, sideframes, and bolsters compared to the UIC two-axle wagon without any bogie. The elements of a bogie on a two bogie wagon (four axles) would usually increase the tare by about 4-5 tonnes compared to a bogieless wagon on two axles.

Improved curve negotiability usually results in a reduced hunting speed due to the lower yaw resistance incorporated in the design to improve curving. On the other hand, the length of a bogieless wagon can be more restricted due to it being less able to accommodate longer lengths which require larger twist displacement that, if not accommodated in the suspension, could produce unsatisfactory wheel unloading. The length parameters are also limited by the tonne axle load (tal) limit on the loaded wagon. The tal requirement could be increased as improved track and bridge structures are built across a network. So, there is an opportunity available to build a longer wagon on a minimum number of wheelsets. The research question, hypothesis, and methodology to test the hypothesis have been decided as below.

Research question:

Is it possible to build a lighter and higher capacity freight wagon without resorting to expensive or exotic new alloys or materials?

Hypothesis:

A low tare wagon is possible by reducing elements in a conventional wagon to achieve a lighter wagon and upgrading axles to maximum tonne axle load.

Methodology:

Develop a method to test the hypothesis.

1.1.1 Aims

1. Development of an alternate concept freight wagon to improve payload productivity (kWh/payload/km).
2. Testing of the wagon concept by using multi-body system simulation and a vehicle acceptance procedure.

1.1.2 Enabling Objectives

1. Develop a robust simulation based vehicle acceptance procedure to test any new wagon including any radical design.

2. Develop a suite of multi-body systems representing existing wagon designs with a view to provide a datum for comparison and test the simulation based vehicle acceptance procedure.
3. Develop a very low tare wagon concept.
4. Perform wagon and train dynamic simulations tests to select a suitable new design.
5. Evaluate the vehicle roadworthiness of the concept wagon using simulation and the vehicle acceptance procedure.

1.2 Summary of Chapters

Chapter 2 gives a review of the relevant literature on wagon design and lightweight wagon options.

Chapter 3 develops the methodology of the thesis.

Chapter 4 includes some preliminary analysis to help achieve the direction to the objective parameters.

Chapter 5 deals with the modifications of testing methods and test parameters to create a robust test procedure. Additional rigorous test methods are developed. A method termed the Vehicle Acceptance Procedure by Simulation (VAPS) has been developed based on the AS7509 standard.

Chapter 6 presents the evaluation of an existing wagon model using VAPS.

Chapter 7 presents optimisation of the length and mass parameters of a two-axle wagon in order to achieve a lightweight, long and high capacity wagon.

Chapter 8 presents the development of the initial suspension concept.

Chapter 9 presents the validation of the modelling approach.

Chapter 10 presents the final concept wagon and the further and more precise modelling and simulation tests of a 'buildable design'.

Chapter 11 presents the energy consumption and productivity comparison of the concept wagon with conventional wagons based on train simulations.

Chapter 12 gives the conclusions.

Chapter 2
Literature Review

2.1 Introduction

Three topics were covered in the literature review. Firstly, the payload productivity and energy consumption perspectives to achieve a highly productive wagon were investigated. Secondly, some existing wagons having low tare were investigated along with various design components of the wagons, in particular the running gear, were explored. Thirdly, the vehicle dynamics issues and test procedures including simulation techniques were included.

2.2 Productivity Considerations of Wagon Design

Productivity is considered as an area for savings in the operation of rollingstock. As the tracks are constrained by the maximum axle load design commonly referred to as the "tonne axle load (tal)" requirement, a target for optimisation is often to reduce the tare (empty mass) of a wagon with a view to providing more payload. Several combinations of methods have been used all over the world to improve wagon productivity (Table 2-1). Most of the attempts have included reduction of the mass of the wagon by using high strength material for the wagon body or removing unnecessary material from the wagon body [10-15]. In addition to reducing mass, load carrying capability can be increased by the careful choice of length of wagon and container.

Table 2-1: Methods to improve wagon productivity

Option	Productivity	Comments
Choice of 70t bogie (4t) instead of 50t bogie (4.5t) and YM bogies (5.5t) [10]	Reduction of weight by 1t in removal of decking, reduction of 1- 3t per wagon due to change in bogie design	Changeover within the existing designs of those used in that study on National Rail fleets of Australia in 1993.
Use of high-strength material for wagon body [11]	Reduction of tare weight by about 0.6~1 tonne per wagon	The weight saving was performed by using high strength material on doors, windows, seats. The wagon body could not be replaced due to poor fatigue performance on welded joints and thereby high strength material is necessary for wagon body construction.
Reduction of un-sprung mass by using lightweight materials or re-design [12]	Reduction of mass by 1.3t for a 4-wagon unit, i.e. 0.325t/ wagon	The reduction was mostly achieved by utilising hollow axles.
In board bearing bogies [12], the bearing housings between the wheels allow shorter axles thus reducing the mass of the axle	Reduction of mass by 10t for a 4-wagon unit, i.e. 2.5t/wagon [12]. The Leila bogie using the inner bearing assembly provides about 0.75t less mass per bogie (1.5t/ wagon) compared to the Y25 bogie [13].	High cost
Introduction of electro-pneumatic braking can reduce the stopping distances of long trains by up to 50% and improve fine-control of train speed [14]	More coasting and less energy lost from braking	
Replacing draft gear, coupler, and yoke assembly with slackless packages	Reduction of tare weight of a 100 unit train by 75t (0.75t/ wagon) [15]	

Getting a suitable length to accommodate as many containers as possible has been the concern of cost-effective rail freight for the last few decades. The capacity of a train within its length can be increased by reducing the free space between wagons and increasing payload (volume and mass).

The longest allowable length of a wagon is constrained by the overthrow and clearance requirements of a rail network and the axle load requirement of the infrastructure. The formulas used for calculating overthrow of a wagon are given in the railway group standard of RSSB [16]. The recent drive to improve capacity encourages the use of modern computing tools to obtain a less conservative clearance requirement. A summary of recent approaches to improve the capacity by considering known dynamics and kinematics is presented in [17].

In order to facilitate higher volume capacity, two types of wagons have been considered in [18]. Of these, 'wetrols' are specialised flat wagons having a low centre section between the bogies that allows the wagon to carry a high structure such as an electric power transformer. However, a large unused space above the bogies will occur due to this central loading. Flat wagons with small wheel diameter bogies also help to carry a comparatively high structure load.

It has been recommended that wagons must be both lower and of shorter bogie centre distance (BCD) for the conveyance of larger and heavier loads [18]. While the low deck height ensures a high load volume capacity, the diameter of wheels needs to be sufficiently large to accommodate heavier loads. The permissible loads on a wheel are limited by the contact stress on wheels and rails. Load capacities and speeds can also be limited by the ability of the wheel to absorb braking energy. For example, on British Rail (BR) the permitted axle load is limited to 11t for wagons with wheels of 520mm diameter running at 120 km/h [18].

If the intermodal freight network requires non-uniform length containers, this makes the problem more complex. Depending on the commodity and type of loading, a wide range of recommendations have been suggested in the International Union of Railways' Developing Infrastructure use and Operating Models for Intermodal Shift (DIOMIS) study based on the average structure of loading per traffic [19]:

- Short single wagons for heavy tank swap bodies
- 60' and 80' wagons for maritime traffic (80' = 4x20')
- 104' and 90' wagons for continental traffic (90' = 2 x 45')
- Articulated wagons having a good length and weight balance
- Pocket wagons for the growing demand of transporting semi-trailers

The recent trend of European railway companies suggests a need for versatile, longer and lighter wagons [20]. Considering demand, supply and infrastructure of European rail companies, a project named Versatile Efficient Longer wagon (VEL-wagon) for European transportation suggested maximum loading dimensions (Table 2-2) [7]. The most suitable concept was determined to be a bogied wagon with a total length of 28.7m over buffers which can accommodate two 45' containers or two semi-trailers or a combination of a 45' container/ 45' Semi-trailer and 20' ISO container (Figure 2-1). The target tare weight for this concept was set at 22 tonnes, while the axle load limit was 25 tonnes. It was also proposed that the bogie wagon can be modified to an articulated wagon if the load is lighter.

Table 2-2: Maximum loading dimension proposed in the VEL-wagon concept study [7]

Type of load	Length (m)	Width (m)	Height (m)	Mass capacity (t)	Axle load (t)
Container 45' PW HC	13.72	2.5	2.896	38.9	25
Common semi-trailer	13.67	2.60	4.5	39	25

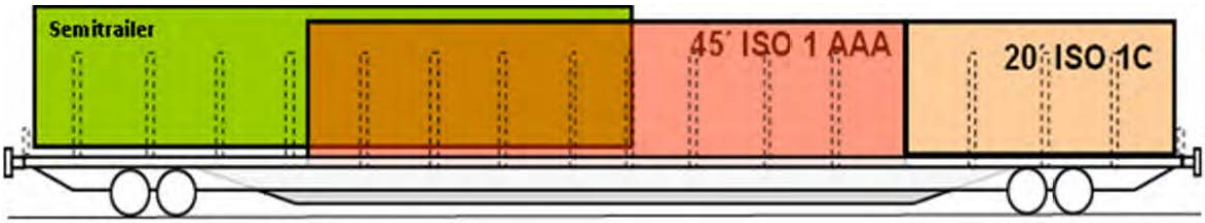

Figure 2-1: Optimised concept based on operation and handling proposed in the VEL-wagon study [7]

2.3 Energy Consumption of Train Operation

The energy consumption depends mainly on resistance on the train which is proportional to mass. The minimum energy required for a trip can be measured by taking account of average train speed, the potential energy requirement to overcome altitude on grades, the sum of the resistance to motion such as curve and propulsion resistances (Equation 2-1) [21].

$$E_{min} = \frac{1}{2} m_t v^2 + m_t g h + \sum_{i=1}^{q} \left(m_i \sum_{j=1}^{r} \left[\int_0^{x=l_{cj}} F_{crj} dx \right] \right) + \sum_{i=1}^{q} \left(m_i \int_0^{x=L} F_{pri} dx \right) \quad \text{2-1}$$

where E_{min} is the minimum energy consumed (J), g is the gravitational acceleration (m/s^2), h is the net altitude change (m), L is the track route length (m), lcj is the track length of curve j (m), m_i is the individual mass of vehicle i (kg), m_t is the total train mass (kg), F_{crj} is the curving resistance for curve j (Newtons/kg), F_{pri} is the propulsion resistance for vehicle i (Newtons/kg), q is the number of vehicles, r is the number of curves, and v is velocity of the train (m/s).

It is to be mentioned here that the energy requirement varies significantly with train handling issues such as the application of brakes or stopping trains at stations as well as signalling conditions. The minimum energy requirement defined by Equation 2-1 means that the train has achieved the speed v and there is no more stopping or speed restrictions due to stations, curve or other track conditions on the whole route. Every time there is a stoppage or speed restriction, the train has to regain kinetic energy to move the train back to target speed, and thus exceeds the minimum energy amount of Equation 2-1.

The second term of Equation 2-1 ($m_t gh$) evaluates the energy required to overcome the potential energy due to the difference in track altitudes (h) or grades. The energy required to increase speed and overcome grade is stored on a train as kinetic and potential energy which can be utilised to overcome the rolling resistance and thus the traction is not considered as wasted [22]. However, if the gained kinetic and potential energy is not utilised by a cruising train, the energy consumed is considered as wasted, such as will occur during braking operations to stop a train or reduce speed on a steep downgrade.

The third term, the energy required to overcome curving resistance on a route, depends on the mass of the train, the number of curves, the length of each curve and the distance travelled. The curving resistance on a curve can

be obtained from an empirical relationship, knowing that it can vary based on rollingstock design and condition, steering performance, cant deficiency, rail profile, rail lubrication and curve radius (Equation 2-2).

$$\boldsymbol{F_{cr} = \frac{6116}{R}} \qquad \textbf{2-2}$$

where F_{cr} is the curving resistance (N/ tonne of wagon mass), and R is the Radius of the curve (m)

Curving resistance (Equation 2-2) is thought to be reduced by about 50% if rail flange lubrication is present on the curve [21]. A stationary wagon on a curve faces about double the resistance of that obtained from Equation 2-2.

The fourth term, the energy required to overcome the propulsion resistance is also directly proportional to the mass and propulsion resistance of the train. There are some empirical relationships available to determine propulsion resistance which differs depending on the type of rollingstock and speed. The modified Davis equation (Equation 2-3) appears to cover a more global perspective compared to other empirical equations as this equation allows user input depending on numerous scenarios.

$$\boldsymbol{F_{pr} = K_a \left[2.943 + \frac{89.2}{m_a} + 0.0306V + \frac{1.741 k_{ad} V^2}{m_a n}\right]} \qquad \textbf{2-3}$$

where F_{pr} is the propulsion resistance (N/ tonne of wagon mass), K_a is the adjustment factor depending on the rollingstock type (1.0 for pre 1950, 0.85 for post 1950, 0.95- container on flat car, 1.05- trailer on flat car, 1.05- hopper car, 1.2- empty covered auto racks, 1.3- loaded covered auto racks, 1.9- empty, uncovered auto racks), k_{ad} is the air drag constant depending on the wagon type (0.07- conventional equipment, 0.0935- containers, 0.16- trailers on flat cars), m_a is the mass supported per axle (tonnes), n is the number of axles, V is the velocity (km/h).

In the modified Davis equation (Equation 2-3) the first two terms are generally representative of journal or bearing resistance [23]. The third term (0.0306V) is proportional to speed and mass and represents flange/ rolling resistance. The fourth term (air resistance) is proportional to an air drag constant, square of speed and is not related to the mass of the train.

The intermodal freight wagons have some empty spaces during operation and so can face larger air resistance than more uniform freight such as in a heavy haul operation. It thus follows that the length of flat wagons needs to be a close match to the typical container load carried over an intermodal operation to reduce the empty space in order to reduce aerodynamic drag and energy consumption. A study [23] has found that loading empty containers instead of leaving empty spaces on wagons is beneficial despite the added mass when considering aerodynamic drag.

In determining propulsion resistance for energy analysis, it is important to note that the empirical equations of curving and propulsion resistance do not cover wheel-rail profile information, centre bowl friction, warp stiffness and numerous types of wagon design shapes subjected to air drag [21]. Hence, it is obvious that calculations based on the empirical equations will vary from the field measurements. However, these equations can act as a starting point for comparing the energy consumption of trains.

A comparison of energy consumption of four typical trains (heavy haul, freight intermodal, Iron Highway and Cargo Sprinter) on two different tracks is available in [24]. The simulation was run for one-way travel with fully

loaded conditions and 5 stoppages using dynamic braking over 50km track sections (heavy haul and undulating track). The paper [24] shows that the freight intermodal train consumes about double the energy consumption per product load compared to the heavy haul train. The energy consumption per product tonnes (payload minus mass of the container or semi-trailer) is even higher for the lighter and shorter Iron Highway and Cargo Sprinter trains due to the lower product tonnes and higher running speed compared to the heavy haul and intermodal freight trains.

2.4 Review on Wagon Design

The components of a wagon can be divided into the wagon body and the running gear. The scope of this thesis is limited to possible modification to the running gear to achieve a lighter wagon. This review is therefore limited to running gear only. Both existing and concept running gears are reviewed.

2.4.1 Existing Running Gear

The running gear comprises bogies and/or axles, wheels and suspension components. The most common running gears are three-piece bogie and UIC-link wagon. In addition, some of the running gears, such as single axle, unitruck and single axle bogie have been used in some of the railways.

2.4.1.1 Three Piece Bogie

Most freight wagons consist of two, two-axle bogies per vehicle [25]. Bogies with only a secondary suspension are usually of the 'three-piece' type and appear to dominate in the countries of the former USSR, the USA, Canada, China, Australia and most countries in Africa and Latin America. The 'Three-Piece-Bogie', comprising three major structural components of wheelsets, sideframes and bolster, is the most common design for Australian freight wagons (Figure 2-2).

Each wheelset in a 'three-piece bogie' is made up of a pair of wheels connected by an axle with bearings on both ends which are fitted into journals in a pair of sideframes. These sideframes connect two wheelsets and transfer loads from the bogie bolster to the wheelsets. The bolster is placed over nests of coil springs which are placed into each sideframe. Sidebearers placed on either side of the centreplate on the bolster restrict the rolling motion of the wagon body.

Three piece bogies can be categorised based on the arrangement of friction damping wedges- "constant force dampers" and "variable force dampers", known in the industry as "the ride control bogie" and "the Barber stabilised bogie" [26]. The ride control mechanism using the constant force damping wedge elements provide greater resistance against hunting motion because the full damping force is available when the wagon is empty. On the other hand, the Barber stabilised mechanism uses variable force damping wedges proportional to the load, which provides more appropriate vertical damping when empty.

The three piece bogie construction allows a lozenging characteristic due to the loose fit between the bolster and each sideframe that allows one sideframe to move ahead of the other of the same bogie. The sideframes are centred and return to correct geometry due to springs and wedge damper forces. The unfavourable lozenging nature results in a lower critical hunting speed on the tangent or straight track compared to a case without the lozenging

phenomenon. The unfavourable lozenging also provides high wheel creep and extra flange resistance and wear on both wheel and rail on a curved track.

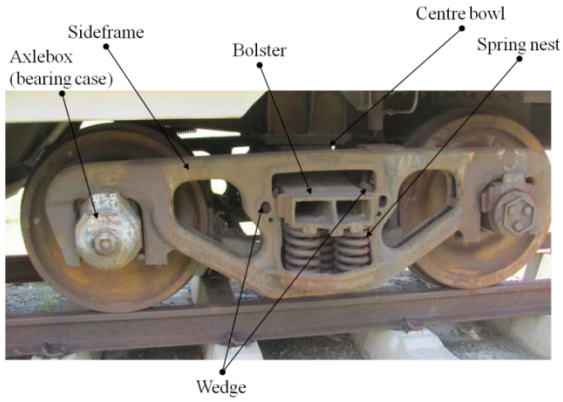

Figure 2-2: Three-piece bogie [27]

Improvements in the three-piece bogie have been achieved by using several strategies such as swing motion, cross-braced and frame-braced methods. The swing motion bogie (Figure 2-3) uses a transom underneath the bolster to carry the spring plank. The transom is connected to each sideframe by a rocker seat assembly that allows some swinging between the bolster and sideframes. The interconnection between the two spring planks on the bolster restricts lozenging of the sideframe. The second set of rockers is set in the connection between the sideframes and pedestals to provide additional swinging between sideframes and the axles. Thus, both hunting and curving performance is improved on a swing motion arrangement compared to the conventional three piece bogie arrangement.

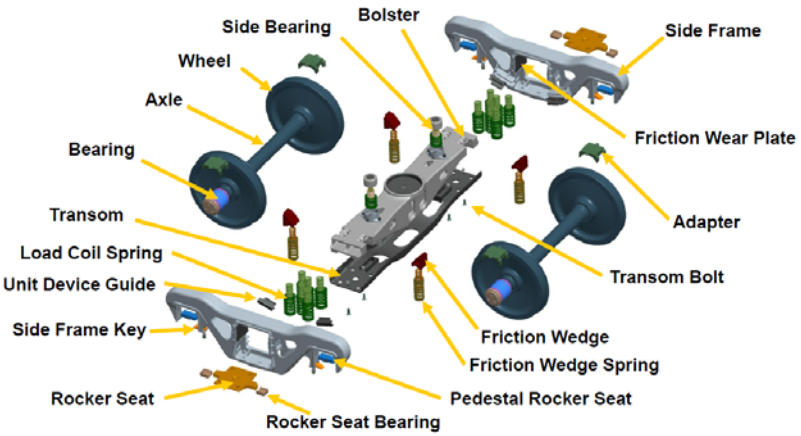

Figure 2-3: Swing motion bogie [28]

The Scheffel bogie, introduced in South Africa in the 1960's to reduce wheel and rail wear due to increased axle load and speed, utilised a sub-frame connected to the axle journals diagonally [26]. In addition to the arrangement of the conventional three piece bogie, a primary suspension was provided by a rubber shear pad between the sideframe and the sub-frame (Figure 2-4). The sub-frame on the Scheffel bogie restricts lozenging to improve hunting behaviour on straight track. The softer primary suspension of Scheffel bogie improves steering by allowing the wheelsets to adopt a radial position on curved track.

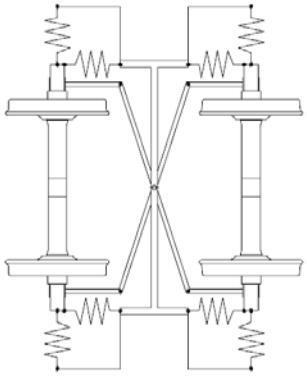

Figure 2-4: Scheffel bogie [26]

Lozenging of the sideframe can also be restricted by connecting the two sideframes as has been done with cross connection links in the frame braced bogie (Figure 2-5a) and as triangular links in the ABB traction bogie (Figure 2-5b). The frame braced bogie uses shear pads between the bearing adapters and sideframes which can improve curving [26].

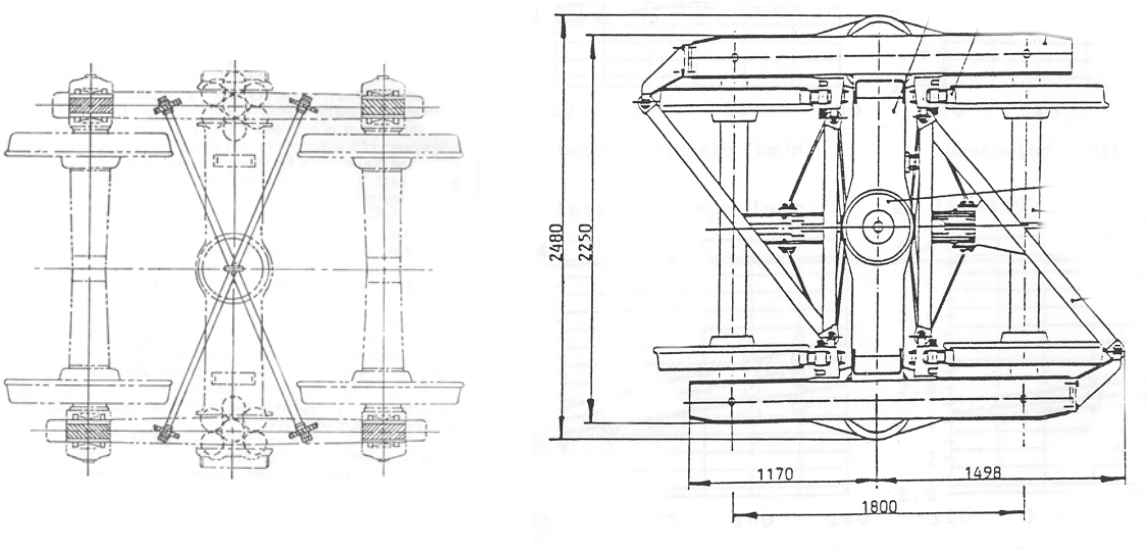

(a) Frame-braced bogie [26] (b) ABB traction bogie [26]

Figure 2-5: Reducing lozenging effect on the three piece bogie

The cross links between the axle boxes or frames in the Scheffel bogie, frame braced bogie or ABB traction bogie interfere with the positions of brake pipes which then lead to an alternate design of the Frame Mounted Shear Stiffener (FMSS) suspension (Figure 2-6). The FMSS suspension provides the inter-axle connection of steering links outside the wheels [26].

Additional steering is provided by two steering arms interconnected by a bushing inside the bolster in the American Steel Foundries (ASF) List AR-1 bogie (Figure 2-7). The steering arm in the List AR-1 bogie increases lateral stiffness and yaw stiffness which is necessary for improved straight and curved track negotiation. The lateral stiffness is increased by maintaining the sideframe alignment with the help of the steering which improves critical hunting speed typically by about 24 km/h [29]. The elastic connection between the wheelsets and the

sideframes increases yaw stiffness which allows longitudinal movement of the axles through the resilient pads and helps radial positioning of the wheelsets.

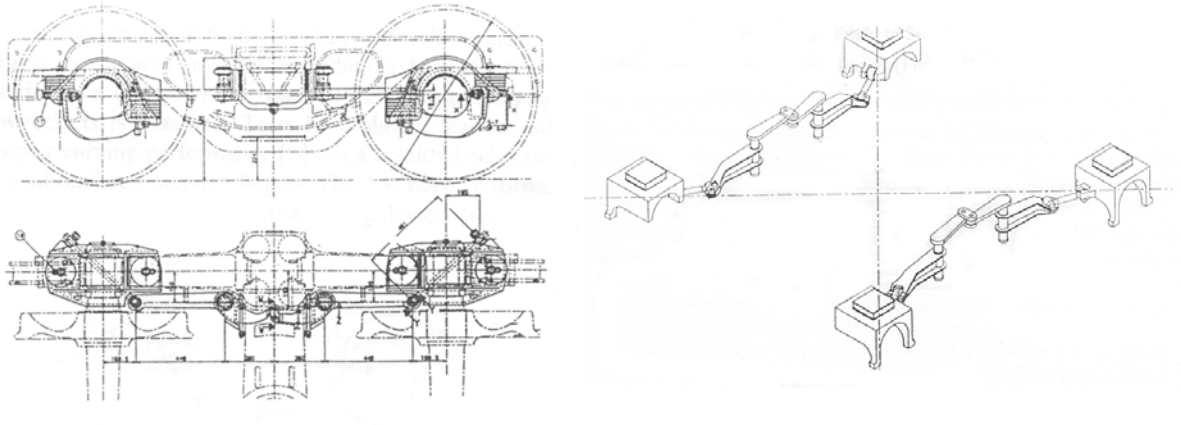

(a) Frame mounted shear stiffener (FMSS) [26] (b) Inter-axle connections [26]

Figure 2-6: Positioning of inter-axle linkage outside the wheels

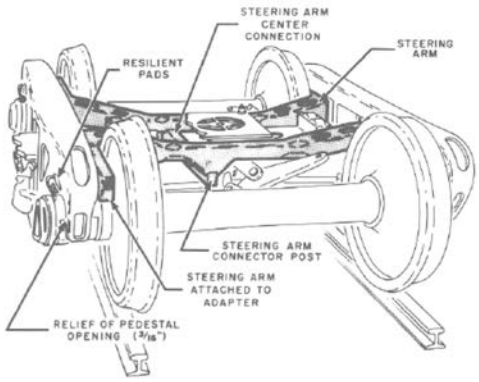

Figure 2-7: ASF List AR-1 bogie [29]

Similar principles to that of the List bogie were used in the British Rail bogie with the exception of the connection point between the steering arms being under the bolster mid-point (Figure 2-8a). The RC25NT bogie (Figure 2-8b) [13] is the other alternative option developed in Germany that uses steering arms and is interchangeable with the Y25 bogie discussed in Section 2.4.1.4.

In the Radial Primary Suspension (RPS) bogie, the steering was provided by connecting the wagon body with the wheelset via sub-frames and anchor links (Figure 2-9) [26]. The sub-frames contain the suspension springs, adapters, and wheel bearings. The sub-frames are positioned at pockets at the end of the bogie frame. The steering linkages on each side of the bogie control the position of the sub-frames. Some longitudinal freedom is given for the sub-frames by allowing them to move on low friction bearing pads within the pockets. The additional longitudinal freedom allows the sub-frames on the outside of the curve to move further apart and the sub-frames of the inside of the curve to move closer together [30]. The radial steering bogie also ensures lower longitudinal and lateral creepages that provide less running resistance and thereby improve energy savings [13].

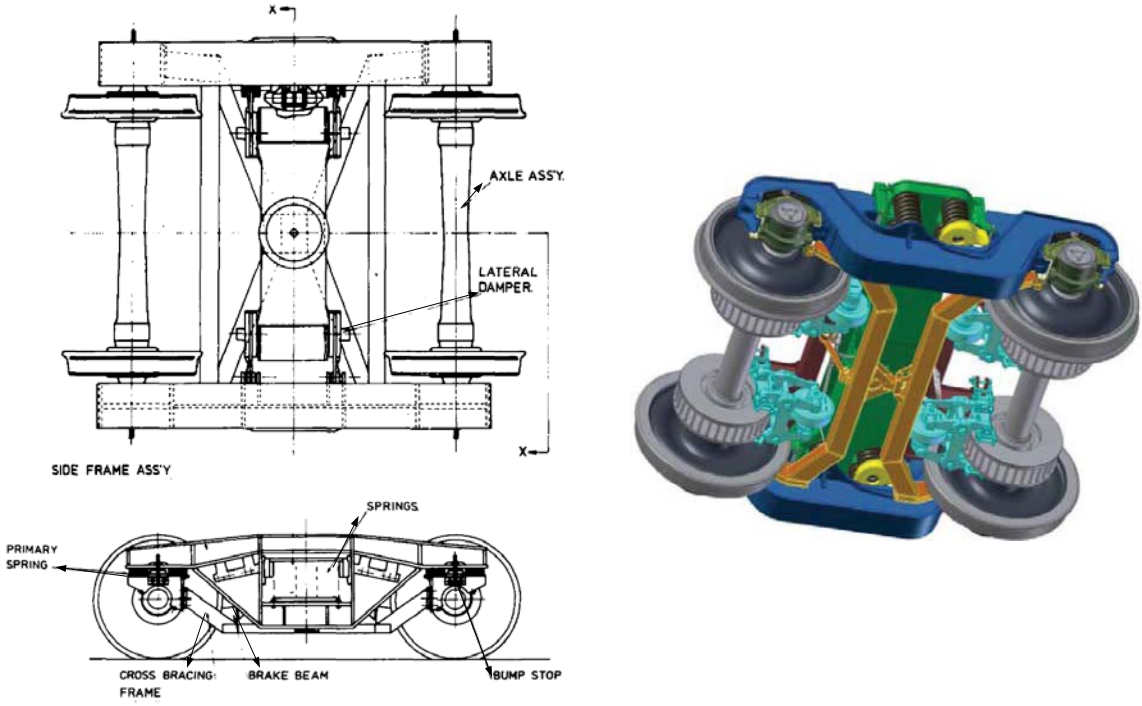

(a) British Rail bogie [31] (b) RC25NT bogie [13]

Figure 2-8: Alternative arrangement of the steering arms

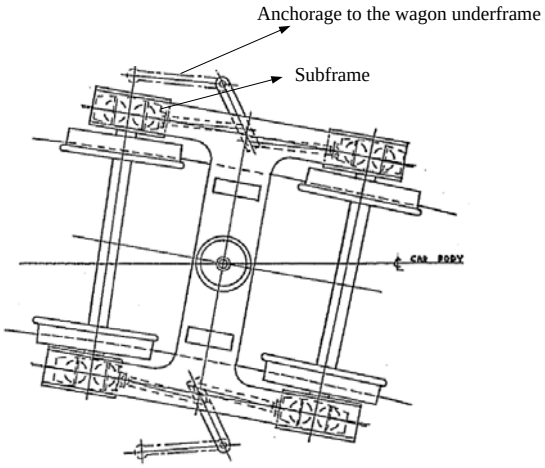

Figure 2-9: Radial primary suspension (RPS) bogie [30]

2.4.1.2 UIC-Link Suspension

The oldest running gear is the link suspension which has been mostly utilised on the single axle arrangement (Figure 2-10). The movement of the double-link between the leaf spring and the wagon body allows yaw and lateral movement of the wheelsets which allows better curving but can reduce critical hunting speed. However, the simplicity and light structure of the suspension system made this the most commonly used suspension system in Europe from the 19th Century [32] until higher speed and capacity requirements emerged.

The vehicle body is connected to the leaf spring by the double-links (Figure 2-11) which provide longitudinal and lateral stiffness to the suspension (Figure 2-12). The double-link is inclined in the longitudinal direction and placed on a vertical plane in the lateral direction when the nominal load is applied [26]. The suspension system rests on

the axle box. The axle guard restricts the horizontal motion of the axle box. The combination of the leaf spring and double-link suspension system provides stiffness and damping in the longitudinal, lateral and vertical directions. The friction between the different parts of the double-link suspension system provides the relevant damping. The leaves in the leaf spring mainly damp the vertical motion. The friction between the link pins and end bearings damps the longitudinal and lateral motions.

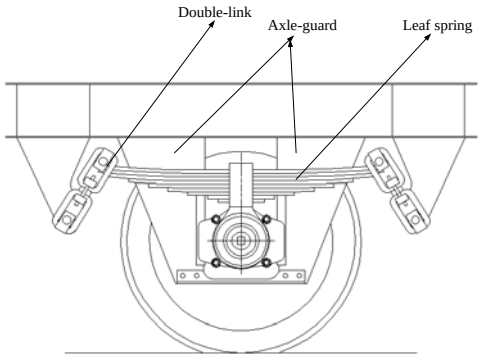

Figure 2-10: UIC double-link single axle [26]

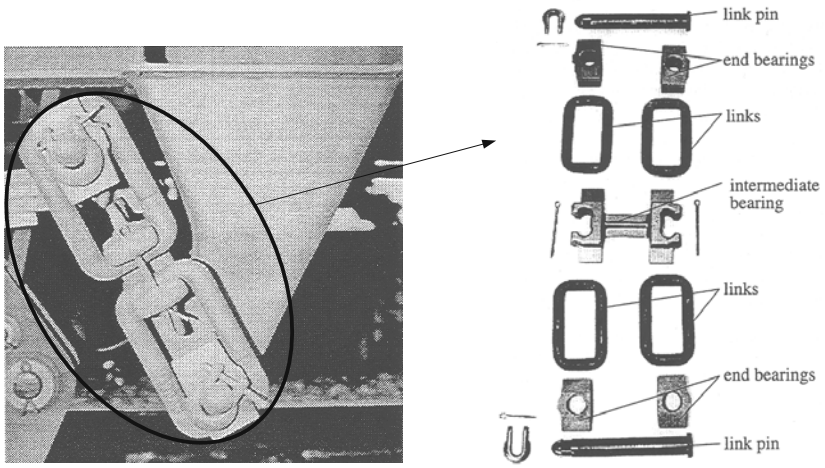

Figure 2-11: Double-link suspension [26]

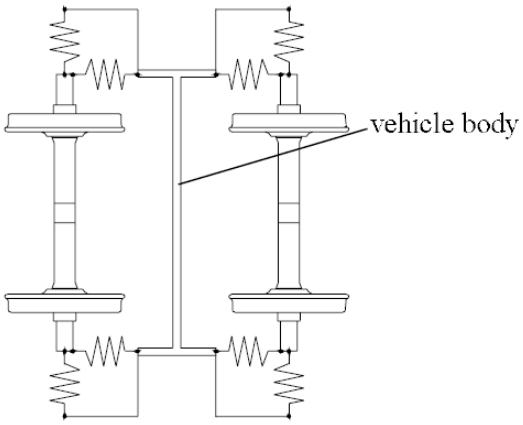

Figure 2-12: Principle of a two-axle link suspension [26]

A few improvements in the damping of the UIC-link suspension for speeds higher than 100km/h have been tested including mechanical damping by an additional leaf (Figure 2-13a) and hydraulic yaw dampers (Figure 2-13b) [26, 32]. Physical test results showed that the possible improvement on the wagon body acceleration could allow speeds up to 160km/h. The resulting response at 160km/h was comparable to a wagon without any damper running at 100km/h.

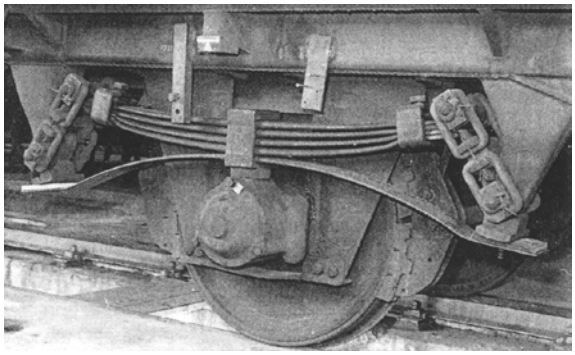

(a) mechanical damping in the UIC-link suspension [26]

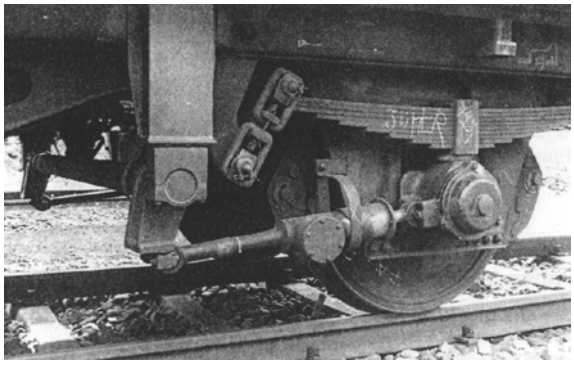

(b) hydraulic damping in the UIC-link suspension [26]

Figure 2-13: Improvement of damping in the UIC-link suspension

2.4.1.3 Single Axle Running Gear - Unitruck

The Unitruck was developed in the 1970s in America with a view to achieve similar performance to that of a bogie while using a single axle [26]. In the Unitruck design, lateral stiffness was provided by a swing action principle [26]. Being built with one axle, it is generally lighter than the conventional three piece bogie. The Unitruck assembly (Figure 2-14a) allows a swinging motion of the wheelset in the lateral direction controlled by the addition of a rocker seat arrangement between the saddle and axle box [26]. The saddle acting as a swing link provides lateral stiffness to the primary suspension. The vertical primary suspension in the Unitruck is provided by coil springs while the friction wedges provide the load dependent friction in the vertical direction. The friction wedges, when forced by the longitudinal movement of the wheelsets, also provide stiffness and damping to the motion.

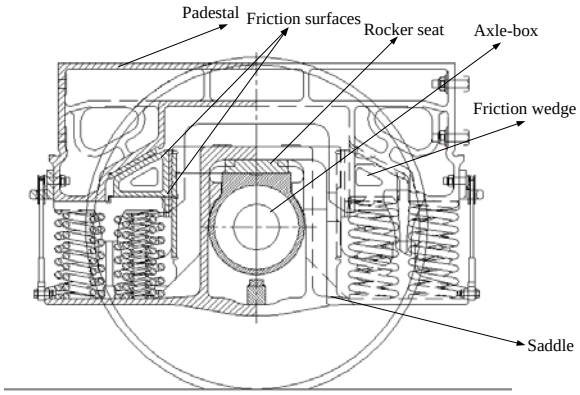

(a) Meridian Rail's Unitruck [26]

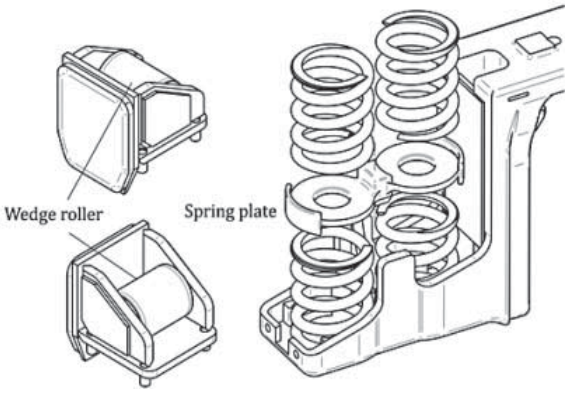

(b) Improvement in Unitruck [13]

Figure 2-14: Unitruck assembly

Further improvement in the Unitruck assembly was possible by replacing the inclined friction wedge surface by a roller that provided reductions in the longitudinal stiffness and damping (Figure 2-14b) [13]. The critical speed can be improved by using a coupling plate in the centre of the coil springs that increases longitudinal stiffness (Figure 2-14b) [13]. The Unitruck principle was further utilised in a 'H' type bogie frame (Figure 2-15) providing similar advantages.

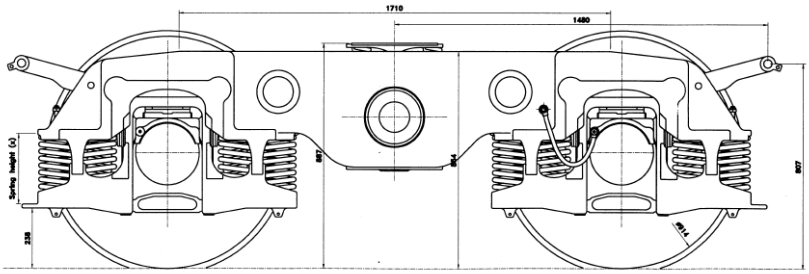

Figure 2-15: Meridian Rail's axle motion bogie [26]

Improvements to track friendly behaviour were achieved by using two dampers in the lateral and vertical directions between the saddle and pedestal of a two-axle running gear on the design of the TF25SA arrangement (Figure 2-16a). The performance on straight track was improved by a longitudinal radial arm between the pedestal and axle box. The end of the radial arm was provided with rubber bushings to allow some radial alignment of the wheelsets on curves. The TF25 bogie version of the TF25SA was also developed (Figure 2-16b). In addition to the primary suspension system used in the single axle running gear, two secondary springs and a traction-centre are used to connect the bogie to the wagon body. The vertically stiff nature of the steel chevron sandwich arrangement (Figure 2-16b) is used as the secondary suspension that allows longitudinal and lateral motions [26].

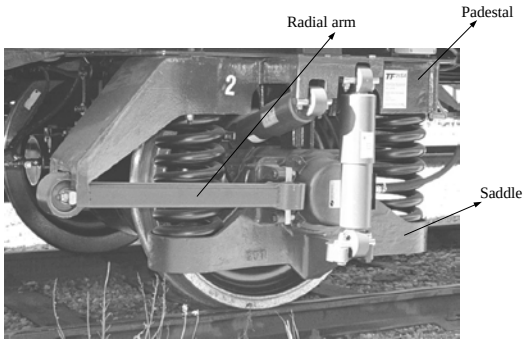

(a) TF25SA [26] (b) TF25 [26]

Figure 2-16: Application of lateral and vertical damper to improve track friendly behaviour

2.4.1.4 Link Bogie and Y25 Bogie

The UIC link suspension was used by DB in the bogie mechanism of the 'link bogie type 931' to improve the design speed to 100 km/h in the 1950's [26]. A later design of the 'link bogie type 665' (Figure 2-17a) was built in the 1980's and introduced parabolic leaf springs, shorter links and a permissible axle load of 22.5 tonnes.

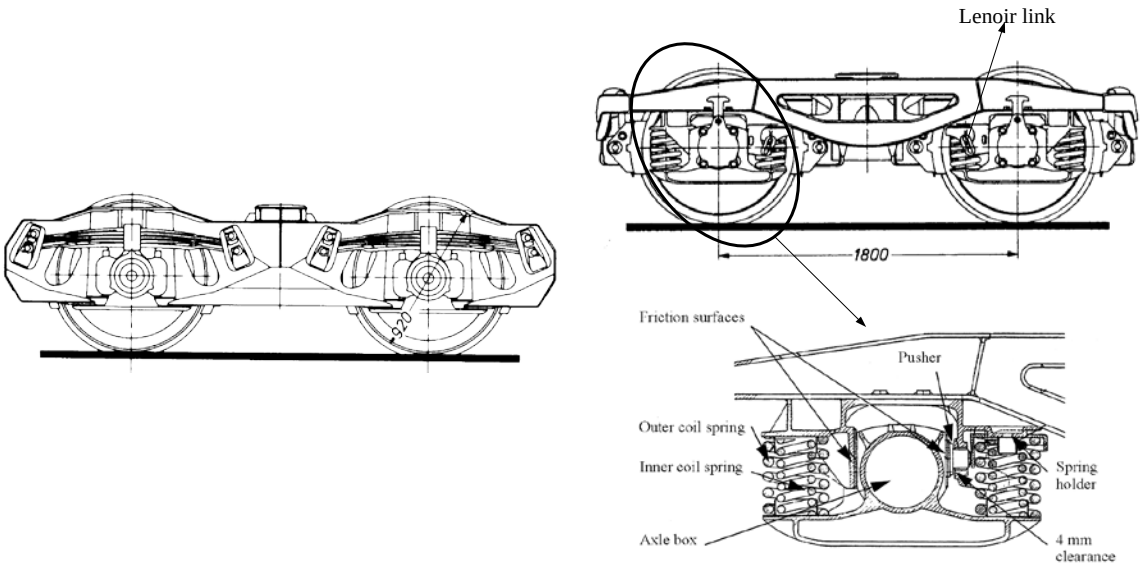

(a) Link bogie (DB bogie type 665) [26] (b) Y25 bogie [26]

Figure 2-17: Link and Y25 bogie

Although the link bogie provided a higher speed compared to the single axle suspension, the weight of the bogie was considered a bit high [26]. A reduction by 100 kg in the bogie design was achieved by SNCF of France when it replaced the leaf spring suspension of the link bogie (type 931) by coil springs in the design of the Y21 bogie [26]. A further modification of the Y21 bogie was performed in 1966 and the Y25 bogie (Figure 2-17b) was developed which has a reduced axle spacing of 1.8m compared to 2m for the Y21 bogie [26].

The damping in the Y25 bogie is provided by the inclined Lenoir link mechanism which is connected between the bogie frame and spring holder (Figure 2-17b). Part of the vertical forces on the outer spring is transmitted to the bogie frame by the Lenoir link which pushes/ pulls the bogie frame via a pusher towards/ outwards of the axle-box over a friction surface. The friction force is thus proportional to the vertical load and damps the motion in the lateral and vertical directions. A narrow gap of 4mm between the pusher and the bogie frame is provided in the longitudinal direction which allows some steering movement of the axle box. However, the connection in the longitudinal direction is still considered quite stiff which then creates poor curving behaviour [26].

In order to lower the longitudinal stiffness, a double Lenoir link suspension is proposed in [33] (Figure 2-18a). Lowering the longitudinal stiffness, however, resulted in a lower critical hunting speed which then encouraged the use of the radial arm technology (Figure 2-18b). Use of radial arm technology did improve the critical hunting speed of the double Lenoir link arrangement; however, the influence of the radial arm technology on the curved track is still under investigation.

The Y37 bogie was designed by SNCF in 1988 to achieve a speed up to 160 km/h (Figure 2-19) [26]. The bolster was made hanging in links on the sideframes that allows maximum lateral motion between the sideframes and bolster up to +/- 58mm on straight track [26]. The longitudinal suspension element was made stiff to provide better hunting characteristics on straight track.

(a) double Lenoir links [33] (b) radial arm providing longitudinal linkage [33]

Figure 2-18: Lowering longitudinal stiffness means in the Y25 bogie

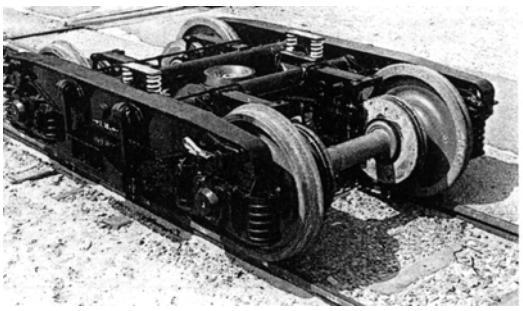

Figure 2-19: Y37 bogie [26]

2.4.1.5 Single Axle Bogie

Application of single axle bogies has been tried in Denmark and Japan. The Danish State Railway (DSB) in cooperation with Technical University of Denmark carried out a project to investigate the dynamics of a single axle KERF (Kurvengesteuertes Einzelradsatz- Fahrwerk) bogie in 1995 [34]. One bogie of a passenger train (Copenhagen S-train) consisting of two wagons was replaced by the single axle KERF bogie and tested for critical hunting speed under different operational and suspension properties [34]. The critical speed was found to be in the range of 150- 180km/h utilising the Hopf-bifurcation and non-linear decreasing velocity method [34]. The mass reduction due to the use of the KERF bogie was achieved by reduction of the number of wheelsets to 10 (Figure 2-20) compared to 16 on a similar urban train [35].

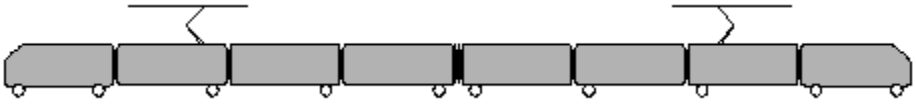

Figure 2-20: Application of the single-axle bogie KERF on a Copenhagen S-train [35]

A similar study to achieve compatibility between hunting behaviour and curving performance for a single axle bogie for a suburban light rail transit commuter vehicle developed by the Japan Railway Engineers' Association was presented in a World Congress on Railway Research conference in 2001 [36]. A traction linkage was used. The theoretical results suggested that the single axle bogie had a poor angle of attack for curves of radius less than 400m.

2.4.2 Concept Suspension Designs Proposed in Patents

A search into patents was performed to investigate if any lighter running gear design compared to the existing running gear is available. As reducing the number of wheelsets on a wagon has been considered as a suitable option to achieve a low tare wagon, the search of concepts was limited to the suspension design with a single wheelset arrangement.

2.4.2.1 Alternatives to UIC leaf spring suspension

In search of replacing the leaf springs on the conventional UIC wagon, a number of alternative arrangements with coil springs are proposed in [37]. Figure 2-21 represents a design of a beam element that can be used as a replacement of the leaf spring. The bearing assembly part 11 of the axle is connected to the beam 14 which is pivotally connected to link 16. The link is placed in the downward and outward direction from the axle. The lower part of the link is pivotally connected to a rod 22 which is connected to a pressure plate 23. The coil spring 24 is mounted between the pressure plate and support block 20 around the rod 22. The upward movement of the axle transfers the motion through part numbers 14, 16, 18 and 22 to compress the coil springs. Vertical damping in this arrangement can be obtained from the frictional arrangement in the pivot points 17, 19 and 21.

A damping device 26 may be incorporated between the link 16 and beam 14 (Figure 2-22a). A damper pad 27 is connected to the pillar through a helical compression spring 28. A member element can be used to pivotally connect the damping device between link 16 and lever arm 18. The compression spring 33 (Figure 2-22a) can be located at the intermediate position of the lever arm 18 (Figure 2-22b). In another form, the helical spring 44 can be placed between the beam 14 and a support surface 44a (Figure 2-22c). The damping device in Figure 2-22a can be replaced by a bar 45 which pivotally connects the two links 16 (Figure 2-22d). In addition, a traction rod 46 can be added between the bearing saddle 49 and support bracket 20 on the vehicle underframe to provide longitudinal stiffness characteristics to the suspension assembly.

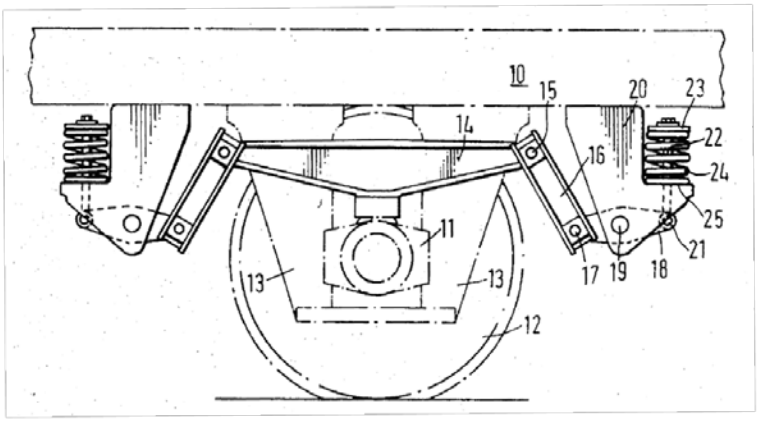

10- underframe of the wagon
11- bearing assembly
12- wheelset
13- pillars
14- forc-and-aft extending beam
16- link
18- lever arm
20- support bracket
22- rod
23- pressure plate
24- spring

Figure 2-21: link and coil spring arrangement as a replacement of leaf-spring and link [37]

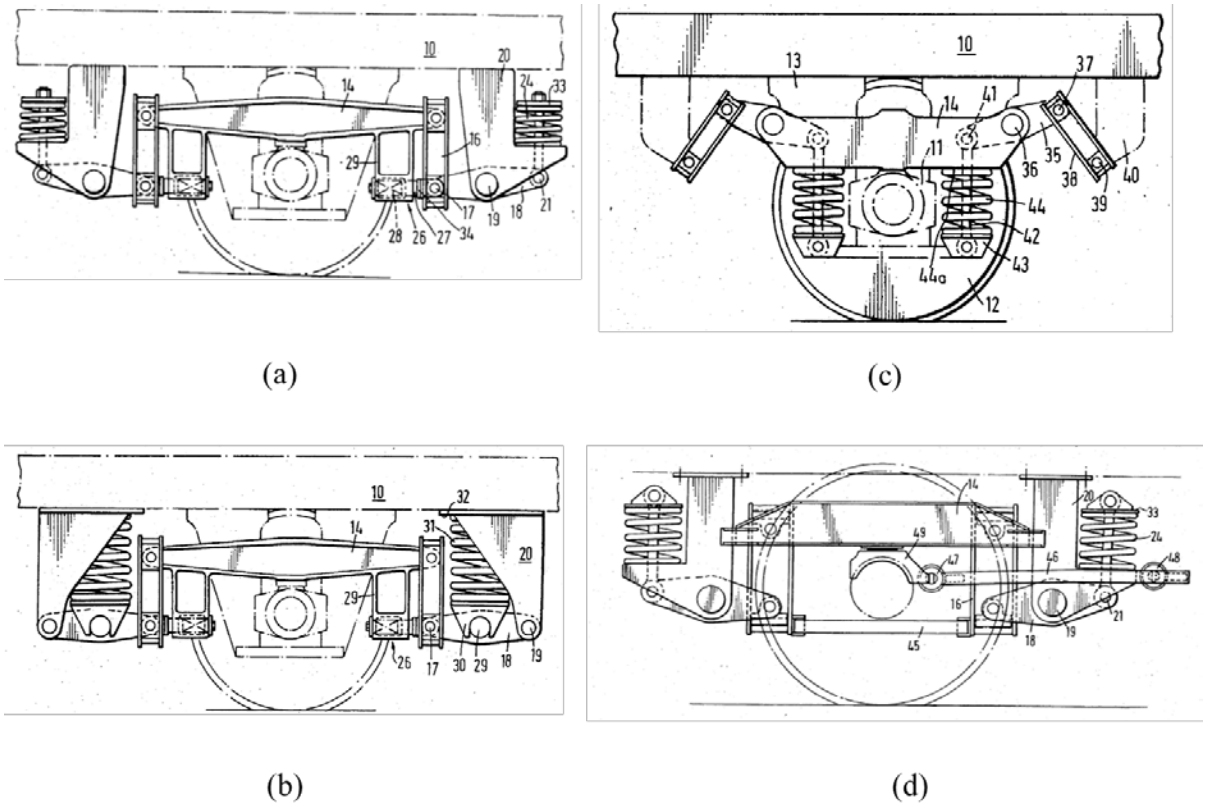

Figure 2-22: Some alternative arrangement of link suspension [37]

2.4.2.2 Two stage leaf spring and traction rod

A new invention in [38] was proposed with a leaf spring design of suspension by adding a traction rod (Figure 2-23) to provide a resilient yaw restraint on the wheelsets. This invention claims to utilise the traction rod to reduce the load on the friction linings in the pivotal mountings of links by providing resilience in the yaw direction. A leaf spring with a two stage characteristic has been used in this innovation [38]. Links can swing about bearing pins to provide lateral movement between the vehicle body and wheelset. Pins 12 are placed through bearing blocks 11 which pass through the eye of the leaf spring and suspension links at the upper ends and through suspension links and brackets 6A or 6B at the lower ends. A separate friction liner with a lower coefficient of friction than the steel to steel friction is proposed in between the pins 12 and bearing blocks 11 with a view to maintaining a consistent level of friction in service. In case of wear, the friction liner is easier to replace than the leaf spring, thus ensuring less maintenance effort than the conventional suspension system.

A traction rod is extended from each axle box 4 towards support bracket 6A on the inboard side of the wheelset or with the outboard side of the wheelset on support bracket 6B (Figure 2-23). The traction rod has a pivotal connection at the axle box through a rubber bush. To ensure the traction rod has adequate length, a pair of supporting blocks 18 is proposed on suspension bracket 6A. It is important to select the resiliency of the rubber bush such that the action of the traction rod does not affect the lateral and vertical movements of the wheelset with respect to the vehicle body which are controlled by the swing link and the leaf spring respectively.

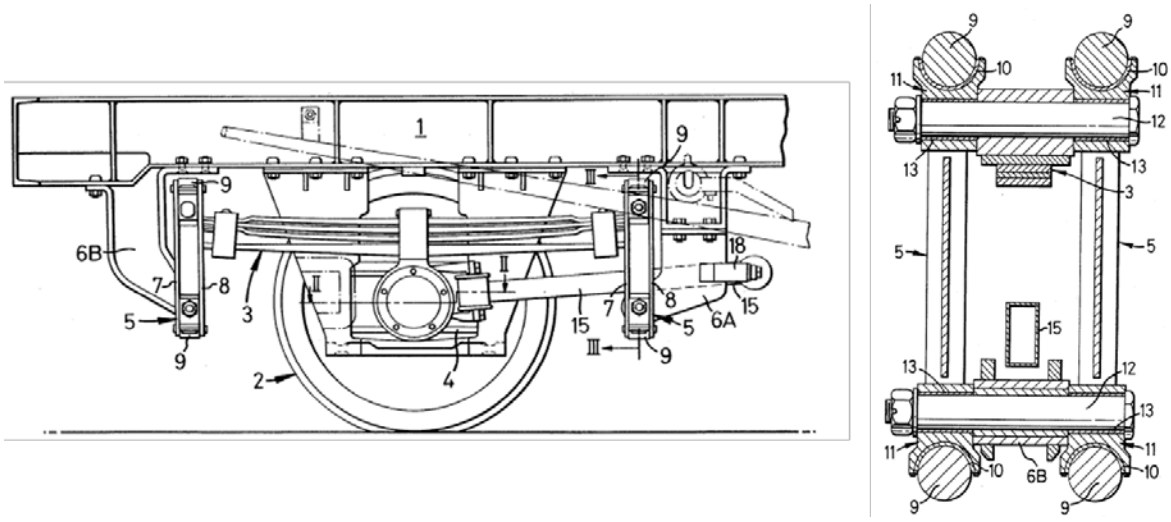

Figure 2-23: Link suspension with traction rod [38] (1- body of the vehicle, 2- wheelsets, 3- leaf springs, 4- axle boxes, 5- suspension links, 6A, 6B- brackets, 9- bearing pins, 10- bearing surface, 11- bearing block, 12- pin, 13- friction liner, 15- traction rod)

2.4.2.3 Single axle suspension system

A single axle suspension system (Figure 2-24) with wings 18 attached to the journal bearings of wheels is proposed in [39]. The wings are extended longitudinally from the journal bearing 10 to accommodate spring seats 20 to attach spring nests 22, 24 and the jaw 32 to attach damper 34 with the longitudinal part 28 of the wagon body. The inclined position of dampers 34 was claimed to provide appropriate damping for the multi stage stiffness for the entire load range of operation. The assembly was claimed to provide sufficient movement to the wagon body 30 compared to the wheelset 12 in lateral, longitudinal, vertical, yaw, pitch and roll directions.

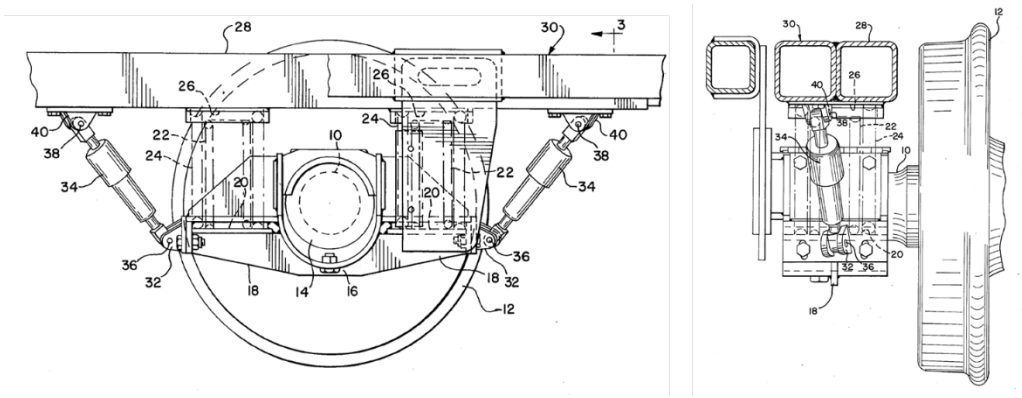

Figure 2-24: Single axle suspension system [39]

2.4.2.4 Improvement to the single axle suspension

With a view to improving the hunting performance of a two-axle vehicle, a ‘three-axles-one-unit’ was proposed in [40]. In this design, three single axle steering bogies are installed under a wagon body. Use of the additional axle per wagon helps to increase the length of the wagon body compared to that of a two-axle bogie by providing improved rigidity of the wagon. The addition of a traction rod 58 was proposed to the single axle suspension system to improve curving and thereby achieve a similar dynamic performance to that of a railway bogie [41].

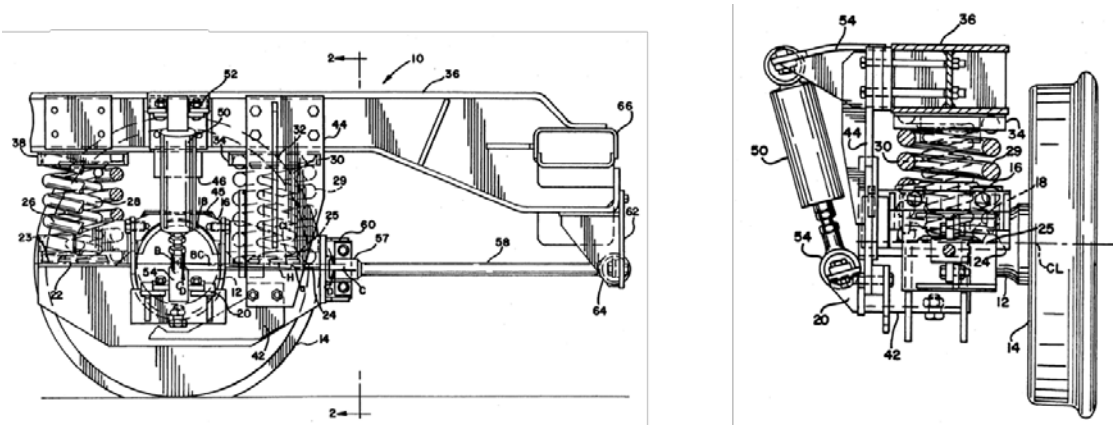

Figure 2-25: Single axle suspension system [41]

A single axle bogie with a sideframe structure was proposed in [42]. The sideframe attachment to the single axle bogie was used to hold the steering arms connected to the wagon body [42]. The rotatable steering arms can be fixed to the wagon body in front of the axle which, on a curved section, pushes the sideframe and hence an additional steering force is applied to the single axle bogie.

2.4.2.5 Spring nests suspension units

Up to three stage spring nests have been proposed to be used in conjunction with wedges and a rubber block over a wheel axle box in [43]. Vertical movement is controlled by the compression of two spring nests and a rubber block (Figure 2-26). The wedges on top of the spring nests provide damping and help to reduce longitudinal movement of the suspension system relative to the wagon body. In addition to the wedges, the rubber block also helps to restrict the longitudinal movement of the suspension unit relative the wagon body up to the position of the stop block.

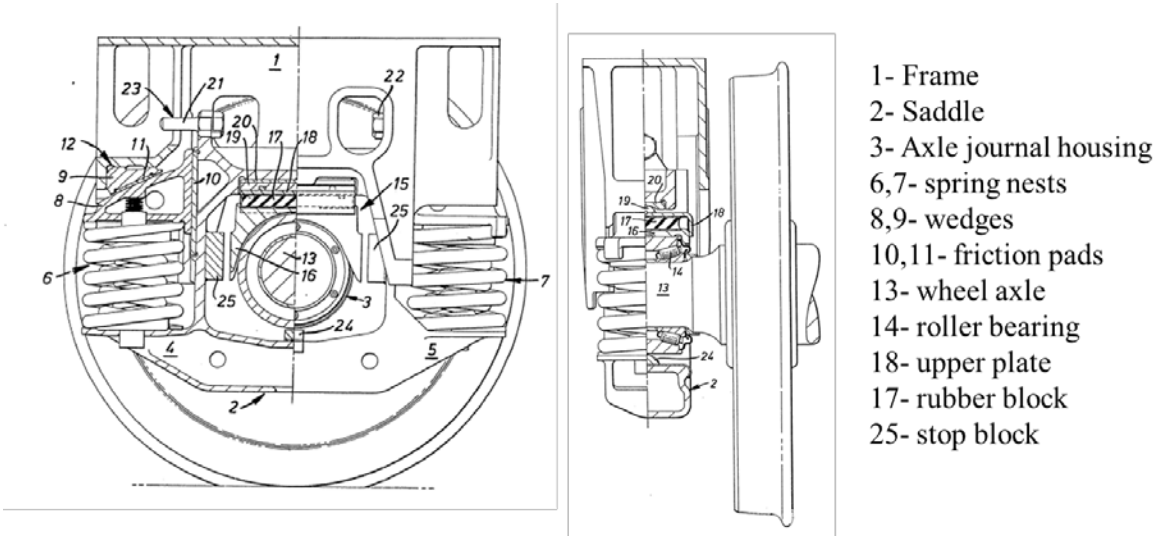

Figure 2-26: Spring nest suspension units [43]

2.5 Wagon Dynamics

Modification of suspension elements require understanding of wagon dynamics. The most important parameter is the confronting requirement of the curve negotiation and stability on a straight track.

2.5.1 Guidance and Curving

The word guidance refers to the ability of a vehicle to follow the geometric layout of the track [44]. The guidance performance depends on the connection mechanisms between the wheelsets and the wagon body, and the dynamics of wheel-rail contact. On a sharp curve, the flange of the outer front wheel comes in contact with the rail which results in a yaw couple on the wheelset (Figure 2-27). As the wheelset is constrained by the longitudinal and lateral stiffness provided by the suspension attached to the rest of the vehicle, the wheelset moves further out in a radial direction to generate opposite longitudinal creep forces [44]. The difference between the travelling distance of the inner and outer wheels of a wheelset on a curved track leads to yaw [45]. The lateral force is balanced by the further yaw movement as the vehicle moves through the curve.

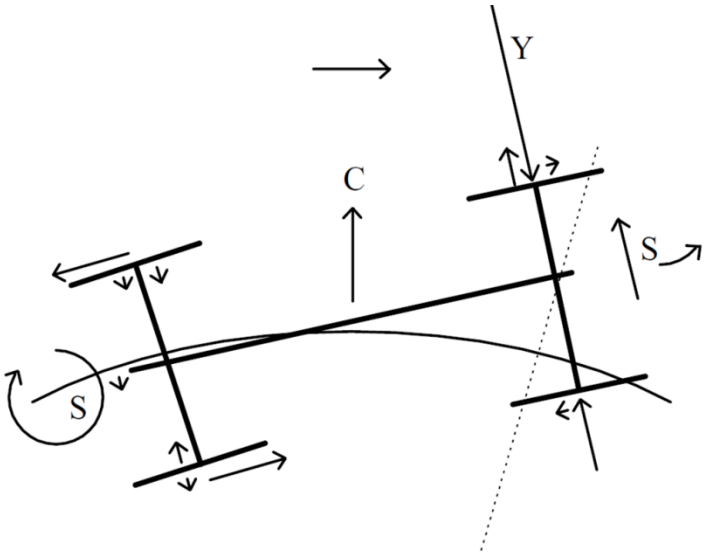

S- the forces applied to the wheelsets by the suspension
C- Centrifugal force
Y- Horizontal component of the normal force between wheel and rail

Figure 2-27: Schematic diagram of a typical attitude of a two-axle vehicle in a curve [44]

The running characteristics in curves are also influenced by the conditions in the wheel-rail contact interface due to the fact that wheelsets in curves gain the radial adjustment through creep forces in the contact zone [46]. Thus the geometry of wheel and rail profiles (and the tractive effort exercised by powered wheelsets such as on locomotives) influences the guiding force of the wheelsets. As an example, the guiding force for the S1002 wheel profile and the UIC 60 rail profile with an inclination of 1:20 have been found to be higher than that of similar wheel-rail profiles with an inclination of 1:40 [46].

Curving and stability considerations play an important role in the design phase of the guiding mechanism [46]. There are conflicting objectives between curving and stability of the vehicle. The longitudinal stiffness of the wheelset needs to be low to generate a sufficiently small steering resistance force that is suitable for reducing wheel and rail wear, but this is in conflict with the need for a high longitudinal stiffness requirement for higher critical hunting speed (Figure 2-28).

The curving requirement leads to the selection of a shorter length for the two-axle vehicle than that of a bogie vehicle. The early bogie designs had very short wheelbases that tended to oscillate violently [44]. The increase of

wheelbase of the leading truck of locomotives in the 1850s improved their stability significantly. Oscillation of bogies had also been reduced by the application of yaw restraint for small relative motions, thus preventing bogie hunting. Yaw damping was provided by the centre friction plate, or alternatively by friction at the side bearers.

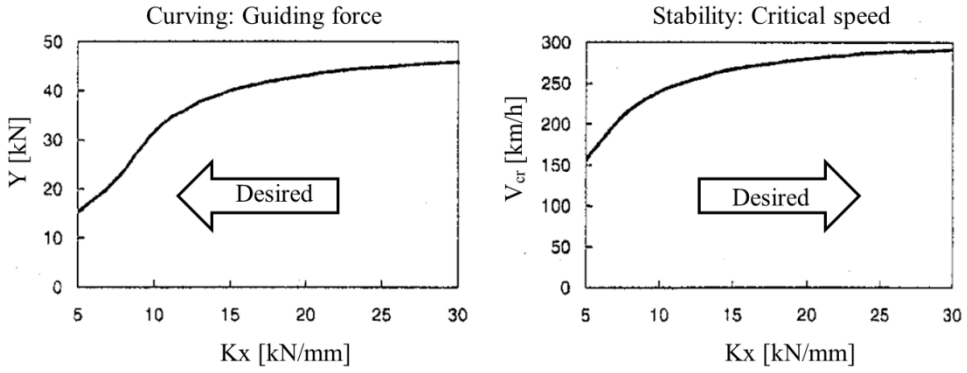

Y- Lateral wheel- rail force, Kx – longitudinal stiffness of the wheelset, V_{cr}- Critical speed

Figure 2-28: Curving and stability considerations during the design of the wheelset guidance [46]

The use of independent wheels has a potential for positive future developments due to the fact that they do not induce longitudinal slip, and wear and noise problems can thus be mitigated [47]. One important advantage of independent wheels is that they do not generate the hunting motion. However, they lack the restoring ability on curves or on any track irregularities and are easily affected by wheel-rail wear and have a tendency to run off the track centre.

Rail vehicles during curving face centrifugal and lateral forces due to curvature [45]. Superelevation adds lateral gravity components to assist curving. The speed at which the centrifugal and lateral gravity components become equal is known as balance speed. The lateral creep force also contributes to balance of forces on the vehicles on the curved track. The vehicle is said to be operating with excess cant if the speed is less than the balance speed, and with cant deficiency if the vehicle speed is higher than the balance speed. The lateral rail force increases with the increase of cant deficiency.

2.5.2 Hunting

The self-excited cyclic lateral motion of the wheelset with respect to its initial position is known as hunting [45]. The hunting phenomenon is the result of the coupling between the lateral and yaw displacements and the creep forces [45]. Due to hunting, significant lateral vibration is introduced which, in severe cases, can cause a derailment. The severity of the hunting motion depends on the speed of the vehicle. The characteristic speed over which the vehicle becomes unstable due to hunting motion is known as the critical speed.

The stable and unstable equilibrium (also called attractor or limit cycle) regions in a typical non-linear system are often represented by a so-called bifurcation diagram [48]. At the limiting line between the stable and unstable regions, the vehicle might lose its stability and another equilibrium solution could be achieved which can abruptly change the vehicle behaviour. The velocity of the vehicle has been determined to be the main influencing parameter in deciding on the equilibrium solution of the system equations. If the velocity of the vehicle is below a certain limit (v_{nlin}) for a certain combination of parameters, all solutions are stable which means the oscillation

will be damped out regardless of the initial conditions (Figure 2-29). At the range of speed between v_{nlin} and v_{lin}, two stable solutions and one unstable solution (the dotted line in Figure 2-29) could co-exist [48] which may provide a misleading conclusion regarding the stability if not examined carefully. Thus it is important to determine the minimum velocity where instability starts (v_{nlin} in Figure 2-29). The v_{nlin} is considered as the critical hunting speed.

There are two instability regions for a rail vehicle. One is at the low speed range associated with the instability of the wagon body which can be controlled by using lateral dampers in the secondary suspension to reduce the amplitude of the wagon body lateral motion [45]. The other type of instability occurs at higher speeds and depends on the bogie suspension design and the wheel-rail geometry [45].

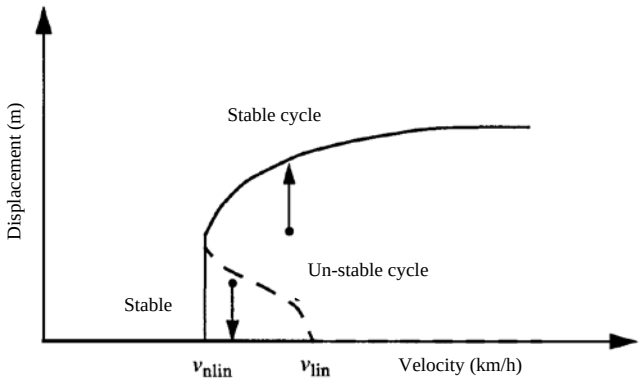

Figure 2-29: Typical bifurcation diagram [48] (V_{nlin}- a solution without oscillation exist, V_{lin}- a sub-critical Hopf bifurcation point where the equilibrium solution loses its stability and a new solution exists)

Wear on wheel and rail affects critical speed. The amount of wear in the wheel-rail contact interface is often characterised in terms of 'equivalent conicity'. According to the British standard EN 14363 [49], equivalent conicity is defined as "*for a given wheelset running on given track it equals the tangent of the taper angle of a tapered profile wheelset whose transverse movement has the same wavelength of kinematic yaw as the wheelset under consideration*". It has been observed on a scale rig test using different worn wheel profiles used in the Korean railway that equivalent conicity increases with flange wear and that critical speed is inversely proportional to equivalent conicity [50].

Although an individual worn wheel profile gives a lower critical speed than that of a new wheel profile, the use of worn wheels on all wheels in a wagon combination can give a higher critical speed [51]. Use of worn wheels in a three piece bogie wagon running in one direction results in about a 25% increase in critical speed compared to that of a wagon with new wheel profiles as observed in [51]. The possible reason behind this fact is the damping out of the hunting motion by the mismatch of hunting between the worn wheelsets of a bogie which gives a lower bogie hunting for the two wheelsets. On the other hand, a worse wheel profile alone does not replicate the worst case situation in service; the combination of rail and wheel need to be considered to determine the worst service worn condition [52].

2.6 Train Configurations

In addition to reducing the mass of a wagon, the possibility of improving mass and payload productivity also exists by varying combinations of axles, lengths, coupler types etc. The tare weight of a wagon can be reduced by either using fewer wheelsets per unit train length or using a lighter material for construction. Various combinations of wheelsets in the wagon have been tried since the introduction of railways [44]. On the other hand, the use of fewer wheelsets increases the axle loads which might have a negative effect on wheel and track damage [53].

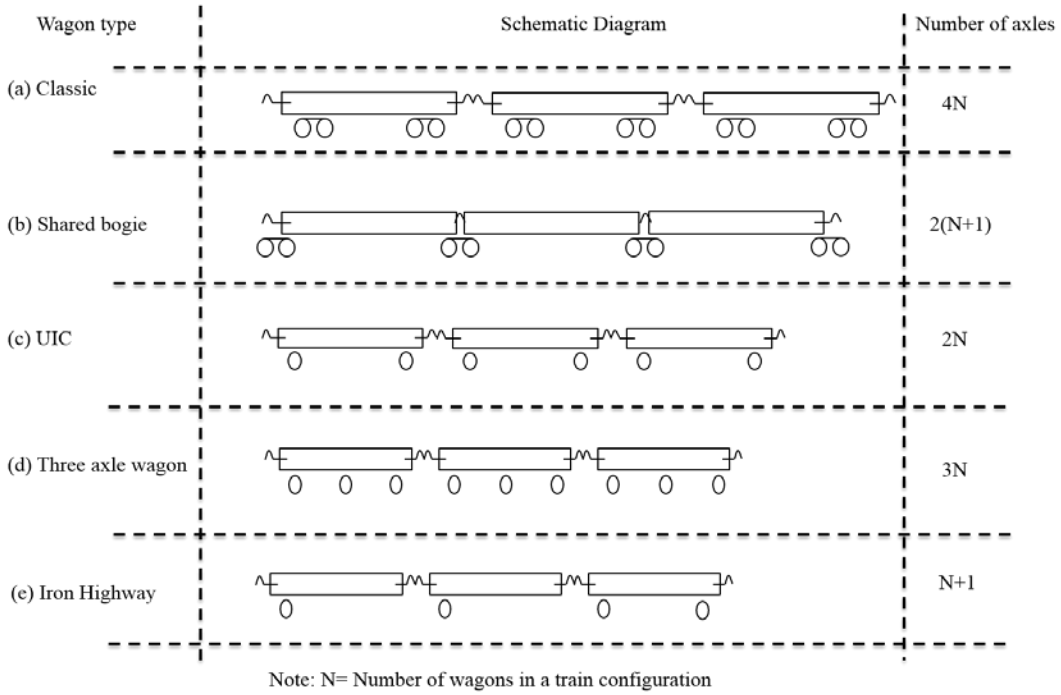

Figure 2-30: Wheel and axle arrangements for wagons (based on container type arrangement)

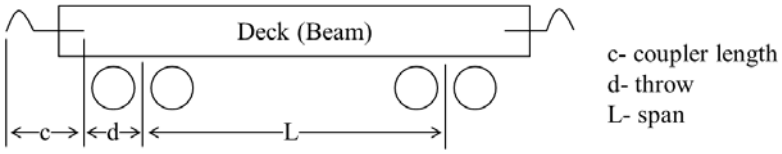

Figure 2-31: Length parameters of a container wagon

Based on the bogie, axle and wheel arrangements, wagons can be divided into several groups such as Classic wagons- two bogies per wagon, Shared bogie wagon- each bogie is shared by two adjacent wagons, UIC wagon- two axles per wagon, three axle wagons, Iron Highway- independent wheels etc. The number of axles in a train configuration can be estimated based on the number of wagons and the arrangement of their axles (Figure 2-30).

The mass density along the length of a train depends on three length parameters, namely overhang (c), wheelbase spacing (d) and the distance between the two inner wheels (L) of a wagon (Figure 2-31).

2.6.1 Normal Rollingstock

The normal train configurations generally consist of using conventional bogie or two-axle wagons (example, Type a and c, Figure 2-30) marshalled in a train suitably designed for the network requirements such as the allowable

tonne axle load (tal), the length of crossing loops, available locomotive power, track topography (curves, gradient) etc. The number of axles needs to be increased to carry a high payload on track with a low allowable axle load. Thus, the two-axle configurations are usually replaced by bogied wagons that reduce the tal to about 50% compared to a two-axle wagon when the high payload is desired. The minimum crossing loop length in a network limits the length of the train. Heavy haul networks are dedicated to the heavy haul trains and it is possible to provide very long crossing loops due to the fact that the heavy haul operations are usually operated outside cities. In the case of intermodal transportation within cities, the length of crossing loops is often limited (as an example, about 600 to 700m in European intermodal routes [54]). So, the length of the intermodal freight trains is usually shorter than heavy haul trains. Due to the variable load requirement in intermodal freight train operations, the locomotive power cannot be chosen as an optimum for a typical operation of the network, compared to the consistent power requirement for the fully loaded condition in heavy haul operation which can be optimised. The axle load limit also restricts the distance between wheelsets on a wagon and on adjacent wagons, and overhang lengths are mentioned in the British standard [18]. As an example, the minimum overhang, axle centre distance and gap between adjacent wagons on 25.5 tal two-axle wagon were 1.524m, 4.572m and 3.048m respectively [18]. The maximum distance between the two axles of 16.4m according to the British standard [18] is significantly higher than the 13m bogie centre distance (BCD) allowable in the ARTC track geometry standard of Australia [55].

2.6.2 Alternative Rollingstock

In search of suitable options for fast and cost effective intermodal transport, a few alternatives are now being considered around the world such as the Iron Highway, Rail Runner and Cargo Sprinter [56].

The Iron Highway system was prototyped in the USA during the 1990s. The system is based on the ‘trailer on flat car’ concept that allows road trailers to drive onto the rollingstock by using a ramp and thus claims reduction of the loading and unloading time. The Iron Highway system uses independent wheels without any solid axle between wheel pairs and the steering is provided by linkages attached to the load bearing platform and wagon body [57]. The continuous platform with movable hitches allows flexibility in trailer sizes that can be loaded on the Iron Highway container wagon.

Trailerail has been used in Australia by Pacific National to transport semi-trailers (without their prime movers) in a train configuration. The system shares one bogie between two semi-trailers which reduces the bogie weight per freight transport. However, due to low life expectancy, Pacific National has started replacing the Trailerail system with five pack container wagons.

The European designed Cargo Sprinter has power units on either end and is used for short haul transport consisting of only a few wagons in between. This arrangement generally gives speed and flexibility of operation. The cost of operation on Cargo Sprinter could be high compared to long freight trains as it needs more drivers for the same amount of payload per trip compared to the long haul operation.

Articulated configurations reduce the number of bogies per unit of configuration and thereby the tare weight. As an example, an articulated configuration requires 6 bogies for 5 platforms instead of 10 bogies for a similar set of

conventional wagons and thus achieves a tare mass of 55 tonnes per articulated consist (11 tonnes per platform) compared to 90 tonnes per non-articulated consist (18 tonnes per platform) with the conventional design [10].

2.7 Longitudinal Train Dynamics

Longitudinal train dynamics (LTD) is defined as the motion of the train as a whole and any relative motions between vehicles in the longitudinal direction of the track [21]. The relative motions between vehicles, also known as 'slack action', occur due to the looseness of the connections between vehicles. The loose or slack connection occurs due to the clearances in the autocoupler knuckles and draft gear assembly pins.

Longer and heavier trains suffer consequences caused by higher in-train forces acting on couplers between wagons. The larger and heavier trains may cause a greater in-train force [21]. The in-train forces in curves push a wagon laterally inward or outward depending on whether the forces are tensile or compressive. The lateral component of the coupler forces can be significant in some cases which can initiate wheel unloading and, in extreme cases, derailment can occur. In the AS7509 standard, a slow speed test is recommended to investigate the effect of coupler forces due to safety issue for physical test. In simulation it is possible to run the test for the service speed on a curved track and this is regarded as a useful test to measure a wagon's response to a reasonable lateral component of coupler force that may occur during service [58].

The dynamic problem in train operation is worse when an empty wagon is marshalled with loaded wagons as in-train forces can cause wheel climb on curves and body and/or bogie pitch that might derail the wagon [59]. The mismatch of coupling heights due to the presence of different weight wagons in a train configuration can lead to wagon lift. Thus it is important to consider the train dynamics inputs such as coupler forces on a wagon when designing a wagon for particular train and route combinations.

With these considerations in mind, very low tare wagons might not be workable in the long train lengths typical of heavy haul operations due to risks of jack knifing, rollover etc. under some operational situations. Jack knifing could occur due to buff (compressive force in the train during braking) forces and the effects are potentially severe on curves when the couplers are angled, increasing the lateral force on the wagon [60]. Examples of jack knifing derailments mentioned in [60] indicate that jack knifing risk is higher for couplers without alignment control, large coupler angles and poor quality track.

Therefore, the development of a longer and lighter wagon might require applying a few control mechanisms such as couplers with alignment control, low coupler length and higher curve radius of track to reduce coupler angle and lateral force, and improved track quality. In addition to the control measures, it is acknowledged that intermodal operations with smaller length trains than most heavy haul operations would produce lower in-train coupling forces. Hence, the jack knifing tendency is less likely on intermodal operations than with the longer train lengths in heavy haul operations.

2.8 Computer Simulations for Rail Vehicles

Australian standard AS 7509.2 recognises Vampire, NUCARS, and Gensys as suitable software packages for vehicle simulation by virtual homologation [61]. In addition to these, SIMPACK, ADAMS/Rail, Simulink and

Matlab have also been used for simulation of railway vehicles. The main scheme of the simulation process is presented in Figure 2-32.

The first stage in preparing a model for the evaluation of dynamics using simulation is the development of equations of motion that represent the vehicle-track system [62]. The equations of motion are usually second order differential equations that can be combined as a set of matrices. Most Multi-Body System (MBS) software packages can automatically convert the vehicle parameters into some suitable equations of motion. The input parameters are added via graphical selection or a list of text files.

Modelling refers to defining connections between the bodies using the input parameters. The solution methods include quasistatic analysis, eigenvalue analysis, frequency response and time history analysis. The outputs obtained from the solution are then post-processed using filtering, plotting, animation etc. based on the particular requirements.

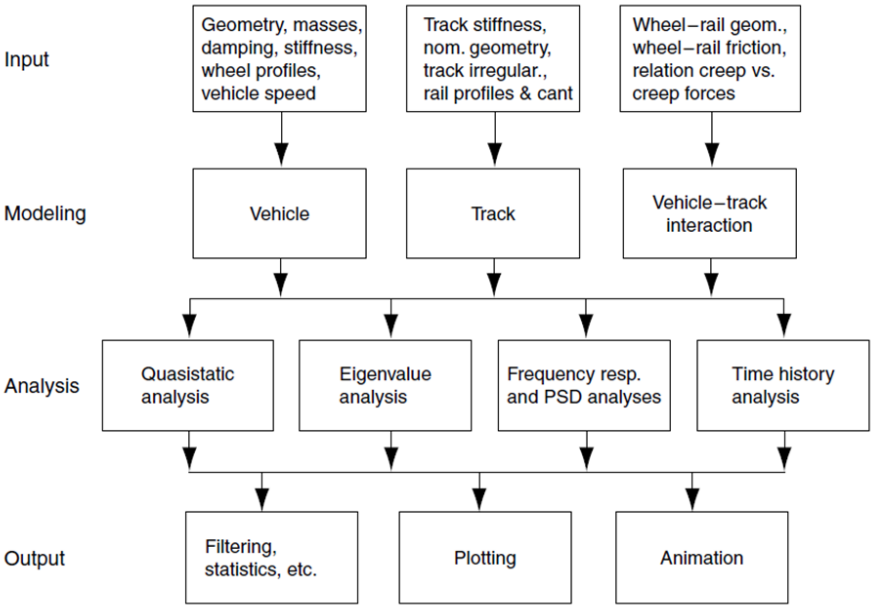

Figure 2-32: A flow chart of process of computer simulation of railway vehicles [62]

2.8.1 Basic Theory of Multi-Body Applications on Railway Vehicles

In a Multi-body System (MBS), a network of bodies is connected to each other by theoretical flexible, massless elements such as springs, dampers, links, joints, friction surfaces or wheel-rail contact elements [62]. A representation of an MBS model defining a rail bogie is shown in Figure 2-33.

The connection points are specified on bodies and are known as nodes. Each of the rigid bodies has a maximum of six degrees of freedom (DOFs) made up of three translational DOFs, namely longitudinal (x), lateral (y) and vertical (z), and three rotational DOFs, namely roll (f), pitch (k) and yaw (p) [62]. The available DOFs of the system are defined by the set of joints and constraints [63]. The movements are controlled by applied force and torque elements or imposed displacements or rotations. Excitation (force, displacement) is introduced to the model so that the response can be evaluated.

In addition to the Cartesian coordinates, a trajectory coordinate system is used in specialised railroad vehicle formulations (Figure 2-34) [45]. In the trajectory coordinate system, the motion of a body (i) within a railroad vehicle model is defined using coordinates that depend on the track geometry. The coordinate system for a body, known as the body-trajectory system, can be defined by X^{ir}, Y^{ir}, Z^{ir} coordinates which are different to the global coordinate system of X, Y, Z coordinates. Considering the known track geometry over a distance, the complete definition of the trajectory coordinate system requires only one time dependent parameter, namely distance travelled, with all other translational and rotational parameters coinciding with the track geometry.

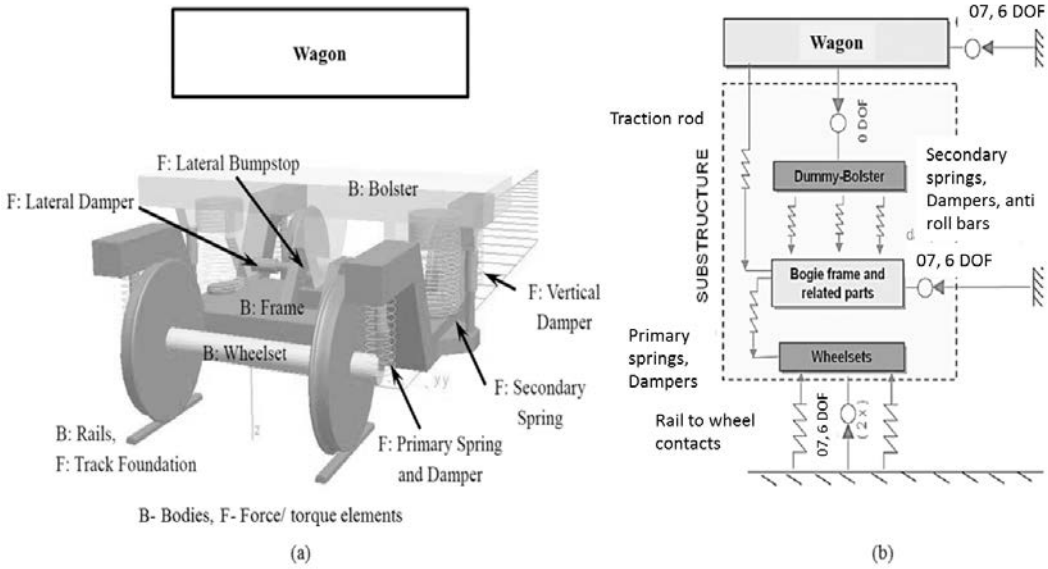

Figure 2-33: (a) MBS model of a bogie [63], and (b) Schematic model topology of a bogie [63]

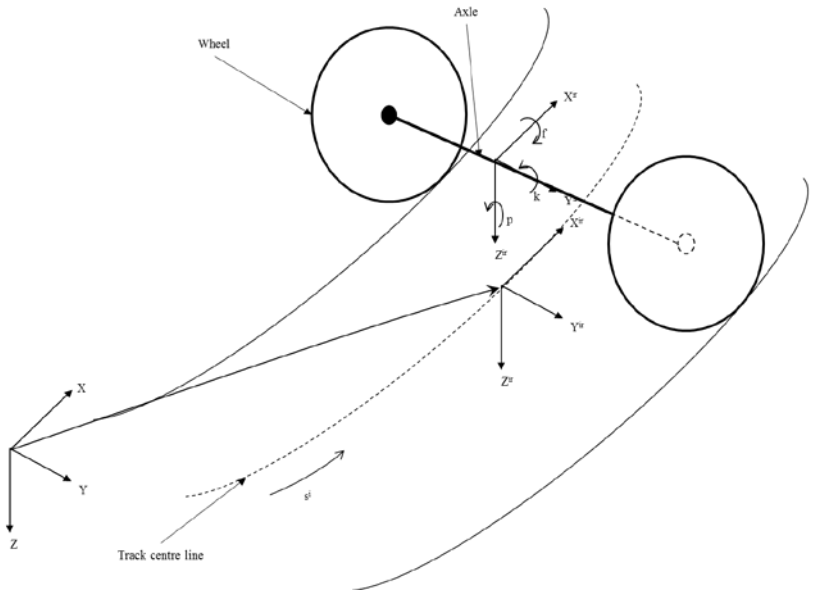

Figure 2-34: Trajectory coordinate system of a rail vehicle formulation [45]

The centre of each body is regarded as the origin of the body coordinate system. The body coordinate system is selected such that it does not have any motion in the longitudinal direction with respect to the trajectory coordinate system. The body coordinate system requires five time dependent parameters comprised of two translational and three rotational parameters defined with respect to the body trajectory coordinate system. Thus, the trajectory coordinates of an arbitrary body *i* in the system can be represented by the following set of coordinates (Equation 2-4).

$$\boldsymbol{P^i} = \left[\boldsymbol{s^i y^{ir} z^{ir} \psi^{ir} \phi^{ir} \theta^{ir}}\right]^{\boldsymbol{T}} \quad \textbf{2-4}$$

where s^i is the arc length coordinate along the track space curve, y^{ir} and z^{ir} are the locations of the centre of the mass in the lateral and vertical directions respectively, $\psi^{ir}, \phi^{ir}, \theta^{ir}$ are the yaw, roll, and pitch angles respectively defining the orientation of the body with respect to the trajectory coordinate system.

2.8.2 Modelling Elements

The first stage of simulation is to develop a set of mathematical equations to represent the vehicle. The main elements of modelling are the wagon subsystem, suspension subsystem, track subsystem and contact modelling between wheel and rail.

2.8.2.1 Modelling of wagon subsystem

Traditionally, the wagon subsystems have been modelled in three ways, namely single wheel, bogie and wagon models based on particular requirements as modelling of a full wagon model is computationally expensive (Figure 2-35) [64]. In the single wheel model (Figure 2-36a), a static wheel load representing the mass of all wagon components is applied on the wheel directly or through the primary suspension. The one bogie or half wagon model comprises two wheelsets connected to the sideframes directly or through primary suspensions (Figure 2-36b). The sideframes carry the mass of the wagon directly or through secondary suspensions. The third type of model considers a single wagon comprising all components where the wagon body is supported by the secondary suspension through bolsters or directly by two bogies. With the increase in computing power, it is now possible to complete simulations of a full wagon model with reasonable computational effort.

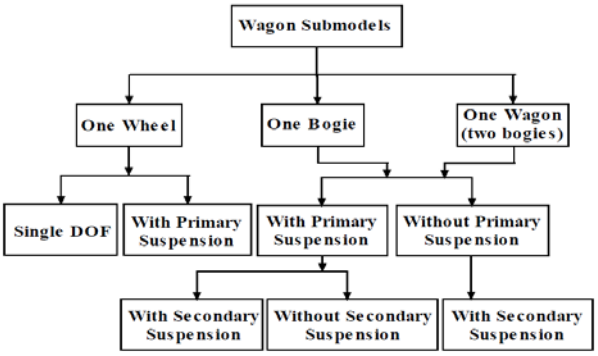

Figure 2-35: Model classification for wagon subsystem [64]

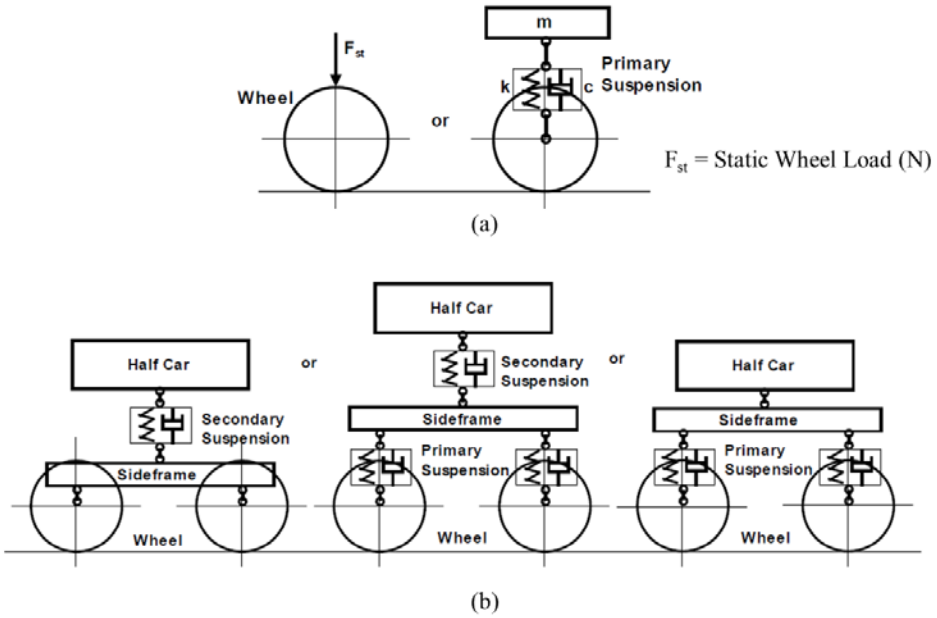

Figure 2-36: Wagon submodels: (a) Single wheel model, and (b) Bogie models [64]

2.8.2.2 Modelling of suspension subsystem

The wagon body and axles are connected by suspension elements. The accurate modelling of suspension elements requires field or laboratory measurements. The key properties in the suspension system often include stiffness, viscous damping, friction damping including friction system pre-load and friction static-dynamic characteristics [65]. In most freight vehicles, primary suspensions are absent due to the relaxed requirements of ride comfort.

The secondary suspension spring carries the vertical load and has been represented by separate vertical and lateral linear springs in numerous literature (Figure 2-37a) [66]. A more accurate model with additional roll torque represented by a shear spring element (Figure 2-37b) has been proposed in [66]. This principle has been implemented in VAMPIRE software with the addition of a shear spring element which also provides second order effects such as bending stiffness.

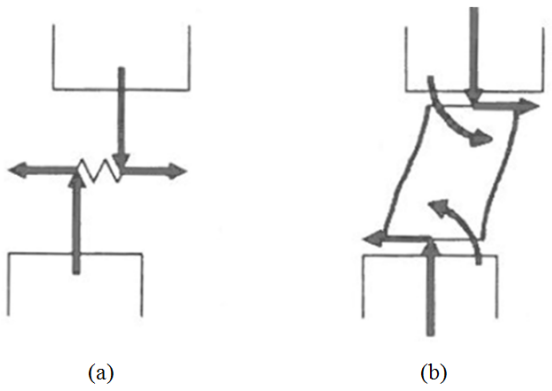

Figure 2-37: Secondary suspension spring model: (a) simple spring model, and (b) shear spring model [66]

Coil springs are more common on bogie wagons. Modelling of coil springs in railway suspension needs to take care of the coupling in different directions and reaction moments due to non-axial vertical forces [65]. The use of

an air spring in place of coil springs has made the modelling more challenging because of the non-uniform properties of the air spring with height [66].

2.8.2.3 Modelling of track subsystem

In most of the commercially available vehicle dynamics system software packages such as NUCARS (a product of TTCI, USA), ADAMS/Rail (a product of MSC Software, USA), and Vampire (a product of AEA Technology, UK), track is considered as a rigid support or as an elastic foundation [64]. The geometry of the track including length, curvature, superelevation, and grade is usually defined at different segments along the length of a track in the vehicle dynamic software (Figure 2-38).

The typical track model used in the function 'wr_coupl_pe3' of the Gensys program [67] is shown in Figure 2-39. While the contact between rail and its supporting track structure can be explained by using spring and damper properties (kyrt_, cyrt_, kzrt_, and czrt_), the contact between wheel and rail can be characterised by 1, 2 or 3 contact points with a stiffness value (knwr_) chosen by the user.

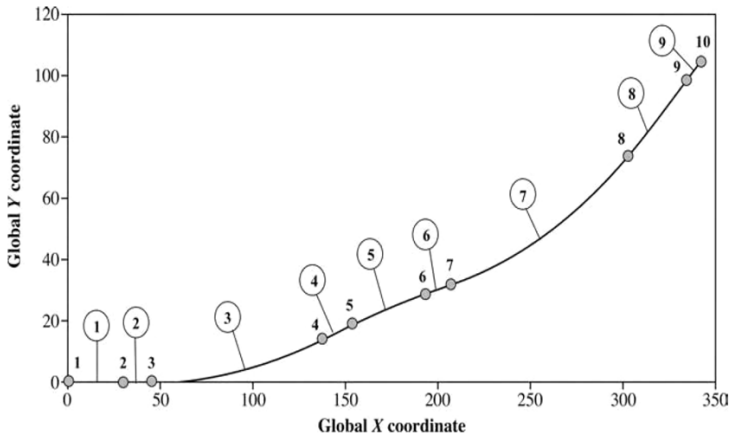

Typical Railroad Input Entries Used to Define a Curved Track

Node No.	Distance (ft)	Curvature (deg)	Super-Elevation (in.)	Grade (%)
1	0	0	0	0
2	100	0	0	0
3	150	5	1.5	0
4	450	5	1.5	0
5	500	−3	−1	0
6	650	−3	−1	0
7	720	7	2	0
8	1020	7	2	0
9	1145	0	0	0
10	1195	0	0	0

Figure 2-38: Typical definition of a track along the length [45]

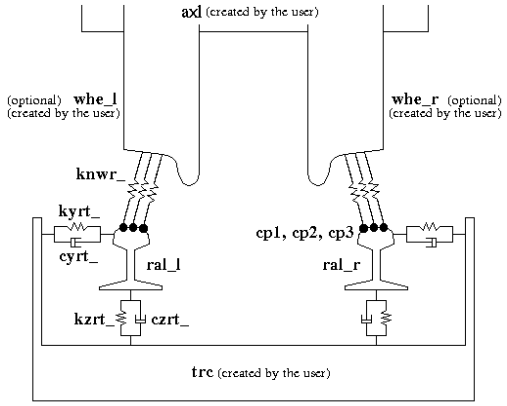

Figure 2-39: Track model in Gensys using function 'wr_coupl_pe3'[67]

2.8.2.4 Contact between wheel and rail

The formulation of contact between wheel and rail found in numerous literature is mostly based on the theory of Hertz. Hertz solved the problem for two bodies in contact with surfaces of second degree [68]. According to Hertz

theory, if two elastic bodies with large curvature radius compared to the contact patch size and having constant curvatures inside the contact patch are pressed together in elastic behaviour within semi-infinite spaces, then the contact surface is considered flat, the shape of the contact surface is an ellipse and the contact-pressure is a semi-ellipsoid [69]. The traditional Hertzian contact model has been found to be inadequate for simulation in rail vehicle dynamic models as the wheel and rail are in multi-point contact [70]. However, Hertz theory is still widely accepted by rail research community to determine shape and size of contact area [45].

The differences in motion of wheel and rail at the contact point generates both rolling and sliding motion (Figure 2-40) [45]. The difference in angular velocity at the contact point generates rolling and/or spin creepages. The relative angular motion (yaw) about the normal of the contact point is known as spin.

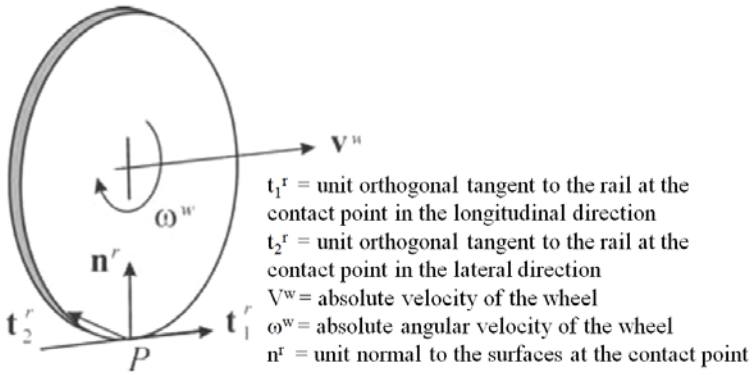

Figure 2-40: Contact frame of wheel and rail [45]

The small slip developed by the tangential strains of two bodies at the contact patch area (in this area particles in contact do not slide relative to each other, can also be termed as a no-slip region) is known as creepage. Creepages can be the longitudinal, lateral or spin type and can be presented mathematically by Equations 2-5 to 2-8.

$$\zeta_x = \frac{(v^w - v^r)^T t_1{}^r}{V} \quad \textbf{2-5}$$

$$\zeta_y = \frac{(v^w - v^r)^T t_2{}^r}{V} \quad \textbf{2-6}$$

$$\varphi = \frac{(\omega^w - \omega^r)^T n^r}{V} \quad \textbf{2-7}$$

$$V = v^{wT} t_1{}^r \quad \textbf{2-8}$$

where ζ_x is the longitudinal creepage, ζ_y is the lateral creepage, φ is the spin creepage, V is the magnitude of the wheel velocity along the longitudinal tangent defined at the contact point, v^w is the velocity vector of the wheel, v^r is the velocity vector of the rail, $t_1{}^r$ is the unit orthogonal tangent to the rail at the contact point in the longitudinal direction, $t_2{}^r$ is the unit orthogonal tangent to the rail at the contact point in the lateral direction, ω^w is the angular velocity of the wheel, ω^r is the angular velocity of the rail, and n^r is the unit normal to the surfaces at the contact point.

The success of a vehicle dynamics model largely depends on the calculation of an accurate contact patch between wheel and rail. The wheel-rail contact is considered as a rolling friction contact that differs from the sliding friction

Coulomb model with an area of adhesion (contact patch) and an area of slip [69], together considered as creepage. The area of slip increases progressively with the increase of the applied forces (Figure 2-41).

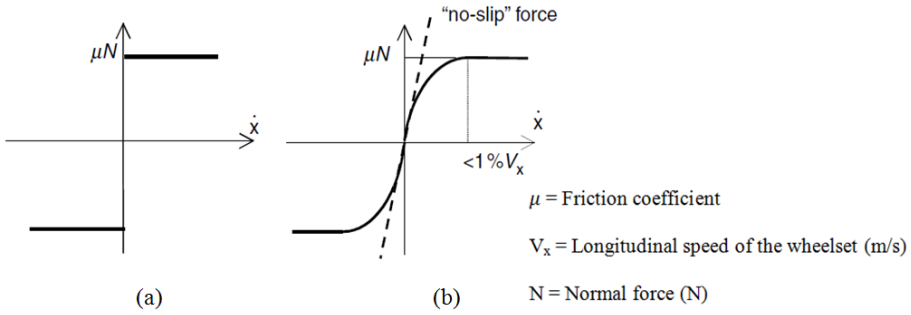

Figure 2-41: Wheel-rail contact: (a) Coulomb's model, and (b) Rolling friction model [69]

The accuracy of estimation of wheel-rail forces depends the use of linear or non-linear representations of wheel-rail contact and coefficient of friction [66]. In a full non-linear approximation, the contact data is derived from the measured wheel and rail profiles [66]. The longitudinal, lateral and spin creepages can be calculated from the parameters for the given lateral shift of the wheelset, such as rolling radii, contact angles and roll displacements of the wheelsets. The creep force depends on the size and ellipticity of the contact patch which can be obtained from the contact data. The saturation of non-linear creep force occurs at μN, where μ is the coefficient of friction chosen by the user and N is the normal load (Figure 2-42).

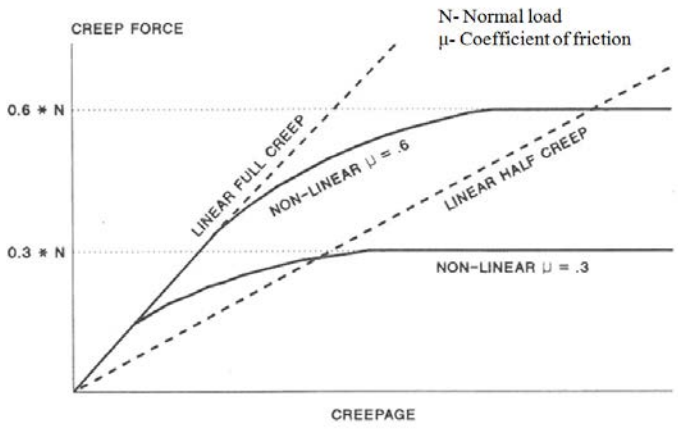

Figure 2-42: Creep force vs creepage [66]

Linear calculations of wheel-rail contact are based on two linear assumptions – constant conicity of wheelsets and a linear creep force vs. creepage relationship [66]. The assumption of constant conicity is only valid for the straight track but becomes poor when lateral displacements are large and the flange contact approaches on a curved section of track. At low conicities such as less than about 0.1, a wheelset may approach flange contact even on a straight track. The second assumption of linear creep force vs. creepage relationship is only valid for small creepage values for full creep coefficients. However, the creep force does not saturate with an increase of creepage values in this case. It has been advised that the slope of the line can be reduced by an appropriate factor, such as half of full creep, to obtain saturation when the creepage value is sufficiently large [66]. The shortcomings of linear approximation include its inability to consider dynamic changes in the wheel loads.

The complexity in formulating wheel-rail contact requires geometric data of wheel profiles and track gauges obtained using machines such as MINIPROF [71]. A method has been described in [72] to develop a geometric function in a tabulated form by using the data of wheel and rail profiles.

Based on the availability of experimental data, Johnson and Kalker established the definitive expressions of the creepage stiffness in the 1960s, introducing variable coefficients depending on the b/a ratio of the contact ellipse (a- contact ellipse semi-axis in rolling/ longitudinal direction, b- contact ellipse semi-axis in lateral direction) which is regarded as the most common method for railway vehicle dynamics study to date [69]. Kalker later developed two computer programs known as CONTACT and FASTSIM based on the strip theory originally proposed by Haines and Ollerton and extended to the three creepages.

The program CONTACT is based on the complete theory of elasticity and can take into account several body shapes and so can model wheel-rail contact [69]. The CONTACT program is able to provide better results compared to other simplified approximations such as FASTSIM but requires high computational time [68] which makes it often unsuitable for vehicle dynamics simulation [73]. On the other hand, FASTSIM is based on the simplified theory that describes the contact surface as a grid separating parallel strips in the direction of the rolling motion. The elements do not have the same length due to the elliptical shape of contact. In order to make the calculation faster, several pre-tabulated tables have been generated using FASTSIM results by Kalker which are being used in the Gensys, NUCARS and VAMPIRE simulation software packages [67, 69].

2.8.3 Inputs of a Multi-Body Model

Inputs to a model are usually specified at each wheelset [62]. The success of any modelling largely depends on the correct values of the parameters of the masses and suspension elements connecting different parts of the model [66]. The representation of the connecting bodies in multi-body simulation software often faces challenges in accurately modelling the actual non-linear behaviour due to the dependence of such parameters on amplitude and frequency. It is not only the ability to select the parameter that best represents the real element but also awareness of the range of operating conditions for which this parameter is appropriate that leads to developing a reliable and accurate vehicle model.

Considering the complexity in determining the parameters for a three piece bogie, a test rig method proposed in [74] uses a sliding plate and hydraulic actuator mechanisms to determine the lateral, shear and warp stiffness of a bogie that can be used in computer simulations. A hydraulic shaker arrangement along with low frequency sine sweep rates installed in the Association of American Railroads (AAR) rail dynamics lab in Pueblo have been used to characterise a bogie in [75]. The characteristic parameters for the modelling purpose chosen in [75] from the test rig were vertical and lateral suspension stiffness, vertical and lateral Coulomb damping, roll stiffness, break away yaw moments for the bogie as well as for the span bolster to the wagon body connection.

Dampers are commonly modelled as linear viscous [76, 77] and Coulomb friction elements [78, 79]. To prevent erroneous high frequency responses, linear dampers need to be modelled in series with a stiffness. Similarly, a very stiff limiting stiffness is needed for the Coulomb friction model to prevent numerical instability [80]. Dampers can also be a complex mix of viscous and friction damping with frequency dependent stiffness. Stability and ride performances mostly depend on the stiffnesses of the yaw spring-dampers which is affected by the choice

of mountings and the bulk modulus of the oil in the damper [66]. It is common that manufacturers cannot provide the complete data on stiffness, friction and damping characteristics and laboratory measurements or estimates based on past experience are often useful.

2.8.4 Solution Methods

The appropriate solution method is dictated by purposes such as customer specification, vehicle acceptance tests, risk assessment and support of other specialists (Figure 2-43) [62]. The primary investigation of any simulation includes running safety, track loading, ride characteristics and ride comfort which are necessary tests for the acceptance of any vehicle [62]. The vehicle model also needs to match customer requirements such as expected dynamic response, the influence of external loads, vehicle gauging, stresses and cumulative load distribution.

Task				Type of analysis	Calculation method				
							Simulation		
					Eigenvalue analysis	Quasi-static analysis	Straight track	Full curve	Curve transition
Internal need				Eigenbehaviour	X		X		
Risk assessment	Customer's specification			Carbody sway in curve		X		X	
		Vehicle acceptance	Safety	Safety against derailment		X		X	X
				Track shift force			X	X	
				Stability	X		X		
				Ride characteristics			X	X	
				Track loading		X		X	
				Ride comfort			X	X	X
				Wear		X		X	
		Support of other specialists		Gauging			X	X	X
				Influence of external loads			X	X	X
				Load collectives			X	X	X

Figure 2-43: Type of analysis and calculation method commonly used in rail vehicle engineering [62]

2.8.4.1 Eigenvalue analysis

The eigenvalues are calculated from the equations of motion and are used to identify natural frequencies and mode shapes. The natural frequency of various modes of the vehicle helps to find possible problems in the model [81]. The vehicle model can be investigated by the values obtained from the eigenvalue analysis for parameters such as eigenfrequencies, eigendamping and eigenmodes [62]. Any asymmetry or unlikely eigenvalue can indicate the presence of incorrect or missing parameters in the model.

Eigenbehaviour analysis uses some basic carbody modes and nomenclature to verify the model (Figure 2-44). There are some standard values available based on experiences for each of these modes. It has been recommended to perform eigenvalue analysis for both empty and loaded conditions, at a very low speed (e.g., 1m/s or zero speed if possible) due to the fact that it is necessary to exclude any kinematic oscillation that can happen at a higher speed [62].

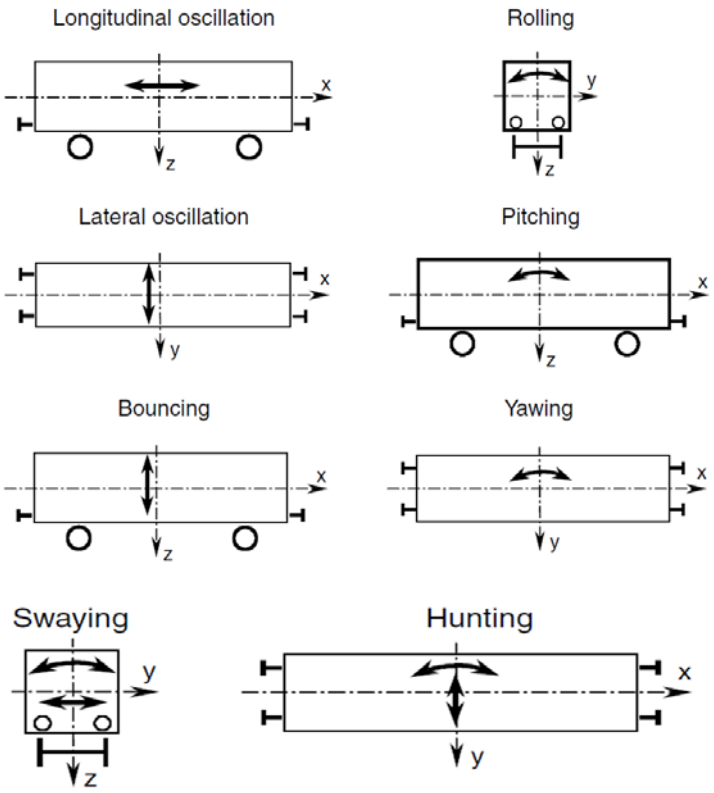

Figure 2-44: Carbody modes [62]

2.8.4.2 Stochastic analysis

In the stochastic analysis, a complex transfer function is calculated from the equations of motion with a view to finding any frequency spectrum of any part of the vehicle corresponding to an input track section [81]. This method is used to find and to remove problems with vehicle ride characteristics where the vehicle acceptance procedure requires the vibration levels to be lower than a limit specified in the frequency spectrum. The stochastic analysis method is useful to evaluate the lateral and vertical behaviours of a vehicle on a track with particular characteristics [62].

2.8.4.3 Numerical integration methods

The implication of Newton's second law in the multi-body system leads to a set of differential algebraic equations (DAE) and ordinary differential equations (ODE). Different interconnections in the MBS may include nonlinearities that may occur at places such as damper blow-off valves or bump stop contacts, rubber or air-spring elements, wedge dampers; all the wheel-rail contact models are non-linear [62].

In order to solve the equations analytically, it is necessary to remove all nonlinearities present in the model. As an option to solve nonlinear equations, numerical methods are being used that integrate equations at small time intervals over the simulation period. The result of each time step is used to predict the behaviour at the next time interval.

The efficiency and sometimes the accuracy of analysis are largely dependent on the choice of time step and integration methods. Numerical time stepping integration (or simulation) provides time series data and can be used to analyse both linear and non-linear models. Where the equations of motion have non-linear elements, the

integration requires very small time steps. The choice of a smaller time step can sometimes improve the numerical stability in the simulation of non-linear systems, but it increases the time required for simulation.

Numerical methods and integrators can be assessed based on the stability, convergence, accuracy and numerical effort. Numerical instability can occur due to the choice of numerical methods and time difference or step size being either too large or too small. As an example, in Figure 2-45 numerical instability occurs with a time step of 0.5ms but does not when the time step is reduced to 0.1ms.

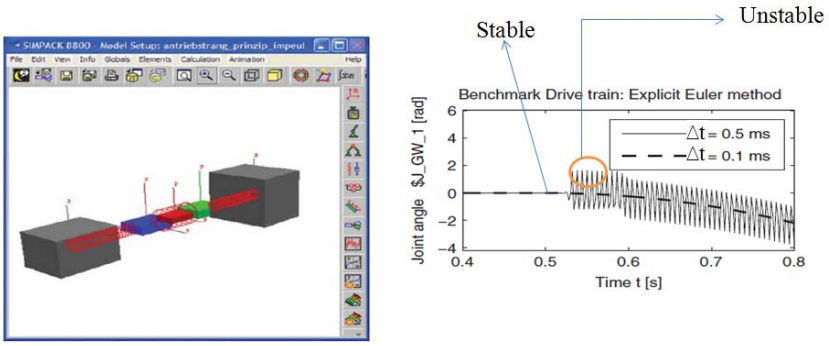

Figure 2-45: Numerical stability [82]

Convergence of a numerical method is an indication of how fast the numerical method will approach an exact solution. Initially, a numerical method approximates the solution using the step wise equations to obtain a result close to the exact solution. The iteration stops when the error between exact and approximate solution comes within a limit.

In order to obtain a good range of accuracy, the numerical effort required can be high depending on model complexity. Implicit methods usually provide better accuracy, but the requirement of further function evaluations at each step makes this method computationally expensive [83]. Conversely, the inability to calculate error at each step of a Runge-Kutta (explicit) method makes it necessary to check different time steps for stable behaviour. On the other hand, in a multi-step predictor corrector method, the error is calculated at each step with the previous steps and, if the result is not within a prescribed error tolerance limit, the iteration continuously looks for a better time step estimate at the previous step without evaluating the function value [83]. The numerical effort in case of the predictor corrector method depends on the limit of error tolerance.

It is also important to provide adequate error tolerance to obtain a robust solution (Figure 2-46) [82]. The FORTRAN ordinary differential equation solver RADAU5 shows that the solution is more robust for low error tolerance of 10^{-5} compared to high error tolerance of 0.03 (Figure 2-46).

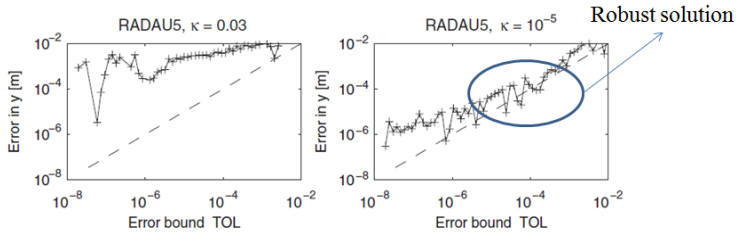

Figure 2-46: Error tolerance and robustness of solution [82]

2.9 Summary

The benefits of a low tare wagon can be realised in terms of payload carrying capability and low energy consumption. The high payload carrying capacity usually requires a high tare to provide the structural strength to carry the high payload. A low tare mass is beneficial as it not only reduces energy consumption to carry the empty load, but also provides an opportunity to raise the payload capability within an axle load limit on a network. A low tare wagon can be obtained using options of high strength low density material; alternate design of rollingstock such as bogied wagon or bogieless wagon; alternate design of train configuration such as non-articulated, articulated or single axle bogies. A review on the alternate design of rollingstock showed that the mass saving of 1-3t per wagon was achieved in different wagons. However, the data on length of the wagons were not always available which made it impossible to compare tare per unit length of the wagons. In intermodal transportation, available loading length is an important parameter for efficient transportation of containers. Based on a European study on intermodal transportation a bogied wagon with 28.7m length (VEL-wagon) suitable to carry a total of 90' of container load has been considered an efficient intermodal wagon.

Bogieless wagons are generally lighter than the bogied wagons. However, bogieless wagons generally provide poor steering and curving compared to bogied wagons. So, application of bogieless wagons on a tighter track curvature would require improvement in the dynamic performance. As an example, increasing longitudinal stiffness on the suspension would increase hunting speed but reduce curve negotiation ability. The stiffness of the vertical suspension can also be changed using multistage suspension elements for a desired outcome. Existing and patented rollingstock designs were reviewed with a view to provide an insight into some possible alternate designs that can be utilised to improve the dynamics of a bogieless wagon.

Some of the alternate designs of bogieless wagons have achieved popularity in intermodal transportation in the European network. However, the length of the bogieless wagon is usually less than the bogied wagon due to less number of axles on a bogieless wagon which restrict the payload capacity due to the axle load limit.

Improvement in computing power and computer simulation techniques on vehicle design have made it possible to model more complex dynamic conditions. The vehicle dynamics standards have also recognised computer simulations as a valid alternative for some physical tests. The success of computer simulation depends on the definition of the model elements (wagon, suspension, track, wheel-rail contact) and selection of a solution method.

Chapter 3
Methodology

3.1 Introduction

The methodology of the thesis has been developed considering the research gap in the field of low tare wagons in particular in the modification of running gear to achieve a lighter wagon. In this chapter, the research gap and methodology of the thesis have been presented.

3.2 Research Gap

The literature review in Chapter 2 shows that the intermodal wagons have the potential to adopt a low tare and longer length design option as the intermodal transportation is not as optimised as some other rollingstock such as the heavy haul wagon. As found in the literature survey, the intermodal wagon needs to be longer and lighter to be competitive with other modes such as the road trailers. A longer wagon needs to have the capacity to carry the maximum container loads on its length. The research gap identified for this thesis is that a long, ultra-light wagon with a high tal (example 40tal) capacity is not yet developed.

In Chapter 1, it is hypothesised that a reduction in tare load is possible by replacing the bogie suspension system with a single axle suspension system without the bogie structures. A bogieless design faces some issues such as poor twist accommodation, poor critical hunting speed [84], and potentially higher axle loads when compared to a bogied wagon. It was hypothesised that an improvement in the design of the single axle suspension would be required. It was also envisaged that more comprehensive simulation tests might be needed to establish fitness for purpose and roadworthiness as the new design might push the boundaries of normal design.

3.3 Methodology of the Thesis

The methodology of the thesis is presented in Figure 3-1. A review of the existing wagon and suspension designs has been performed in Chapter 2. The review showed that improvement of dynamic performance of a single axle suspension could be possible by trialling potential modifications of the suspension system as have been proposed in numerous literature and patents presented in Chapter 2. While it is obvious that improving dynamics can be possible with exotic innovations, the relevant cost saving on fuel consumption may not be sufficiently large when a costly suspension system is used. In freight transportation, the ride quality is generally less important as opposed to its need for passenger transportation. So, providing derailment safety in the freight wagons could be adequately ensured, a moderate ride quality could be adequate. Hence, an approach is necessary to ensure an optimum suspension with the minimum number of additional elements or modifications.

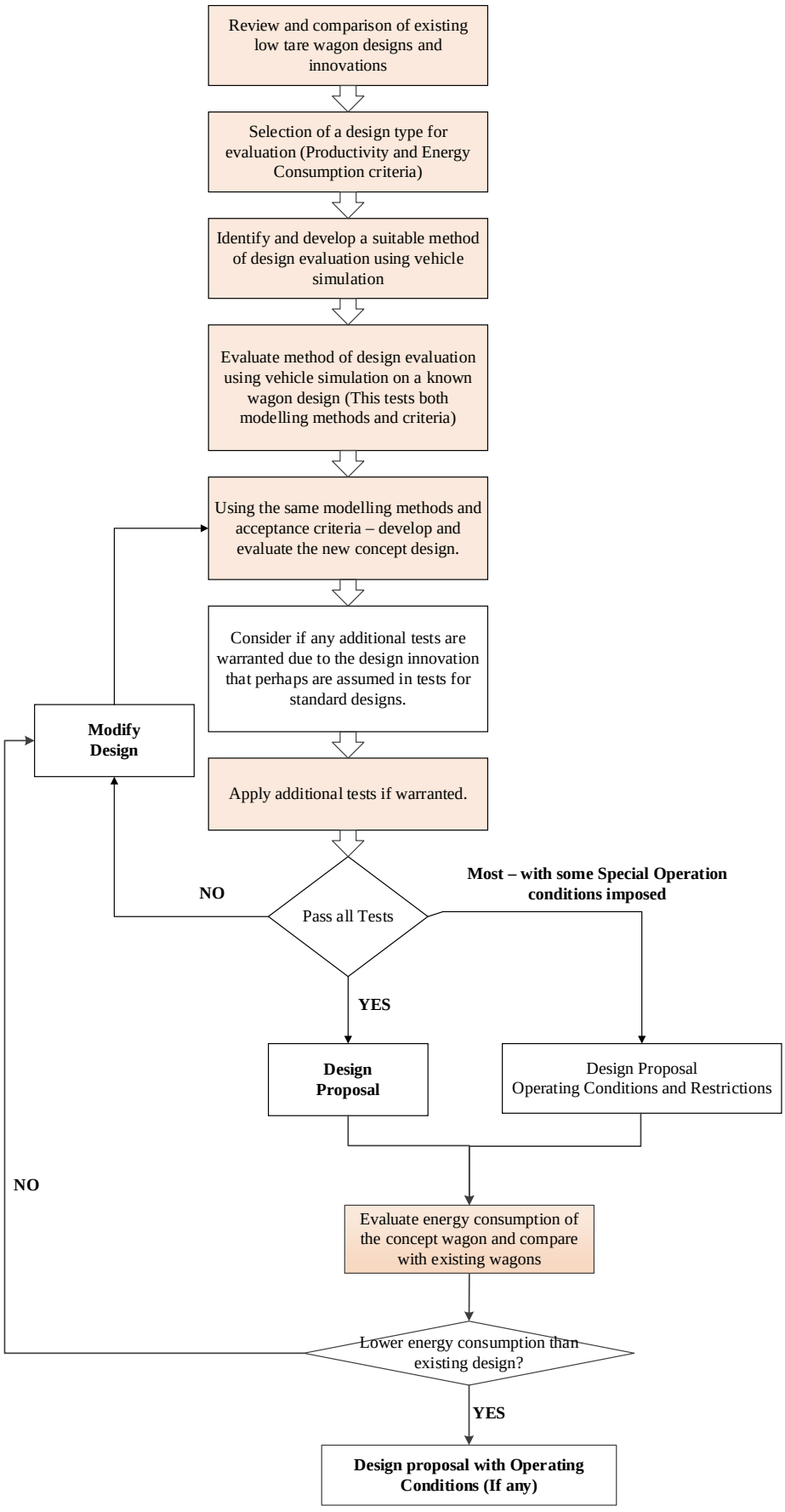

Figure 3-1: Methodology of the thesis

Before testing and optimising wagon parameters, it is necessary to conduct a preliminary analysis to identify the starting design parameters such as length, tare, and payload of the wagon that may produce a wagon concept with the desired performance on payload productivity and energy consumption. This analysis must also examine simple design parameters such as chassis bending deflection and bogie centre distance (BCD). The preliminary analysis has been performed in Chapter 4. The preliminary analysis is important to reduce simulation effort at the early stage by selecting tentative design parameters. It is also required that the design must push boundaries to ensure innovation.

After selecting the preliminary design parameters, it is important to identify and define the method of testing a wagon by 'vehicle dynamics simulation'. In the Australian context, the standard AS7509 [61] developed by the Rail Industry Safety and Standards Board (RISSB) uses some parts of standards of other organisations such as AAR [85] and RSSB [86, 87] while developing test conditions for the Australian conditions. The AS7509 standard also acknowledges and explicitly allows the use of simulations. It is also a performance based standard used successfully in several different safety jurisdictions. Hence, in this study, the AS7509 standard has been used as a starting point for a general set of simulation tests.

Another thing to note is that, because AS7509 is a performance standard, defect sizes are based on certain levels of allowable defects as specified by any applicable network standard. The level generally specified as a starting point for roadworthiness tests is the "urgent class 2" defect which requires inspection within 24 hours and repair within 7 days. Clearly, wagons must be able to accommodate defects of this type with some safety margin. The margins required are specified in the AS7509 standard. In Australia on the standard gauge network, this is usually the ARTC standard [55] and the common name for the "urgent class 2" defect is the "P1" response or limit. So, further to AS7509, the ARTC Standard is assumed for the specification of defect magnitudes. As a starting point, the proposed design will be tested for Australian track conditions and needs to pass all the relevant roadworthiness tests mentioned in the AS7509 standard.

The test parameters set out in AS7509 are based on typical existing rollingstock. The introduction of new rollingstock with radically different parameters may require additional tests. As an example, a shorter wagon may result in a higher wheel unloading ratio compared to that of a longer wagon on the allowable track defects as found in a derailment study [88]. Furthermore, suspension resonance on a cyclic track defect may induce an unacceptable response on a smaller track defect magnitude which may not be addressed or detected by the track inspection procedure as the smaller amplitude is less than the P1 level [89]. The resonance condition depends on both the wavelength of the track defects and the vehicle parameters such as the distance between bogies and speed. So, some additional tests are needed when the proposed length and mass of the rollingstock would be significantly different to existing rollingstock.

It was hypothesised that tests further to AS7509 should be considered for the introduction of a radical design. These are developed in Chapter 5 and, combined with the selected tests from AS7509, the result is designated as the Vehicle Acceptance Procedure by Simulation (VAPS). The simulation tests were performed using the Gensys simulation software package which is one of the simulation tools accepted in the AS7509 standard. The Gensys simulation software has been evolving since 1971 and has gone through a series of developments and validations [90].

The debugging of the wagon dynamic model was performed using the Wagon Model Acceptance Procedure (WMAP) method presented in [91]. The VAPS method was firstly evaluated on an existing wagon design to validate the approach and provide a datum from an accepted design (Chapter 6). Having tested the VAPS approach on an existing wagon, it was then applied to new wagon concepts.

The concept development was performed starting with a tutorial model of a two-axle wagon available in the GENSYS simulation software [92] and systematically applying the tests of the VAPS while trialling the design parameters (Bogie Centre Distance, Overhang) in Chapter 7. Initially, two different suspensions were developed for the empty and the loaded conditions of the concept wagon. It was reasoned that studying simplified suspensions of the empty and loaded suspension systems separately would help to achieve the design parameters in a shorter time. The simplified parameters of these suspensions were then combined to form one suspension element for the concept wagon. The modelling approach of the concept suspension was validated using input data from Royal Institute of Technology, Sweden (KTH) [93] and Technical University of Denmark (DTU) [94], and the model validation is included in Chapter 9. The final suspension element was then evaluated under practical considerations (Chapter 10). The new suspension concept design was modified several times to give a degree of optimisation. The process of evaluating the performance of the concept suspension has been included in Chapter 10. Finally, it is necessary to check if the final suspension concept still performs satisfactorily in a practical design. The final concept wagon has been simulated in Chapter 10. A comparison of energy consumption on different rollingstock was also performed (Chapter 11).

3.4 Summary

A research gap and a methodology for the thesis has been established. A long, low tare, high axle load wagon which could make intermodal transportation competitive with other modes is not currently researched. It is speculated and proposed that further dynamic analysis and tests (beyond those in the Australian Standards) will be needed to give a more robust evaluation of the new design. In improving the design of the long, low tare wagon, a simulation based strategy involving modifications of some of the elements of rollingstock is proposed to achieve a degree of optimisation in the design of a suitable single axle suspension.

Chapter 4
Preliminary Analysis

4.1 Introduction

In this chapter, a preliminary analysis of design and objective parameters of various wagons has been performed as part of the methodology. A comparative analysis of a selection of rollingstock vehicle systems has been performed to identify suitable initial design parameters (length, mass, suspension) for the concept wagon.

4.2 Selection of the Design Type

Selection of the design type was performed based on the potential market, and on the improvement in the two objective parameters of productivity and energy consumption. The recent trends of increasing fuel cost, growing road network congestion, changes to regulation of heavy road vehicle driver hours and community concerns around greenhouse emissions, safety, and amenity have created a competitive position for the utilisation of rail compared to road freight [95]. However, intermodal rail transportation has to have the necessary tools to compete with road freight.

The intermodal rail operation faces challenges of efficient loading to minimise any mismatch of wagon length with container (already well optimised) length to avoid leaving empty spaces on a train. Thus, the length of intermodal freight wagons plays an important role in defining the maximum load carrying capability of a train. The length parameters would need to be multiples of 20' to be able to provide flexibility in the loading of standard containers (20', 40', 60' etc.). Having a 65' deck length would allow further flexibility of carrying a very long 65' container. The maximum payload capacity on a 65' loading length would be up to 72t considering 3x20' containers.

Having less axles, a two-axle wagon has a higher axle load than that of a bogied wagon which usually has four axles per wagon. Traditionally, two-axle wagons are short or carry a lighter payload in order to meet the axle load limits. Having short wagons would require more wagons having two axles compared to using bogied wagons in order to carry a similar length of load or number of containers. So, a possible improvement in the existing low tare two-axle wagon would be the idea of a longer two-axle configuration, assuming that the resulting higher axle loads are permitted on the network. A quantitative indication of achieving high payload on low tare is often used to compare the performance of rollingstock using the “weight factor” (the payload/tare ratio) [5].

The positioning of multiple containers would require a wagon deck length multiple of 20' to accommodate the most common types of containers. Choice of various length parameters also needs to consider constraints on a track network. The ARTC track geometry standard dictates a maximum limit on bogie centre distance of 13m [55]. A limit on the minimum axle centre distance is also sometimes applied due to specific conditions of particular routes such as the presence of bridges designed to standards only suitable for low tal and hence the wagon might require a higher number of axles [96, 97]. However, in this thesis, it was assumed that the concept wagon would be suitable for a route with upgraded bridges, and low tal limits would not be applied.

The operational flexibility of a rail fleet lies in the flexibility of changing the rollingstock for different types of freight. Some optimised container wagon designs (two-pack, five-pack configurations) using shared bogies often lack the flexibility of shuffling the wagons when required as the shared bogie wagons are semi-permanently coupled. The shared bogie wagons, if not properly loaded, could end up leaving empty space in the train consist. So, this thesis is restricted to the study of an independent wagon-chassis design to ensure maximum flexibility in usage.

Based on the discussion in this section, the following objective parameters and constraints of the proposed design have been set as a guide to selecting a suitable design of wagon:

- Objective parameters:
  - A low tare wagon giving high payload/tare ratio
  - Energy consumption per payload per distance would be lower than the closest competitor in terms of capacity and application
- Constraints:
  - A long wagon capable of carrying at least a 65' container
  - A maximum payload of 72 tonnes considering carrying three 20' containers
  - Independent/ flexible fleet requirement (single independent chassis)
  - Maximum axleload limit of 42 tonnes

4.3 Payload Productivity

Payload productivity can be seen as a measure of efficiency in carrying a payload. 35 wagon configurations comprising 29 intermodal, 2 heavy haul and 4 concepts wagons (a generated UIC wagon, a generated shared bogie wagon, a VEL wagon and a concept wagon target set out in this section based on payload productivity) have been compared in terms of productivity in intermodal operation (Table 4-1). Four performance parameters (Payload/ Tare, Utilisation of length, Payload per loading length and Tare per wagon length) presented in [5] as part of the DIOMIS project in Europe were considered in this Chapter to evaluate productivity of these wagons in the intermodal application. The top five performing wagons based on the productivity performance parameters were marked as green shaded cells and the bottom five performing wagons were marked in bold italic font in Table 4-1. It is clear that the existing intermodal wagons (Wagons 1-29) provide less payload per tare ratio and payload per loading length compared to those of heavy haul operations (Wagons 30, 31). However, the intermodal wagons provide significantly lower tare per wagon length (example: 680kg/m on wagon 8) compared to the heavy haul options (example: 2308kg/m on wagon 30). The higher payload per loading length on the intermodal wagons can only be possible on bogied wagons (four axles) due to the restricted tal requirement.

A wide variation in length combinations depending on the type of loading (ISO containers, semi-trailers or swap bodies) leads to a recommendation to design the train configuration to best suit the length utilisation on a train.

Generally, 60' (18.288m) wagons provide the best utilisation of space when carrying a mix of 20' and 40' ISO containers [5]. The 60' wagons are usually built on two bogies (4 axles) which have tare weights ranging from 17.4t to 23.4t (wagon types- sgnss, sgns, sgjs) [5, 98].

The Versatile Efficient Longer (VEL) wagon concept study revealed an overall length (length over buffers) requirement for a wagon of 28.7m (suitable to carry 2x 45' containers, Wagon 34 in Table 4-1) to provide the most efficient combination of loading for European transportation [7]. The 28.7m wagon on two bogies would reduce the tare by about 4.5t (weight of a bogie) compared to a similar length (27.6m) wagon such as sggmrss (Wagon 22 in Table 4-1) on three bogies (articulated) that would improve the payload per tare.

Heavy haul operations obviously have a different objective to that of intermodal operations as the former need to carry a homogeneous and often very dense load under the same operational conditions nearly all the time. Thus, the heavy haul wagons are designed for specific load requirements that may require high tare (21, 22.4t on wagons 30, 31 which operate in the Pilbara and Hunter Valley networks of Australia respectively) to provide structural strength to carry a high payload such as 142 and 120t in wagons 30, 31 (Table 4-1). Hence, tare per wagon length was found to be higher for heavy haul operations. However, the overall payload performance parameters would be less when the full trip is considered as heavy haul operations usually carry payload in only one direction and are empty on the return leg.

The payload productivity parameters are further presented in graphical plots (Figure 4-1) to establish a trend to improved productivity parameters. The first obvious indicator is high payload and low tare which is shown in Figure 4-1a. High tare is usually used in the existing wagons to accommodate a higher payload. So, having a very low tare with a high payload, which is an important objective of this thesis, would be a significant modification from the existing rollingstock.

Utilisation of train length depends on the wagon length, loading length, and length of couplers or buffers. The utilisation of length is usually higher on wagons with fixed uniform load such as most heavy haul operations. Intermodal transportation faces the challenge of carrying non-uniform containers along the same train length. The efficiency in utilisation of length on intermodal wagons is therefore largely dependent on the choice of container lengths for a specific train operation. In this study, the intermodal load is standardised to the maximum available container sizes suitable for the loading length. The desired improvement in the utilisation of train length is shown in Figure 4-1b. The couplers or buffers do not carry any load. A reduction of length of buffer would allow more utilisation of train length (Figure 4-1c).

Table 4-1: Payload productivity of various wagons

Wagon ID	Generic name	Length over buffers (mm)	Loading length of a wagon (mm)	Utilisation of train length (%)	Tare (t)	Payload (t)	Payload/ Tare	Payload/ loading length (t/m)	Tare/ length over buffers (kg/m)	Source
		*l+ 2*cpl*	*l*= b+ 2*a	*l/(l+ 2*cpl)*						
1	UIC	13860	12500	90	13.5	26.5	2.0	2.1	974	[4]
2	UIC	16550	14500	***88***	16	24	***1.5***	1.7	967	[4]
3	UIC	16550	15100	91	16	24	***1.5***	***1.6***	967	[4]
4	UIC	16550	14500	***88***	17.5	22.5	***1.3***	***1.6***	1057	[4]
5	UIC	16550	15100	91	17.5	22.5	***1.3***	***1.5***	1057	[4]
6	UIC	16550	14500	***88***	17.5	22.5	***1.3***	***1.6***	1057	[4]
7	UIC	16550	15100	91	17.5	22.5	***1.3***	***1.5***	1057	[4]
8	sgns	13530	11700	***86***	9.2	30.8	3.3	2.6	680	[4]
9	sgns	14040	12800	91	12.5	27.5	2.2	2.1	890	[4]
10	sgns	19640	18400	94	17	63	3.7	3.4	866	[4]
11	sgns	15640	14400	92	17	73	4.3	5.1	***1087***	[4]
12	sgns60	19740	18500	94	20	70	3.5	3.8	1013	[4]
13	Lgns	13860	12620	91	12.3	32.7	2.7	2.6	887	[5]
14	sgkkmss	19130	15890	***83***	18	46	2.6	2.9	941	[5]
15	sgmns	17540	16300	93	18.3	71.5	3.9	4.4	1043	[5]
16	Sdgmns	18340	13720	***75***	21	69	3.3	5.0	***1145***	[5]
17	Sgjs	21000	18400	88	23.4	56.5	2.4	3.1	***1114***	[5]
18	Sgns	19640	18400	94	20	70	3.5	3.8	1018	[5]
19	Sggns	23890	22590	95	22	68	3.1	3.0	921	[5]
20	Sggnss	25940	24700	95	21.5	68.5	3.2	2.8	829	[5]
21	Sggrss	26400	25160	95	26	109	4.2	4.3	985	[5]
22	Sggmrss	29590	27640	93	29.5	106	3.6	3.8	997	[5]
23	Sggmrss	33940	32200	95	32	104	3.3	3.2	943	[5]
24	Sffggmrrss	36440	32240	88	39	89	2.3	2.8	1070	[5]
25	Sdggmrss	33940	30840	91	34.5	108	3.1	3.5	1016	[5]
26	Sdggmrss	33940	32200	95	32.9	102	3.1	3.2	969	[5]
27	Sdggmrss	34030	31522	93	35	100	2.9	3.2	1029	[5]
28	Sdggmrss	34030	31480	93	34	100	2.9	3.2	999	[5]
29	RQTY	20985	19812 (1)	94	18	72	4.0	3.6	858	[6]
30	Pilbara	9100	8200 (2)	90	21	142.4	6.8	17.4	***2308***	
31	Hunter Valley	15840	14936 (2)	94	22.4	120.4	5.4	8.1	***1414***	
32	UIC_gen (3)	15600	12192	***78***	8	37	4.6	3.0	513	
33	Articulated_gen (3)	20800	19812 (1)	95	20	86	4.3	4.3	962	
34	VEL Concept	28700	27432	96	25	106	4.2	3.9	871	[7]
35	Concept wagon	20697	19812 (1)	96	8	72	9.0	3.6	387	

Notes: Green shaded cells are the top 5 performers and the bold italic fonts are the bottom 5 performers for the desired utilisation/productivity parameters among the wagons compared here; all wagons are suitable for intermodal container transportation except wagons 31 and 32, although the loading length of the heavy haul wagons were considered as carrying ISO containers; (1) Assuming a 65' container load, (2) assumed from figures of similar rollingstock, (3) _gen refers to Parameters obtained from simulation models in Gensys or CRE-LTS; l- loading length, cpl- length of coupler, a- overhang length, b- Bogie Centre Distance (BCD) for bogied wagon or Axle Centre Distance (ACD) for two-axle wagon

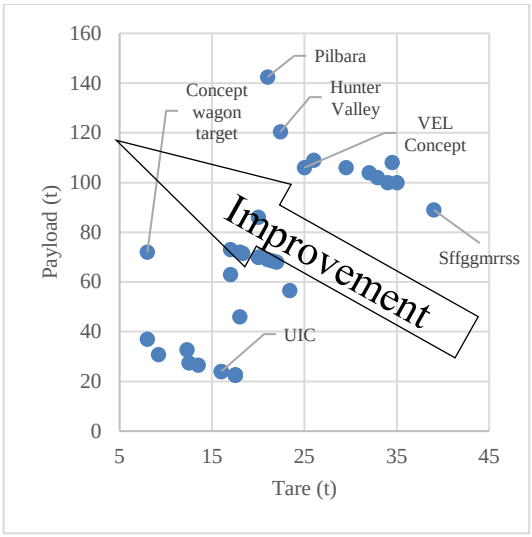

(a) Payload vs Tare

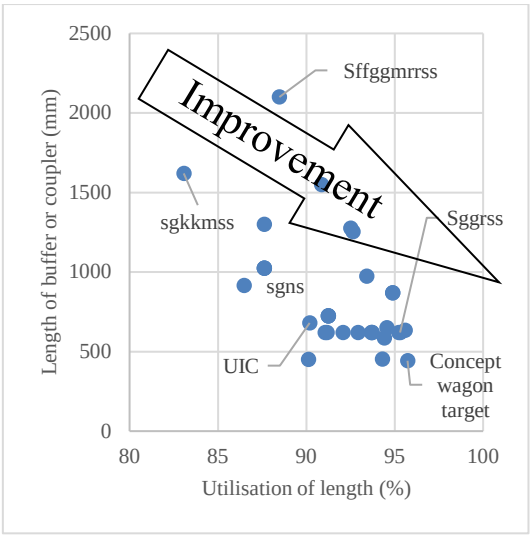

(c) Payload/Tare ratio corresponding to length of buffer

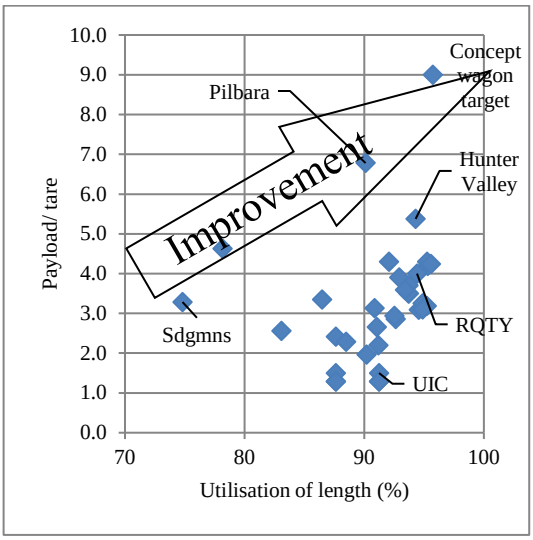

(b) Utilisation of train length corresponding to payload/Tare ratio

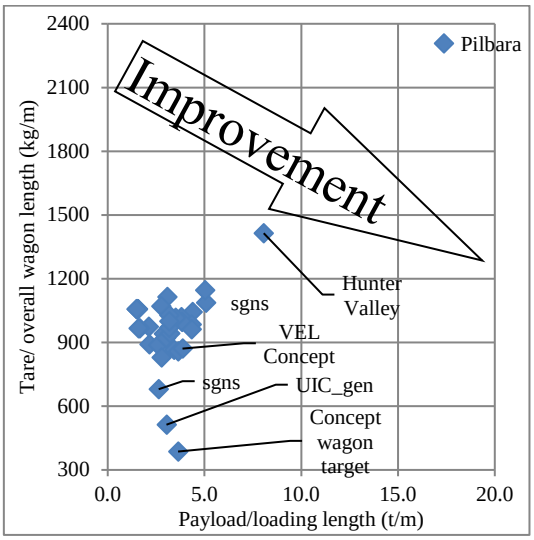

(d) Payload/ loading length corresponding to Tare/overall wagon length

Figure 4-1: Desired improvement parameters (The results are plotted from Table 4-1, only few of the wagons are labelled to show a trend and better readability in this Figure 4-1)

The last graphical plot (Figure 4-1d) is an indicator of relative proportion of mass to the relevant length parameters. The loading length needs to be utilised by the payload efficiently which can be measured as payload per loading length ratio. When moving containers, intermodal transportation faces the issue of length utilisation more than the accommodation of higher payload. So, the payload per loading length in intermodal transportation is less than that of heavy haul operations. The tare load per unit of wagon length needs to be low if the payload per unit length is low.

A concept wagon mass and length target were set as wagon body mass of 6000kg (making an approximate tare of 8000kg assuming a bogieless, two-axle arrangement, axle mass of 1000kg), a payload of 72000kg and length of 19.8m. The assumed mass of 1000kg for each axle was made similar to a conventional two axle wagons having a maximum payload of 37000kg. The mass of axles for the intended higher payload of 72000kg could be higher than 1000kg or an alternative design can be achieved to restrict the axle mass to 1000kg. The detail design of axle

has been left as a future scope of this work. The concept wagon target values provide payload/tare ratio of 9 which is even higher than some of the heavy haul operations (examples wagons 30, 31). The length parameters were chosen to provide better utilisation of length for standard ISO containers (20', 40').

4.4 Bending Stress and Deflection Considerations

A preliminary calculation was carried out to investigate buildability of a low mass chassis. For simplification, the load on the wagon deck is assumed uniformly distributed over the entire wagon deck including the overhangs (Figure 4-2a). The fatigue loading (due to aerodynamic load, traction, braking, track defects) consideration is not performed in this thesis as detail design on strength and material selection has been left as a future scope. The support points (R1 and R2) representing the two bogie connections were assumed as fixed type connections (Figure 4-2a, Figure 4-2b). The rigid connections were further moved to the end of the wagon chassis (Figure 4-2c) for simplified analysis in this section. The simplified approximation of the rigid connections at the end of the wagon chassis will produce higher bending moments compared to the positions of supports at the BCD as the '*l*' parameter will be higher in Equations 4-2, 4-3 [99]. The maximum bending moment (Figure 4-2d) obtained from Equations 4-2 and 4-3 was used to calculate the maximum bending stress (Equation 4-4). The bending deflection at any point along the chassis from one fixed end can be determined from Equation 4-5 [99]. The maximum bending deflection occurs at the mid-point of the chassis ($x= l/2$) and was evaluated using Equation 4-6.

$$\boldsymbol{M_x = \frac{w}{12}\left(6lx - l^2 - 6x^2\right)} \quad \textbf{4-1}$$

$$\boldsymbol{M_1 = M_2 = -\frac{wl^2}{12}} \quad \textbf{4-2}$$

$$\boldsymbol{M_3 = \frac{wl^2}{24}} \quad \textbf{4-3}$$

$$\boldsymbol{\sigma_{bmax} = \frac{M_{max}C}{I}} \quad \textbf{4-4}$$

$$\boldsymbol{\delta_x = \frac{wx^2}{24EI}(l - x)^2} \quad \textbf{4-5}$$

$$\boldsymbol{\delta_{max} = \frac{wl^4}{384EI}} \quad \textbf{4-6}$$

where R_1 and R_2 are the reactions provided by the two bogies (N); M_1, M_2 and M_3 are the three bending moments at various positions of the wagon deck (Nm); w is the load per unit length (N/m), M_{max} is the maximum bending moment among M_1, M_2, and M_3; I is the second moment of area (m^4), C is the distance from the neutral axis where the stress is maximum (m), σ_{bmax} is the maximum bending stress (N/m^2), δ_{max} is the maximum bending deflection (m), E is the modulus of elasticity (N/m^2, 207Gpa for steel).

The evaluation of moment of inertia in Equation 4-4 requires sectional properties of the chassis. In vehicle dynamics simulation, the chassis is usually considered as simplified rectangular beam elements presenting the empty and loaded outlines with assumed uniform load (Figure 4-3a). In this thesis, a realistic chassis having one rectangular and two triangular beams underneath the rectangular wagon floor or deck was also considered (Figure 4-3b) using an approximation of a drawing of a typical RQTY wagon.

A simplified chassis approximation having rectangular outlines of 19.812m X 3m X 0.6m and assuming an 8mm wall thickness (tw, Figure 4-4) would give a chassis mass of 8862kg (using a conventional steel AISI 1030 density of 7800kg/m^3) which is still higher than the target empty wagon body mass of 6000kg obtained in Section 4.3 (payload productivity). It is possible to change the design of deck elements and/ or select a high strength material to achieve such a mass. In this study, the material selection and detail design procedure of the chassis is not included. For the current study, it was decided to check if the bending property of the low mass chassis is acceptable.

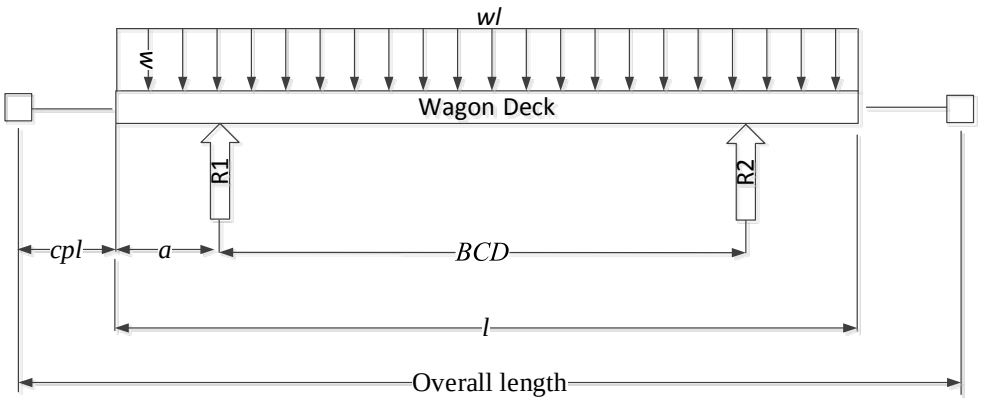

(a) Load distribution on a wagon chassis assuming uniform load over the length

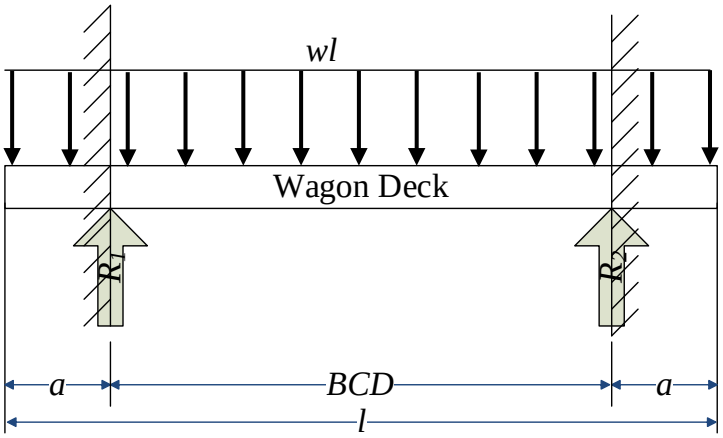

(b) Rigid connection at the BCD

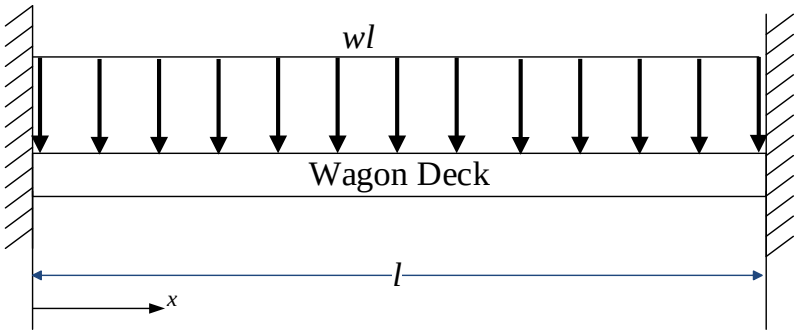

(c) Assumed rigid connection for calculation of bending moment and deflection in this section

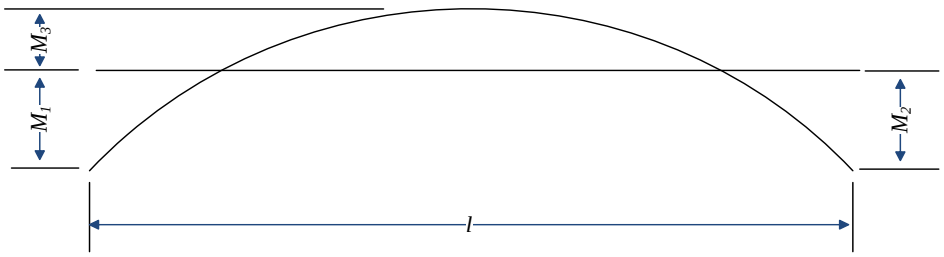

(d) Bending moment diagram for both end fixed structure

Figure 4-2: Load distribution on a wagon chassis

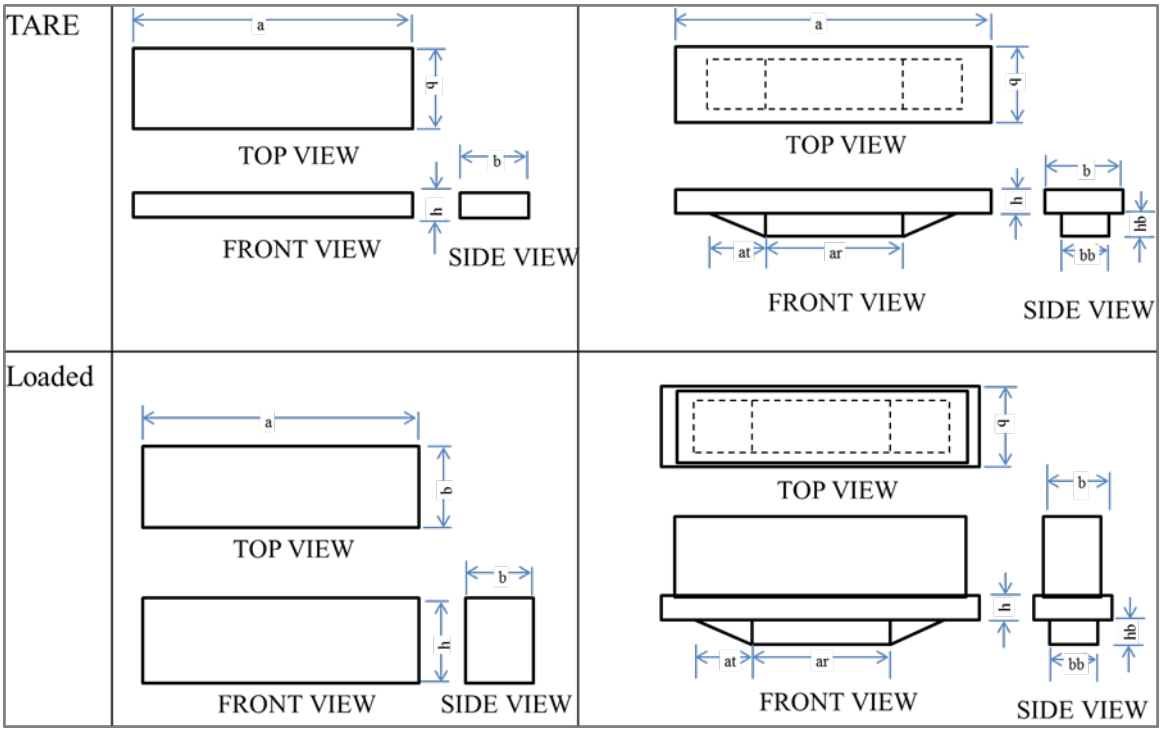

(a) Simplified Chassis (b) Realistic Chassis

Figure 4-3: Schematic diagram of the chassis configurations (a- length, b- width, h- height, at- length of the triangular beam, ar- length of the rectangular beam, bb- width of the beams, hb- height of the beams)

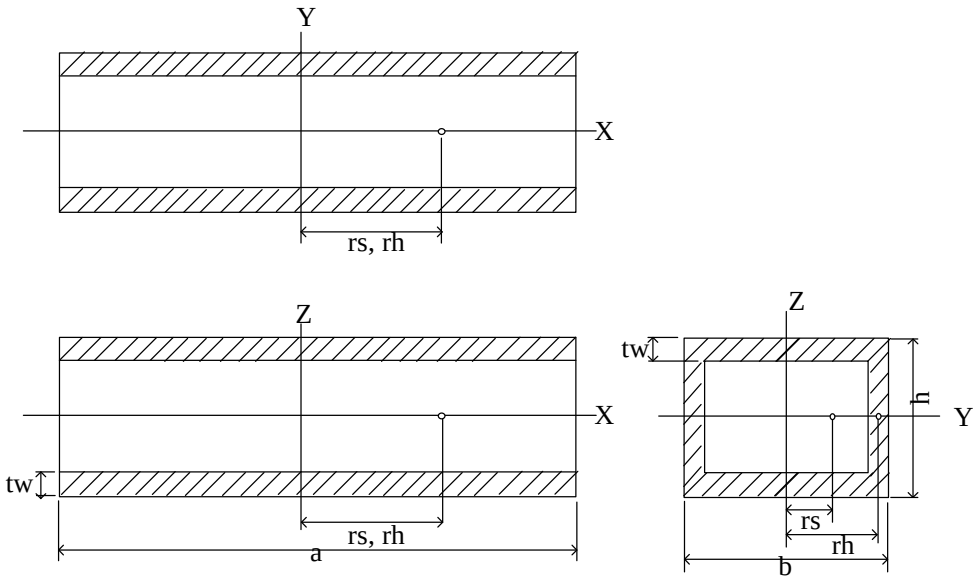

Figure 4-4: Hollow box approximation of a beam element

The target mass of the overall empty chassis (6000kg) as obtained in section 4.3 was distributed among the 3 beams and 1 deck element of the realistic chassis (Figure 4-3b). At the initial concept development stages (Chapters 7-8) mass components were chosen as 2206, 794, 794 and 2206kg on the beam 1, beam 2a, beam 2b and wagon deck elements of the realistic chassis.

The second moment of area on the simplified and realistic chassis using the hollow box approximations were 0.0044 and 0.00923 m^4 respectively which indicates that the maximum bending stress on the realistic

approximation would be lower and hence the factor of safety on the realistic chassis would be higher compared to those on the simplified chassis approximation.

The maximum bending stress on the simplified and realistic chassis arrangements for the loading length of 19.812m was evaluated as 85MPa and 75MPa respectively which would give a factor of safety of 4.37 and 4.95 respectively (considering conventional steel material AISI 1030, yield strength of 370MPa).

The maximum bending deflection on the realistic chassis (8mm) was reduced to about half of that of the simplified chassis (16.7mm) on the 19.812m loading length using Equation 4-6. The realistic chassis on the overload conditions showed that the maximum bending deflection on 90% overload is 15mm (Table 4-2) which is considered acceptable based on the typical limits on bending deflection (55- 79mm on the 19.812m beam, using *l*/250 criteria [100-102]).

Table 4-2: Maximum bending stress and deflections on realistic chassis (Loading length 19.812m, maximum static load 78000kg, material AISI 1030, yield strength 370MPa)

Loaded mass (kg)	Overload (%)	Maximum Bending Stress (MPa)	Maximum Bending Deflection (mm)	Factor of safety
148200	90	143	15.4	2.59
140400	80	135	14.6	2.74
132600	70	128	13.8	2.90
124800	60	120	13.0	3.08

From the analysis in this section, it can be seen that it is possible to build a 6000kg chassis on a 19.812m long beam within acceptable bending parameters. The selected mass distribution of 6000kg on a simplified chassis has been used in the wagon concept development stages in Chapters 7 - 9. The realistic chassis approximation is used in Chapter 10.

4.5 Mass moment of inertia of chassis

A representative solid body approximation is generally used to determine mass moments of inertia in vehicle dynamics simulations. The mass moments of inertia of a rectangular section and a triangular wedge type section can be calculated using Equations 4-7 to 4-12 [103] based on solid body approximation.

$$J_{f_R} = \frac{1}{12}m(b^2 + h^2) \quad \textbf{4-7}$$

$$J_{k_R} = \frac{1}{12}m(a^2 + h^2) \quad \textbf{4-8}$$

$$J_{p_R} = \frac{1}{12}m(a^2 + b^2) \quad \textbf{4-9}$$

$$J_{f_T} = \frac{1}{36}m(3b^2 + 2h^2) \quad \textbf{4-10}$$

$$J_{k_T} = \frac{1}{18}m(a^2 + h^2) \quad \textbf{4-11}$$

$$J_{p_T} = \frac{1}{36}m(2a^2 + 3b^2) \quad \textbf{4-12}$$

where m is the mass of the body (kg), a is the length of the body (m), b is the width of the body (m), h is the height of the body (m), J_{fR}, J_{kR}, J_{pR} are the mass moments of inertia for the rectangular body along longitudinal (roll),

lateral (pitch) and vertical (yaw) directions (kgm^2), $J_{fT,}$ $J_{kT,}$ J_{pT} are the mass moments of inertia for the triangular body in roll, pitch and yaw directions (kgm^2).

The simplified chassis (Figure 4-3a) overestimates the moments of inertia in the empty condition in the roll, pitch and yaw directions by about 79, 136 and 136% (Table 4-3) respectively when compared to that of the realistic chassis (Figure 4-3b). The overestimation in the loaded condition is less obvious as it is dominated by the mass component of the loaded container and hence is reduced to 42, 30 and 31% in the roll, pitch and yaw directions respectively.

When loaded, the realistic chassis with the assumed mass elements gave a higher centre of gravity than that of the simplified chassis (2.28m compared to 2.0m on the simplified chassis, Table 4-3). The higher centre of gravity may result in higher roll displacements for the realistic chassis in the curved section or on any track defect that may produce roll movement. In addition to that, the lower roll inertia of the realistic chassis also encourages higher roll movement when any lateral force is applied.

Table 4-3: Mass moment of inertia of simplified and realistic chassis configurations for concept wagon using solid box distribution

Chassis	Elements	Length	Width	Height	Mass	Mass moment of inertia (% increase from the realistic chassis)			Centre of gravity from top of rail
		a	b	h		J_f	J_k	J_p	
		m	m	m	kg	kgm^2	kgm^2	kgm^2	m
Simplified Chassis	Empty wagon	19.812	3	0.6	6,000	4680 (79%)	196438 (136%)	200758 (136%)	0.80
	Loaded wagon	19.812	3	3.038	78,000	118491 (42%)	2611341 (31%)	2609850 (31%)	2.0
Realistic Chassis	Rectangular Beam	7.4	1.4	0.66	2206	440	10147	10427	0.67
	Triangular Beam 1	2.37	1.4	0.66	794	149	267	377	0.78
	Triangular Beam 2	2.37	1.4	0.66	794	149	267	377	0.78
	Wagon Deck	19.812	3	0.2	2206	1662	72165	73812	1.10
	Empty Container	17.655	2.35	2.4	6450	6064	170634	170507	1.20
	Loaded Container	17.655	2.35	2.4	72000	67695	1904754	1903329	2.40
	Empty wagon	19.812	3	0.86	6000	2616	83026	84957	0.86
	Loaded wagon	19.812, 17.655	3, 2.35	3.26	78000	83495	2000999	1988323	2.28

The mass moment of inertia calculated using the solid body approximation in the simulation process has been further evaluated on a realistic hollow beam approximation for the chassis and container elements. Mass moment of inertia is higher for a mass placed further from the centre of rotation ($I = Mr^2$, I is the mass moment of inertia, kgm^2, M is the equivalent mass placed at distance r from the axis of rotation). In a hollow beam approximation (Figure 4-4), the distance (rh) of the mass considering a hollow box distribution from the pivot axis X is higher than the distance (rs) of the mass considering a solid box distribution (Figure 4-4). The difference between the distances 'rs' and 'rh' is high along the X axis or roll direction, but there is no difference between the rs and rh in the yaw and pitch directions due to the uniform distribution of mass about the Y (pitch) and Z (yaw) axes. Hence, the solid box approximation showed less mass moment of inertia about the x axis compared to the realistic empty

box distribution of a hollow box (example: roll moments of inertia for solid box compared to hollow box approximation, S/H for the beam1, beam 2a, beam 2b and deck being 0.57, 0.59, 0.59 and 0.89 respectively, Table 4-4). The pitch and yaw moments of inertia of different elements of the solid box approximation were found to be lower or similar to that of the realistic chassis (S/H- 0.82 ~ 1.00, Table 4-4).

Table 4-4: Inertia parameters of the realistic chassis using hollow box, solid box, and dynamic approximations

Parameters		Length	Width	Height	Mass	Mass moment of inertia			Cg from top of rail
		a	b	h		*Jf*	*Jk*	*Jp*	
		m	m	m	kg	kgm^2	kgm^2	kgm^2	m
Beam1, tw= 8mm	Solid Beam 1	7.4	1.4	0.66	53333	10647	245314	252089	0.67
	Hollow Beam 1	7.4	1.384	0.64	51446	9990	236541	242975	0.68
	Empty box (solid - hollow)				1888	657	8772	9113	0.67
	Solid box distribution, sim	7.4	1.4	0.66	1888	377	8683	8922	0.67
	S/H					0.57	0.99	0.98	
Beam 2a, tw= 8mm	Solid Beam 2a	2.37	1.4	0.66	8541	1602	2872	4060	0.78
	Hollow Beam 2a	2.37	1.384	0.644	8238	1505	2761	3886	0.79
	Empty box (solid - hollow)				302	97	111	174	0.78
	Solid box distribution, sim	2.37	1.4	0.66	302	57	102	144	0.78
	S/H					0.59	0.91	0.82	
Beam 2b, tw= 8mm	Solid Beam 2b	2.37	1.4	0.66	8541	1602	2872	4060	0.78
	Hollow Beam 2b	2.37	1.384	0.644	8238	1505	2761	3886	0.79
	Empty box (solid - hollow)				302	97	111	174	0.78
	Solid box distribution, sim	2.37	1.4	0.66	302	57	102	144	0.78
	S/H					0.59	0.91	0.82	
Deck, tw= 8mm	Solid deck	19.812	3	0.2	92720	69849	3033150	3102381	1.10
	Hollow deck, 8mm thick	19.812	2.984	0.184	84848	63198	2775571	2838291	1.10
	Empty box (solid - hollow)				7873	6651	257578	264090	1.10
	Solid box distribution, sim	19.812	3	0.2	7873	5931	257535	263413	1.10
	S/H					0.89	1.00	1.00	
	Loaded container and Empty_Solid box, Deck 4mm	19.812, 17.655	3, 2.35	3.26	78438	83943	2055516	2044576	2.2805
	S/H				1	0.99	1.00	1.00	

Note: tw is the wall thickness (m), cg is the centre of gravity position, S is the solid box approximation, H is the hollow box approximation, C is the chosen mass distribution, considering coupling height h_c of 1.1m from top of rail, cg from top of rail= h_c-h_d/2, h_c-h_d-h_{b1}/2, h_c- h_d-h_{b2}/3

4.6 Preliminary Train Simulation to Select a Design Type Based on Energy Consumption

Preliminary train simulations have been carried out to compare the energy consumption of some top-performing wagons in Table 4-1 (UIC_gen, articulated_gen, Pilbara, Hunter Valley). In addition, the payload on the UIC_gen wagon was increased to 72t (termed as UIC_link_80t) to check a possible advantage on the energy consumption parameter by the increase of payload.

In the train simulations, the trains were configured having three head-end locomotives and 100 wagons. All trains were operated using the same throttle settings to ensure the same driving strategy. The trip distance varied between 33.1 and 34.7 km among the trains due to the inertia effect of the trains. The heaviest wagon in the loaded condition (Pilbara) was found to provide the least energy consumption per payload per distance (0.018 kWhr/t/km, Table 4-5). The lowest tare wagon of the four considered wagons, the UIC_gen (two-axle UIC-link) wagon, was found to have the highest amount of energy consumption per payload per distance (0.029kWhr/t/km) among the wagons considered in this section. This two-axle UIC-link wagon at its typical operational limit of 22.5tal could only carry a 37t payload which is low compared to other wagons and makes the energy consumption per payload high.

Table 4-5: Preliminary result of normalised energy consumption of some wagons by train simulation

Wagon type	Tare	Payload	Gross	Tonne axle load	Payload/ Tare	Energy consumption per payload per distance
	tonne	tonne	tonne	tonne		kWhrs/tonne/km
UIC_gen	8	37	45	22.5	4.63	0.0290
Articulated_gen	20	86	106	26.5	4.30	0.0201
Pilbara	21	121.4	142.4	35.6	5.78	0.0183
Hunter Valley	22.4	98	120.4	30.1	4.38	0.0190
UIC-link_80t	8	72	80	40	9	0.0191

Note: _gen refers to generated value from the in-built simulation model data in Gensys or CRELTS

The UIC-link_80t wagon provided a similar energy consumption per payload per distance (0.019kWhr/t/km) compared to those of existing heavy haul wagons (Hunter Valley and Pilbara), and better than the UIC_gen and articulated (shared bogie) wagons (Table 4-5). So, having a higher payload on a two-axle wagon would allow lower energy consumption per payload per distance than that on the existing two-axle wagon (0.029kWhr/t/km). A further analysis of energy consumption and productivity parameters has been performed in Chapter 11.

4.7 Summary

A preliminary analysis has been performed to identify initial parameters of the desired concept wagon to achieve the objective parameters set out in this Chapter. A bogieless, 19.812m (65') long wagon with a 72t payload capacity and having a low tare of about 8t has been selected as the starting parameters for the concept design evaluation. The constraints are identified as a maximum 42 tonne axle load and further operational restrictions that might evolve during further testing.

Chapter 5
Vehicle Acceptance Procedure by Simulation (VAPS) development

5.1 Introduction

The conventional railway vehicle dynamics standards have historically been primarily aimed at physical tests. As a consequence, tests have evolved that are practical and have wide applicability as the track defects and geometry changes have to be physically put on track to enable the tests. Recently, some roadworthiness standards are allowing vehicle simulations as alternatives to some physical tests. A review on existing vehicle acceptance procedures showed variations in measuring methods and parameters among different countries [104]. Some of the standards on vehicle acceptance procedures recommend using statistically significant assessment of data for practical tests such as in [87, 105] or limit values from physical tests or simulation tests [61]. Actual track data can be used in simulations to obtain comparable statistical results of those prescribed in the European standards such as [86, 87] , and examples of such simulations can be found in [106]. A method has been developed to determine validation limits of the simulation parameters within some standard deviation limits using field track data as proposed in [107]. One consequence of allowing simulation as a method of testing is that more tests can now be specified which opens the opportunity to improve the robustness of roadworthiness tests by testing more conditions. The other important fact about the standards is that they evolve in the context of typical rollingstock designs. A new radical design may need to be evaluated for different conditions as typical track defect limits for typical rollingstock designs may not be adequate for a new design with very different length and suspension parameters. In this chapter, a vehicle acceptance procedure by simulation (VAPS) has been established for use in this thesis.

5.2 Vehicle Acceptance Procedure by Simulation (VAPS)

In the context of developing a process of evaluation of a freight wagon design by VAPS, some of the tests mentioned in the AS7509 standard can be excluded. Four of the nine tests included in the AS7509 standard are excluded in the VAPS method as shown in Table 5-1. These tests, however, would be completed at a later design stage and are not included in this thesis. As the model of the wagon is based on known physical parameters and clearances (Sections 5, 10 of AS 7509), static tests pertaining to twist and transitions (Section 6 of AS 7509) will be covered as part of the later detailed design. The base ride acceleration test (Section 4 of AS 7509) is not included as ride comfort is not considered a priority for typical freight wagons excluding sensitive freights. The wind loading test (Sections 11 of AS 7509) is not performed at this stage realising that lateral wind load on a very low tare weight will induce a higher rollover tendency compared to heavier conventional wagons. The wind load consideration is left as a separate problem. It is reasoned that wind issues may have solutions in operational control or ballasting of empty containers.

The measurement of critical speed is not included in the AS7509 standard. Instead the standard requires that a wagon does not hunt at operating speeds. However, for a new design, the measurement of critical speed is

necessary as it would be an initial indicator of the performance of the chosen wagon. So, measurement of critical speed is included in the VAPS method.

Thus, a total of 5 tests (measuring critical speed, hunting test at 110% of the maximum service speed, curve negotiation, negotiation of cyclic track irregularities and negotiation of isolated track irregularities) have been adopted for the VAPS method (Table 5-2).

Table 5-1: Wagon dynamics tests in the VAPS

Section of AS7509	Tests as per AS 7509	VAPS	Comment
3	Hunting	√	
4	Base ride acceleration	X	Excluded for the freight wagon design as this requirement is not a safety-related issue, ride comfort is more important for passenger rollingstock
5	Horizontal and vertical curve negotiation	X	Static test, Calculation by using a formula to determine if the vehicle has adequate clearances to negotiate the tightest horizontal and vertical curves
6	Transition curve negotiation	X	Calculated as Static design parameters, such as static twist test, bogie rotational resistance
7	Rollover	√	Curve negotiation at maximum cant deficient speed limit
8	Negotiation of isolated track defects	√	
9	Negotiation of cyclic track defects	√	Modification of track defects
10	Longitudinal forces in curves	X	Static calculation based on length of couplers, track radius
11	Wind loading	X	Implications of a lightweight wagon to be evaluated in terms of energy benefits and operation restrictions at a later stage

Note: √- included, X- not included

Table 5-2: Tests adopted in the VAPS method

Test number in VAPS	Tests	Comment
1	Critical speed test	Measuring nonlinear critical speed by simulation
2	Curve negotiation test	Equivalent to rollover test in the AS7509 standard
3	Hunting test	Following AS7509 standard, measure hunting proneness at a design speed
4	Negotiation of cyclic track irregularities	
5	Negotiation of isolated track irregularities	

Before starting the tests by simulation, it is necessary to build and debug a multibody model of the wagon. A method to debug a wagon multibody model has been developed recently and is known as Wagon Model Acceptance Procedure (WMAP) method [91]. As per the WMAP method, the developed multi-body system of the wagon needs to go through stage1 or model check and debugging test, and stage2 or dynamic test of the vehicle by simulation. For stage1 of the WMAP (or model checking), rules are taken mostly from the manuals and technical documents on GENSYS [108] (Table 5-3). The limit values and test conditions for the dynamic analysis of the vehicle model (stage2) are mostly taken from the Australian standards AS7509.2 and AS 7508.2 [61, 109]. Some of the debugging methods (visual model check, numerical instability, and critical speed test) are included in this thesis as part of investigations in different sections. However, the detailed model debugging tests are not included in detail in this thesis for brevity. Some examples of model debugging can be found in [58, 91, 110]. The VAPS method developed in this thesis includes all the dynamic tests of stage 2 of WMAP and some additional tests.

The five selected tests for the VAPS method have been proposed in a five-step procedure as shown in Figure 5-1. The first step of the VAPS is the critical speed test where the critical speed of a wagon is determined. The second step deals with determining the curve negotiation ability of a wagon by using different speed conditions and a selected minimum track radius for a network. The third step is a further check of the hunting nature of a wagon at a design speed and on a typical track with superimposed irregularities. The fourth step deals with the wagon's ability to negotiate cyclic track defects. The fifth step is the test for the negotiation of isolated track defects. Steps 4 and 5 include additional tests based on track defect size corresponding to the vehicle geometry as developed in Section 5.3 of this thesis. Each step provides either the pass status or quantified operational parameters such as critical hunting speed, minimum track radius at the desired cant deficiency, maximum allowable service speed, permitted cyclic and isolated track defects. The simulation techniques of the tests in the VAPS method are included in Chapter 6.

Table 5-3: Brief description of stage 1 tests of WMAP [91]

Test	Description	Track conditions
1. Automatic syntax error checking	Wagon model code is checked using an automatic syntax checking program such as RUNF_INFO (GENSYS) [108, 111]	1km ideal tangent
2. Visual model check	Create a 3D plot of the wagon model to observe any geometry errors (not observable by syntax checking programs) [108]	
3. Quasistatic analyses: a) Vertical car-body deflection b) Lateral car-body deflection	Observe effects on suspension components, bogie movements, and wheel loads when applying a) downward and b) rightward displacements on the car body [108]	
4. Modal (eigenvalue) analysis	Calculate eigenvalues at zero speed for the wagon model. Errors include negative damping and high absolute eigenvalues (~5000 rad/s) [108, 112]	
5. Time-stepping analysis – numerical instabilities	Run the wagon model at high speed and check for unexpected motions. Check effects of altering time-step on instabilities [108]	
6. Critical speed	Apply an initial car-body disturbance and decelerate the empty wagon from a high speed to determine when hunting stops [108]	3km ideal tangent

For the purposes of this thesis, the VAPS method will be used in two ways. Firstly, any existing wagon or a concept can be tested following the solid line flow path in Figure 5-1. The VAPS method is applied on an existing wagon in Chapter 6 to provide a datum for comparison.

Secondly, the VAPS method can be used for evolving a concept as shown by the dotted line flow path in Figure 5-1. In the development of a concept method, design parameters such as the Bogie Centre Distance (BCD), overhang length, and mass of a selected wagon design can be modified to meet the objective parameters. Alternative concept wagons can, therefore, be evolved and methodically tested. The iterative process at the early steps of simulations tests includes only the critical speed and curve negotiation to roughly quantify the design parameters. Application of the VAPS method to develop a concept starting with a tutorial model is presented in Chapter 7.

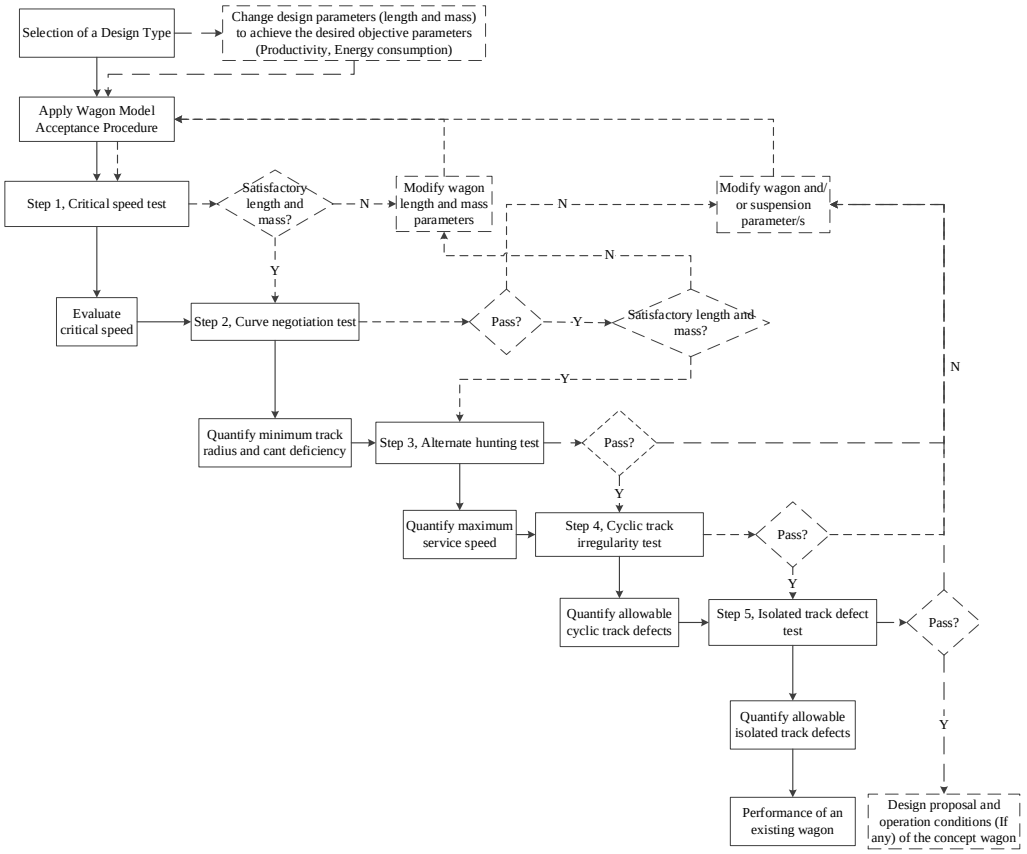

Figure 5-1: Wagon dynamics tests for testing any wagon and developing a concept wagon (Note: Dotted lines refer to the development of a concept wagon phase, solid lines refer to design evaluation of an existing wagon or the developed concept; Y- Yes, N- No)

5.2.1 Acceptable Limits on Derailment Criteria and Accelerations

The most important outputs of any dynamics test are the derailment parameters which are lateral to vertical wheel force ratio on any wheel (wheel L/V ratio), lateral to vertical force ratio on any axle (axle sum L/V ratio) and wheel unloading ratio. The lateral and vertical forces on each wheel are calculated from the wheel-rail contact theory (Kalker's simplified theory) in the simulation package Gensys which is then used to calculate the wheel L/V ratio (Equation 5-1) and axle sum L/V ratio (Equation 5-2). The wheel unloading ratio is calculated using Equation 5-3.

$$\boldsymbol{Wheel}\frac{\boldsymbol{L}}{\boldsymbol{v}} = \frac{\boldsymbol{L_w}}{\boldsymbol{V_w}} \quad \textbf{5-1}$$

$$\boldsymbol{Axle}\frac{\boldsymbol{L}}{\boldsymbol{v}} = \left(\frac{|\boldsymbol{L}|}{\boldsymbol{v}}\right)_{\boldsymbol{wr}} + \left(\frac{|\boldsymbol{L}|}{\boldsymbol{v}}\right)_{\boldsymbol{wl}} \quad \textbf{5-2}$$

$$\boldsymbol{U} = \left(\mathbf{1} - \frac{\boldsymbol{Q_d}}{\boldsymbol{Q_s}}\right) \quad \textbf{5-3}$$

where, L_w is the lateral wheel load (N), V_w is the vertical wheel load (N), $\left(\frac{|L|}{v}\right)_{wr}$ and $\left(\frac{|L|}{v}\right)_{wl}$ are the lateral to vertical wheel force ratio on the right and left rails, $\left(\frac{L}{v}\right)_a$ is the axle sum lateral to vertical wheel force ratio, U is the wheel unloading ratio, Q_d is the dynamic wheel load (N), Q_s is the static wheel load (N).

The derailment parameters in AS7509 are specified as being maintained over a distance (2m) or time (50ms) in different tests to exclude high-frequency transients. At 144km/h, the holding time of 50ms is 2m. So, for less than

this speed, 50ms is a shorter track distance and would include more transients. In this thesis, the 50ms criteria are used as conservative values as freight speed of 144km/h is considered a high value and it is expected that allowable freight speed would be less than 144km/h.

The wheel unloading ratio and wheel L/V ratio have been filtered using a 4th order low-pass Butterworth filter with cut-off frequency of 10Hz. The 10Hz is a reasonable approximation of 50ms (half a wavelength), is still conservative and includes more transients than 50ms. The limit values of wheel L/V ratio, axle sum L/V ratio, wheel unloading ratio, and accelerations are presented in Table 5-4. The acceptable wheel unloading ratio is as high as 0.9 on curved track when aggregated dynamics due to wind on a curved section is considered (section 11 of AS 7509). In this study, the wheel unloading ratio of 0.9 has been chosen as an acceptable criterion. The AS7509 standard recommends using a dry rail condition (wheel rail friction coefficient of 0.4).

Table 5-4: Limit values for acceptable conditions

Parameters	Limit value
L/V wheel ratio	1.0
L/V axle sum ratio	1.5
Wheel unloading ratio	0.9
Maximum lateral acceleration	0.5g
Maximum vertical acceleration	0.8g
Average (over 5s) peak lateral acceleration for hunting test	0.35g

Note: L/V wheel, L/V axle sum, and wheel unloading ratios need to be filtered over 50ms window using a low pass filter with cut-off frequency of 10Hz

5.3 Track Defect Geometry

As AS7509 is a performance-based standard, some of the tests in that standard require complying with the specific track defect limits in the relevant track network standard (such as ARTC standards in the standard gauge network in Australia). The track defect limits mentioned in the track standards are set based on the experience of the network and the running behaviour of the existing rollingstock. As an example, the Australian standard AS 7509 does not specify that the wavelength of the pitch and bounce test should be equal to the BCD because the standards were written with the expectation of mechanical joints (at 40ft or 45ft lengths). It was not envisaged that wagons would face pitch and bounce cyclic irregularity from track defects of the same wavelength as the BCD. However, on continuously welded rail, cyclic track defects are generally generated from repeating wagon responses [113]. The cyclic defects are initiated on a continuously welded rail track when an isolated track defect is present on the track. The isolated track defect could result in a bounce, pitch, sway, yaw or a combination of motions depending on the shape of the isolated track defect and these motions then exert an increased force on the track at repetitive oscillations during the subsequent wagon responses. If similar rollingstock are operated at consistent speeds (such as heavy haul or modern intermodal modes) on the same track, the same force sequence is exerted at the same points which reinforces and grows the same defect shapes. Thus several defects are generated at fairly equal distances forming a cyclic track defect pattern corresponding to the BCD of the wagons running over the track. The cyclic defect occurring at the BCD of a wagon could excite resonance in the suspension and so resonance conditions need to be added with the existing test parameters (speed and the wavelength of track defects).

The track defect shape is considered as sinusoidal for both the cyclic and isolated track defects in the AS 7509 standard. In the case of isolated track defects in the AS7509 standard, the shape could be different from that of a

sine wave as the development of the isolated track defect could be due to different issues, e.g., joints, special track work, fixed structure etc., but a sinusoidal shape is still generally assumed as a reasonable approximation of all defect shapes.

The wavelength of the isolated vertical track defect types mentioned in the AS7509 standard could be bad or good for a wagon depending on its BCD and the wavelength of the track defect. As an example, the 20m chord length for measuring the vertical track defects as per the ARTC track geometry standard [55] gives allowable track defects of 66mm at 80km/h for the ARTC P1 (inspection within 24 hours) condition. If the defect shape spanned the 20m wavelength, a wagon with 10m BCD would face more severe pitch movement on that allowable vertical track defect compared to a wagon with longer BCD. On the other hand, a track defect could be much shorter than 20m as the standard does not specify shape. As an example, wagon A produces more pitch (θ_2) on the shorter wavelength of track defect compared to that obtained with the longer wavelength ($\theta 1$) (Figure 5-2). However, the chord-based measurement method would represent the same P1 for both the shorter and longer wavelength. So, having a short wavelength of track defect could be severe.

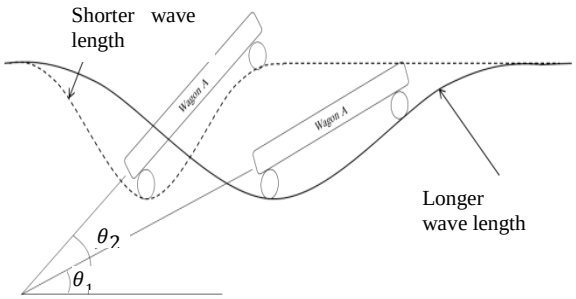

Figure 5-2: Variation in the pitch motion of a wagon depending on the change of wavelength of a track defect

A way to provide similar dynamics on all wagons is to use track defects which are equivalent to the track defects in the track maintenance standard but with wavelengths adjusted to the wagon BCD. A method to obtain equivalent track defects has been included in section 5.3.2.

5.3.1 Resonant Condition for Cyclic Track Defects

The Australian standard AS 7509 specifies a test for resonance for the harmonic roll test but does not require a test for resonance for the pitch and bounce test. In this study, the resonance criteria have been implemented in all three modes of pitch, bounce, and roll tests to replicate a possible worst-case situation for vehicle dynamics. In order to excite resonance, the wavelength of the vertical track defects (includes vertical alignment, twist, and roll) are set to correspond to the BCD of the wagon. The lateral cyclic track defect test is not added as the lateral cyclic track defects are not included in vehicle dynamics standards. However, lateral track defects effect roll motion. The hunting motion replicates a severe lateral and roll motion of the wagon and hence can be considered as an alternative to including cyclic lateral track defect tests. A modification of the defect wavelength based on BCD is presented in Table 5-5. The resonance speeds for various modes can be obtained using Equations 5-4 to 5-7.

$$\boldsymbol{V = f_n \lambda} \qquad \textbf{5-4}$$

$$\boldsymbol{f_n = \frac{1}{2\pi}\sqrt{\left(\frac{4K}{M}\right)}} \qquad \textbf{5-5}$$

$$f_{np} = \frac{1}{2\pi}\sqrt{\left(\frac{4K(a/2)^2}{I_y}\right)} \quad \textbf{5-6}$$

$$f_{nr} = \frac{1}{2\pi}\sqrt{\left(\frac{4K(l/2)^2}{I_x}\right)} \quad \textbf{5-7}$$

where V is the velocity (m/s), f_n is the natural frequency of linear motion (1/s), f_{np} is the natural frequency of pitch mode (rotation about lateral axis), f_{nr} is the natural frequency of roll mode (rotation about longitudinal axis), λ is the wavelength (m), K is the stiffness of a suspension system of the wagon (N/m), M is the sprung mass (kg)-mass of wagon body and bolsters (for a bogied wagon), I_x and I_y are the moment of inertia (kgm^2) about longitudinal (roll) and lateral (pitch) axes, a is the bogie centre distance (m), l is the lateral distance between suspensions (m).

Table 5-5: Track defects applicable for the vehicle performance test

	Defect wavelength (m)		Proposed defect wavelength (m)					
Track irregularity (mm)	ARTC track standard [55]	AS7509	Vertical		Lateral	Twist	Hump	Harmonic roll
			Pitch	Bounce				
Vertical alignment (mm)	20		4*acb	2*acb				
Lateral alignment (mm)	10				10			
Long twist (mm)	14					2*acb		
Short twist (mm)	2					2*aca		
Vertical hump (mm)		10					10	
Harmonic roll		2*acb						2*acb

Note: acb- half BCD, aca- half axle centre distance of a bogie or consider aca is 1m for a two-axle wagon, the vertical hump defect is fixed for all wagons as this parameter is a design fixed value for any fixed structure on the track

5.3.2 Equivalent Track Defect

A method to determine the equivalent track defect geometry has been proposed in this section using the shape equations mentioned in the AS7509 standard (Equation 5-8).

$$Z = \frac{H}{2}\left\{1 - \cos\frac{2\pi X}{L}\right\} \quad \textbf{5-8}$$

where H is the maximum depth of the irregularity (m), L is the wavelength of the irregularity (m), Z is the vertical coordinate of the shape (m), X is the longitudinal coordinate of the shape (m).

The track defect size mentioned in the track geometry standards (such as, ARTC [55]) is based on chord measurements and has been converted for the BCD of a wagon (Figure 5-3). The chord wavelength could be longer or shorter than the BCD, but it will usually be longer. The longer chord length of the two cases is made the base shape in the graphical plot (Figure 5-3). The BCD along with the shape curve is then superimposed on the base shape. The amplitude of the defect on the BCD is then changed (the equivalent amplitude) until a similar shape to that of the chord wavelength is found. As an example, the chord wavelength (20m) and amplitude (increased by 20% over the AS7509 value, e.g., 66mm is increased to 79.2mm corresponding to the ARTC P1 limit for 80km/h) have been used to develop an equivalent track defect based on a wagon with BCD of 12m (Figure 5-3). The equivalent amplitude for the 12m wavelength has been obtained as 52mm. The BCD and equivalent amplitudes thus constitute the equivalent track defect.

It can be noted here that the slope and curvature (rates of change of slope) of the equivalent track defect are not exactly the same as that of the longer chord based track defect. The equivalent track defect has a steeper slope and a sharper peak than these of the chord based track defect (Figure 5-3). In practice, actual track defects as detected can be of any shape and could also be sharper, so it is still reasonable to use the shorter defect despite its different slope and curvature.

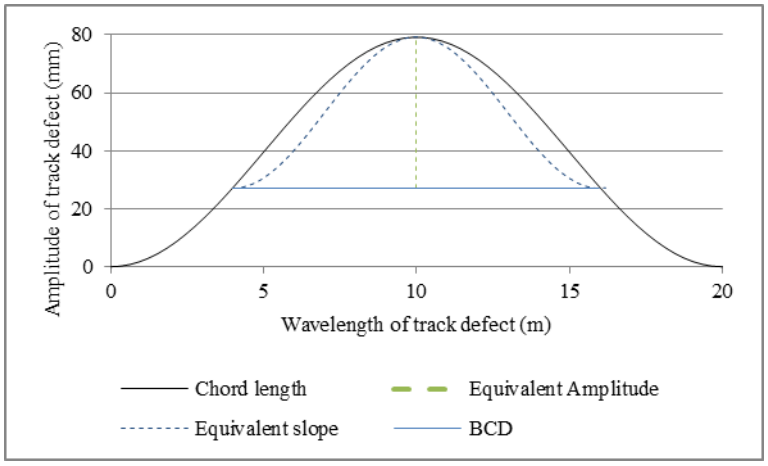

Figure 5-3: Adjusting wavelength and amplitude of the irregularity according to rollingstock requirement using similar peak method (standard wavelength is 20m as per the ARTC top irregularity measurement by chord, 120% of P1 vertical irregularity limit corresponding to 80km/h as per the ARTC track geometry and AS7509 requirement)

Table 5-6: Example of modification of P1 limits for a design rollingstock with BCD of 13.82m

Steps in determining track defect amplitude	Type of an isolated track defect	Wavelength of a track defect (m)	Speed (km/h)				
			40	60	80	100	115
			Amplitude of a track defect (mm)				
ARTC P1 limits	Lateral	10	44	44	34	24	18
	Vertical	20	71	71	66	56	51
	Long twist Non transition	14	60	60	52	46	40
	Long twist transition	14	64	64	55	49	42
	Short twist	2	18	18	16	14	12
Raise by 20% as per AS 7509	Lateral	10	52.8	52.8	40.8	28.8	21.6
	Vertical	20	85.2	85.2	79.2	67.2	61.2
	Long twist Non transition	14	72	72	62.4	55.2	48
	Long twist transition	14	76.8	76.8	66	58.8	50.4
	Short twist	2	21.6	21.6	19.2	16.8	14.4
Modify for BCD of 13.82m (Wavelength of 2acb), bounce and roll/ twist mode	Vertical	13.82	**67.0**	**67.0**	**62.0**	**53.0**	**48.0**
	Long twist Non transition	13.82	**72.0**	**72.0**	**62.4**	55.2	48
	Long twist transition	13.82	**76.8**	**76.8**	**66.0**	**58.8**	**50.4**
Modify for BCD of 13.82m (Wavelength of 4acb), pitch mode	Vertical	27.64	**103.0**	**103.0**	**96.0**	**82.0**	**74.0**

The ARTC track geometry standard [55] does not give separate defect levels for cyclic track defects. AS 7509 provides some default values for cyclic track defects based on approximations of rail joint spacing which are about 20-40% of the values provided in the vertical defect limits corresponding to priority #1 for track maintenance activity, also known as the P1 defect level. The vertical defect limits need to be modified based on the BCD of the design wagon concept to ensure application of an equivalent track defect for wagons with different BCDs. An example of equivalent track defect limits is presented in Table 5-6.

5.3.3 Type of Track Defects

To approach the problem of variation in track defect length on rollingstock systematically, 4 different track defect types have been developed in this section to check the effect of the track defect length and repetition on the response of a wagon. The methods are presented as the following defect types:

- Type A – Using the standards as they are (AS7509 and ARTC Track Geometry Section 5; Pitch and bounce cyclic defects as per AS7509, Harmonic roll as 40% of the defect limit requiring inspection within 24hours, also known as the P1 limit as per AS7509, Isolated defects as per P1 limits of ARTC track geometry standard).
- Type B – Reduced defect size, wavelength similar to chord length (less severe than Type A). The defect is reduced to evaluate the operating limits of the vehicle if it fails Type A tests.
- Type C – Wavelength is same as the BCD of the wagon, defect amplitude of Type A.
- Type D – Tuned to wagon (equivalent track defect) 'Type A' Amplitude is reduced by a graphical method to obtain the equivalent defect, wavelength is same as the BCD of the wagon.

The Type A track defect represents the minimum performance requirement set by the AS7509 standard. The AS7509 standard refers to individual track owner's standards when identifying shape and size of the track defect. However, in case of the absence of any track defect data, the AS7509 generally gives some default data for a test, such as 20mm cyclic bounce or pitch test amplitude over 12.2m or 13.7m wavelengths. The harmonic roll assessment as per AS7509 [61] requires using 40% of the P1 limit as per the ARTC track geometry standard [55]. The Type B track defect is introduced when a wagon fails on Type A as it could be the case that the wagon could run under some reduced performance criteria (slower speeds, higher track maintenance standards). Type C is the first step towards using a track defect tuned for the BCD of the wagon. In Type C, the wavelength of the track defect is changed to BCD, but the amplitude remains the same as Type A. So, there is a strong possibility that Type C could be too severe for some wagons when the BCD is shorter than the chord length of Type A (Figure 5-4). It could be argued that a fairer test for the wagon would be achieved using the equivalent track defect (discussed in section 5.3.2) amplitude for the BCD as developed as Type D. The equivalent track defect (Type D) is the modified Type A defect tuned to the wagon BCD. The modifications in cyclic pitch and bounce tests consider a variation of defect amplitude due to the changed circumstances of generating the cyclic defect by repetitive wagon responses on a continuously welded rail track. Due to the absence of available data on cyclic track defects due to repetitive wagon responses, it is possible to have a cyclic track defect at the typical cyclic defect amplitude of 20mm that could be as low as 20% of the P1 limit. The sensitivity analysis of the cyclic track defect size is not included and 40% of the P1 limit is chosen as a starting parameter to test cyclic pitch and bounce tests in this thesis. The amplitude of the harmonic roll test for Type D is similar to that for Type A, but the

wavelength is changed to BCD. The isolated track defect was tuned to the wagon BCD to make it equivalent to the P1 limit on the considered rollingstock.

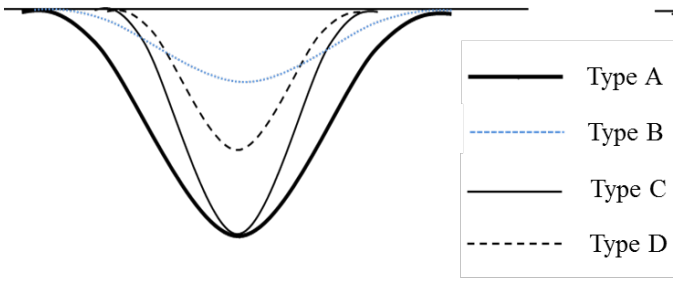

Figure 5-4: Severity of type of defects based on BCD of a wagon and wavelength of track defect

5.3.4 Test Speeds

It is also necessary to specify operating speeds for the simulation tests in VAPS. Four different speeds can be used to describe the cases of interest:

- Speed 1- the low-speed situation at the cant excess (Ce), applied on curved sections.
- Speed 2- the speed at which resonance occurs (depends on the wagon BCD, suspension parameters, mass and natural frequency).
- Speed 3- the test speed representing 10% higher (as per AS 7509) than the design speed (Speed 3a) and/ or modified speed limit (Speed 3b). The design speed could be increased or decreased from the intended speed limit based on the results of the simulation.
- Speed 4- the speed corresponding to the intended cant deficiency (Cd) limit, applied on curved sections.

Different track defect sizes are specified for different speed limits in [55]. The speed on a curved section is dictated by the allowable cant excess (low-speed criteria, Speed 1) and cant deficiency (high-speed criteria, Speed 4) on a network. If a track defect occurs on a curved section, the dynamics are affected by the combined effect of the geometry of the curve and the track defect. If speed 4 is less than speed 3a on a curved track, it is adequate to test at Speed 4. On a straight track, Speed 1 and Speed 4 are not required. Speed 2 and Speed 3a generally determine the worst response on a straight track. In some cases, there is a need to reduce the intended speed limit which can be defined as Speed 3b. Speed 2 is particularly important for cyclic track defects where resonant response needs to be tested.

As resonance depends on wavelength and suspension characteristics, it can be lower or higher than the intended speed limit (Speed 3a). If the resonance speed (Speed 2) is higher than Speed 3a, the wagon need not be tested at Speed 2. The resonance conditions need to be tested when Speed 2 is lower than Speed 3a. In addition to that, severe responses could also then be obtained at the maximum speed (Speed 3a). So, it is also necessary to test the wagon at the intended speed limit in addition to the resonant speeds. A provision is kept in this method to use a lower speed limit (Speed 3b) than the target limit (Speed 3a) if the wagon failed to pass on the track defect geometry at Speed 3a.

5.3.5 Application of Type of Track Defects

A systematic approach applying 4 different defect levels has been presented in Figure 5-5. Generally, all wagons should pass the type A criteria (wavelength and amplitude of standards). If a wagon fails to pass the type A, the defect magnitude could be reduced (type B) to check the capability of the wagon and specify operating restrictions. The type B track defect is considered as the least severe test of the four defect types mentioned in this method. It is only considered if Type A tests are failed. On the other hand, if a wagon passed the type A test, it is necessary to check for further tests such as types C and D tests. An alternative path to apply the type of defect methodological approach (dotted path in Figure 5-5) is to start with the Type D defect knowing that the worst situation for cyclic track defect would be type D. If a wagon fails at Type D the Type A approach should be checked. The alternative path would reduce the number of simulations to evaluate the defect negotiation ability of a wagon. The possible outcomes could be defined as type B, C or D compatible; type B with stricter maintenance and reduced type D.

As for a lower performing wagon, a type B track defect can be further described as a track corresponding to defect band (Table 5-7) to make it suitable to compare with the ARTC standard. If a wagon failed to negotiate the P1 defect level corresponding to the design speed a reduced amplitude of track defect need to be tested. The reduced amplitude of track defect would establish the track defect band for the wagon. Defect band A to G represents the worst (defect band A) to the best track (defect band G) in the ARTC track network

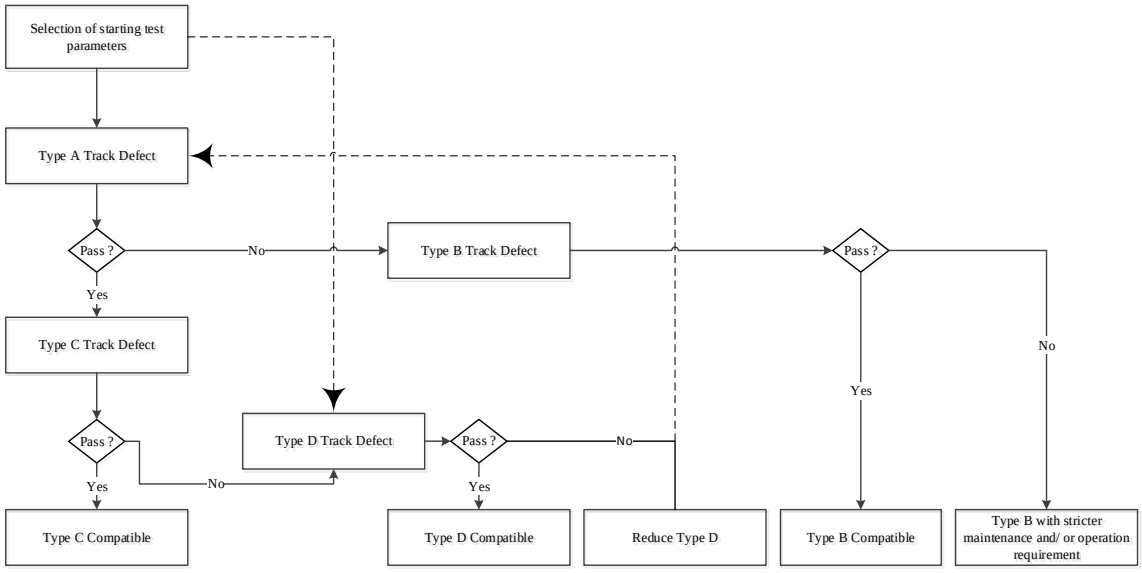

Figure 5-5: Application of the type of defect method to perform track defect tests

Table 5-7: Defect band of the track

Speed bands (km/h)					Defect Band
40	60	80	100	115	
					A
					B
P1	P1				C
		P1			D
			P1		E
				P1	F
					G

Notes: P1 is the track maintenance level requiring inspection within 24 hours. Defect band A is the worst track, G is the best track in the ARTC track network

5.4 Summary

The VAPS method defined a list of suitable tests for testing a wagon and developing a new wagon concept. The parameters of track defect geometry have been modified to create possible higher responses compared to the fixed track defect sizes mentioned for some of the tests in the AS7509 standard and further tests for cyclic track defects and investigations of suspension resonance were defined. A method to determine an equivalent track defect geometry based on the BCD of a wagon was also developed.

Chapter 6
Testing the VAPS method with an existing wagon (RQTY)

6.1 Introduction

In this chapter, an existing design, the RQTY container wagon which is a typical three-piece bogie wagon, has been evaluated using the proposed vehicle acceptance procedure by simulation (VAPS) method discussed in section 5.2. This is to provide a datum of performance parameters for later comparison with the new concept wagon development. The RQTY container wagon specification has been used in this study as the length and capacity/ gross mass parameters of an RQTY wagon are similar to that of the desired concept wagon. The three-piece bogie model used in this study has been described in [114] and has been simulated in several papers [115-117]. The detailed model parameters of the three-piece bogie model used in this study have been presented in Appendix 1.

The chassis of the RQTY wagon has been considered as the realistic type (having 4 beam elements- one rectangular deck, one rectangular beam under the deck and two triangular beams under the deck) as described in section 4.4. The wagon body mass and inertia parameters based on the realistic chassis approximation is presented in Table 6-1. The empty mass of the RQTY wagon body is 10000kg. The bogie centre distance (BCD) of the RQTY wagon is 14.94m and the overhang length beyond each bogie is 2.13m which makes a total wagon length of 19.2m. The tare mass and gross mass of the RQTY wagon are 16.88 tonne and 90.88 tonnes respectively.

Table 6-1: Moment of inertia calculation considering realistic beam and deck elements for RQTY wagon

RQTY_ARTC	a, ar, at (Figure 4-3)	b, bb (Figure 4-3)	h	Mass	Jf	Jk	Jp	Centre of gravity
	m	m	m	Kg	kgm^2	kgm^2	kgm^2	M
Beam1 (rectangular)	7.4	1.4	0.66	3676.5	734	16,910	17,377	0.67
Beam 2a (triangular)	2.37	1.4	0.66	1323.5	248	445	629	0.78
Beam 2b (triangular)	2.37	1.4	0.66	1323.5	248	445	629	0.78
Deck	19.82	3	0.2	3676.5	2,770	120,365	123,110	1.1
Empty Container	17.655	2.35	2.4	6450	6,064	170,634	170,507	1.2
Loaded Container	17.655	2.35	2.4	72000	67,695	1,904,754	1,903,329	2.4
Empty Wagon	19.82	3	0.86	10000	4,361	138,527	141,746	0.9
Loaded Wagon	19.82, 17.655	3, 2.35	3.26	82000	92,956	2,064,181	2,045,075	2.2

6.2 Step 1 Critical Hunting Speed Test on the RQTY Wagon

There have been numerous debates in the literature on methods of obtaining the critical hunting speed for lateral instability or hunting for a railway vehicle by mathematical analysis and railway engineering standards. Due to the high number of non-linear elements in the running gear, it is always preferable to use simulation to determine the critical speed of a railway vehicle. A list of methods can be found in [118] - decreasing velocity without additional force or track excitation, bifurcation diagram, single excitation- oscillation damped, single excitation-

measurement of track shift force, rms accelerations [87], track irregularity- measurement of track shift force, rms accelerations.

The decreasing velocity method uses a high starting velocity as the initial excitation which then gradually decreases with time. The critical speed is measured at a point when the lateral movement of wheelsets is damped out. The bifurcation diagram (Figure 2-29) uses the plot of lateral movement with respect to speed. Minimum speed for lateral instability is obtained at the nose of the diagram. In the single excitation methods, the excitation can be applied in the form of a force on the wagon or a lateral track irregularity. Outputs from excitation methods can be analysed by means of lateral movement of wheelsets, track shift force or lateral acceleration. In the case of lateral movement of wheelsets, the critical speed is taken as the velocity when the lateral oscillation of wheelsets stops. In the case of track shift force and lateral acceleration values, there are values mentioned in the standards which determine the limiting conditions up to which the wagon is considered free of hunting.

The decreasing velocity method appears to give the lowest critical speed among all these methods [118]. So, in this study, the decreasing velocity method has been used to provide a conservative critical speed in the design. An initial excitation was used to activate the limit cycle behaviour. The excitation on the RQTY wagon model was provided by applying an initial disturbance to the wagon body in lateral (0.15m/s) and yaw (0.15rad/s) directions. The speed was decreased at a rate of 5km/h/s from an initial speed of 140km/h (Figure 6-1a).The critical speed was taken as the speed where the lateral displacement of wheelsets approached zero (Figure 6-1).

Generally, the critical speed decreases with increasing friction coefficient between the wheel and rail [119]. The critical speed has been found to have a larger decrease for a friction coefficient between 0.3 and 0.4 (example, 270-310km/h on a four car articulated vehicle, wheel-rail equivalent conicity of 0.4) while decreasing slowly between 0.4 and 0.5 (example, 260-270km/h) [119]. The recommended wheel-rail friction coefficient for non-linear bogie stability analysis is 0.4 to 0.5 [62]. In this chapter, the wheel-rail friction coefficient of 0.4 is used for datum purposes. In all stability analysis cases, Kalker's full creep coefficient has been used in this study as recommended for non-linear bogie stability analysis [62].

The wheel-rail profile conditions are recommended to match with typical track and operational conditions for the stability analysis. As the detailed sensitivity analysis of worn wheel and worn rail profiles is not in the scope of this study, two cases of new and worn wheel profiles combined with a new rail profile have been used to establish a datum case.

The WPR2000 wheel tread profile is designed as a worn profile shape for operation on the New South Wales network of Australia [120]. The WPR2000 wheel profile is considered to have good curve negotiation ability on a typical track which will not give a high critical speed due to the conflicting nature of curving and hunting stability. The other important fact is that appropriate worn wheel and rail profiles for evaluation of critical hunting speed are not specified in the Australian standards. Decisions regarding the choice of appropriate worn wheel and rail profiles are left with the individual network organisations having regard to the typical operational scenarios on a network. So, the WPR2000 wheel profile, both new and in a service worn condition were used in this Chapter to observe the effect of wheel profile on critical speed. The new and service worn WPR2000 wheel profiles give equivalent conicity's of 0.148 and 0.264 respectively when matched with a new AS60 rail profile. The equivalent

conicity was determined using a linearisation method based on the measured wheel and rail profiles described in the European standard EN 15302 [105]. The KPF program GENSYS simulation software uses the principles of EN15302 and has claimed a close match with the benchmark calculation described in the EN15302 standard [121]. The wheel-rail contact patch has been generated by using the KPF program in the GENSYS simulation software.

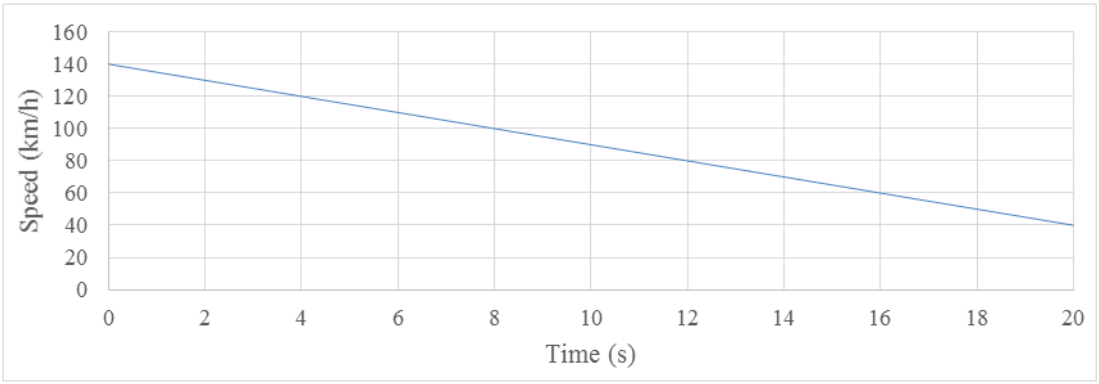

(a) Decreasing velocity to evaluate critical hunting speed

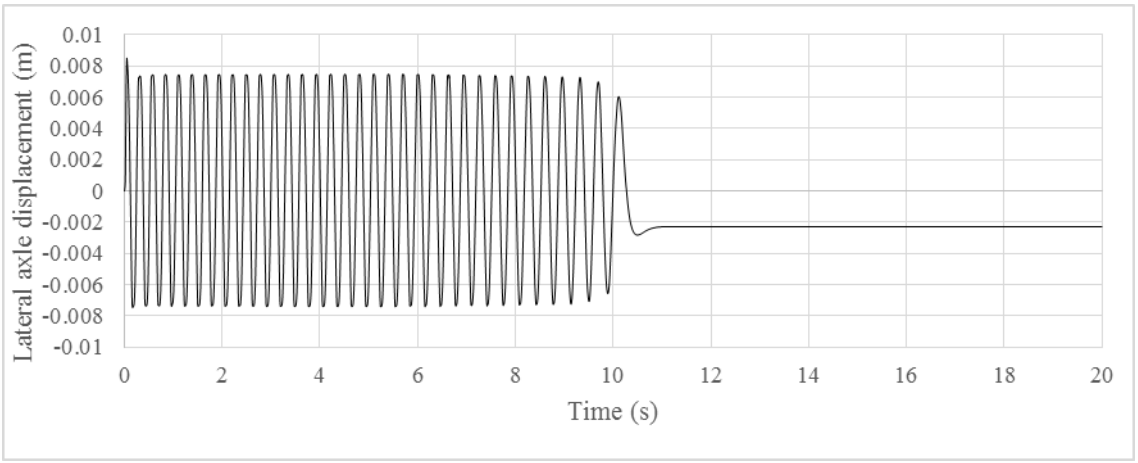

(b) New WPR2000 wheel profile

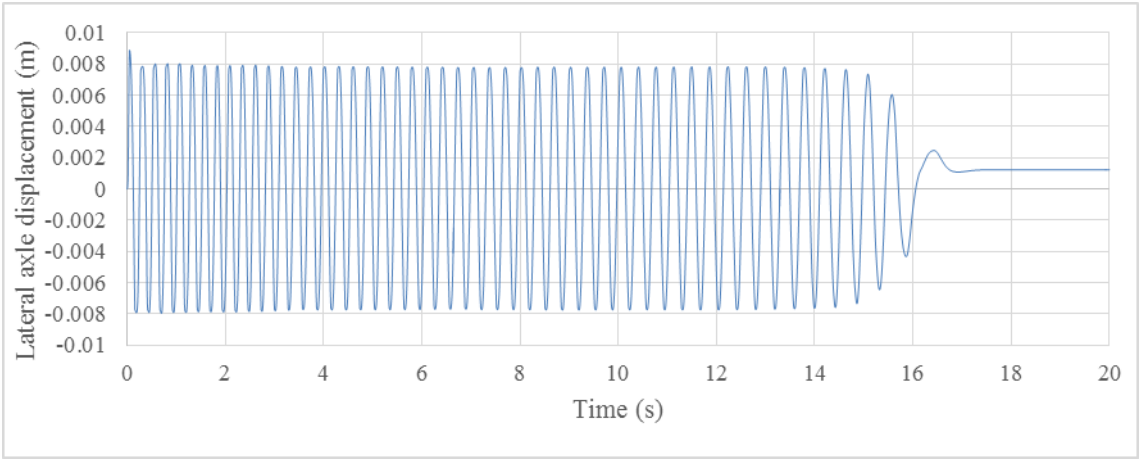

(c) Service worn WPR2000 wheel profile

Figure 6-1: Critical speed of the RQTY- wagon using decreasing velocity method, new AS60 rail profile, Track without any irregularity

The critical speeds have been found to be 85 and 55km/h for the new (Figure 6-1b) and service worn WPR2000 wheel profiles respectively (Figure 6-1c). It is important to note that uncertainty in wheel-rail contact geometry with the track can result in up to 20% variation in the measurement of critical speed [118]. The service worn wheel profile of WPR2000 used in this study provides a 35% lower value of critical speed than that obtained for new wheel conditions. The service worn profile of WPR2000 is therefore considered as a worse parameter for simulation study and was not used further for datum purposes. At the concept development stage, the new wheel and new rail profiles were chosen as these would provide a better dynamical outcome. The new WPR2000 wheel and new AS60 rail profiles were chosen for the remaining stages of the simulation study of the RQTY wagon and development of the new concept. Effect of wheel rail profiles (having higher equivalent conicity compared to a new wheel new rail combination) on a final concept is included in Section 10.14.

6.3 Step 2- Curve Negotiation Test

The curve negotiation tests have been performed using both the empty and loaded conditions of a single wagon. The curve negotiation tests were performed at speeds corresponding to both the desired cant deficiency (110mm) and cant excess (75mm) conditions. Railway companies use Equation 6-1 to determine the allowable maximum and minimum speeds for curves by using applied cant, cant deficiency, and cant excess parameters. Cant deficiency and cant excess are the parameters which are set to dictate the limiting speeds at which a vehicle should be able to negotiate curves of a particular radius without derailment (high speed, derail over high rail) or rollover (slow speed, rollover along the low rail).

$$V = \sqrt{\frac{E_e * R}{11.82}} \qquad \textbf{6-1}$$

where E_e is the equivalent cant (applied cant + cant deficiency) (mm), V is the speed (km/h), R is the radius of the track curve (m).

Track irregularity levels corresponding to FRA track classes have been chosen based on the speed limit on a curved track. The FRA track classes are categorised in terms of speed limits (Table 6-2). The higher FRA track class numbers indicate better or smoother track. Hence, a wagon passing a test on a rougher track would mean that the wagon would be suitable for smoother track at the same speed. The FRA class 1 and 2 tracks are the worst two track classes that are used for maintenance yard/ shunting trains and are not included in the simulation study. The roadworthiness standards of the Association of American Railroads (AAR) recommend using FRA class 5 or smoother track [85]. However, in this study, the rougher FRA track class 3 and class 4 tracks were also used to provide a more severe test than the standard test for datum purposes.

A 300m radius track with the applied cant of 125mm was used to check the curve negotiability of the wagon under tracks with different FRA track irregularities. The corresponding speeds are 77.2 km/h (at the cant deficiency of 110mm) and 35.6 km/h (at the cant excess of 75mm) which are within maximum allowable speed limits on FRA track classes 4 and 2 respectively (Table 6-2). As the class 2 track is kept outside the scope of simulation tests, the slow speed test was performed on class 3 or smoother than track class 3. It can be mentioned here that, if a curve allows speed corresponding to 110mm cant deficiency limit, the applicable track irregularities on a 300m radius track should correspond to FRA class 4 or smoother. So, the slow speed test on a rougher track than class 4 would be a stricter test and was chosen as a suitable condition for datum tests.

Table 6-2: Maximum allowable speeds on different track classes as per FRA track standards [122, 123]

FRA Track Class	Maximum allowable speed (km/h)
1	16
2	40
3	64
4	96
5	128
6	177

The minimum length of transition derived in the ARTC standard [55] is based on the uniform rate of change of superelevation deficiency or excess and difference in deficiency (Equation 6-2). The minimum length over which the superelevation ramp needs to be produced can be determined using Equation 6-3.

$$L_t = \frac{V * \Delta C_d}{3.6 * C_r} \quad \textbf{6-2}$$

$$L_r = \frac{E_r * \Delta C_a}{1000} \quad \textbf{6-3}$$

where L_t is the length of the transition length (m), V is the speed (km/h), ΔC_d is the difference in cant deficiency between the two adjacent track sections, C_r is the rate of change of superelevation deficiency or excess (mm/s), L_r is the length over which the superelevation needs to be developed (m), E_r is the superelevation ramp rate (1 in _, 500 in this case as set for typical limits in the ARTC standard [55]), ΔC_a is the difference in applied superelevation (mm).

The ARTC standard [55] mentions that, if the calculated superelevation ramp length (L_r) is greater than the available transition length (L_t), the remaining ramp can be provided on the straight and curved sections. In this thesis, the maximum length of the two length parameters (L_t and L_r) have been used as the transition length as an initial assessment. As an example, the 110mm cant deficiency speed on a 300m radius track gives a minimum transition length (L_t) of 67.4m using 35mm/s as the rate of change of superelevation deficiency, and 110mm as the difference in cant deficiency. Using a superelevation ramp rate of 1 in 500, and difference in the applied cant of 125mm gives a minimum ramp length of 62.5m using Equation 6-3. The minimum length of the two length parameters of 62.5m (when using 110mm cant deficiency speed on a 300m radius track) was used in simulation approach as it would provide a steeper transition compared to a longer transition length and hence a worse case of track twist situation.

The curve entry and exit transition sections generates a track twist condition. A wagon would face the most sever twist condition if the ramp length is the same length of the BCD. However, the ramp length (67.4m on a track with radius of 300m as obtained from Equation 6-2 and 6-3) would be a lot higher than the intended wagon BCD of 13.8m which means that the vehicle would not face the worst track twist situation on a curved track of radius 300m and more. The worst condition of track twist can occur in a cyclic harmonic test or in an isolated track defect tests.

The type of transition curve in the ARTC network is a clothoid [55]. In the clothoid type transition, the curve is a third-degree parabola with a linear superelevation ramp along the track length [124]. The clothoid type transition sections have been widely used as it has been easier to maintain alignment of clothoid type transitions than

complicated S-shaped curves (example, Ruch curve) that needs to smoothen near the curve entry and exit transitions [125]. In the clothoid transitions, the curve entry and exit transition are not smoothed (Figure 6-2) which creates a sharp change in curvature and can create problems in numerical integration. The vehicle reactions do not change significantly between the clothoid and Ruch type transitions as investigated in [126]. So, the Ruch type transition section can be used instead of the clothoid type transition, realising that the vehicle reactions are not affected significantly due to this change and the results can be accepted as applicable for clothoid type transition sections. It is also possible to maintain an S-shaped curve due to the availability of modern tamping machine equipped with microcomputers which can easily calculate necessary correction values [126]. For the current study, the Ruch type transition curve is chosen.

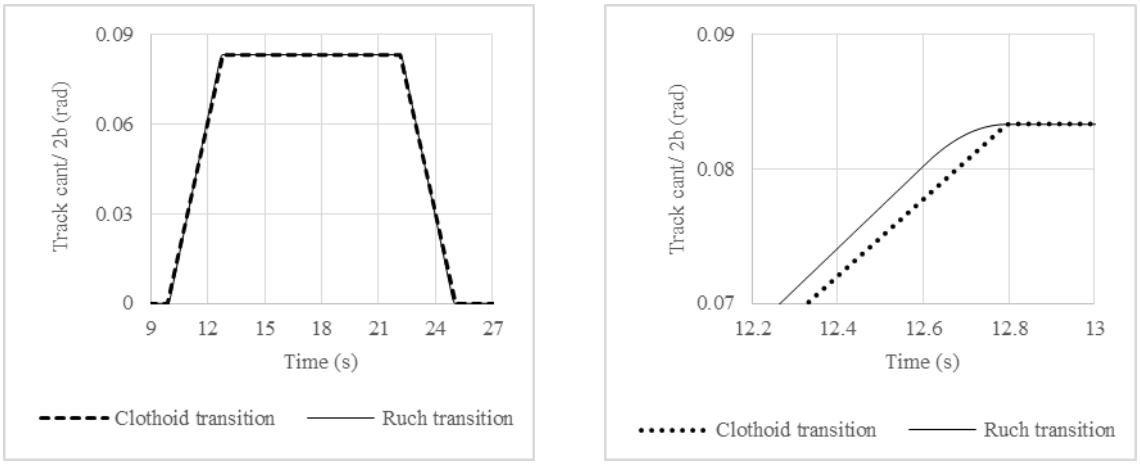

(a) Clothoid and Ruch transitions on the full curve

(b) Clothoid and Ruch transitions zoomed at the curve entry

Figure 6-2: Clothoid and Ruch transitions

The wheel-rail friction coefficient (0.4) corresponding to dry weather approximation and full creep condition was used in the curve negotiation test following similar conditions used in the critical speed test.

The initial trials on the RQTY wagon revealed that it faced a high wheel unloading ratio (1.03) and was assumed to derail under dry weather and full creep conditions (Figure 6-3). The wheel unloading could occur due to suspension arrangements and wheel-rail contact conditions. The suspension arrangements of the RQTY wagon are intended to be a datum for this thesis and hence cannot be modified. So, the possible improvement is to modify the test condition by modifying the wheel-rail contact condition. The dry wheel-rail contact conditions have a steep slope on a typical creep vs. creep-force (Figure 6-4, Figure 6-5) curve [127].

In reality, the slope of the creep force vs. creep curve is less than that obtained by Kalker's linear theory [127]. Kalker's linear theory assumes a linear relationship between wheel-rail contact and creep which is adequate to investigate the cases where creep is low. At high creep, the slope of the force vs. creep plot decreases with creep (Figure 6-5). The decrease in the slope is usually modelled by a reduction factor (typical values are 0.6-0.85 for dry rails and 0.2-0.5 for wet rails [127]) [128]. In this thesis, the creepage reduction coefficient of 0.6 is used as an approximation of dry contaminated rail following the value corresponding to normal levels of contamination as mentioned in [62]. The use of the different friction conditions for contaminated rail significantly changed the wagon dynamics and reduced the maximum wheel unloading ratio to 0.84 (Figure 6-3).

The reduction of wheel unloading ratio on the dry contaminated rail can be explained by considering the rolling and sliding motion on the contact between wheel and rail (Figure 6-4). The contaminated rail condition allows more rolling before reaching the sliding zone. The availability of roll motion in the contact zone on the contaminated rail reduces yaw movement of the wheelset (-4 and -6 mrad on contaminated and dry contact respectively, at 12.3s, Figure 6-3b). The negative yaw angles on the front wheelsets in both the dry and contaminated condition indicate an underradial position (Figure 6-6) which allows flange contact at the front of the centre line of the wheelset axle. The dry rail provided a greater underradial angle (negative yaw angle 6 mrad) than the contaminated rail (negative 4mrad) at the point of possible derailment (at about 12.3s, Figure 6-3b). The high yaw angle on the dry rail increases lateral creepage and results in lateral creep force being inclined upward (Figure 6-6) which has a tendency to lift the wheelset [128]. The flange force on the high rail acts with the centripetal action of the wagon to increase the tendency to roll over along the high rail which creates wheel unloading on the low rail (right rail on the RHC). In addition to the rollover effect, the wheel unloading is also being generated due to the twist moment created by the long and rigid wagon body as the wagon negotiates cant ramps. Thus, a combination of factors effect curve and transition negotiation ability of this wagon. As the dry contaminated rail was found to be a suitable test condition for the RQTY wagon under the given test parameters, it is decided to use the dry contaminated rail with the same parameters as described above for all simulations of the RQTY wagon.

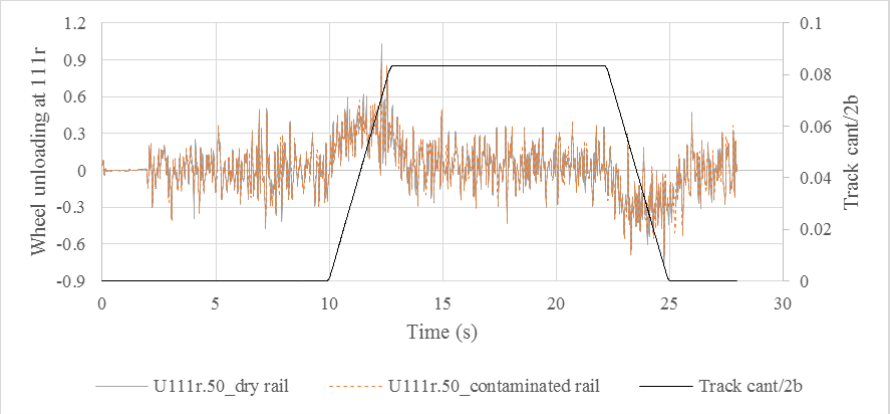

(a) wheel unloading ratio and Track cant/2b on the right-handed 300m radius track

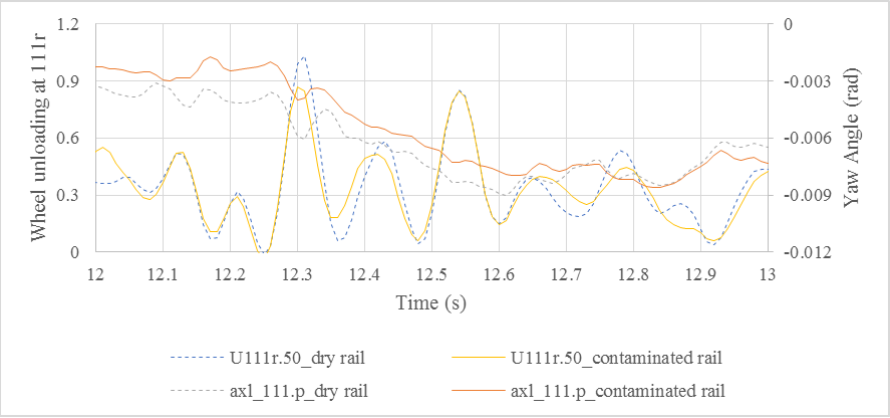

(b) Wheel unloading ratio and yaw angle on front axle of the front bogie in dry and contaminated rail conditions

Figure 6-3: Effect of wheel-rail contact condition on steering

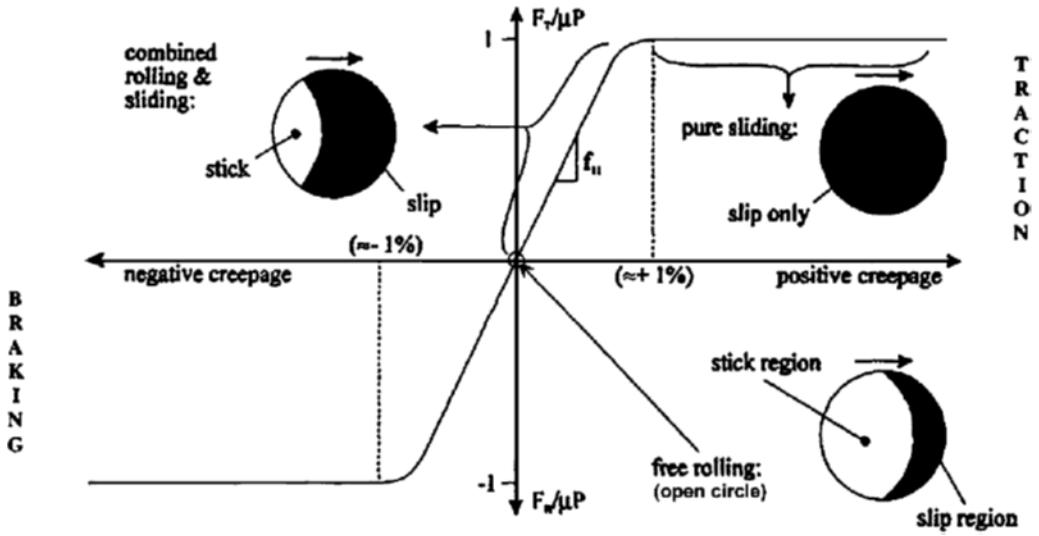

Figure 6-4: Schematic diagram of rolling and sliding on wheel-rail contact [129]

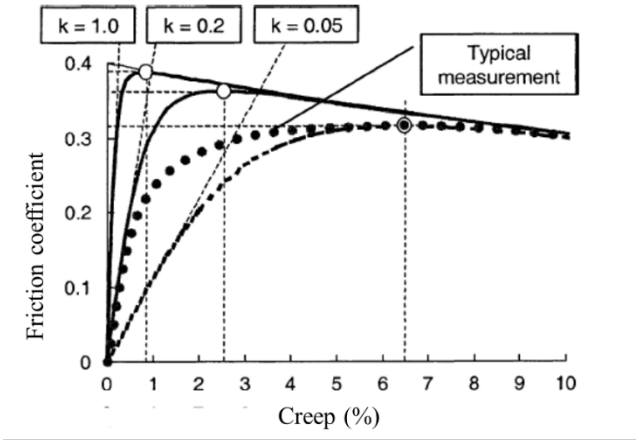

Figure 6-5: Adjustment of friction coefficient vs creep curve [127] [k is the reduction factor of the slope, also termed as Kalker's coefficient]

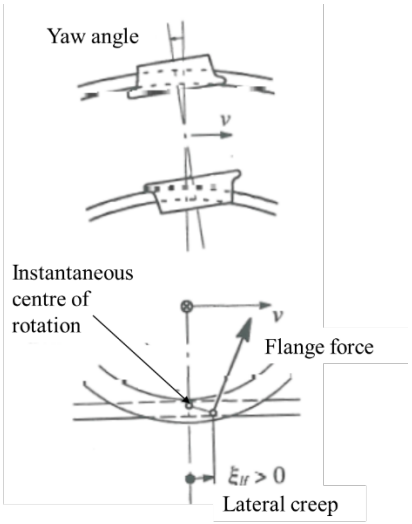

Figure 6-6: Underradial position of wheelset [128]

The simulation cases selected for investigating the curve negotiation ability of the RQTY wagon are presented in Table 6-3. Suitable track classes were chosen from Table 6-2 corresponding to the operating speed.

Table 6-3: Simulation cases for curve negotiation test on the RQTY wagon (Track radius 300m)

Simulation cases	Load (kg)	Speed (km/h)	FRA track class
1, 2	0, 72000	77.2	4
3, 4	0, 72000	35.6	3

The simulation results for the RQTY wagon on the 300m radius curve at both the high and low-speed conditions are given in Table 6-4. The derailment parameters (L/V ratio and wheel unloading ratio) in the empty conditions (cases 1 and 3) have been found to be higher than those in the loaded conditions (cases 2 and 4). The vertical loads (V) on wheels in the loaded wagon are much higher than those in an empty wagon which reduces lateral to vertical wheel load ratio on the loaded wagon. In addition to that, wheel loads differ on the curved section depending on the centrifugal force (depends on velocity, and track radius) and mass.

Table 6-4: Results of step 2 test on the RQTY wagon (Track radius 300m)

Case	Load	Maximum L/V wheel								Maximum L/V axle			
		111l	111r	112l	112r	121l	121r	122l	122r	111	112	121	122
1	E	0.66	0.44	0.54	0.28	0.84	0.38	0.49	0.3	1	0.71	1.04	0.74
2	L	0.53	0.43	0.54	0.42	0.4	0.56	0.42	0.67	0.92	0.9	0.95	1.06
3	E	0.98	0.44	0.56	0.42	0.96	0.43	0.7	0.44	1.39	0.93	1.37	1.09
4	L	0.77	0.45	0.77	0.44	0.44	0.4	0.47	0.46	1.2	1.19	0.84	0.86
Case	Load	Maximum Wheel unloading ratio								Maximum Lateral acceleration (m/s^2)		Maximum Vertical acceleration (m/s^2)	
		111l	111r	112l	112r	121l	121r	122l	122r	ay1	ay2	az1	az2
1	E	0.83	0.87	0.58	0.73	0.66	0.85	0.67	0.72	3.09	3.21	5.74	4.83
2	L	0.27	0.57	0.22	0.5	0.27	0.52	0.23	0.48	2.71	2.75	2.89	2.85
3	E	0.62	0.61	0.64	0.53	0.54	0.57	0.59	0.59	2.96	2.84	3.35	2.81
4	L	0.42	0.3	0.42	0.22	0.46	0.33	0.45	0.25	1.87	2.09	1.59	1.57

Note: E- Empty wagon, L- Loaded wagon; 111l- from right to left- l/r means left or right wheel, 1- axle number of 1- bogie number of 1- wagon number; 121r means right wheel of the first axle of the second bogie of first wagon etc.

The right wheels on the front axles of the front bogie (111r) and rear bogie (121r) in case 1 (Empty, 110mm cant deficiency condition) showed maximum wheel unloading ratios of 0.87 and 0.85 respectively among all the four cases (Table 6-4, Figure 6-7). The graphical plot showed that wheel unloading ratio was maximum at the curve entry on wheel number 111r (at 12.3s) and at the exit transition of the curve on wheel number 121r (at 24.5s) (Figure 6-7c).

The centrifugal inertia is proportional to the square of speed which reduces the gravitational load on the low rail and generates an additional load on the high rail, i.e. the left rail on the right-handed curve (RHC), when running on a cant deficiency condition. So, the wheel unloading ratio is higher on the low rail (right rail on the RHC) due to less gravitational wheel load on the low rail at cant deficiency speeds.

In reality, the wagon body usually allows some flexibility which helps to negotiate track defects. In the simulation approach in this study, the wagon body is considered as a rigid solid body. The dynamic effects on wheel loads due to the twist track defect creates unequal loading on all the wheels [130]. In real wagon structures, there is some chassis and body flexure, so the rigid body approximation in the simulation represents a worst case situation by not allowing any flexure when negotiating a twist track defect. More elaborate models can be used to do this – but just standard solid body modelling is used here. The effect of wagon body rigidity on available twist adjustment by the wagon body can be explained using equation 6-4 ([131]).

$$\Phi = \frac{TL}{GJ} \qquad \textbf{6-4}$$

$$J = \beta a b^3 \qquad \textbf{6-5}$$

where Φ is the twist angle (rad), T is the applied torque (Nm), *L* is the length of body (m), *a* is the short side of the cross-sectional area where torque is applied (m), *b* is the long side of the cross-sectional area where torque is applied (m), *G* is the modulus of rigidity (N/m^2), *J* is the polar moment of area of a rectangular section (m^4), β is a factor that depends on the a/b ratio.

As the rigidity (*G* in Equation 6-5) increases, the twist angle on the wagon body decreases. The amount of twist angle on the wagon body increases with the increase of length, hence a longer wagon is likely in practice to provide more flexure. Torsional moments on the wagon body are higher at the points of changing cant such as the curve entry transition (12- 13s in Figure 6-8a) and exit transition (24- 25s in Figure 6-8a) positions. The maximum wheel unloading ratio of 0.87 was found on the front right wheel (111r) at about 12.3s (Figure 6-8b). The front right wheel is positioned on the low rail on the RHC. At the curve entry position, cant becomes the maximum (125mm in this case), so the height difference between left and the right wheels also becomes the highest among other positions on the track. The rear bogie remains on the transition section when the front bogie meets the curve entry point. The height difference of the wheels on the rear bogie is less than the height difference of the wheels on the front wheels which creates a torsional moment on the wagon body. As the wagon body was modelled as a rigid body, no flexure was available and the front right wheel failed to generate adequate wheel load and a high wheel unloading ratio (0.87) is obtained on wheel #111r at the curve entry point. An opposite situation developed on the exit transition when the maximum wheel unloading ratio (0.85) occurred on the right wheel of the front axle of the rear bogie (wheel # 121r) at about 24.54s (Figure 6-8c). At 25.24s, the front axle clears the curved section of the track at 77.23km/h (track file starts at 2m ahead of the front axle in this simulation, it would take 0.09s to pass the 2m distance, so 25.24s would give adequate time for the front axle to cross the exit transition) but the rear axles remained on the transition section which produces a torsional moment on the front axle and wheel unloading occurred on the rear bogie (wheel number #121r, right wheel on low rail).

The added vertical track irregularities changed the track vertical position under the wheels which, when combined with the cant ramp, can increase or decrease the difference in vertical positions between the left and right wheels. As an example the exit transition and the position of high wheel unloading ratio in Figure 6-8c have been investigated in Figure 6-9 and Table 6-5. The front axle positions at the exit transition (25.06s, Figure 6-9a) are located at a point of zero cant when the rear axles are still on the transition section positioned at a track cant of 26.6mm (using a lateral semi-distance between the rolling points of left and right rail of b= 0.75m). The superimposed vertical track irregularities create an overall difference in rail height of 1.4mm on the front axle and

18mm on the rear axle when the front axle is on the exit transition (Table 6-5). The same procedure is applied on the position of a high wheel unloading ratio on wheel #121r at 24.54s (Figure 6-8c). The combination of cant ramp and vertical track irregularities creates a rail height difference of 32.4mm on the rear axle (#121) and 23.3mm on the front axle (#111). The height difference between right and left rail has created a torsional moment on the wagon body which further influenced the wheel unloading ratio as seen in Figure 6-7 and Figure 6-8.

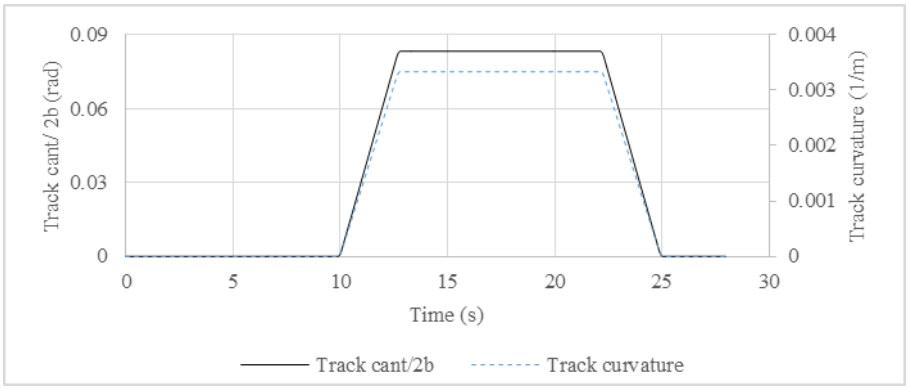

(a) Track geometry

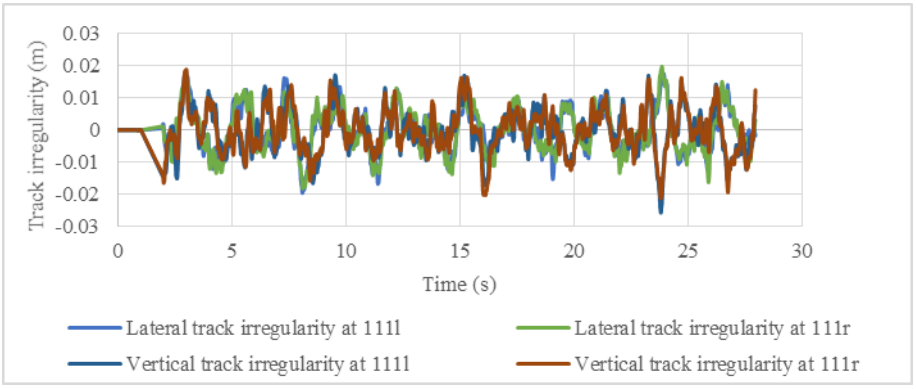

(b) Applied track irregularities

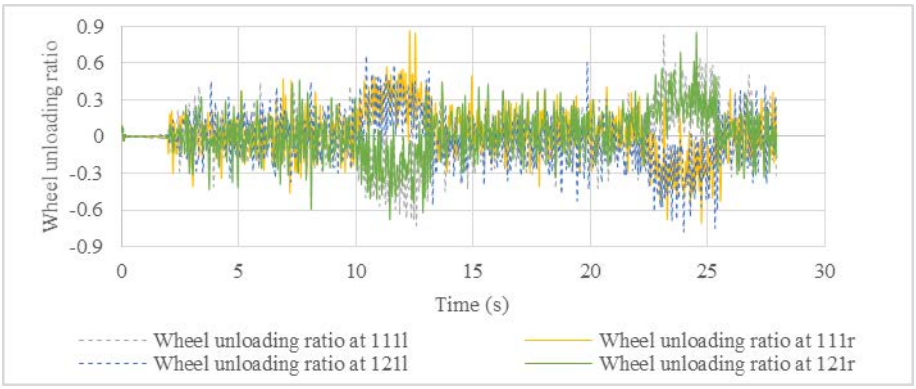

(c) Wheel unloading ratio

Figure 6-7: Case 1 of step 2 tests on RQTY wagon (Curve radius 300m, cant deficiency 110mm, FRA class 4 track irregularities, tare mass) [Notes: positive track curvature and track cant refer to a right-handed curve, positive lateral track irregularity refers to rightward lateral track irregularity, positive vertical irregularity refers to downward track irregularity, positive wheel unloading ratio means wheel unloading, negative wheel unloading refers to wheel overloading, b – lateral semi-distance between nominal contact on two rails]

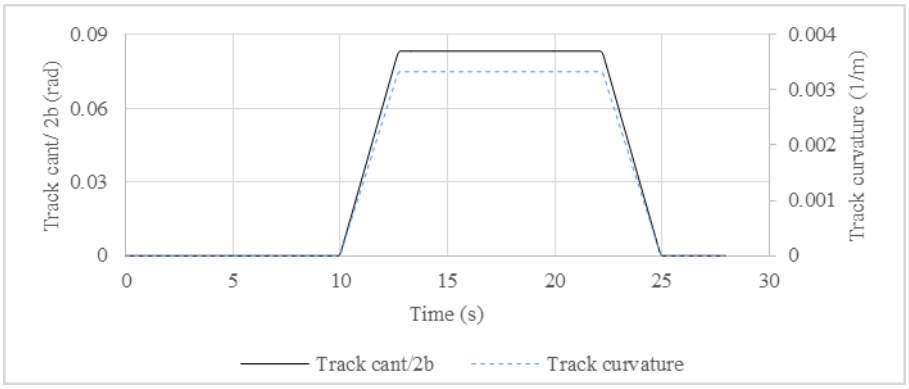

(a) Track geometry

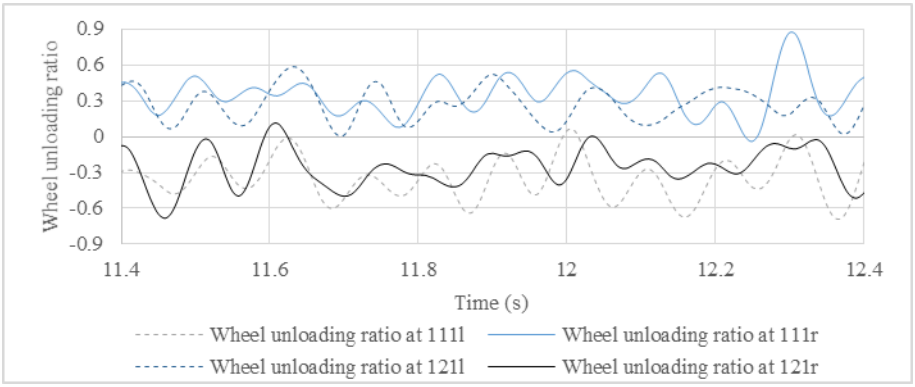

(b) Wheel unloading ratio near curve entry position

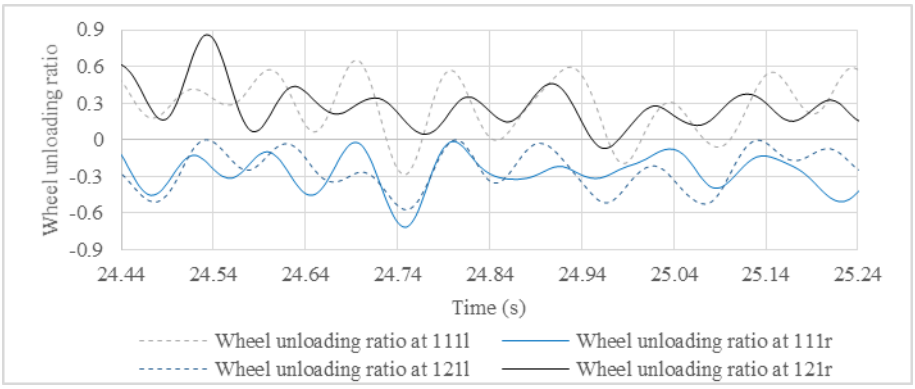

(c) Wheel unloading ratio near exit transition position

Figure 6-8: Effect of twist moment on transition negotiation (case 1 of step 2 tests on the RQTY wagon, Curve radius 300m, cant deficiency 110mm, FRA class 4 track irregularities, tare mass)

The high-speed conditions (cant deficiency of 110mm) generated higher wheel unloading ratios on the low rail (111r, 112r, 121r, 122r) than those on the high rail (111l, 112l, 121l, 122l) in both the cases 1 and 2 (Table 6-4). The L/V wheel ratios have been found to be higher on high rails in an empty condition which also indicates a higher lateral wheel load on the high rail as centripetal force moved the wheels towards flange contact on the high rail (case 1, Table 6-4). The loaded condition generated higher L/V wheel ratios on the high rails than those on low rails on the front bogie axles (111 and 112), but the opposite on rear bogie axles (121 and 122). The vertical load on the low rail at the rear bogie axles in the loaded condition (case 2) became low due to the combined effect of wagon dynamics and track irregularities. The length and positioning of irregularities affect the lateral and vertical load on the wagon wheelsets. In this thesis, detailed quantification of variation due to track irregularities is not included.

Of the four cases (Table 6-2), the maximum L/V wheel ratio (0.98 on the left wheel of the front axle of the front bogie, number 111l) was observed in case 3 (Table 6-4, Figure 6-10). Case 3 is a slow speed situation where the gravitational load is likely to dominate over the centripetal action. So, the low rail experiences higher vertical wheel load than the high rail. Low wheel load on the high rail (Left wheel on RHC) also means a higher lateral to vertical wheel load (L/V wheel) ratio on the left wheel such as occurred on wheels 111l and 121l in case 3 (Figure 6-10c).

Both the extreme L/V wheel ratios on wheel numbers 111l and 121l in case 3 occurred in the transition sections of the curve. It is also evident that the L/V ratio is higher on curved and transition sections than on the straight sections of the track (Figure 6-10c). The curved sections create larger variation in the vertical wheel loads on low and high rails which gives greater variation in wheel L/V ratio and wheel unloading ratio than those on the straight track sections.

The step 2 tests indicate that the RQTY wagon is capable of successfully negotiating a 300m radius track curve at the 110mm cant deficiency and 75mm cant excess speeds on a dry contaminated rail condition.

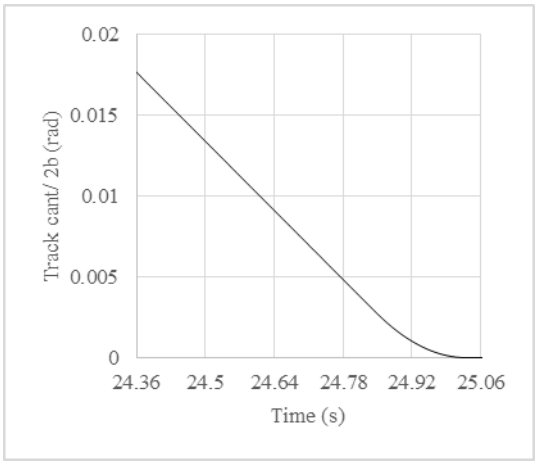

(a) Track cant at the exit transition

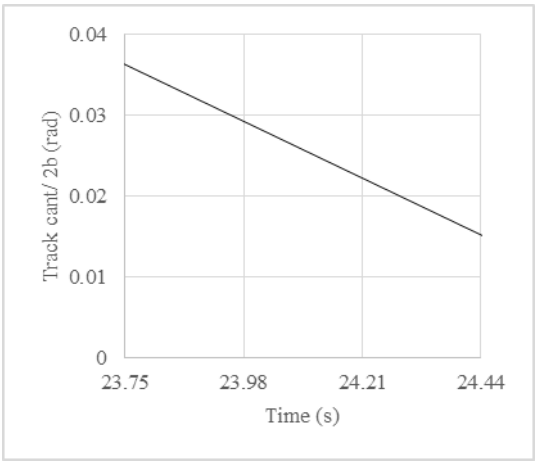

(c) Track cant near the high wheel unloading ratio on wheel #121r

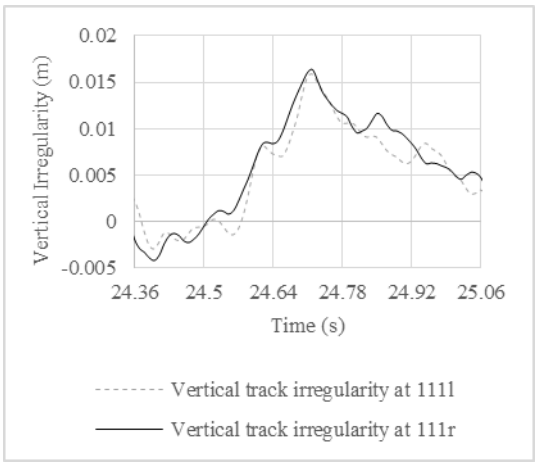

(b) Vertical track irregularity at the exit transition

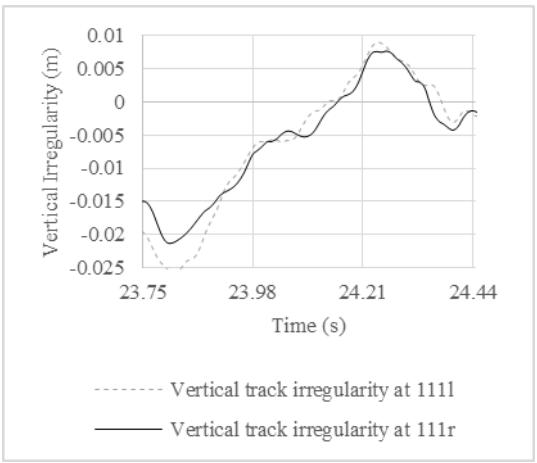

(d) Vertical track irregularity near the high wheel unloading ratio on wheel #121r

Figure 6-9: Effect of vertical irregularity and applied cant on curve negotiation test (case 1 of step 2 tests on the RQTY wagon, Curve radius 300m, cant deficiency 110mm, FRA class 4 track irregularities, tare mass)

Table 6-5: Effect of vertical irregularity and applied cant on curve negotiation test (case 1 of step 2 tests on the RQTY wagon, Curve radius 300m, cant deficiency 110mm, FRA class 4 track irregularities, tare mass)

	Front axle (#111) At the exit transition (25.06s)					
Time (s)	Wheel number	Vertical Irregularity (m)	Cant (m)	Position due to cant and vertical irregularity (m)	Position due to cant and vertical irregularity (mm)	Difference in rail height (mm) (1)
25.06	111r	0.00473	0	0.00473	4.7	1.4
25.06	111l	0.00335		0.00335	3.3	
24.36	121r	-0.0019	0.0266	0.01142	11.4	18
24.36	121l	0.0023		-0.00658	-6.6	
	At the position near a high wheel unloading ratio at wheel #121r (23.75s)					
Time (s)	Wheel number	Vertical Irregularity (m)	Cant (m)	Position due to cant and vertical irregularity (m)	Position due to cant and vertical irregularity (mm)	Difference in rail height (mm) (1)
24.44	111r	-0.00155	0.0228	0.00985	9.9	23.3
24.44	111l	-0.002		-0.0134	-13.4	
23.75	121r	-0.01495	0.0545	0.012275	12.3	32.4
23.75	121l	-0.00196		-0.02011	-20.1	

Note: (1) difference between right and left rail, positive displacement refers to downward

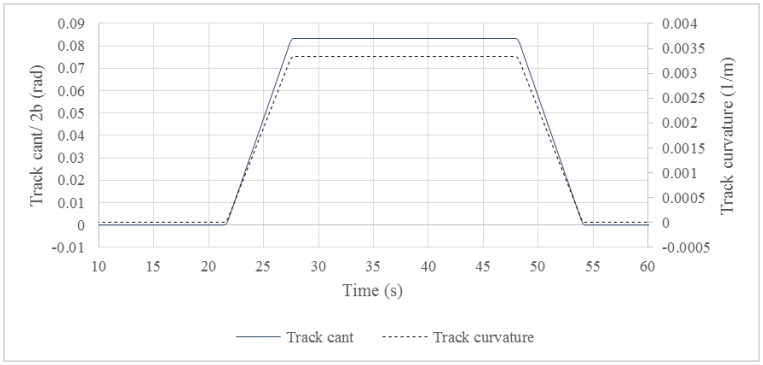

(a) Track geometry

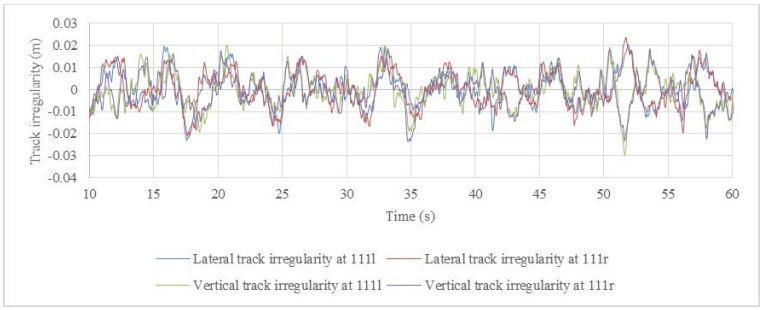

(b) Applied FRA track class 3 irregularities

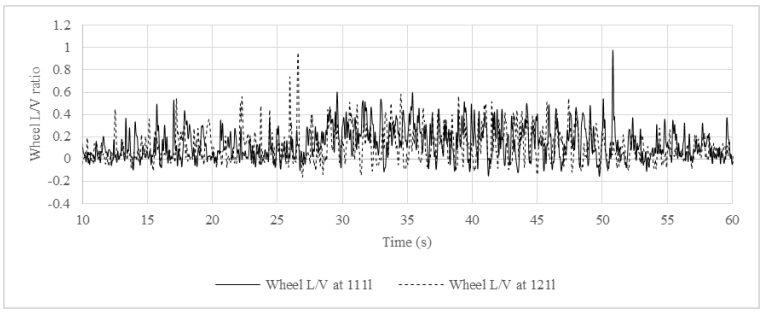

(c) Wheel L/V ratio

Figure 6-10: Case 3 of step 2 tests on RQTY (Curve radius 300m, cant excess 75mm, FRA class 3 track irregularities, tare mass)

6.4 Step 3- Hunting Test on a Long Track with Track Irregularities on the RQTY Wagon

Step 3 is a hunting test that includes track irregularities to assess operability of a wagon in the given track and operational conditions. According to the Australian standard AS7509, the hunting test aims to observe the derailment proneness at 110% of the design speed. This is to ensure that the design speed is less than the critical speed. Availability of accelerometers makes it possible for this to be assessed with physical tests and such a method uses lateral acceleration values measured near the bogie centres at the wagon floor level. The test can also be done using simulation.

The lateral acceleration values at the bogie centres are used in different standards to evaluate hunting [61, 119]. The Australian freight rollingstock standard (AS7509) allows an average peak lateral acceleration of 0.35g (3.43m/s^2) over 5s using a low pass filter with a cut-off frequency of 10Hz [61], determined by Equation 6-6 over a minimum of 5 seconds.

$$\boldsymbol{A = \frac{\sum_{i=1}^{M} Max\,(i) + Abs\left(\sum_{j=1}^{N} Min\,(j)\right)}{M+N}} \qquad \textbf{6-6}$$

where A is the average peak acceleration in units of 'g', M is the number of positive peaks (maxima) that occurred over a minimum 5 seconds evaluation period, N is the number of negative peaks (minima) that occurred over a minimum 5 seconds evaluation period, i and j are integers from 1 to M or N respectively, Max (i) and Min (j) are the magnitudes of the positive and negative peaks (g).

A 2 km straight track has been used for the hunting simulation. The speed is set at 10% above the speed board limit of 80km/h, i.e. 88km/h for the typical empty RQTY wagon operating on ARTC network track. In order to run the wagon at 88km/h, the track class should be corresponding to FRA class 4 or smoother quality (FRA class 5, 6 etc.). Two simulation tests have been performed on FRA class 4 and 5 tracks (Table 6-6).

Table 6-6: Step 3 tests on the tare RQTY wagon at speed of 88 km/h on FRA class 4 and 5 tracks on a 2km track section

FRA track class	Numerical integrator (Backstep control Y/N)	Maximum L/V wheel								Maximum L/V axle			
		111l	111r	112l	112r	121l	121r	122l	122r	111	112	121	122
4	N	0.54	0.5	0.45	0.48	0.49	0.49	0.49	0.53	0.81	0.75	0.73	0.76
5	N	0.27	0.25	0.2	0.19	0.23	0.16	0.17	0.16	0.46	0.3	0.29	0.27
4	Y	0.54	0.53	0.45	0.45	0.49	0.52	0.49	0.51	0.81	0.73	0.78	0.74
FRA track class		Maximum Wheel unloading ratio								Maximum Lateral acceleration (m/s^2)		Maximum Vertical acceleration (m/s^2)	
		111l	111r	112l	112r	121l	121r	122l	122r	ay1	ay2	az1	az2
4	N	0.7	0.69	0.53	0.88	0.69	0.67	0.43	***1.02***	3.37	***3.72***	3.55	3.18
5	N	0.33	0.34	0.28	0.31	0.36	0.38	0.27	0.29	1.96	1.75	5.42	4.61
4	Y	0.60	0.56	0.44	0.56	0.56	0.56	0.57	0.46	3.03	***3.91***	5.46	6.28

Note: Y- with backstep control, N- without backstep control, the shaded cells are outside the vehicle acceptance criteria as discussed in Chapter 5

All values of derailment parameters and accelerations were within the acceptable limits except the wheel unloading ratio at the rear right wheel of the rear bogie (wheel # 122r, Table 6-6). A further investigation of the values of wheel unloading ratio at 122r showed that there was a high wheel unloading ratio at around 23s (Figure

6-11b). Considering the moderate track condition (lateral and vertical track irregularities about 15mm leftward and 5mm upward respectively, Figure 6-11a) and no pattern of hunting near 23s, the unusual value may be generated from numerical instability. So, a further simulation test was performed using a two-step Runge Kutta integrator with backstep control instead of the two-step Runge Kutta integrator without any back-step control (Figure 6-11b).

The two-step Runge Kutta integrator with backstep control showed a reduced wheel unloading ratio of about 0.46 in place of 1.02 found with the two-step Runge Kutta integrator without any backstep control (Figure 6-11b). The change of numerical integrator changed all other derailment parameters (Table 6-6). The maximum lateral acceleration on the rear bogie (3.91m/s^2) was still greater than the acceptable limit of 3.43m/s^2 (Table 6-6). A further calculation was performed to measure average peak acceleration over 5s as mentioned in the AS 7509 standard. The peak acceleration values on the rear bogie were obtained as local maxima and minima values (Figure 6-12). The maximum value of the average acceleration over 5s was found as 0.8m/s^2 which is within the acceptable limit of the AS7509 standard. As the average lateral acceleration values obtained over ≥5s was within the acceptable limits (0.35g) it can be stated that the RQTY showed acceptable performance in the context of hunting tests on class 4 track at 80km/h speed based on the tests performed in this section.

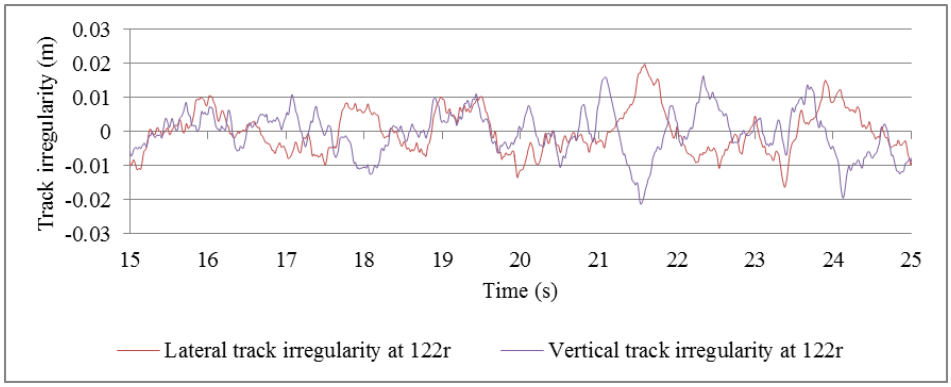

(a) Applied FRA track class 4 track irregularity

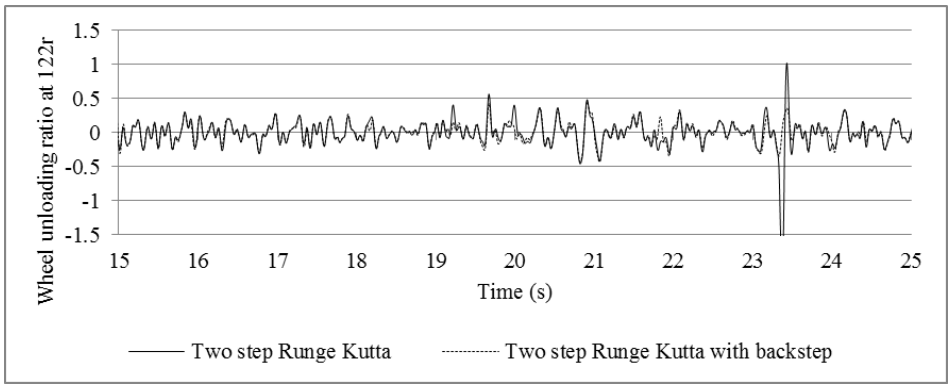

(b) Wheel unloading ratio using a Runge Kutta numerical integrator with and without backtep control

Figure 6-11: Step 3 tests on RQTY wagon (straight track, tare wagon, speed 88 km/h, FRA track class 4)

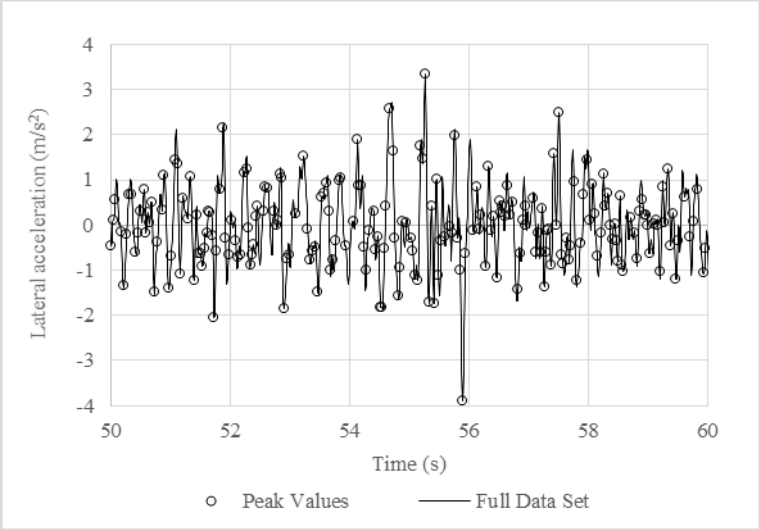

Figure 6-12: Peak value analysis of lateral acceleration at the rear bogie centre (ay2)

6.5 Rerun of Steps 1 and 2, Due to Change in Numerical Integrator

Having found an abnormal value in the wheel unloading ratio with the computationally cheaper two-step Runge Kutta solver without backstep control, it is required to rerun the first two steps with the better solver- Runge Kutta solver with backstep control. To reduce simulation effort, the step 2 tests were not simulated at this stage as the curved track of step 2 tracks can also be evaluated in step 5 tests having isolated track defects on the curved section. Only step 1 is performed at this stage with the two-step Runge-Kutta solver having backstep control (Figure 6-13). The numerical integrator with the backstep control did not change the step 1 outcome significantly. In step 1, no track irregularities were added which is why the simpler solver was used successfully.

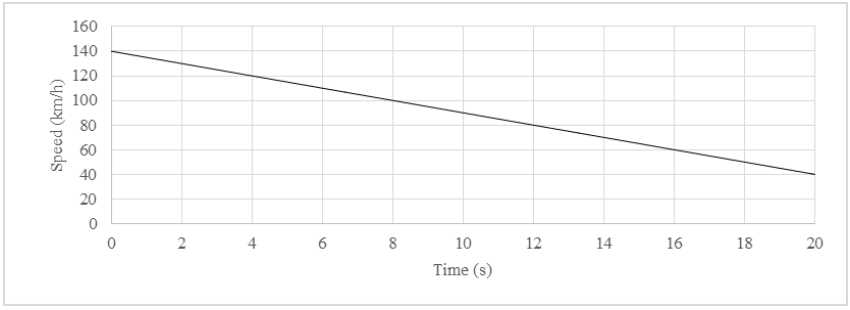

(a) Decreasing velocity

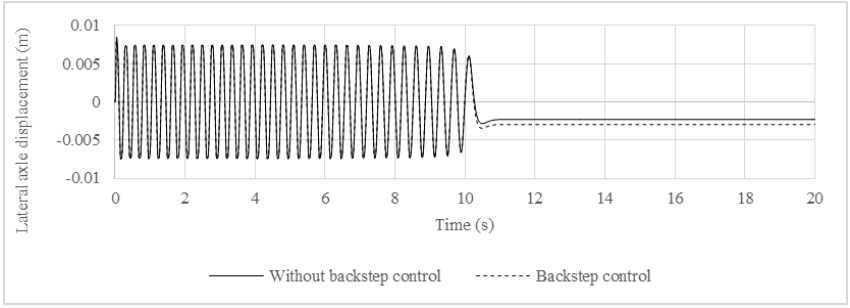

(b) Lateral axle displacement

Figure 6-13: Rerun of step 1 test on RQTY wagon with and without backstep control of the two-step Runge-Kutta integrator

6.6 Step 4- Cyclic Track Defect Tests on the RQTY Wagon

Cyclic track defects are used to test the adequacy of suspension damping of a vehicle as per the AS7509 requirement. For the pitch test, the test track has been chosen with a cyclic vertical defect wavelength of twice the BCD which will ensure one bogie to be at the highest and another bogie to be at the lowest point on the track defect to replicate the worst pitch situation (Figure 6-14a and Figure 6-14b). For the bounce test, the worst case situation would be having a cyclic vertical track defect with the wavelength of the same length as the BCD (Figure 6-14c and Figure 6-14d). The harmonic roll assessment is carried out to observe the vehicle's ability to negotiate a track that has a series of cyclic vertical irregularities on both rails as specified by AS7509. The two rails have different irregularity positions in the harmonic roll mode (Figure 6-14e). At least three irregularities in one rail and two irregularities on the other rail were provided as per the Australian Standard AS 7509 [61]. The positioning of irregularities on both rails has been intended to generate a rolling resonant response from the vehicle at a speed that corresponds to resonant frequency. The vertical track irregularities for the harmonic roll assessment are either all humps or all dips, positioned at 180^0 phase difference between the two rails (Figure 6-15) [61].

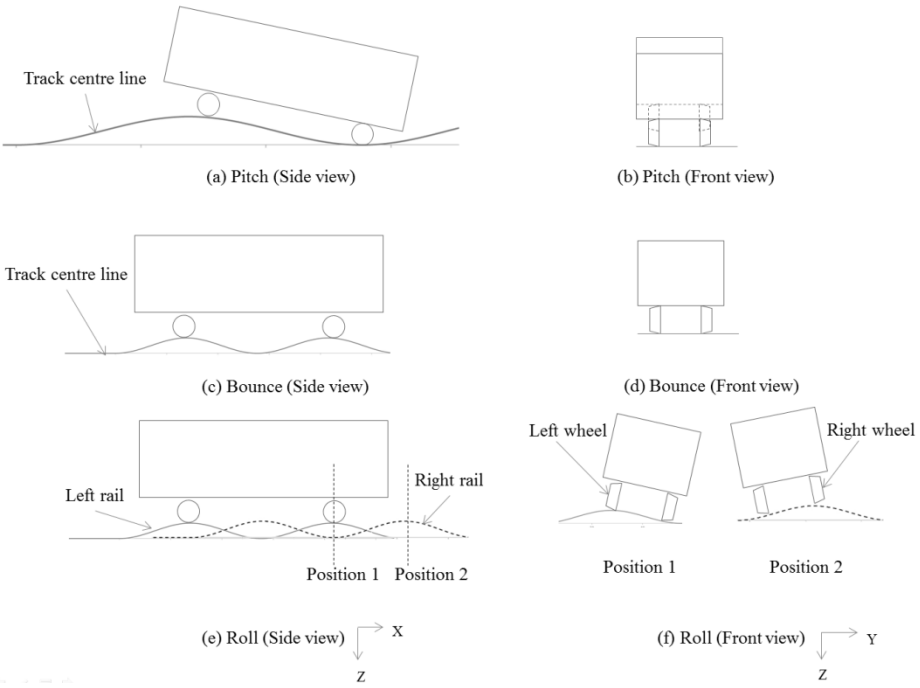

Figure 6-14: Track arrangement for cyclic track defect test

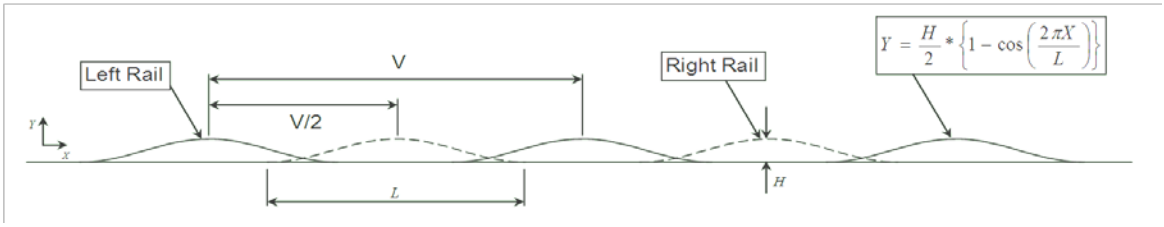

Figure 6-15: Harmonic roll assessment [61] (Note: wavelength V is the BCD of the wagon)

The size of track defect geometry was chosen as per the track defect type method developed in section 5.3.3. The type D cyclic defects (as it represents an extreme case as discussed in Section 5.3.3) were applied on the RQTY

wagon. The equivalent defect amplitudes (a method developed in section 5.3.2) obtained for the bogie centre distance of 14.93m of the RQTY wagon are 22m and 36mm (40% of the equivalent P1 limits) for the bounce and the pitch mode respectively for a service speed of 80km/h. The track was chosen without any other irregularities as they may damp out resonance.

The velocities corresponding to resonant responses obtained from the natural frequency of the RQTY wagon and BCD parameters (Equations 5-4 to 5-7) were all found to be greater than or equal to 104 km/h for bounce, pitch and roll motions in both the empty and loaded conditions. All resonance velocities were, therefore, higher than the design speed of 80 km/h for the considered wagon (Table 6-7). So, the speed for evaluation was chosen as 110% of the design speed as per the AS 7509 standard, i.e. 88 km/h in this case.

Table 6-7: Resonance frequencies and velocities for the RQTY wagon (BCD of 14.93m, Overhang length of 2.132m)

Load conditions	Natural frequency (Hz)			Resonant velocity (km/h)		
	Vertical	Pitch	Roll	Bounce	Pitch	Roll
Empty wagon	5.54	7.79	5.58	298	419	300
Loaded wagon	2.02	2.72	1.95	107	145	104

A total of 6 simulation cases were performed to check derailment criteria and wagon body accelerations on cyclic track defect tests (Table 6-8). The results showed that all the simulation cases passed the vehicle acceptance parameters (Table 6-9). The bounce resonant velocity based on the suspension and wagon length parameters for case 2 (loaded conditions, bounce mode) is 107 km/h (Table 6-7) which is higher than the test speed of 88 km/h, so resonance will not occur. An example plot showing a variation of wheel load along the applied cyclic track defect (bounce mode) is given in Figure 6-16. As long as all the parameters remain within acceptable values, such a pattern would be considered acceptable for the wagon.

Table 6-8: Simulation cases for the Step2 tests on the RQTY wagon

Case	Load (kg)	Test Mode
1, 2	0, 72000	Bounce
3, 4	0, 72000	Pitch
5, 6	0, 72000	Roll

Table 6-9: Simulation results for step 4 tests on the RQTY wagon at speed of 88 km/h, track without any irregularity, Type D Track defects

Case	Maximum L/V wheel								Maximum L/V axle			
	111l	111r	112l	112r	121l	121r	122l	122r	111	112	121	122
1	0.07	0.07	0.08	0.08	0.07	0.07	0.08	0.08	0.15	0.15	0.15	0.15
2	0.05	0.05	0.06	0.06	0.05	0.05	0.06	0.06	0.1	0.11	0.11	0.12
3	0.07	0.07	0.07	0.07	0.07	0.07	0.07	0.07	0.13	0.13	0.13	0.13
4	0.05	0.05	0.05	0.05	0.05	0.05	0.05	0.05	0.1	0.1	0.1	0.1
5	0.1	0.1	0.07	0.07	0.1	0.11	0.07	0.07	0.07	0.07	0.07	0.07
6	0.11	0.16	0.12	0.16	0.08	0.12	0.09	0.13	0.07	0.07	0.06	0.06
Case	Maximum Wheel unloading ratio								Maximum Lateral acceleration (m/s^2)		Maximum Vertical acceleration (m/s^2)	
	111l	111r	112l	112r	121l	121r	122l	122r	ay1	ay2	az1	az2
1	0.12	0.12	0.12	0.12	0.12	0.12	0.12	0.12	0	0	1.17	1.17
2	0.42	0.42	0.42	0.42	0.42	0.42	0.43	0.43	0	0	4.4	4.43
3	0.08	0.08	0.08	0.08	0.08	0.08	0.08	0.08	0	0	0.42	0.54
4	0.15	0.15	0.15	0.15	0.15	0.15	0.15	0.15	0	0	0.54	0.54
5	0.29	0.27	0.32	0.25	0.31	0.27	0.29	0.26	1.19	1.19	0.26	0.39
6	0.36	0.26	0.35	0.23	0.33	0.21	0.33	0.2	2.91	1.85	0.68	0.96

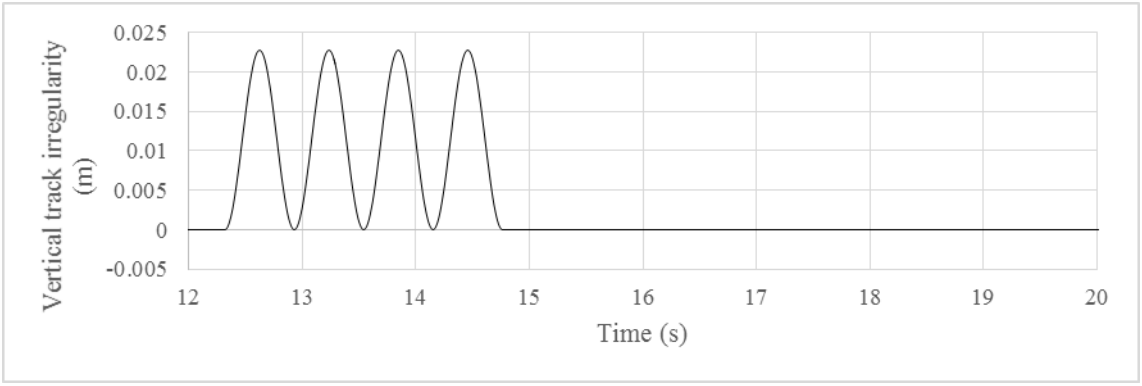

(a) Vertical cyclic track defects

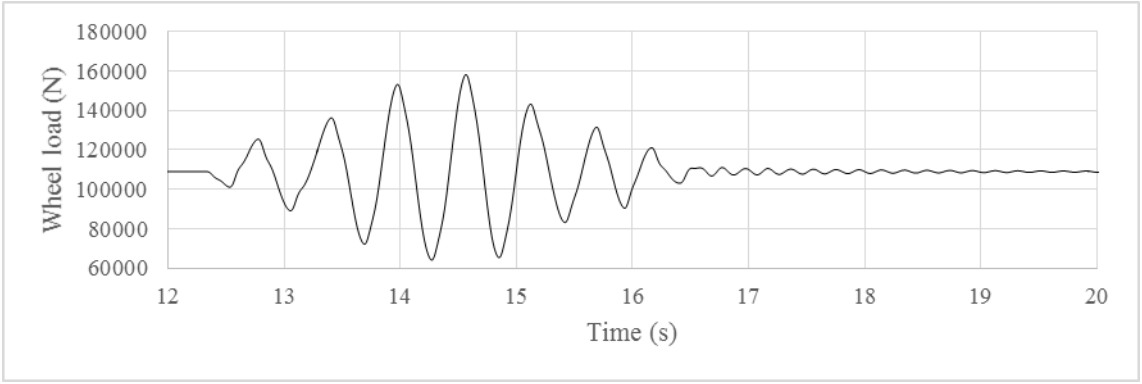

(b) Wheel loads corresponding to positions of the applied vertical cyclic track defects

Figure 6-16: Case 2 (bounce test on loaded wagon) of the step 4 tests on the RQTY wagon

6.7 Step 5- Isolated Track Defect Tests on the RQTY wagon

An isolated track defect is a large defect at a single location on the track. An isolated track defect can be vertical (dip), lateral (kink on a curve) or any combination such as horizontal alignment and superelevation. Vertical, lateral and twist track defects have been considered for assessment of the vehicle taking guidance from AS 7509.

The isolated vertical track defect can occur in the form of the flat hump (e.g., at a level crossing) or vertical dip (e.g., local subsidence due to poor drainage, ballast pumping, ballast sinking into the soil below etc.). Vertical track defects could occur on one rail or both rails.

The lateral track defects generally occur on both rails at the same time. So, there is no change in relative position of the rails with respect to one another and both right and leftward curves would produce similar dynamics. The lateral track defects have been applied on both the outward (curve sharpening) and inward (curve flattening) direction on a curved track.

In addition to the vertical and lateral track defects, long and short twist track defects may also be present in the track and are included in the standard of the ARTC network operator [55]. Twists are the variation in height between the two rails along relatively short lengths of the track. In the simulation, twists have been provided on the track by introducing a dip defect on one rail only.

The Australian standard AS7509 presents sample track parameters for the isolated track defect test (Figure 6-17, Figure 6-18) but it is also mentioned that the dimensioning of track defects could need to be changed if further research shows different requirements [61].

The ARTC track standard does not limit positioning of the isolated track defects which then raises speculation regarding the potential presence of such track defects on any section of track including curved sections. Of the different isolated track defects, the hump is expected to occur on straight sections only due to the fact that the cause of a flat hump is the presence of a level crossing. Logically a hump needs to be evaluated for a straight section of a track only as per AS 7509. The other isolated defects such as vertical dip, lateral and twist tests have been applied on a curved section of a track in simulation to provide the worst-case scenarios with the additional dynamics due to the height difference between the two rails and centrifugal inertia, body roll, steering etc.

Figure 6-17: Flat hump [61]

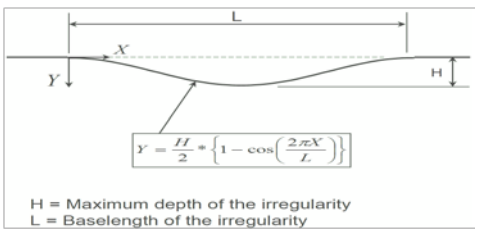

Figure 6-18: Vertical dip [61]

The Type A track defect (as AS7509 standard and ARTC track geometry standard) approach as per the method developed in section 5.3.3 has been considered as a starting point to test the RQTY wagon. The wavelength and amplitudes of the Type A track defect geometry for the isolated track defect test are shown in Table 6-10.

Table 6-10: Isolated track defect limits for test purpose (20% above the ARTC P1 limits [55] as per the AS7509 recommendations, Type A track defect as per the methodology section)

Type of an isolated track defect	Wavelength of track defect (m)	Speed (km/h)				
		40	60	80	100	115
		Amplitude of track defect (mm)				
Lateral	10	52.8	52.8	40.8	28.8	21.6
Vertical	20	85.2	85.2	79.2	67.2	61.2
Long twist Non transition	14	72	72	62.4	55.2	48
Long twist transition	14	76.8	76.8	66	58.8	50.4
Short twist	2	21.6	21.6	19.2	16.8	14.4

The isolated lateral, vertical and twist track defects have been applied on the curved section of a 300m radius curved track. Initially, thirteen simulation cases with different isolated track defects and loads have been performed to obtain a reasonable test condition (Table 6-11). Four different modes of operations are listed- P- isolated lateral and vertical track defects on both rails of a curved track; Q- isolated twist, DIP on the low rail of a curved track; R- isolated twist, DIP on the high rail of a curved track; S- isolated twist on a straight track.

In the case of the isolated vertical track defect (Mode P), vertical track defects on both rails were considered. The straight track tests on the lateral and vertical track defects were not considered necessary as the wagon was required to pass the same defects test on a curve. In the case of an isolated vertical track defect on one rail, the defect creates a twist type defect which is included in Mode Q and Mode R on curved track (Figure 6-19). In the case of the twist track defect test, the track defect on a straight track (Mode S) was also performed as twist track defects on a curved track produce a derailment outcome.

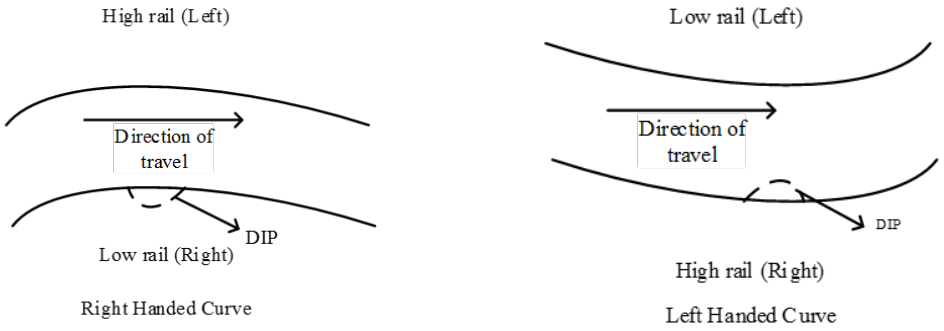

(a) Mode Q- DIP on low rail (b) Mode R- DIP on high rail

Figure 6-19: Schematics test modes to apply isolated track defects on a curved section

Table 6-11: Simulation cases for the step 5 tests on the RQTY wagon

Case	Load (kg)	Test Mode	Track	Track radius (m)	Speed (km/h)	Track irregularities
1, 2	0, 72000	P	1	300	77.23	FRA5
3, 4	0, 72000	P	1	-300	77.23	FRA5
5	0	P	1 (Reduced track defect)	-300	77.23	FRA5
6, 7	0, 72000	Q	2	300	77.23	FRA5
8, 9	0, 72000	R	2	-300	77.23	FRA5
10, 11	0, 72000	Q	2	300	77.23	FRA6
12, 13	0, 72000	R	2	-300	77.23	FRA6
14, 15	0, 72000	S	2	Straight	88	FRA5
16	0	S	2	Straight	88	FRA6

Note: P- isolated lateral and vertical track defects on both rails of a curved track; Q- isolated twist, DIP on the low rail of a curved track; R- isolated twist, DIP on the high rail of a curved track; S- isolated twist on a straight track. Track 1- isolated lateral, vertical track defects and a flat hump and Track 2- long and short twists

Two different tracks have been considered to add different isolated track defects in the simulation. The first track (Track 1) contains isolated lateral and vertical track defects and a flat hump (Figure 6-20) and the second track (Track 2) contains long and short twists (Figure 6-26). A 300m radius track curve was superimposed on the first track such that the isolated lateral, vertical and twist track defects fall within the curved section of the track. The isolated track defects were provided at adequate separation distances (100-300m apart in different cases) to give wagon dynamic responses time to settle before a new defect is confronted. The curve radius was changed to the leftward direction (negative radius, cases 3, 4, 5, 8, 9, 12 and 13) to allow the track defects to occur in the opposite mode from that of the initial rightward (positive radius, cases 1, 2, 6, 7, 10 and 11) direction. By changing the direction of the track curve, the isolated vertical defect on the high rail was thus converted to a vertical track defect on the low rail, and the lateral track defect initially towards the outside of the curve (sharpening, cases 1 and 2) was thus converted to towards the inside of the curve (flattening, cases 3, 4 and 5).

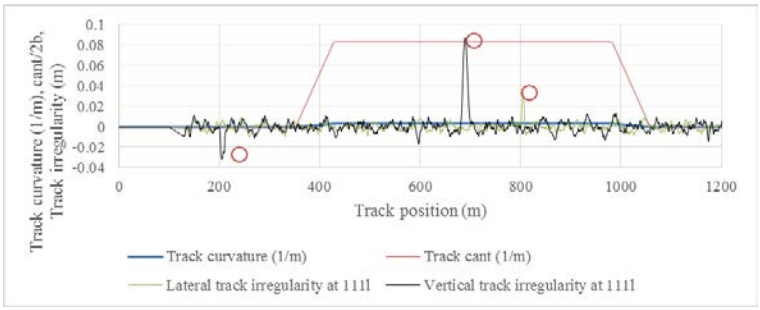

(a) Track geometry, isolated track defects and superimposed FRA track class 5 irregularities

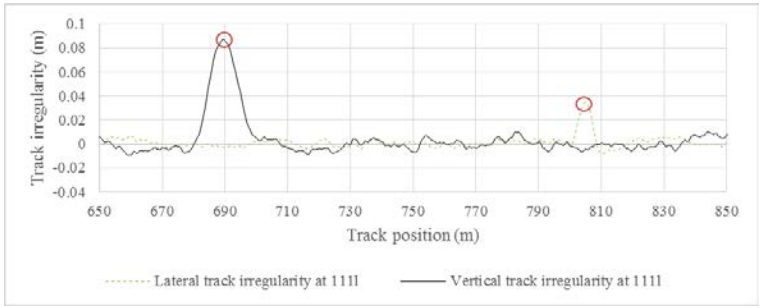

(b) Applied isolated lateral and vertical track defects with the FRA track class 5 irregularities

Figure 6-20: Track 1 containing a vertical hump, isolated vertical and lateral irregularities superimposed with FRA class 5 track irregularities corresponding to P1 limits of 80km/h (circles indicate the peaks of the applied isolated track defects)

The RQTY wagon passed the test with the applied hump, vertical and lateral track defects on both rails when the vertical defect was provided as a DIP and the lateral track defect was provided as a sharpening of the curve (cases 1 and 2, Table 6-12). The lateral track defects in cases 3 and 4 provided curve flattening affect. The RQTY wagon showed an unacceptable L/V ratio of 1.02 at the front axle of the rear bogie (#121r) in the empty condition (Case3, Figure 6-21). The unacceptable L/V ratio occurred near the point of the isolated lateral track defect (Figure 6-21a, Figure 6-21c) corresponding to the Type A defect limit for the 80km/h test speed (40.8mm over 10m wavelength) as per Table 6-10. Due to the isolated lateral track defect of 36.8mm at about 38s (case 5, Figure 6-22a), the lateral load on wheel number 121r reached to approximately 29.3kN (case 5, Figure 6-22b) corresponding to a vertical wheel load of about 27.13kN which creates an unacceptable wheel L/V ratio. In the case of a flattening type lateral track defect (cases 3, 4), the lateral wheel creep forces increase because the wheel moves closer to the gauge face. The standard tests being too severe for the RQTY wagon then led to establishing a datum case with reduced amplitude of allowable lateral track defect. As a trial, the isolated lateral track defect corresponding to the Type A defect limit for 115km/h was chosen which reduces the lateral track defect to 21.6mm from 40.8mm in case 3 (Table 6-10) which then reduced the lateral load to 20.2kN (case 5, Figure 6-22b) and thereby reduced the wheel L/V ratio to an acceptable level of 0.75 on wheel #121r (case 5, Table 6-12).

Cases 6, 8 and 9, i.e. a twist track defect having a DIP on the low rail for the empty condition (case 6) and a twist track defect having a DIP on the high rail on both the empty and loaded conditions (cases 8 and 9) fail on the wheel unloading ratio criterion (Table 6-12).

The wheel unloading ratio on a loaded wagon can be less than that of an empty wagon due to the additional vertical load on the wheels of the loaded wagon. Case 6 for an empty wagon failed on wheel unloading ratio on the front right wheel (i.e. on the low rail) of the first bogie at the short twist track defect corresponding to a DIP on the low rail (Figure 6-23a, Figure 6-23b, Figure 6-23c), but case 7 for a loaded wagon passed the twist track defect on the low rail (Figure 6-24).

As the wagon was running at a speed corresponding to the 110mm cant deficiency, the centrifugal action pushed the wagon towards the high rail and, in combination with the torsional moment on the rigid wagon body created by unequal wheel loads, a high wheel unloading ratio occurred on the low rail.

In the case of the DIP on the high rail (cases 8, 9), both the empty and loaded conditions failed to meet the acceptance criteria. The DIP on the high rail (Figure 6-25a) lowered the vertical position of the wheel on the high rail which then further reduced the wheel load on the low rail (1.5kN on #111l) (Figure 6-25c) due to the rollover tendency along the high rail at a speed with cant deficiency. The reduced wheel load on the low rail created an unacceptable wheel unloading ratio on the low rail (Case 9, Wheel #111l, Table 6-12).

As for determining a reasonable test parameter in this thesis, a further run of simulations was performed using the FRA class 6 track irregularities on the curved track (Cases 10-13 in Table 6-10). The FRA class 6 track, although it reduced the long twist track defect to 67mm, failed to create a reasonable outcome for the wagon. Further simulations were carried out on a straight track using FRA class 5 irregularities and a twist track defect (Cases 14, 15) to establish a datum test condition that the RQTY wagon passed.

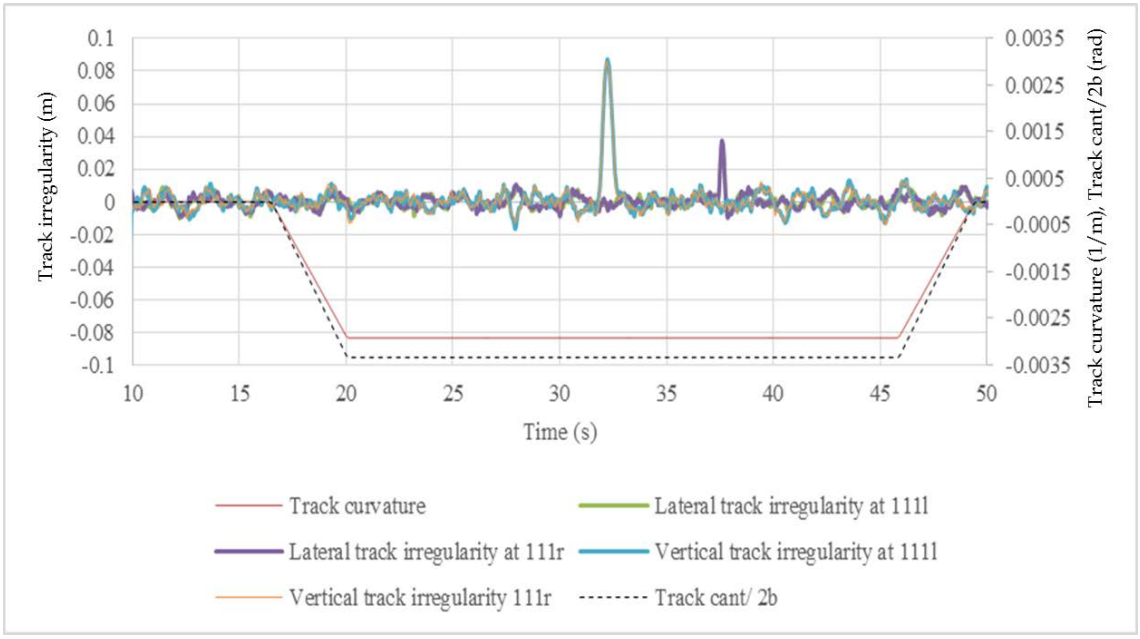

(a) Track geometry, isolated track defects and superimposed FRA track class 5 irregularities

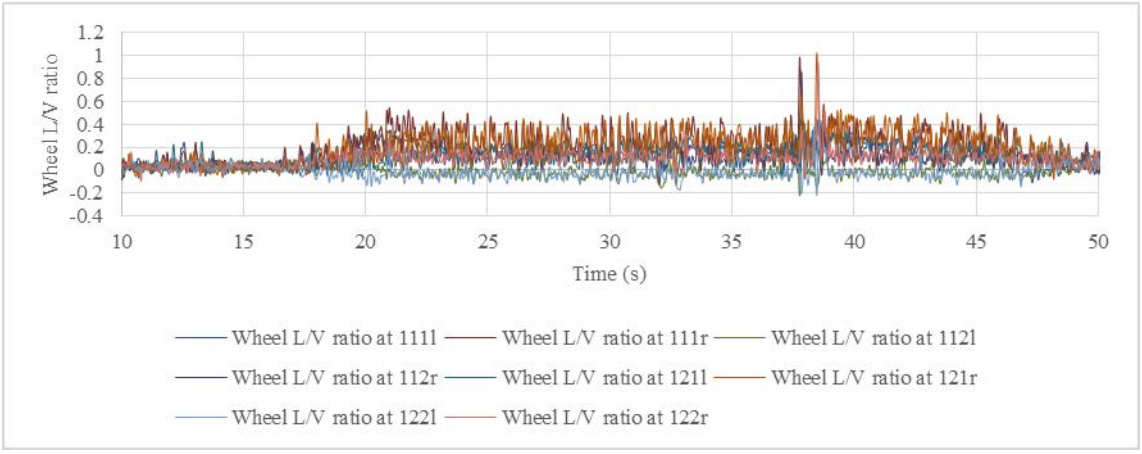

(b) Wheel L/V ratio

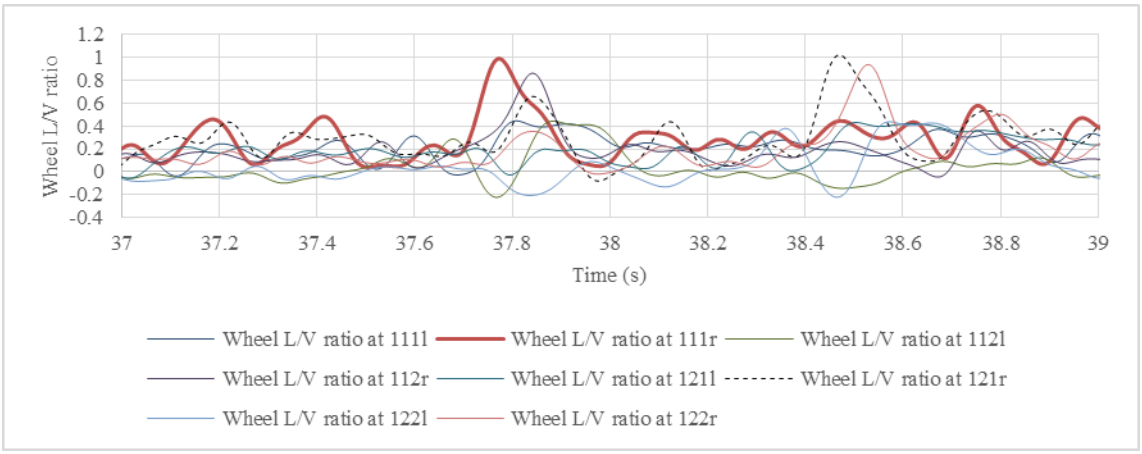

(c) Wheel L/V ratio near isolated lateral track defect

Figure 6-21: Wheel L/V ratio in case 3 (Lateral track defect towards inside of the curve, vertical track defect as a top defect on both rail) of step 5 tests on RQTY wagon

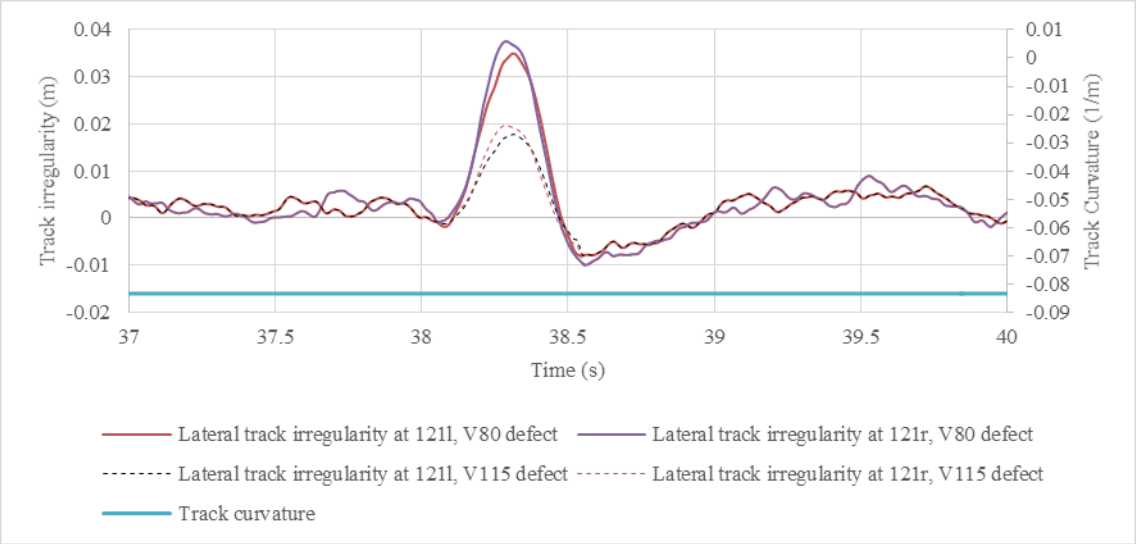

(a) Track geometry near isolated lateral track defect

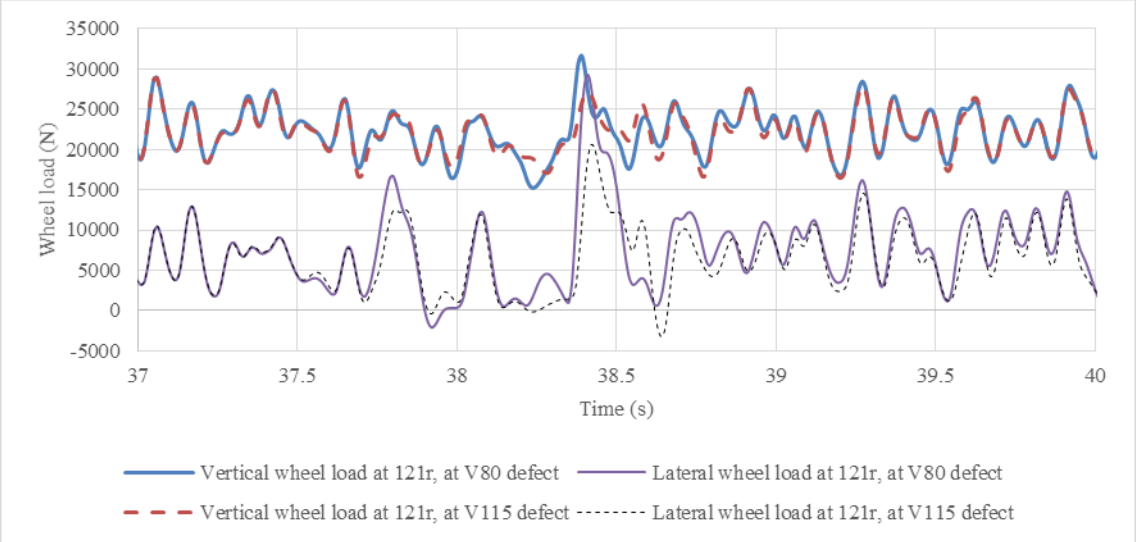

(b) Wheel loads near isolated lateral track defect

Figure 6-22: Effect of lateral track defect on wheel lateral and vertical load (Cases 3- V80 and 5- V115 of step 5 tests on RQTY wagon, Empty condition)

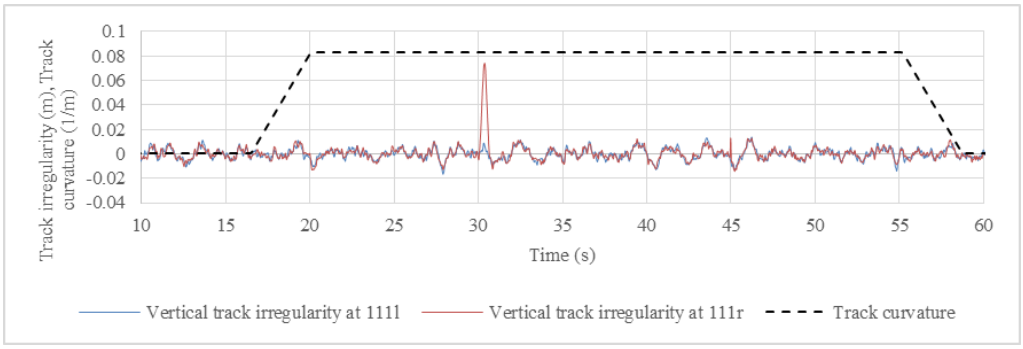

(a) Track geometry, isolated track defects and superimposed FRA track class 5 irregularities

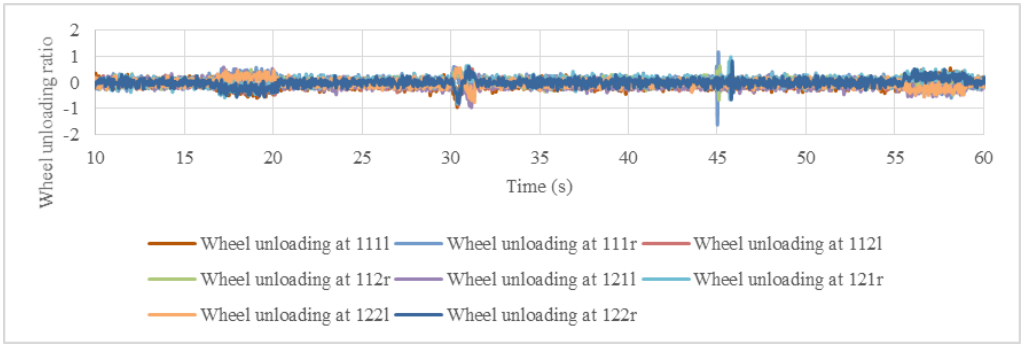

(b) Wheel unloading ratio

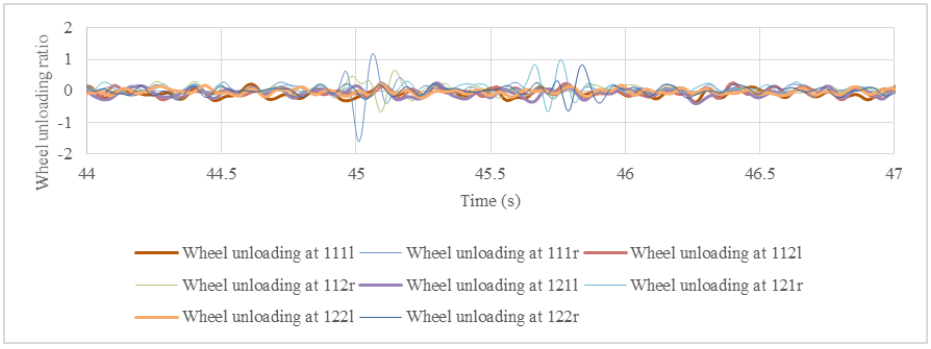

(c) Wheel unloading ratio near a short twist track defect

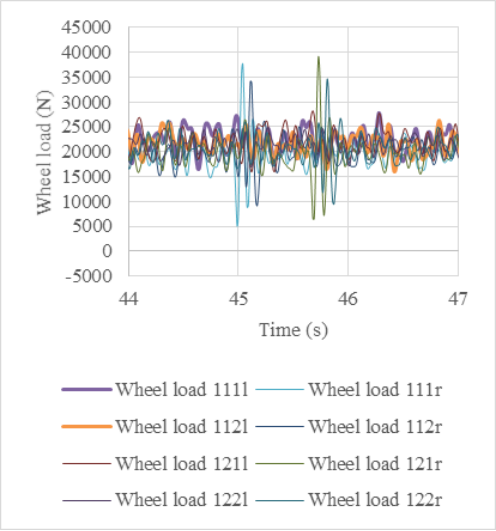

(d) Wheel load near a short twist track defect

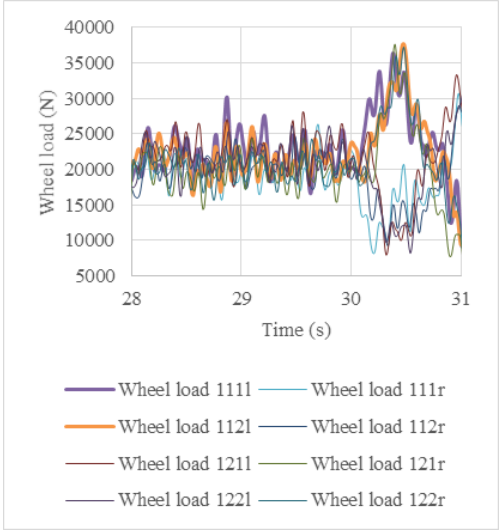

(e) Wheel load near a long twist track defect

Figure 6-23: Case 6 of step 5 tests on the RQTY wagon (Isolated twist track defect test, Empty condition, DIP on low rail, FRA class 5 track)

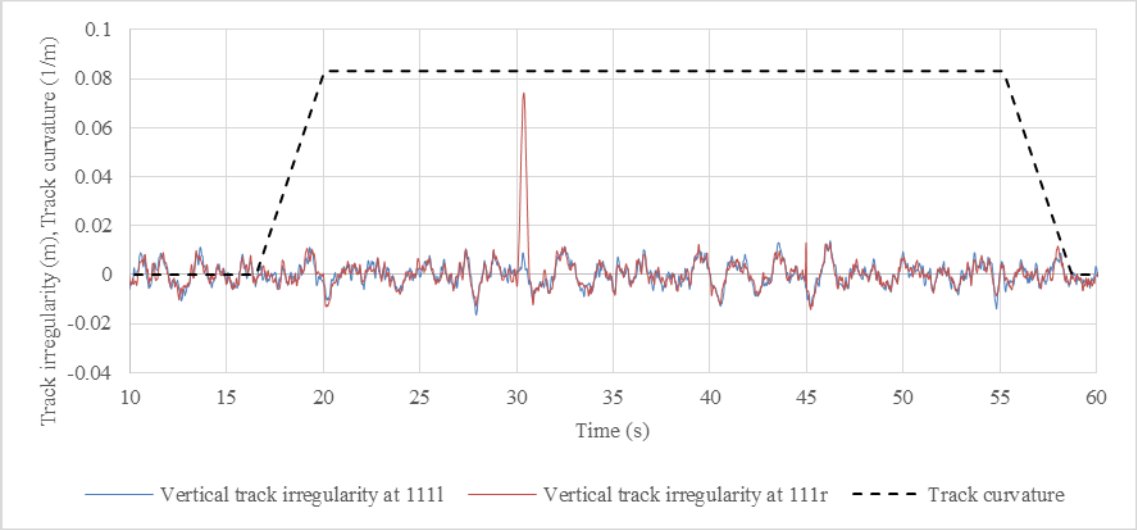

(a) Track geometry, isolated track defects and superimposed FRA track class 5 irregularities

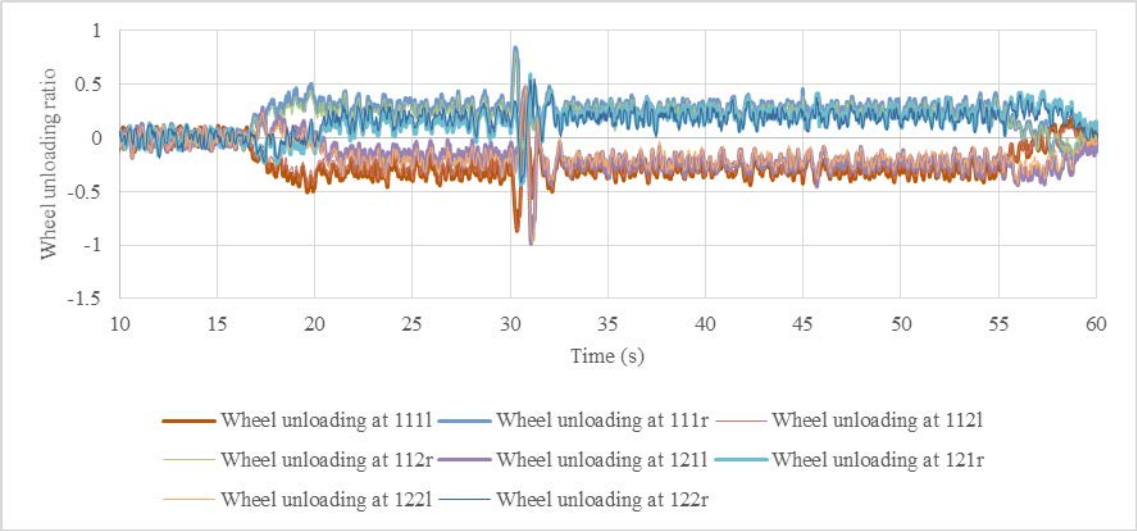

(b) Wheel unloading ratio

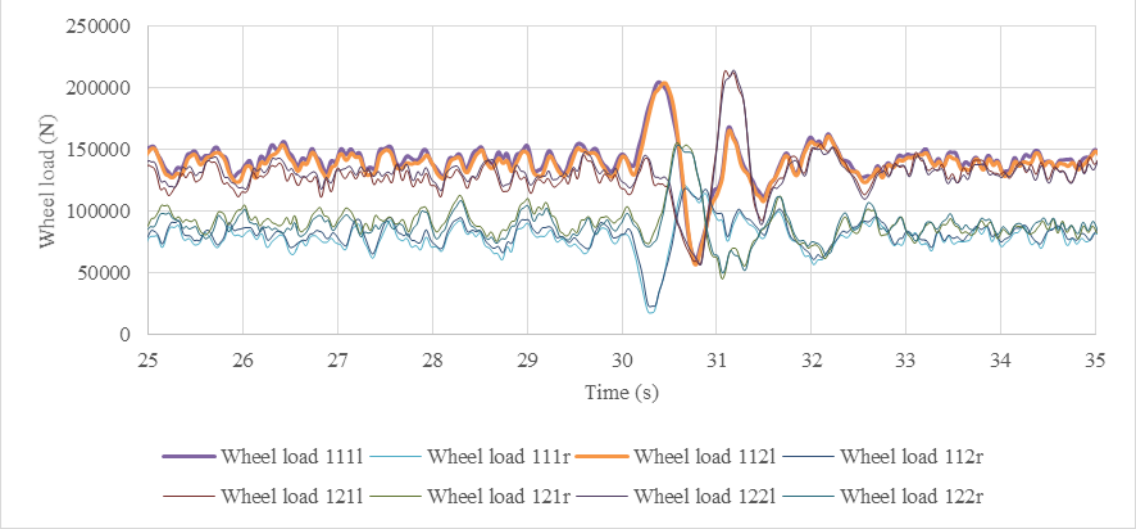

(c) Wheel load near an isolated long twist track defect

Figure 6-24: Case 7 of step 5 tests on the RQTY wagon (Isolated twist track defect test, loaded condition, DIP on low rail, FRA class 5 track)

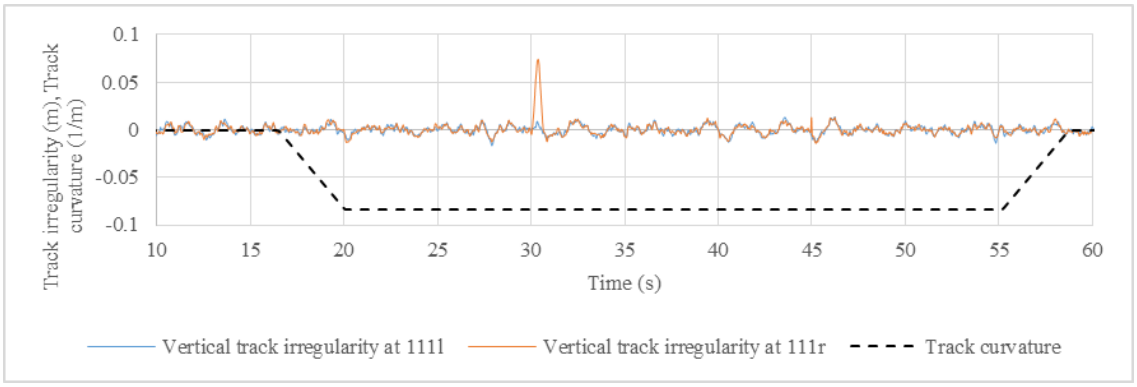

(a) Track geometry, isolated track defects and superimposed FRA track class 5 irregularities

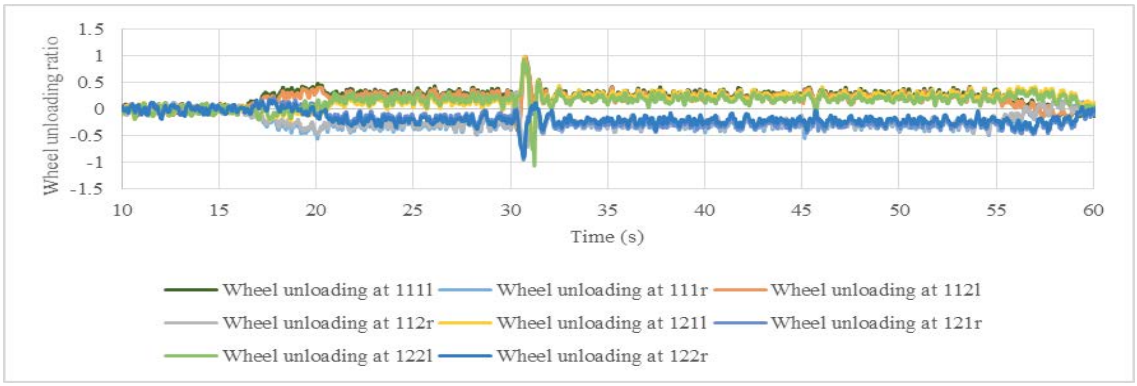

(b) Wheel unloading ratio

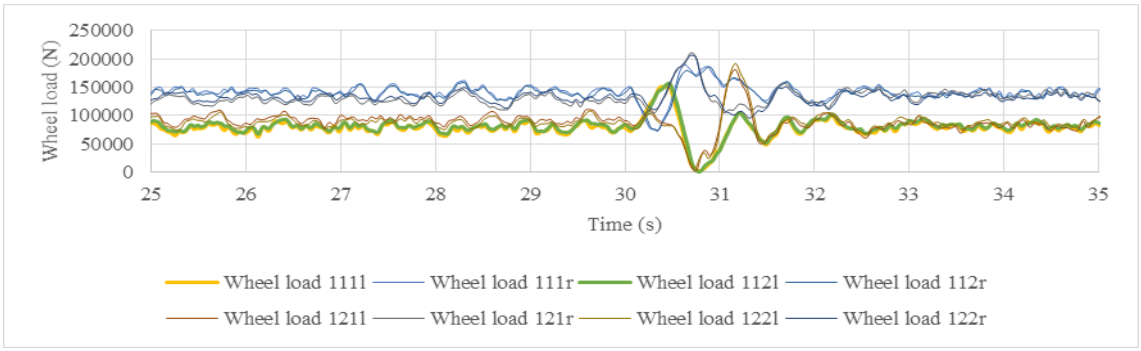

(c) Wheel load near an isolated long twist track defect

Figure 6-25: Case 9 of step 5 tests on the RQTY wagon (DIP on high rail, loaded condition, FRA class 5 track)

The loaded condition passed the tests (Case 15). But the empty condition (Case 14) failed to pass the test on wheel unloading ratio at the rear right wheels at the long twist defect (Figure 6-27b). The superimposed FRA class 5 track irregularities (Case 14) were then changed to FRA class 6 (Case 16). The FRA class 6 reduced the amplitude of twist track defect to 69.2mm from 74mm on the FRA class 5 track. The reduced amplitude of the twist track defect due to smoother superimposed FRA class 6 track irregularities improved the dynamics of the wagon and Case 16 passed the acceptance criteria (Table 6-12). Thus, the twist test on a straight track with FRA class 6 track irregularities was adopted as a datum test condition.

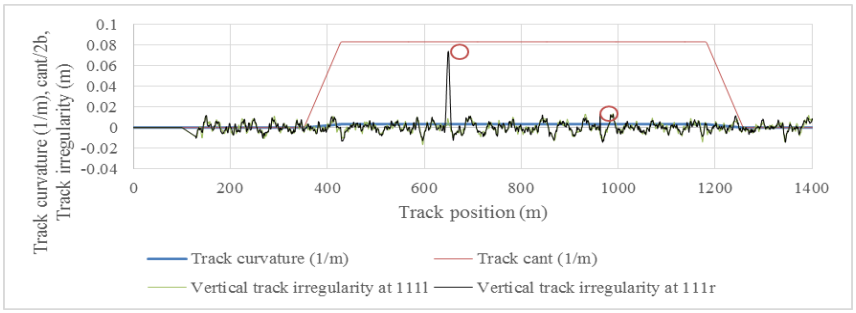

(a) Track geometry

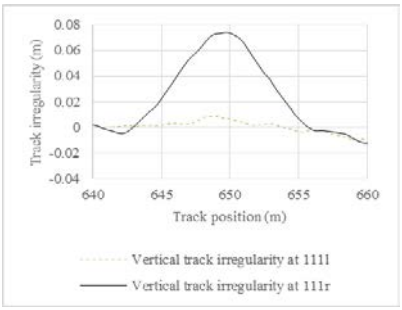

(b) Long twist

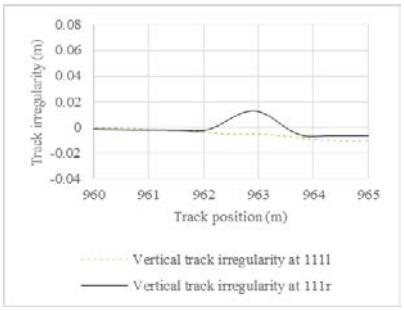

(c) Short twist

Figure 6-26: Track 2 containing isolated long and short twist irregularities corresponding to P1 limits of 80km/h superimposed with FRA class 5 track irregularities (circles indicates the peaks of the applied isolated track irregularities)

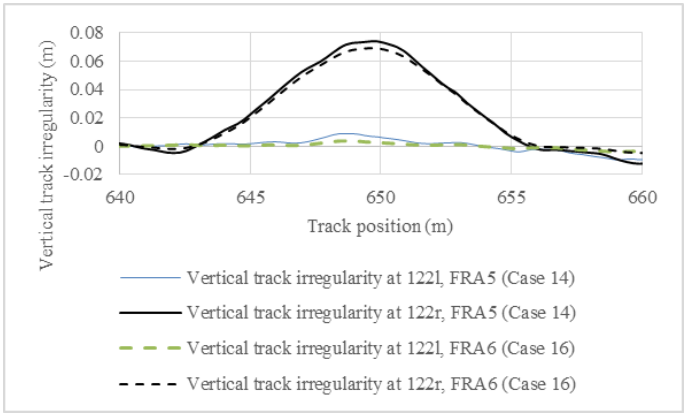

(a) Isolated vertical track defects superimposed on FRA track classes 5 and 6

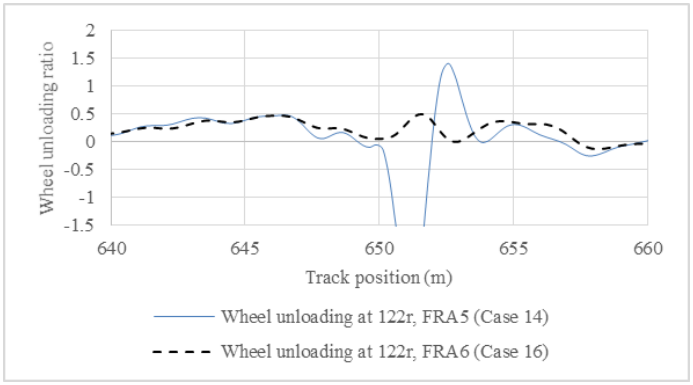

(b) Wheel unloading ratio near an isolated long twist track defect

Figure 6-27: Track irregularity and wheel unloading ratio in cases 14 and 16 (Straight track, speed 88km/h)

Table 6-12: Results of the step 5 tests on the RQTY wagon (Cases 1-6 are on a 300m radius curved track, Cases 7-8 are on a straight track)

Case	Maximum L/V wheel								Maximum L/V axle			
	111l	111r	112l	112r	121l	121r	122l	122r	111	112	121	122
1	0.75	0.54	0.58	0.52	0.86	0.46	0.7	0.49	1.08	0.89	1.21	1.03
2	0.65	0.43	0.64	0.42	0.41	0.85	0.43	0.73	1.05	1.02	1.25	1.03
3	0.45	0.99	0.44	0.86	0.43	***1.02***	0.44	0.94	1.34	1.18	1.4	1.24
4	0.43	0.69	0.44	0.68	0.63	0.42	0.69	0.43	1.09	1.05	1.04	1.08
5	0.4	0.73	0.34	0.59	0.4	0.75	0.37	0.61	1.08	0.91	1.1	0.94
6	0.73	0.37	0.34	0.24	0.79	0.36	0.28	0.25	0.95	0.54	0.97	0.46
7	0.65	0.43	0.67	0.42	0.41	0.82	0.42	0.8	1.07	1.08	1.22	1.21
8	0.36	0.83	0.24	0.3	0.37	0.78	0.3	0.39	1.03	0.49	1.09	0.53
9	0.43	0.87	0.42	0.85	0.62	0.41	***1.64***	0.44	1.3	1.27	0.98	***1.95***
10	0.71	0.35	0.31	0.2	0.44	0.36	0.27	0.23	0.92	0.39	0.71	0.46
11	0.66	0.43	0.68	0.42	0.41	0.82	0.42	0.84	1.07	1.08	1.22	1.26
12	0.34	***1.05***	0.17	0.28	0.35	0.68	0.24	0.27	1.35	0.34	0.97	0.49
13	0.43	0.89	0.42	0.84	0.64	0.41	***1.71***	0.42	1.32	1.26	1.01	***2.05***
14	0.44	0.5	0.55	0.47	0.44	0.27	0.48	0.36	0.57	0.67	0.56	0.56
15	0.18	0.24	0.16	0.2	0.31	0.26	0.17	0.32	0.34	0.24	0.2	0.21
16	0.36	0.3	0.39	0.33	0.32	0.31	0.39	0.43	0.47	0.46	0.4	0.41
Case	Maximum Wheel unloading ratio								Maximum Lateral acceleration (m/s^2)		Maximum Vertical acceleration (m/s^2)	
	111l	111r	112l	112r	121l	121r	122l	122r	ay1	ay2	az1	az2
1	0.55	0.59	0.4	0.52	0.6	0.53	0.47	0.47	4.64	3.83	5.43	5.90
2	0.3	0.58	0.31	0.56	0.29	0.43	0.27	0.43	***5.46***	***5.74***	3.25	3.21
3	0.63	0.52	0.54	0.46	0.75	0.65	0.46	0.47	***5.47***	***5.38***	5.31	5.95
4	0.57	0.21	0.55	0.2	0.43	0.24	0.47	0.25	***5.8***	3.94	2.75	3
5	0.63	0.51	0.45	0.46	0.69	0.65	0.45	0.47	3.99	3.22	5.4	5.9
6	0.6	***1.18***	0.55	0.64	0.6	***0.99***	0.57	0.83	3.12	3.7	4.00	4.70
7	0.44	0.85	0.49	0.8	0.48	0.6	0.48	0.55	***5.2***	3.37	3.67	3.40
8	0.72	0.78	0.64	0.57	***0.9***	0.69	0.67	0.64	3.15	3.7	3.73	4.88
9	***0.98***	0.33	***1***	0.32	***0.99***	0.23	***0.94***	0.17	2.63	4.48	3.91	4.13
10	0.56	***1.11***	0.57	0.59	0.57	0.84	0.59	0.63	3.45	4.01	4.30	3.49
11	0.43	0.86	0.47	0.8	0.45	0.55	0.42	0.52	4.73	2.95	3.24	3.47
12	0.65	***0.9***	***1.11***	0.65	0.73	0.53	0.59	0.59	3.24	3.82	4.68	4.78
13	***0.98***	0.36	***0.98***	0.35	***0.97***	0.23	***0.93***	0.18	1.75	3.31	3.52	4.16
14	0.71	0.63	0.71	0.44	0.79	0.67	0.77	***1.41***	3.76	4.01	4.24	4.11
15	0.73	0.74	0.72	0.68	0.76	0.43	0.82	0.37	3	3.86	5.07	5.40
16	0.74	0.71	0.7	0.65	0.69	0.75	0.61	0.68	4.15	3.69	3.74	2.63

6.8 Summary

A typical RQTY wagon has been tested by simulation to confirm the reasonable tests prescribed in the methodology. The RQTY wagon passed step 1 to step 4 tests as described in the methodology section. The step 5 tests were needed to be modified several times due to failure to meet the VAPS criteria. The outcomes of different steps of the VAPS method applied on the RQTY wagon are listed below:

- The critical hunting speed for the RQTY wagon model was determined as 85 km/h using new WPR2000 wheel and new AS60 rail profiles (step 1).
- The RQTY wagon could negotiate a minimum of 300m radius track curve (step 2) at the given simulation parameters on FRA class 4 and above (smoother) track when operating at the maximum cant deficiency limit of 110mm and cant excess limit of 75mm.
- The hunting test on long track simulation (step 3) with FRA class 5 track irregularities reveals that the RQTY wagon could operate at speeds of up to 80km/h without exceeding the derailment and acceleration parameters.
- When considering the cyclic track defect test (step 4) as per the method described in Chapter 5, the RQTY wagon passed all tests for speeds of up to 80 km/h.
- The step 5 tests on the isolated lateral and vertical track defects were applied on a 300m radius track curve using a type A track defect as per the methodology (Section 5.3.3). The track defect that the RQTY wagon could pass was smaller than the maximum allowed for the curve speed and was that corresponding to 115km/h if FRA class 5 track irregularities were used on a 300m radius track curve at 110mm cant deficiency.
- The step 5 tests on the isolated twist track defects were failed on a 300m radius track curve at 110mm cant deficiency. It was found to be impossible for this wagon to pass the isolated twist test on this curvature. The maximum twist track defect of 62.4mm over a 14m wavelength has been considered suitable for the datum RQTY wagon when maximum service speed is aimed at 80km/h on a straight track.

The following test conditions are therefore adopted for the comparative simulation testing of a concept wagon:

- Step 1 tests can use new WPR2000 wheel and new AS60 rail profiles.
- Step 2 tests are to be performed on a 300m radius curve using 110mm cant deficiency and 75mm cant excess
- Step 3 tests should aim for a design speed of 80km/h or more with FRA class 5 track irregularities
- Step 4 tests should utilise the type D track defect for any wagon (as per section 5.3.3)
- Step 5 tests on isolated lateral and vertical track defects could be performed on a 300m radius track curve, but the isolated twist track defect tests should be performed on straight track only as the datum case for tests by simulation established in this Chapter.
- It can be further noted that assumptions in the modelling such as the rigid body approximation make the simulation situation worse as the usual flexibility on a real wagon deck and body would have helped the twist track defect negotiation. Furthermore, the AS7509 standard does not recommend to perform the twist test in a dynamic situation. The other important observation is that the RQTY wagon was

commissioned before AS7509 was written. Furthermore, the isolated track defect tests were optional in the first version of the AS7509 standard. So, there is a possibility that the problem of twist negotiation for a RQTY wagon with the added dynamic situations as performed in this Chapter may not have ever been an achievable criterion for the design.

- The primary objective of this Chapter of testing the VAPS method to establish datum test conditions for any wagon has therefore been achieved, and the Datum test conditions are listed in Table 6-13.

Table 6-13: Datum test parameters

VAPS steps	Input parameter	Test methods
1	New WPR2000 wheel and new AS60 rail profile Smooth track without any irregularity	Decreasing velocity method Wheel-rail friction coefficient 0.5 Full creep condition Second order Runge-Kutta with Back step control
2	Track radius 300m Cant deficiency 110mm Cant excess 75mm Applied cant 125mm Ruch type transition FRA track class 4	Wheel-rail friction coefficient 0.4 Creep reduction factor 0.6 (dry condition) Second order Runge-Kutta with Back step control
3	Straight track, 2km long track Test speed 88km/h FRA track class 4	Sampling requirement to calculation for average acceleration over ≥5s Wheel-rail friction coefficient 0.5 Full creep condition Second order Runge-Kutta with Back step control
4	Straight track, type D track defect Smooth track without any superimposed irregularity over the cyclic track defects	Wheel-rail friction coefficient 0.4 Creep reduction factor 0.6 (dry condition) Second order Runge-Kutta with Back step control
5a	Isolated lateral and vertical track defects on curved track (300m radius, cant deficiency 110mm, 75mm). Type A track defect, Applied cant 125mm, Ruch type transition, FRA track class 5, track defect band F which is 3 band lower than the required condition of 110mm cant deficiency (corresponding speed of 77.23km/h) on the 300m radius track.	Wheel-rail friction coefficient 0.4 Creep reduction factor 0.6 (dry condition) Second order Runge-Kutta with Back step control
5b	Isolated twist track defect on a straight track at test speed 88km/h, FRA class 6 track	

Chapter 7

Length and Mass Optimisation by VAPS as a Means of Developing a New Concept Wagon

7.1 Introduction

A new concept wagon can be developed using the VAPS method developed in Chapter 5. In this chapter, the starting model for a single axle UIC swing link suspension was chosen from a tutorial model available in the Gensys simulation software package [92]. The tutorial model was developed based on tests on UIC link and leaf spring suspension parameters in the Royal Institute of Technology, Sweden (KTH) [132].

In this Chapter, the length, mass and suspension parameters of the tutorial model were modified in a systematic way using the VAPS method (Figure 7-1) to obtain similar performance to that of the datum wagon (Chapter 6). Firstly, the BCD, overhang lengths and mass of the wagon deck of the tutorial model were varied to observe the effect of length and mass on critical speed. Secondly, curve negotiability was tested with suitable length and mass parameters. As mentioned in Chapter 5, the first two steps of the VAPS were performed several times to achieve an optimum parameter set for stability and curve negotiation ability to reduce simulation effort at the early stage of concept development. Having found a reasonable combination of length and mass for a desired critical speed, the tutorial model was then tested for the remaining steps (steps 3-5) of the VAPS method. A list of development stages of concepts with reference Figures, Tables and Sections is provided in Appendix 2.

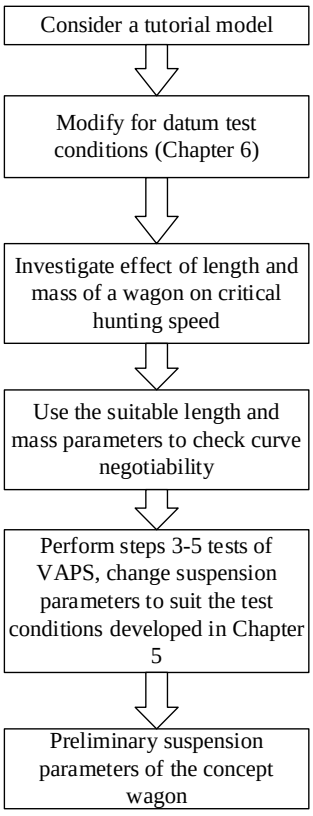

Figure 7-1: Methodology to develop length, mass and suspension parameters of a concept wagon

7.2 Modelling of the Tutorial Model

Figure 7-2 details the tutorial wagon model which comprises one wagon body 13; two wheelsets 15, suspension elements (vertical 1, longitudinal 2 and lateral 7), suspension stops 3, 8; friction buffer 5; contact modelling between wheel and rail 9, rail to track connections 10, 11 and track to ground connections 6, 12. All masses were modelled as rigid bodies. The empty wagon body mass was 6000kg and loaded wagon body mass was 43000kg. Axle boxes were included in the wheelset bodies. The simplified chassis approximation (Figure 4-3a) was used to define the wagon body inertia parameters.

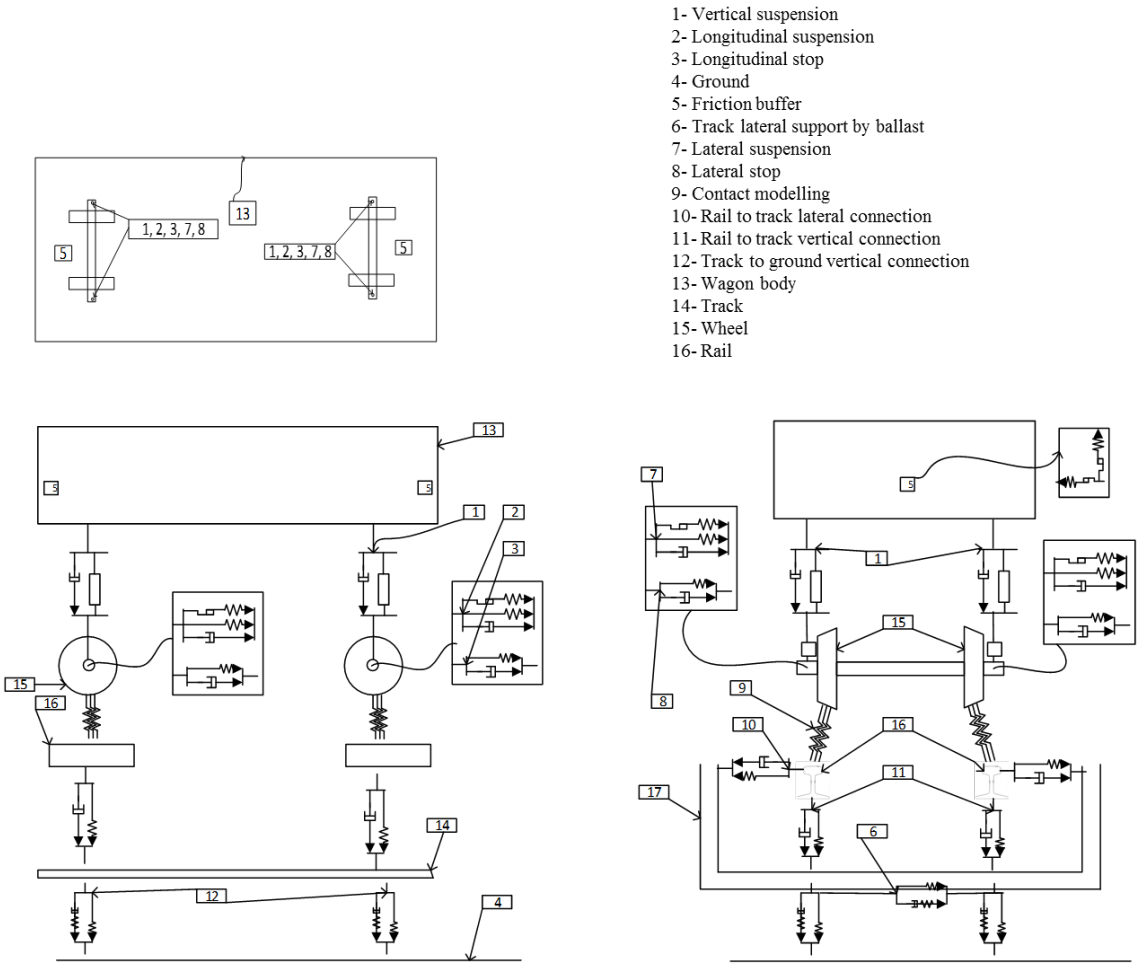

Figure 7-2: Full wagon model of the library model

The tutorial model was firstly modified for the datum conditions (Concept- 1) developed in Chapter 6 (new WPR2000 wheel profile, new AS60 rail profile, 1:20 rail inclination, wheel-rail friction coefficient of 0.4). The wheelset inertia parameters were also changed to that used in the datum condition. The addition of suspension mass with the wheelset inertia was not performed at the concept development stages. However, the inertia corrections of the wheelset was performed on the final concept in Chapter 10. All other parameters were kept similar to the tutorial model (Table 7-1) for the initial assessment of dynamics.

Table 7-1: Tutorial and Concept- 1 wagon model parameters

Parameter	Equations	Units	Tutorial model in Gensys		Modified for Datum conditions (Concept- 1)	
			Empty	Loaded	Empty	Loaded
Wagon body mass, mc		Kg	6000	43000		
Axle centre distance, BCD		M	12	12		
Overhang		M	1	1		
Wheel profile			S1002	S1002	WPR2000	WPR2000
Rail profile			UIC 60	UIC 60	AS60	AS60
Rail inclination			1 in 40	1 in 40	1 in 20	1 in 20
Vertical Suspension Parameters						
Vertical Stiffness, kz		kN/m	1600	1600		
Friction force (Damping)	2*(3000+7600*mc_fact)	kN	±6	± 21.2		
Stiffness at changing direction, kfz	20*(3200e3+1600e3*mc_fact)	MN/m	64	96		
Vertical damping, Cz	$C = 2 * \zeta * \sqrt{\frac{mC}{4} * Kz}$, ζ= 0.05	kNs/m	4.9	13.1		
Longitudinal Suspension Parameters						
Longitudinal Stiffness, kx	78e3+422e3*mc_fact	kN/m	78	500		
Stiffness at changing direction, kfx	7.5*kx	kN/m	585	3750		
Friction force (Damping)	2*(2000+9000*mc_fact)	kN	4	22		
Longitudinal damping, Cx	$2 * \zeta * \sqrt{(mC/4 * Kx)}$, ζ= 0.05	kNs/m	1.08	7.33		
Longitudinal stop position		mm	± 20	± 20		
Longitudinal stop stiffness		MN/m	4	4		
Lateral Suspension Parameters						
Lateral Stiffness, ky	123e3+377e3*mc_fact	kN/m	123	500		
Stiffness at changing direction, kfy	25*ky	kN/m	3075	12500		
Friction force (Damping)	2*(2450+7750*mc_fact)	kN	4.9	24.4		
Lateral damping , Cy	$2 * \zeta * \sqrt{(m\_C/4 * Ky)}$; ζ= 0.05	kNs/m	1.4	7.3		
Lateral stop position		mm	20	20		
Lateral stop stiffness		kN/m	55	55		
Friction buffer at both end of wagon						
Friction force in lateral and vertical plane		N	700	700		
Series stiffness with the friction blocks		MN/m	20	20		
Wheel-rail contact						
Friction coefficient at wheel-rail contact, μ			0.5	0.5	0.4	0.4
Contact Stiffness normal to the surface, knwr		MN/m	2400	2400		
Rail track						
Vertical Stiffness, kzrt		MN/m	230	230		
Lateral Stiffness, kyrt		MN/m	17	17		
Vertical rail track damping, czrt		kNs/m	50	50		
Lateral rail track damping, cyrt		kNs/m	10	10		
Track- ground						
Vertical contact stiffness, kztg		MN/m	220	220		
Lateral contact stiffness, kytg		MN/m	40	40		
Vertical track ground damping ratio, ζ_{Zt}			0.36	0.36		
Lateral track ground damping ratio, ζ_{Yt}			0.55	0.55		

Notes: mc_fact= mc/ 37000, based on maximum load of 37000kg on loaded wagon mass of 43000kg (gross mass 45000kg, 22.5 tonne axle load); the modified parameters were left blank where the library model parameters are used instead

7.2.1 Theory of UIC Link and Leaf Spring Suspension

In the leaf spring and links suspension system, the vertical stiffness is provided by the leaf springs and the horizontal stiffness (longitudinal and lateral) is provided by the links acting similar to pendulums. The pendulum action occurs in both the longitudinal and lateral directions. The swing movement on the links has a tendency to restore the wagon mass to its equilibrium position. The restoring force is governed by gravity and so provides a gravitational stiffness in longitudinal and lateral directions. The moment of the links that provide swing movement is dependent on the geometry of the links which can be changed due to vertical load. So, the longitudinal and lateral suspension parameters are modelled as load dependent parameters in the tutorial model.

In the tutorial model, a single stage leaf spring suspension is assumed which provides a single vertical stiffness (1.6 MN/m). The tutorial model uses some empirical equations (Table 7-1) to define the load-dependent stiffness parameters for lateral and longitudinal directions. The tutorial model, however, does not include variation in the longitudinal and lateral suspension parameters due to changes in vertical load. The difference in vertical loading on a straight track is less significant than that on a curved track. On a curved track, the outer suspension would face more vertical load at a cant deficient speed which would make the stiffness and hysteresis higher on the outer wheels compared to inner wheels. For simplicity, the tutorial model was not modified for dynamic stiffness values (due to variable dynamic vertical load) at this stage in this thesis. The dynamic stiffness (longitudinal and lateral) is incorporated in the final developed concept wagon (Chapter 11). As the tutorial model defines longitudinal and lateral suspension based on static vertical load, different suspension parameter sets for the empty and loaded conditions were necessary for simulation which required two different wagon models for the empty and loaded conditions.

The friction on the bearing at connection points among the leaf spring, links and wagon body provide friction damping to the UIC link suspension system. Typically, a Coulomb friction damper with a stiffness parameter in series (Figure 7-3) is generally used to model the force element. The ideal force-displacement characteristic of a friction damper, also known as the Coulomb friction model, is shown in Figure 7-3a. The initial displacement is characterised by a stiffness parameter (k_2) placed in series with a friction element (μN) (Figure 7-3c). The characteristic force-displacement for the stiffness in series with the friction damping can be represented by Figure 7-3b. Friction damping restricts the movement of the attachment up to a certain force known as the break out force (F_D). When the force in the connection reaches F_D, the attached components start to slide over one another and the damping force does not exceed F_D.

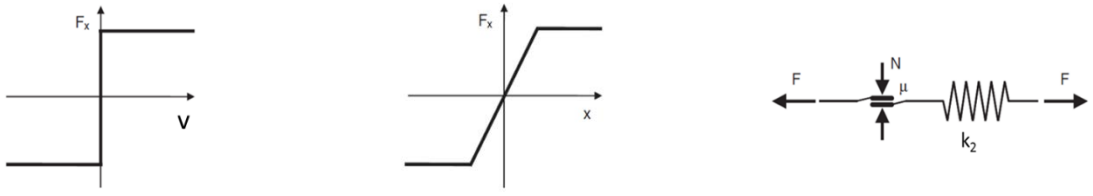

(a) Coulomb friction model

(b) Coulomb friction model with a stiffness parameter in series

(c) Schematic diagram of a Coulomb friction element with a stiffness parameter in series

Figure 7-3: A culomb friction damper

A basic hysteresis loop for a typical friction damping and linear stiffness as occurs in a leaf spring with double-link suspension is shown in Figure 7-4 which depicts two stiffness elements (k_1 and k_2) acting together up to a displacement characterised by F_D. When displacement reaches a value of $F_D/(k_1+k_2)$, sliding occurs in the friction damper and only k_1 provides the stiffness. The theoretical hysteresis loop for the friction damper arrangement of Figure 7-4a is shown in Figure 7-4b. Due to the presence of geometrical tolerances between the components, wear, corrosion and other lubrication between the components of the link suspension system, energy is dissipated and, in practice, a hysteresis loop like the one shown in Figure 7-4c is obtained by a model derived from experimental measurements on leaf spring suspensions [93, 133].

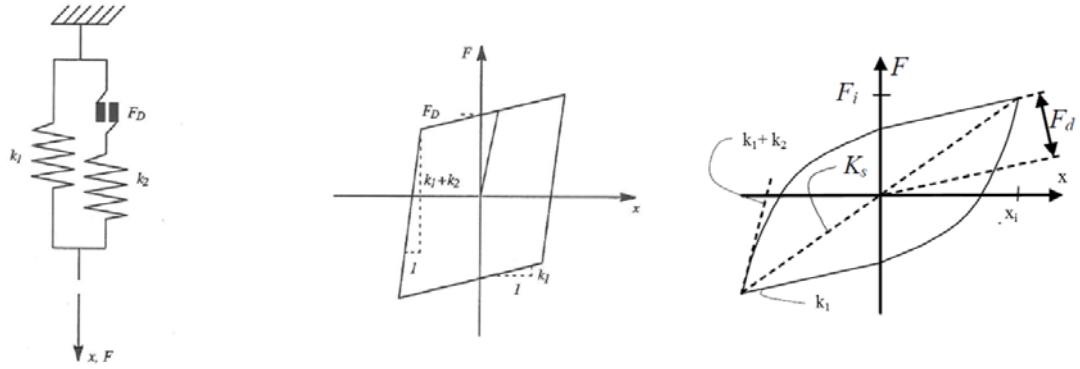

(a) Representation of a friction damper [133]

(b) Theoretical force-displacement characteristics of a friction damper and stiffness parameter shown in (a) [133]

(c) Typical experimental force-displacement characteristic of a lateral link suspension [93]

Figure 7-4: Friction damper characteristics typically used in vehicle dynamics

7.2.2 Main Suspension Parameters of the Concept- 1 Model

The Concept-1 model uses friction damper models similar to Figure 7-4a to model the horizontal stiffness (longitudinal and lateral) elements and an exponential function (Figure 7-4c) to model the vertical stiffness parameters. The longitudinal and lateral suspension elements are represented by one stiffness element, one friction damper element and one small damping element for modelling purpose in parallel connections (Figure 7-5). The vertical suspension element constitutes one friction damping element in parallel with one small viscous damper and one friction buffer element for modelling purpose (Figure 7-6).

The slope on the force-displacement plots of the longitudinal and lateral suspension elements at the start and end of loading and unloading cycles (k_1+k_2 as per Figure 7-4c; kfx, kfy in Table 7-1) were modelled as functions of the load-adjusted stiffness parameters (kx, ky) which made a stiffer transition between the loading and unloading cycles in the hysteresis loop of the loaded cases compared to that of the empty cases in both the longitudinal and lateral suspensions (Figure 7-7). Furthermore, the kfy parameters were stiffer than the kfx parameters as obtained from the empirical equations (Table 7-1). The modelling of the kfx and kfy parameters does not consider the typical exponential behaviour at the end of loading and unloading cycles on a leaf spring suspension (Example point B, Figure 7-7a).

The vertical suspension element was modelled as having an exponential type transition during the loading and unloading cycles (Figure 7-4c) which was generated in the modelling by a stiffness element in series with a friction damper [134]. The empirical equations in the tutorial and concept- 1 models have been used to model the

hysteresis loop in the vertical suspension (Figure 7-7e, f). A small viscous damping element was added to the vertical suspension to improve the stability of the model (Figure 7-6). In reality, there is no additional viscous damping in the physical suspension system comprising the UIC link and leaf springs.

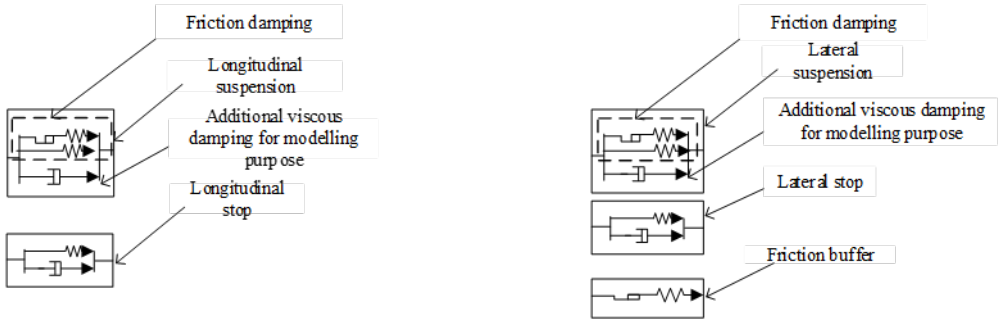

(a) Modelling of longitudinal suspension elements (b) Modelling of lateral suspension elements

Figure 7-5: Modelling of longitudinal and lateral suspension elements of the tutorial model

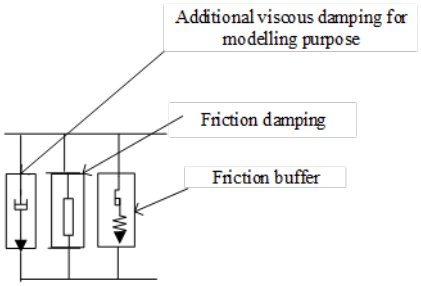

Figure 7-6: Modelling of the vertical suspension elements of the tutorial model

Stiffness and friction damper elements were included in a library element in the Gensys software to create smooth changes in friction force near the transition points between the loading and unloading cycles. The friction function was used to form a closed loop in the hysteresis loop (modelling) which is different to the empirical measurements of the exponential type nature of leaf springs that did not form a closed loop in the hysteresis loop [135]. The difference between the Fancher's equation in [135] and measurements on UIC link and leaf spring suspensions at KTH lies at the response points on the hysteresis loop (Figure 7-8). Responses from both the Fancher's equation (β1) and KTH measurements (α1) form a closed hysteresis loop at point 1 in Figure 7-8. At point 2, responses from the Fancher's equation (β2) do not form a closed loop. However, the KTH measurements (α2) found a typical closed hysteresis loop at point 2 [93]. The tutorial and concept-1 models hence used a closed loop hysteresis loop for modelling friction damper.

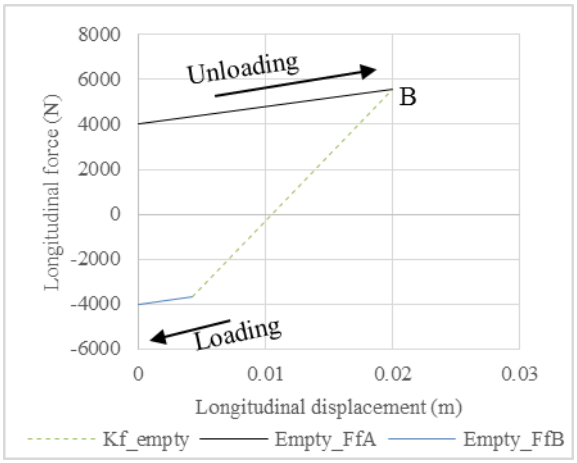

(a) Longitudinal suspension, empty

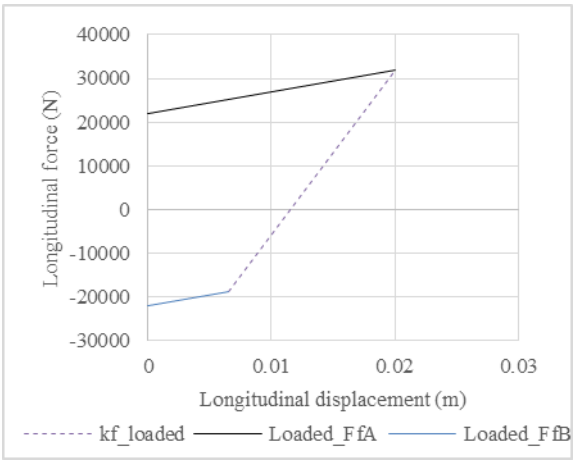

(b) Longitudinal suspension, loaded

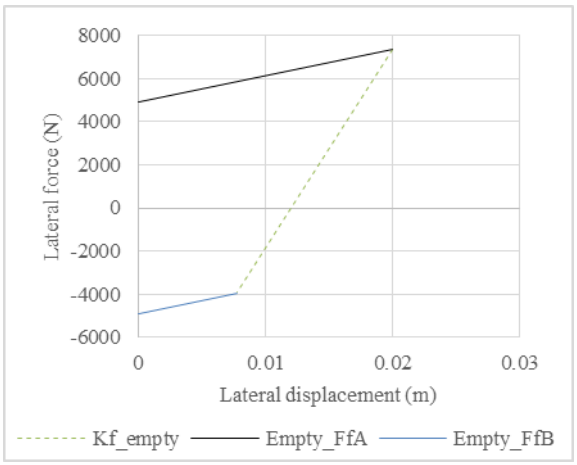

(c) Lateral suspension, empty

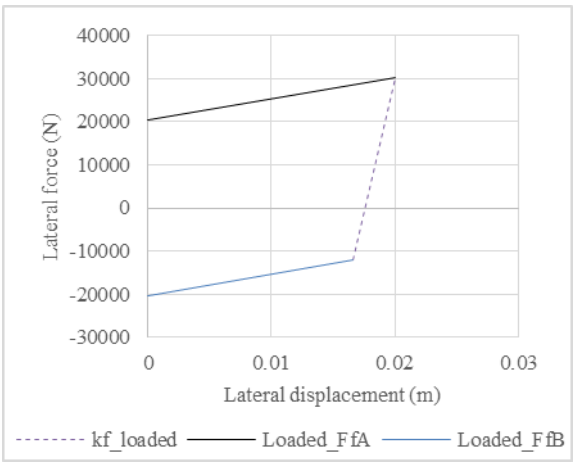

(d) Lateral suspension, loaded

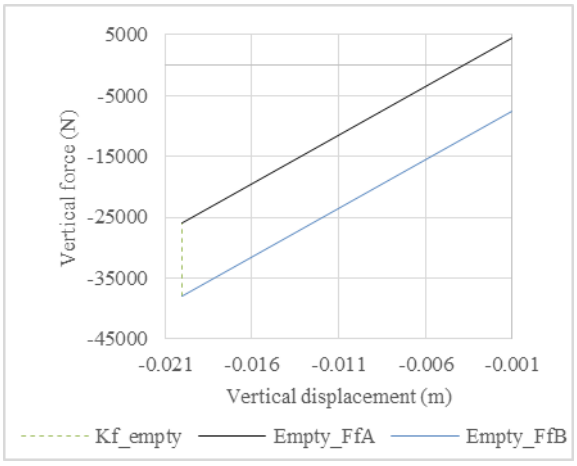

(e) Vertical suspension, empty

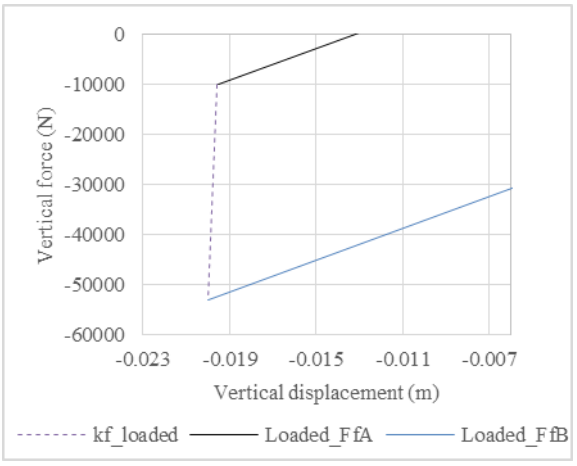

(f) Vertical suspension, loaded

Figure 7-7: Hysteresis loop in the suspension elements of the tutorial model of a two-axle wagon with UIC link suspension (Concept- 3a, Empty- 6000kg; Concept- 3b, Loaded- 43000kg, the exponential smoothing is not added in these plots)

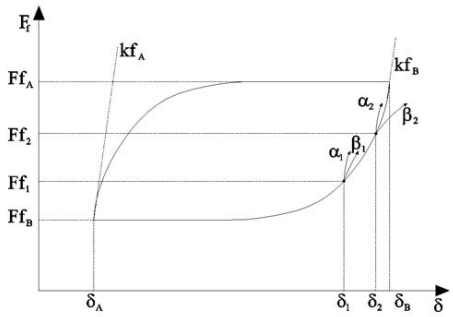

Figure 7-8: Force-displacement characteristics for friction force in leaf spring suspension (α- the response based on experiments on UIC link and leaf spring suspensions [93], β- the response based on experiments on truck leaf springs [135]

7.2.3 Other Suspension Elements of the Concept- 1 Wagon Model

Besides the main suspension, bump stop elements (Figure 7-9) were added to model hard limits in the longitudinal and lateral directions. The standard assembly of a wheelset on a UIC link suspension system allows maximum longitudinal displacement of ±22.5mm [136] and maximum lateral movement of 20mm towards the left and right of the wagon [136] (Figure 7-9). The longitudinal and lateral stops were modelled as a hard stiffness at ±22.5mm in the longitudinal direction (Figure 7-10) and 20mm in the lateral direction (Figure 7-11).

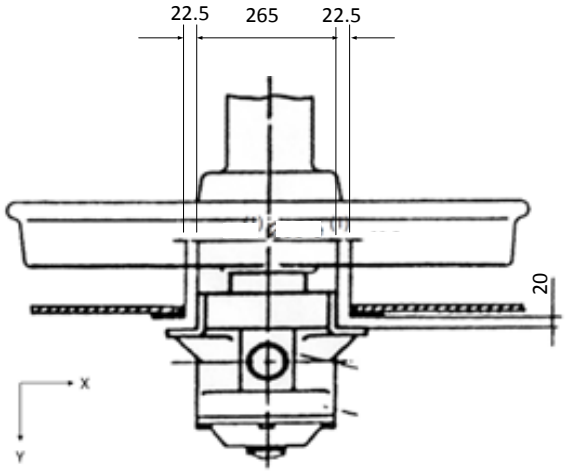

Figure 7-9: Typical longitudinal and lateral stop positions on a wheelset of UIC wagons [136]

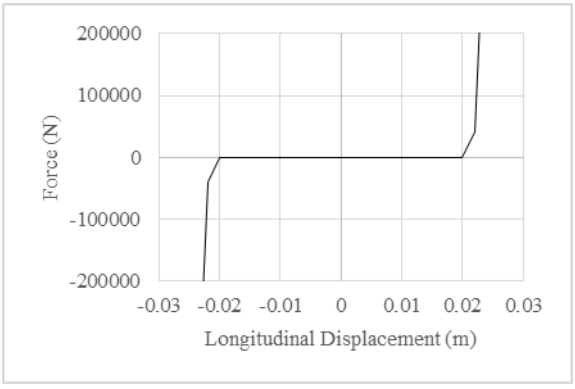

Figure 7-10: Longitudinal stop model between axlebox and wagon body in the Concept-1 model

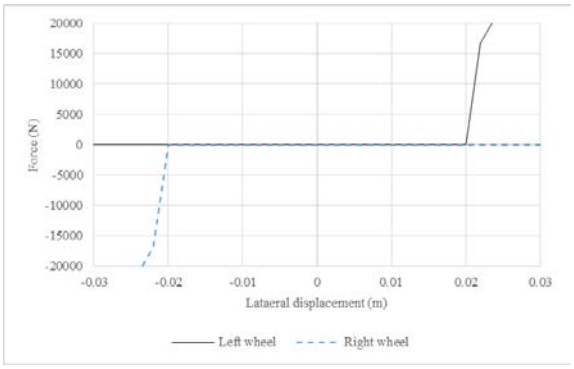

Figure 7-11: Lateral stop model between axlebox and wagon body in the Concept-1 model

The tutorial model has two friction buffer elements on a wagon situated at a distance of 1.8m in front of the front axle and to the rear of the rear axle. The buffer element was modelled as a friction block moving over the lateral-vertical plane (Figure 7-12a) based on the resultant force (Equation 7-1). The friction force (Ff0) of the friction block arrangement was considered as 700N and the series stiffness (K) elements provide a high stiffness of 20MN/m (Figure 7-12b). Sliding only occurs when the displacement exceeds Ff0/K, i.e. about 0.035mm in this case.

$$F_{tot} = \sqrt{F_{k1}{}^2 + F_{k2}{}^2} \qquad 7\text{-}1$$

where F_{tot} is the resultant spring force on the two-dimensional surface (N), F_{k1} is the spring force in the first direction, example lateral (N), F_{k2} is the spring force in the second direction, example vertical (N).

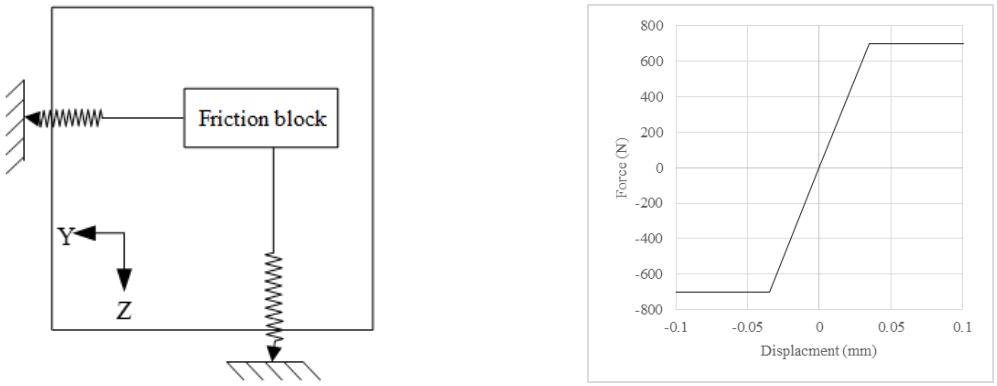

(a) Friction block arrangement in the friction buffer (b) Characteristic of the friction block

Figure 7-12: Friction damper on the buffer at the end of concept- 1 wagon (Friction force 700N, series stiffness 20MN/m, Y- lateral, Z- vertical)

The wheel-rail contact, track, and rail models in the tutorial model were modified (concept- 1) to match the datum test conditions (Appendix- 1) as used in the RQTY wagon simulations in Chapter 6.

7.3 Step 1- Critical Speed Test on the Concept-1 Wagon Model

The critical speed for hunting of the Concept-1 wagon model was evaluated for different length and mass combinations. The length of the wagon was considered a multiple of length parameters of standard containers. The bending deflection and stress consideration in Section 4.3 revealed that it is possible to have a BCD of 19.812m in the possible dynamic loaded condition range (90% overload of 78t) for the concept wagon. So, in this section, the BCD was chosen less than 19.812m by adjusting the length of overhangs to accommodate a target

loading length of 19.812m. The spacing between two axles on the Concept-1 wagon model is set as the difference between the length of the load (or length of the wagon assuming 100% utilisation of deck length) and overhang using the relationship aca= (la- ov), where aca is half distance of the BCD, la is the half length of the container, and ov is the overhang on each side. The BCD term is also used for the two-axle wagon though two-axle wagons do not have bogies. The term "axle centre distance" in the case of a two-axle wagon is a better wording, but it can create confusion with the axle centre distance within a bogie in a bogied wagon. The critical speed was measured using the decreasing velocity method with force excitation events on the wagon body and axles as discussed in Chapter 6.

The critical speed was found to increase with the increase of the length of the wagon and the decrease of overhang lengths (Figure 7-13). Overhang length has a greater effect on the critical speed of shorter wagons (example: 79-84 km/h 'la' of 9.9m; 71-82 km/h on 'la' of 7.62m and 54-78 km/h on 'la' of 6.096m) (Figure 7-13a, and Figure 7-13b). Based on the analysis in this section, the overhang length was chosen as 3m at each end of the target deck length 19.812m (gives a critical speed of 79.7 km/h on the half-length of wagon of 9.906m, Figure 7-13a) to reduce the BCD to 13.8m which is close to the BCD of 13m as per the ARTC track geometry standard [55].

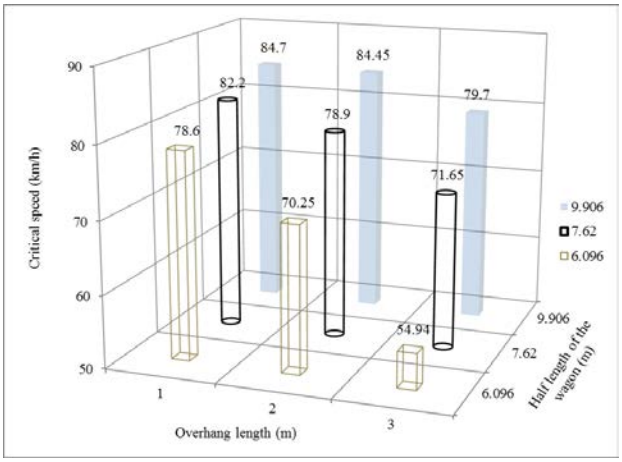

(a) Critical speed with respect to overhang and half length of the wagon

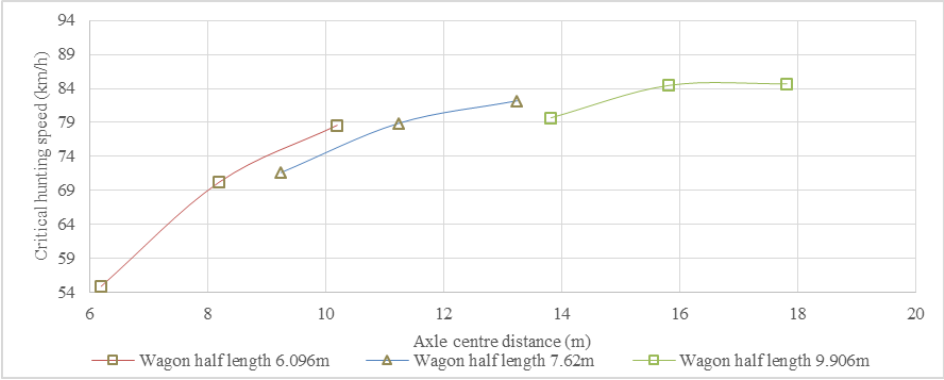

(b) Critical speed with respect to axle centre distance

Figure 7-13. Effect of length on critical speed on concept- 1 wagon (Decreasing velocity method, Empty mass of the wagon is 6000kg)

7.4 Step 2- Curve Negotiation Test on the Concept-2 Model

The chosen BCD (13.812m) and overhang length (3m) based on the analysis (step 1 test, section 7.3) on the Concept-1 wagon model has been further evaluated for curve negotiability (Step 2 tests of the VAPS). The Step 2 tests were performed using the datum test conditions developed in Chapter 6. The Concept-1 model with the changed BCD (13.812m) and overhang length (3m) is termed as the Concept-2 model. The track irregularity, curve radius and suspension parameters were varied in the Concept-2 model as different cases to investigate the curve negotiability of the empty and loaded wagons (Table 7-2).

The empty wagon with chassis mass of 6000kg failed in all derailment parameters on a 300m radius track when the vertical suspension of stiffness 1.6 MN/m was used as per the concept- 1 model (Cases 1, 2; Table 7-2, 7-3). Case 1 failed on both the curved and the transition sections (Figure 7-14b, c). The derailment parameters were within the limit values on the curved section in case 2 (Table 7-3, Figure 7-15b), but above the limit values at the exit transition (Table 7-3, Figure 7-15c). The FRA class 6 track in case 2 provided smoother track (smaller irregularities) than the FRA class 4 track in case 1 which reduced the derailment parameters in case 2 compared to those in case 1.

Table 7-2: Simulation cases on an empty Concept- 2 wagon (two-axle wagon, Curve Cant 125mm, empty wagon body mass 6000kg)

Case	Load (kg)	Track class (FRA track class)	Curve Radius (m)	Cant deficiency (mm)	Vertical suspension (kN/m)
1	0	4	300	110	1600
2	0	6	300	110	1600
3, 4	0	6	300	110, -75	50
5, 6	72000	6	300	110, -75	1600
7, 8	72000	6	300	110, -75	3380

Table 7-3: Results of the step 2 tests on the two-axle wagon using the Concept- 2 wagon model

Case	Maximum L/V wheel				Maximum L/V axle		Maximum Wheel unloading ratio				Maximum Lateral acceleration (m/s^2)		Maximum Vertical acceleration (m/s^2)	
	11l	11r	12l	12r	11	12	U11l	U11r	U12l	U12r	ay1	ay2	az1	az2
1	***2.66***	***1.86***	***7.46***	***2.1***	***2.87***	***7.33***	***1.16***	***1.21***	***1.3***	***1.33***	***5.3***	***5.74***	***9.67***	***9.48***
2	***2.02***	0.47	***1.08***	***3.31***	***2.25***	***3.44***	***1.12***	***1.13***	***1.13***	***1.1***	3.01	4.19	2.51	3.63
1_curved	0.56	0.48	***1.60***	0.96	***1.51***	***1.94***	0.72	***1.19***	***1.30***	***1.13***	***4.79***	***5.74***	***7.64***	***7.67***
2_curved	0.85	0.44	0.44	0.73	1.28	1.12	0.40	0.95	0.88	0.63	2.30	4.03	2.14	2.04
3	0.99	0.43	0.39	0.60	1.41	0.90	0.47	0.49	0.60	0.58	2.70	3.92	2.44	2.43
4	0.95	0.44	0.32	0.75	1.39	1.04	0.46	0.46	0.52	0.44	1.18	2.05	0.90	0.90
5	0.61	0.42	0.42	0.88	1.01	1.29	0.42	0.58	0.42	0.53	1.79	2.42	6.60	3.38
6	0.92	0.43	0.39	0.58	1.34	0.96	0.44	0.37	0.50	0.28	1.06	1.11	6.59	1.78
7	0.76	0.42	0.42	0.94	1.17	1.34	0.33	0.61	0.47	0.58	1.88	2.40	7.15	2.73
8	1.08	0.43	0.39	0.71	1.51	1.08	0.51	0.49	0.60	0.34	1.13	1.12	7.15	1.63
8_curved	0.69	0.43	0.39	0.54	1.11	0.92	0.43	0.21	0.52	0.09	1.13	1.12	1.13	1.18

Note: Bold italic fonts in the shaded cells are the values outside the acceptable values discussed in Chapter 3. In the case of wheel unloading ratio reaching 1.0, the contact between wheel and rail is removed, so the simulation results beyond that point are invalid and the wagon is assumed to be derailed.

At the start of the transition, the wagon faced a twist track condition where the wheels moved to different vertical positions relative to each other and the torsional moment on the wagon body changed. A way to reduce the difference in vertical position of the wheels and thereby reducing torsional affect is to allow softness in the

suspension. The stiffness of the vertical suspension was then reduced to 50kN/m (which is only 3% of the initial vertical stiffness 1.6MN/m of the Concept-1 model, cases 3-4, Table 7-3). The consequence and practical consideration of a very low stiffness value has been evaluated in a later section 7.8. The reduced vertical suspension stiffness reduced the wheel L/V ratio and the wheel unloading ratio in cases 3-4 (Table 7-3). The reduced vertical stiffness allowed the wagon to negotiate the transition curve on the track curve radius of 300m (Cases 3-4) (Table 7-3).

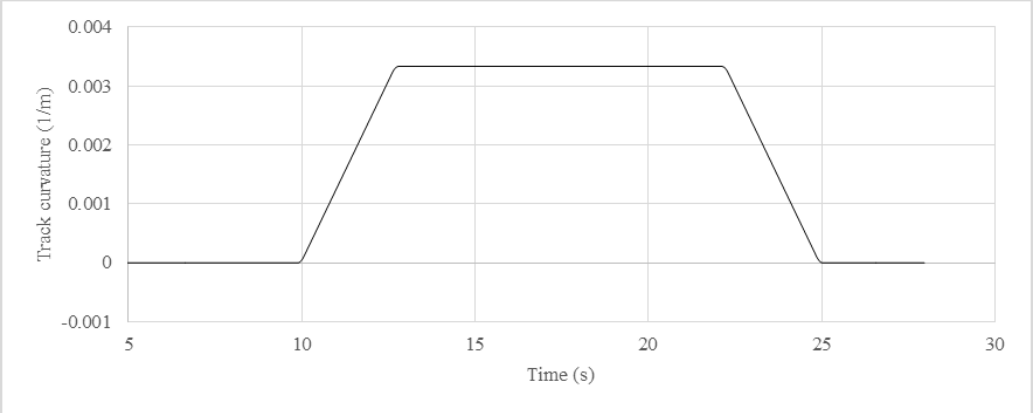

(a) Track curvature

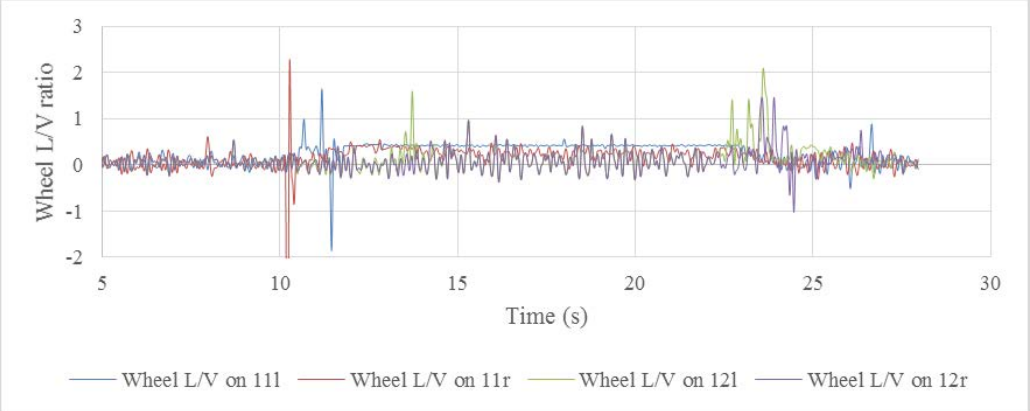

(b) Wheel L/V ratio in case 1

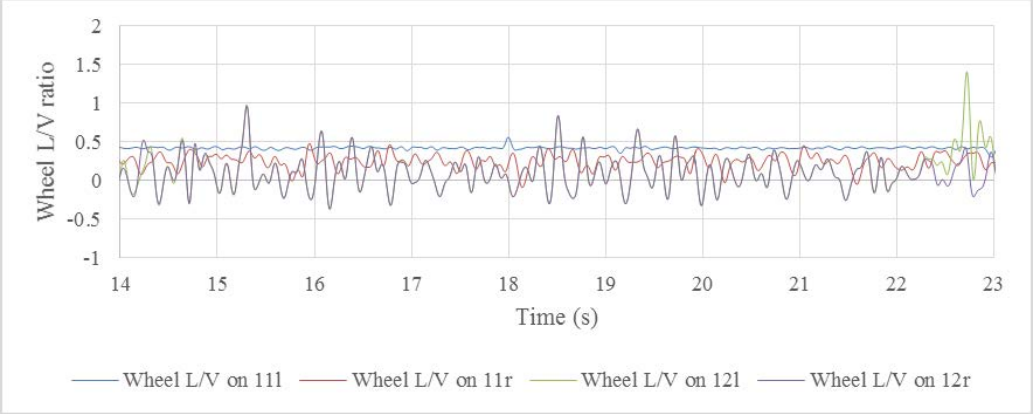

(c) Wheel L/V ratio in case 1 on curved section

Figure 7-14: Step 2 tests on the Concept-2 wagon model (Case 1, FRA class 4 track, Empty- 6000kg, Track radius 300m, Vertical suspension stiffness 1.6MN/m)

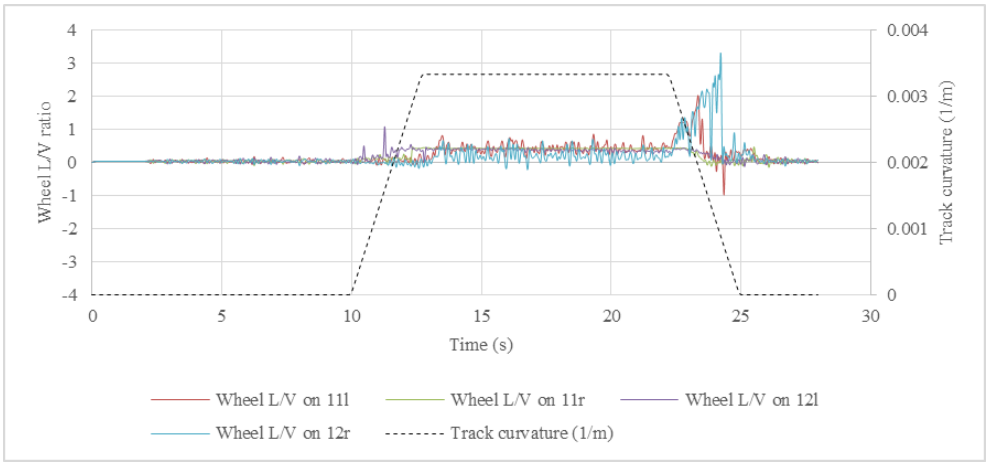

(a) Wheel L/V ratio in case 2

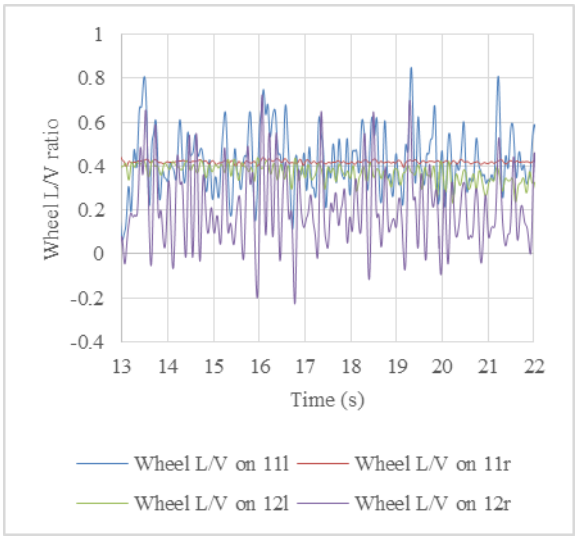

(b) Wheel L/V ratio in case 2 on curve section

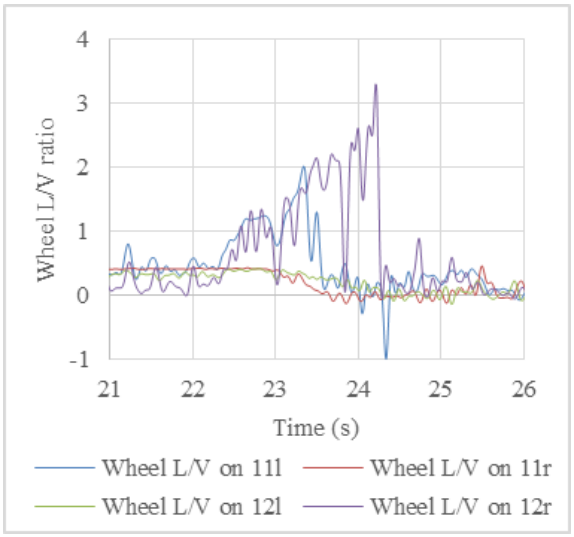

(c) Wheel L/V ratio in case 2 on exit transition section

Figure 7-15: Step 2 tests on the Concept-2 wagon model (Case 2, FRA class 6 track, Empty- 6000kg, Track radius 300m, Vertical suspension stiffness 1.6MN/m)

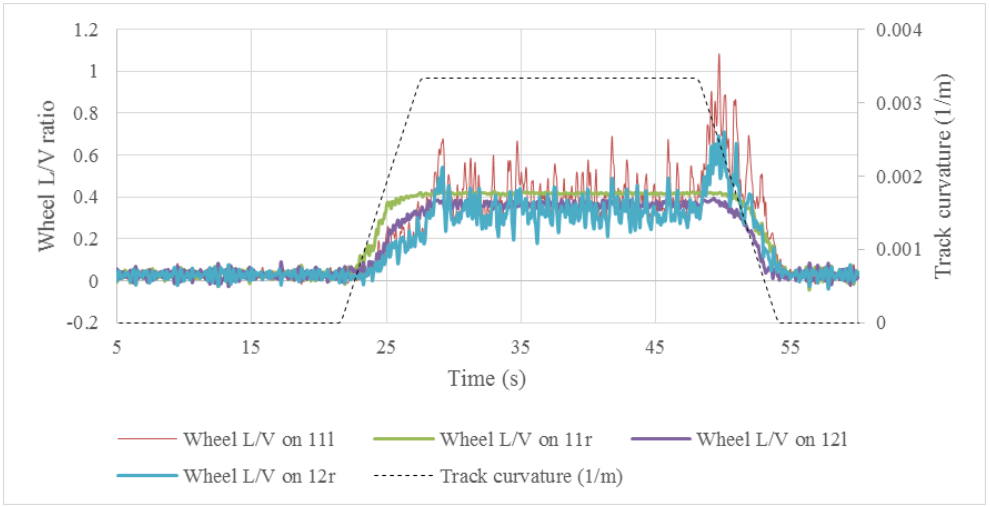

Figure 7-16: Step 2 tests on the Concept-2 wagon model (Case 8, FRA class 6 track, Loaded- 78000kg, Track radius 300m, Vertical suspension stiffness 3380kN/m)

The loaded condition (Cases 5-6) passed all the derailment criteria (Table 7-3) using the vertical stiffness of 1.6MN/m. However, the vertical stiffness of 1.6MN/m of the model is not suitable for the intended maximum payload of 72t as the loaded wagon body mass of 78t would create a vertical displacement of about 120mm which is high and not suitable for such a wagon design. So, a stiffer vertical suspension is necessary for the high payload of 72t. The vertical suspension for the loaded condition has been chosen as 3.38 MN/m as a trial (cases 7, 8, Table 7-3) which would provide a vertical displacement of 57mm at a loaded wagon body mass of 78t. The loaded conditions were then tested using the vertical stiffness of 3.38 MN/m for the cant deficient and cant excess conditions. The loaded wagon passed the tests in the cant deficient condition (case 7, Table 7-3). But, the wheel L/V ratio on the left wheel for the cant excess condition on the loaded wagon (case 8, Table 7-3) was above the acceptable limit in the exit transition region (Figure 7-16). Further modification of the suspension system to make it suitable for a slow speed condition in an exit transition for the loaded condition was not performed here as the further modification of the suspension is sought based on practical operation and buildiability as performed in the following section 7.8 and Chapter 10. .

The changed vertical stiffness parameter in step 2 requires a rerun of the step 1 test as per the VAPS method. The changed vertical stiffness of 50kN/m in the empty condition did not change the critical speed (82km/h, Figure 7-17) significantly compared to that obtained in the step 1 tests using vertical stiffness of 1.6 MN/m (79.7km/h, Figure 7-13a). The following parameters were selected at the end of the step 2 tests:

- Two different wagon models for the empty and loaded conditions. The vertical stiffness for empty and loaded wagon models were 50 kN/m in empty (Concept-3a) and 3.38 MN/m in loaded (Concept-3b) conditions.
- FRA track class 6.

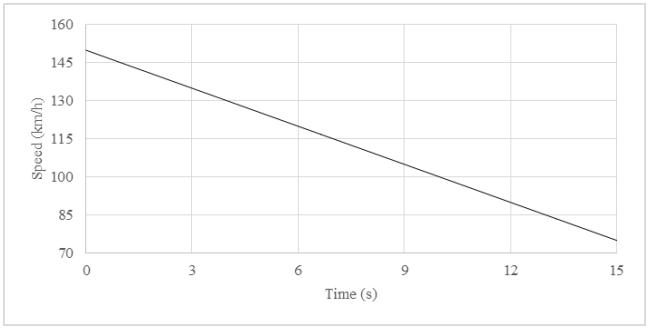

(a) Decreasing velocity for measuring critical hunting speed

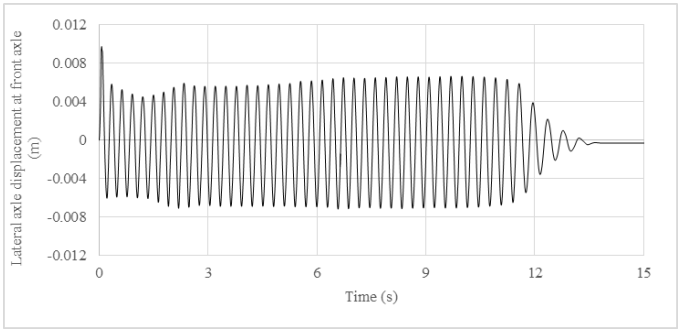

(b) Lateral axle displacement on front axle

Figure 7-17: Rerun of Step 1 test on the Concept- 3a wagon model (BCD 13.8m, Overhang 3m)

7.5 Step 3- Alternate Hunting Test on Concept-3a Wagon Model

The Concept-3a wagon model (Empty wagon with 50kN/m vertical spring) with the selected parameters in steps 1 and 2 were tested on a 2km long straight track with FRA class 4 (case 1) and class 5 (case 2) track irregularities (Table 7-4). The speed was set at 10% above the design speed of 80km/h as per the datum condition. The concept-3a wagon model passed the requirement of wagon body hunting in both these cases (Table 7-4). So, the concept-3a wagon model is suitable for FRA class 4 or smoother track at the design speed of 80km/h.

Table 7-4: Results of step 3 tests on the initial model with the two-stage suspension

Case	Maximum L/V wheel				Maximum L/V axle		Maximum Wheel unloading ratio				Average peak lateral acceleration over 5s (m/s^2)	
	11l	11r	12l	12r	11	12	U11l	U11r	U12l	U12r	ay1	ay2
1	0.75	0.78	0.61	0.76	0.85	0.74	0.82	0.71	0.84	0.74	2.05	1.83
2	0.35	0.4	0.35	0.32	0.3	0.24	0.66	0.64	0.7	0.67	1.34	1.59

7.6 Step 4- Cyclic Track Defect Test on Concept-3a and Concept-3b Wagon Models

The cyclic track defects for the Concept-3a and Concept-3b wagon models were set (Table 7-5) as per the type D defect (modified for the BCD of 13.812m of the Concept-3a and Concept-3b wagon models) used in the datum tests. The resonant velocities in the empty condition (Concept-3a, Table 7-6) were less than the design speed (80km/h) but were higher than the design speed in the loaded condition (Concept-3b). On a wagon with a single stiffness value the natural frequency is inversely related to the mass, so the empty wagon would generally possess a higher natural frequency and thereby higher resonance speed compared to the loaded wagon. In this case, the two different wagon models having a low stiffness value (50kN/m) for the empty wagon and a high stiffness value (3.38MN/m) for the loaded wagon provided higher resonance frequency for the loaded condition than that of the empty condition.

As the loaded condition gave resonance speeds higher than the design speed limit, the cyclic track defect tests in the loaded condition were simulated for the design speed (Table 7-7). Six simulation cases were tested for the cyclic track defect tests (Table 7-7).

Table 7-5: Track defect geometry for cyclic track irregularity test (axle centre distance 13.812m)

Speed (km/h)	ARTC P1 vertical track defect limits (Wavelength of track defect 20m) (mm)	Raise P1 limit by 20% as per AS 7509 (mm)	Equivalent amplitude of the track defect (Type D) obtained by graphical method		40% of the Type D track defect amplitude (mm) for cyclic track defect test	
			Bounce and Roll (wavelength of BCD)	Pitch (wavelength of 2*BCD)	Bounce and Roll (wavelength of BCD)	Pitch (wavelength of 2*BCD)
40	71	85.2	67	103	26.8	41.2
60	71	85.2	67	103	26.8	41.2
80	66	79.2	62	96	24.8	38.4
100	56	67.2	53	82	21.2	32.8
115	51	61.2	48	74	19.2	29.6

Table 7-6: Resonance frequencies and velocities for the concept-3 wagon model (Axle centre distance of 13.812m, TARE mass of the wagon body 6000kg, loaded wagon body mass 78000kg)

Load conditions	Natural frequency (Hz)			Resonant velocity (km/h)		
	Vertical	Pitch	Roll	Bounce	Pitch	Roll
Empty wagon	0.92	1.11	0.99	46	55	49
Loaded wagon	2.10	2.53	2.25	104	126	112

Table 7-7: Simulation cases for step 4 tests on Concept-3a and Concept- 3b wagon models

Case	Mode	Load (kg)	Speed (km/h)	Track defect amplitude (mm)
1	Bounce	0	46	26.8
2	Bounce	72000	88	24.8
3	Pitch	0	55	41.2
4	Pitch	72000	88	38.4
5	Roll	0	49	26.8
6	Roll	72000	88	24.8

Table 7-8: Results of the step 4 tests on the Concept-3a and Concept- 3b wagon models (Empty wagon body mass 6000kg, loaded wagon body mass 72000kg)

Case	Maximum L/V wheel				Maximum L/V axle		Maximum Wheel unloading ratio				Maximum Lateral acceleration (m/s^2)		Maximum Vertical acceleration (m/s^2)	
	11l	11r	12l	12r	11	12	U11l	U11r	U12l	U12r	ay1	ay2	az1	az2
1	0.09	0.09	0.09	0.09	0.17	0.17	0.09	0.09	0.08	0.08	0.00	0.00	0.57	0.55
2	0.05	0.05	0.05	0.05	0.10	0.10	0.33	0.33	0.33	0.33	0.00	0.00	1.81	2.04
3	0.07	0.07	0.07	0.07	0.15	0.15	0.06	0.06	0.06	0.06	0.00	0.00	0.39	0.38
4	0.05	0.05	0.05	0.05	0.09	0.09	0.33	0.33	0.33	0.33	0.00	0.00	0.78	0.8
5	0.10	0.08	0.08	0.09	0.07	0.07	0.42	0.44	0.42	0.44	0.53	0.54	0.30	0.34
6	0.17	0.19	0.19	0.20	0.12	0.12	0.68	0.58	0.67	0.59	1.97	1.75	1.85	1.6

All the derailment parameters in both empty and loaded conditions were found within the limit values when cyclic track defects were applied (Table 7-8). As an example, the bounce test in loaded conditions (case 2) is shown in Figure 7-18. Considering all values of acceptance parameters were within acceptable limits, it was decided to move on to the next step of wagon dynamics tests on isolated track defects.

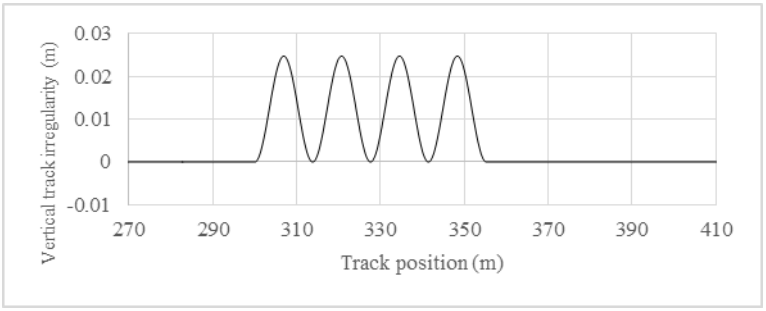

(a) Vertical cyclic track defect for the bounce test

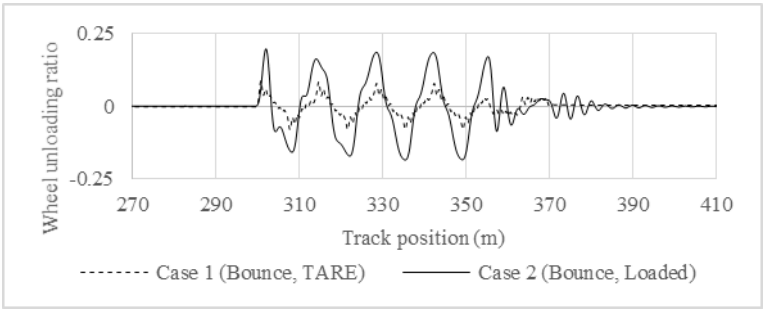

(b) Wheel unloading ratio on front left wheel

Figure 7-18: Cyclic Bounce test in cases 1 (Concept- 3a) and 2 (Concept-3b) wagon models

7.7 Step 5- Isolated Track Defect Test on Concept-3a and Concept-3b Wagon Models

The stiffness parameters of the two suspensions obtained in step 2 tests (50kN/m in empty, Concept-3a and 3.38MN/m in loaded, Concept-3b) have been used in Step 5 tests. The datum test parameters established in Chapter 6 have been used in cases 5-7 in Table 7-9. The Concept-3a and Concept-3b wagon models were also tested in some other test conditions to quantify the performance parameters of the two-axle wagon (cases 1-4 and 8-15).

Table 7-9: Simulation cases for step 5 tests on Concept-3a and Concept- 3b wagon models (Type A track defects)

Case	Mode of tests	Load (kg)	Track radius (m)	Track irregularity (FRA track class)	Speed band (km/h)	Amplitude of the applied track defects limits, P1 (mm)	Track Defect Band
1, 2	Isolated lateral, vertical and hump	0, 72000	300	5	80	79.2, 40.8, 25	D
3, 4	Isolated lateral, vertical and hump	0, 72000	-300	5	80	79.2, 40.8, 25	D
5	Isolated lateral, vertical and hump	0	-300	5	115	61.2, 21.8, 25	F
6, 7	Twist, straight track	0, 72000	Straight	5	80	66	D
8, 9	Twist, straight track	0, 72000	Straight	6	80	66	D
10, 11	Twist, straight track	0, 72000	Straight	6	100	55.2	E
12, 13	Twist, straight track	0, 72000	Straight	6	115	48	F
14, 15	Twist, straight track	0, 72000	Straight	6		45	F

In cases 1-4, the track defect limits corresponding to 80km/h (band D) were applied (Table 7-9). The wheel L/V ratios near the entry of the curve in case 1 (Figure 7-19c) was above the acceptable limit of 1.0. In case 1, the vertical track irregularity changes were about ±12mm (near simulation time of 20 second, Figure 7-19a) near the curve entry position. While the positioning of FRA track irregularities over the test track was not evaluated in this thesis, a combination of track irregularity and track geometry could change the outcome of the tests. Case 1 showed no wheel L/V ratio outside the acceptable limits near the applied isolated vertical track defect (Figure 7-19d). Further investigation showed that the Concept-3a model passed the derailment parameters at the steady curved section and through the isolated vertical track defect (measured from 21s simulation time, Figure 7-19c, Table 7-10). The lateral acceleration in the steady curved section of case 1 was still outside the recommended value as per AS7509 standard (Figure 7-19e) when the isolated lateral track defect was applied (near 37s in Figure 7-19a).

Case 3 failed on wheel unloading ratio on the front left wheel on the low rail (0.94 at #11l, Table 7-10). The unacceptable wheel unloading ratio in case 3 occurred at about 37.6s when the isolated lateral track defect was applied outward (sharpening of the curve) on the curved section (Figure 7-20a, Figure 7-20b). This lateral track defect resulted in the position of the rail moving towards the flange of the wheel on the low rail but further away from the flange of the wheel on the high rail. So, additional lateral movement of the wheel tread is available on the high rail. However, because the wagon is running at the cant deficient speed, the wagon moves towards the high rail and the applied curve sharpening track defect on the high rail reduced the available lateral displacement on the high rail. So, flange contact occurred on the high rail. The flange contact along the high rail due to the cant deficient speed created a rollover tendency of the wagon which then increased the wheel unloading ratio on the

low rail (Figure 7-20b, Figure 7-20c). The applied isolated track defect in case 3 was then reduced to the P1 limit corresponding to a speed band of 115km/h (defect band F) as per ARTC track network in case 5 (which is also a datum case in Chapter 6). Case 5 passed all the derailment parameters (L/V wheel, L/V axle and wheel unloading ratio). The case 5 failed in the maximum lateral acceleration criteria (Table 7-10) which is not a safety concern and can be improved once a final concept is developed. So, the Concept-3a model passed the similar test conditions of the datum isolated lateral and vertical track defect tests. The Concept-3a model failed in cases 1 and 3 which are stricter than the datum test and could be avoided. The Concept-3b model passed cases 2 and 4 which indicated that the loaded wagon in dynamic condition could pass stricter dynamic tests compared to the empty condition.

Table 7-10: Results of step 5 tests on the Concept- 3a (Empty) and Concept- 3b (Loaded) models

Case	Maximum L/V wheel				Maximum L/V axle		Maximum Wheel unloading ratio				Maximum Lateral acceleration (m/s^2)		Maximum Vertical acceleration (m/s^2)	
	11l	11r	12l	12r	11	12	U11l	U11r	U12l	U12r	ay1	ay2	az1	az2
1	***1.03***	0.43	0.46	0.65	1.45	0.96	0.64	0.77	0.74	0.81	***6.79***	***5.43***	6.51	6.69
2	0.73	0.42	0.43	0.89	1.13	1.29	0.48	0.79	0.58	0.74	4.4	4.47	7.16	4.46
3	0.45	0.96	0.71	0.55	1.35	0.98	**0.94**	0.79	0.69	0.67	**8.09**	**5.14**	6.51	6.69
4	0.43	0.67	0.99	0.43	1.08	1.41	0.84	0.41	0.72	0.51	4.34	3.91	7.16	4.46
5	0.45	0.96	0.63	0.41	1.35	0.95	0.89	0.64	0.68	0.67	**5.58**	4.34	6.51	6.69
6	0.28	0.3	0.35	0.32	0.36	0.31	0.67	0.8	0.7	0.71	3.74	3.93	5.48	5.47
7	0.23	0.29	0.2	0.26	0.28	0.34	**1.02**	**1.03**	**0.93**	**1.03**	2.76	2.05	7.16	4.86
8	0.23	0.28	0.25	0.26	0.32	0.31	0.57	0.77	0.53	0.63	3.41	3.61	3.33	3.86
9	0.25	0.27	0.19	0.27	0.31	0.29	**0.92**	**1.03**	0.87	**1.04**	2.71	2.23	7.16	5.04
10	0.21	0.25	0.23	0.24	0.26	0.26	0.57	0.65	0.53	0.6	3.35	3.52	3.47	3.84
11	0.22	0.21	0.16	0.25	0.23	0.23	0.76	**0.98**	0.76	**0.99**	2.14	1.77	7.16	4.25
12	0.2	0.23	0.21	0.23	0.21	0.2	0.56	0.66	0.53	0.58	3.25	3.41	3.46	3.81
13	0.19	0.19	0.16	0.24	0.14	0.19	0.66	0.87	0.64	**0.91**	1.68	1.76	7.16	4.07
14	0.19	0.22	0.21	0.22	0.21	0.2	0.56	0.66	0.52	0.58	3.25	3.41	3.46	3.69
15	0.18	0.19	0.14	0.23	0.12	0.18	0.63	0.82	0.6	0.87	1.58	1.78	7.16	4.07
1_steady curved	0.97	0.43	0.46	0.65	1.34	0.96	0.64	0.77	0.74	0.81	***6.79***	***5.43***	4.64	4.08

Note: Bold italic fonts in the shaded cells are the values outside the acceptable values discussed in Chapter 3. In the case of wheel unloading ratio reaching 1.0, the contact between wheel and rail is removed, so the simulation results beyond that point are invalid and the wagon is assumed to be derailed

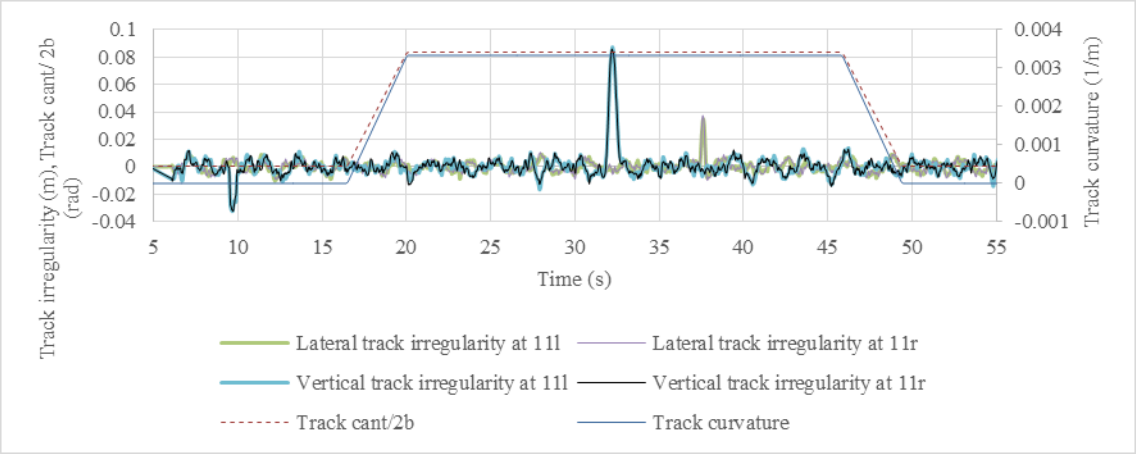

(a) Track geometry including applied isolated track irregularities

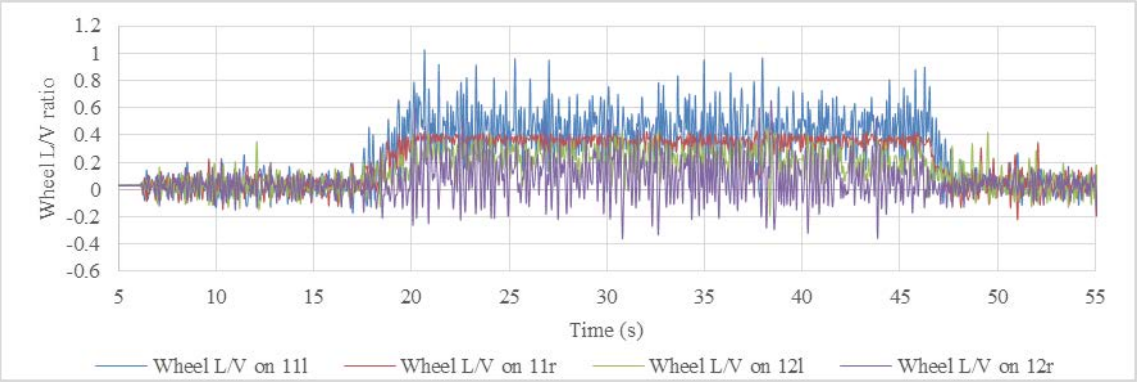

(b) Wheel L/V ratio on full test sections

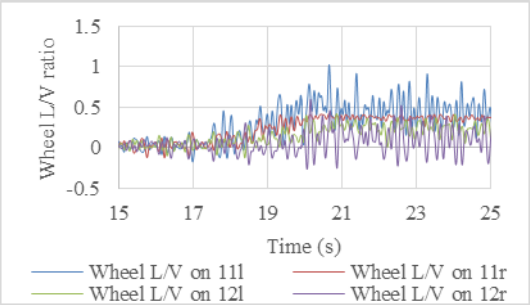

(c) Wheel L/V ratio on transition section

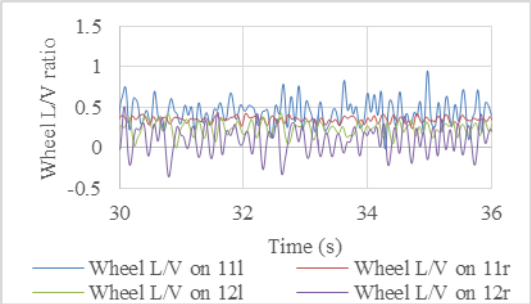

(d) Wheel L/V ratio where isolated vertical track irregularity was applied

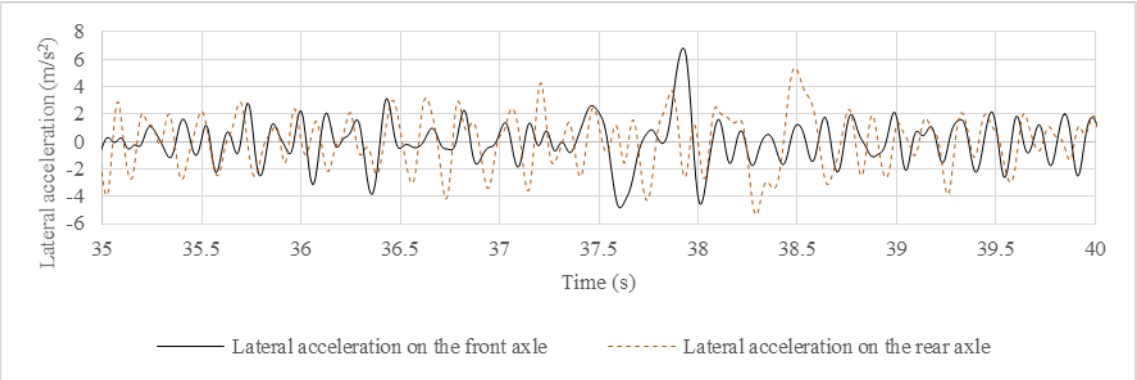

(e) Lateral wagon body accelerations where isolated lateral track irregularity was applied

Figure 7-19: Case 1 of step 5 test on the Concept- 3a wagon model (Empty- 6000kg, Track radius 300m RHC, Cant deficiency 110mm)

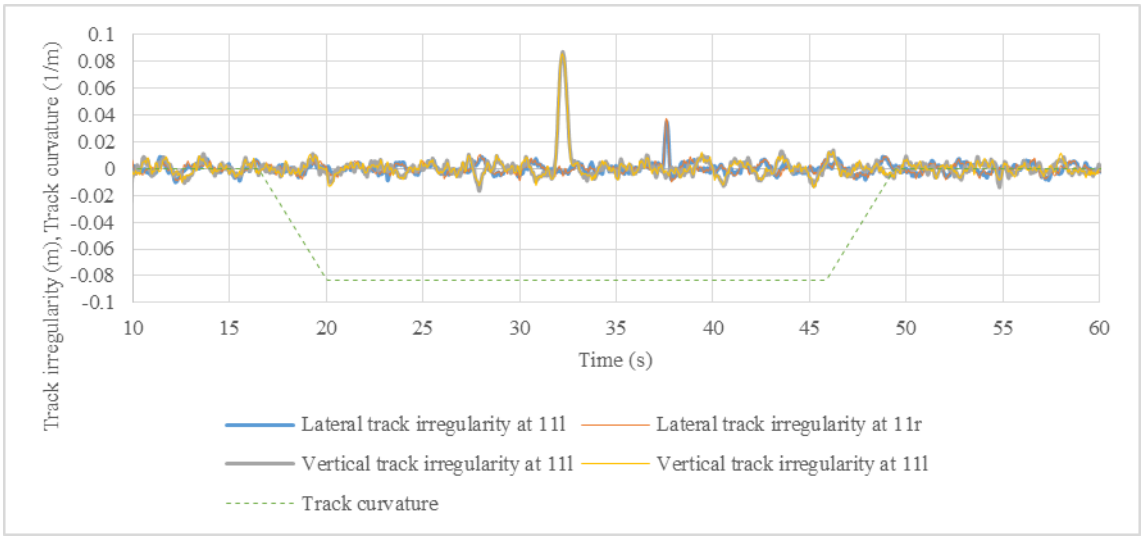

(a) Track geometry including applied isolated track irregularities

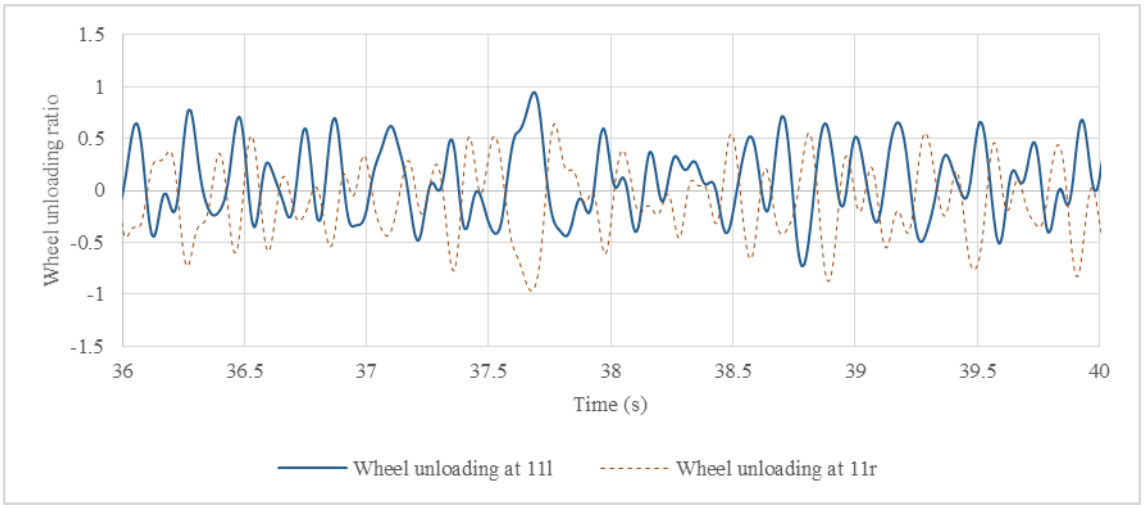

(b) Wheel unloading ratio near applied isolated track defect

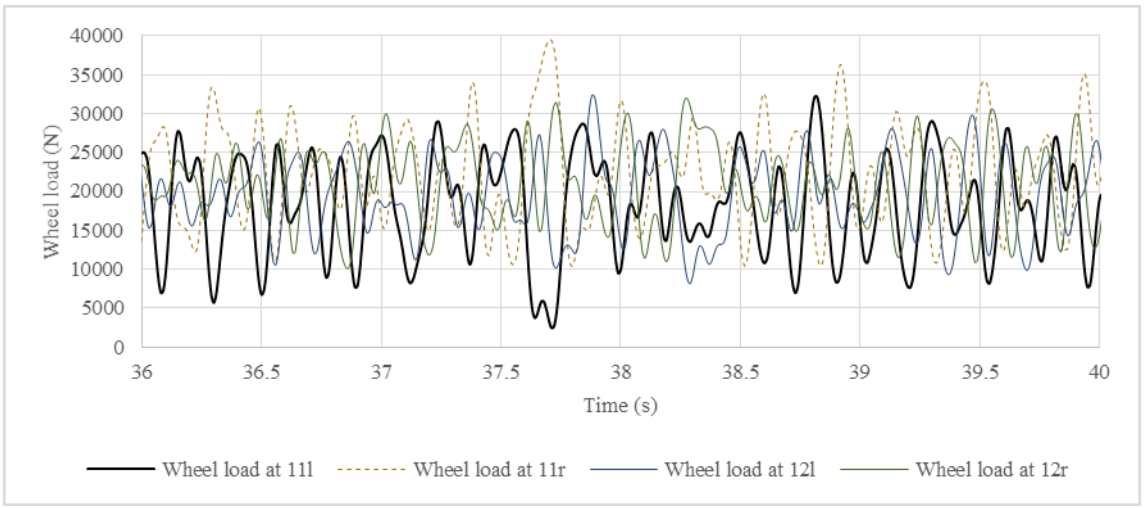

(c) Wheel loads near applied isolated track defect

Figure 7-20: Case 3 of step 5 tests on the Concept- 3a wagon model (Empty, FRA track class 5, track defect limit corresponding to the speed band of 80km/h, Track radius 300m left-handed curve, flattening lateral track defect)

The isolated twist track defects were applied in cases 6-7 according to the datum test conditions (Table 7-9). The Concept- 3a (Empty wagon) model (case 6) passed the datum twist test conditions, but the Concept- 3b (loaded wagon) failed on wheel unloading ratio at long twist track defects in case 7 (Figure 7-21). At the start of the long twist track defect (dip on the right rail), wheel #11r failed to follow the twist track defect and load on that wheel became zero at about 26.5s (Figure 7-21c) which increased the wheel unloading ratio to 1 (Figure 7-21b) and derailment was assumed at that point. Hence the data beyond 26.5s was disregarded. The suspension displacement on wheel #11r went to a maximum of 30mm upward suspension displacement from the initial settled position of 50mm in the loaded case at 26.5s of simulation (Figure 7-21e).

The high stiffness of the loaded suspension restricted suspension travel and so failed to allow the wheel to follow the track (Figure 7-22).The suspension on the left wheel (#11l) in the loaded case allowed more compression (-90mm, Figure 7-23b) than that on the right wheel (-70mm, Figure 7-23a) which also explains the higher vertical wheel load on the left wheel (about 310kN) compared to zero load on the right wheel at 26.5s (Figure 7-21c). The high wheel load on the left wheel occurred as the right wheel failed to share the load by not being able to follow the twist track defect. It therefore follows that adequate suspension travel is required to achieve better dynamic performance on an isolated twist track defect.

The empty case (case 6) with low vertical suspension stiffness of 50kN/m allowed suspension displacement of up to 40mm on wheel #11r corresponding to the wheel load of about 7kN (i.e. wheel unloading ratio of about 0.5 on the empty 6000kg wagon, Figure 7-23c). Wheel #11l displaced to ±18mm from the initial position compared to +42 to -27mm on wheel #11r in the empty case (Figure 7-23c and Figure 7-23d). Thus, allowable movement on the right wheel suspension (low rail on the RHC) allowed the right wheel to follow the DIP on the low rail which gave an acceptable wheel unloading ratio on the right wheel. The empty wheel unloading ratios were all below 0.8 (cases 6, 8, 10, 12 in Table 7-10) and better than the loaded cases (cases 7, 9, 11, 13 in Table 7-10) which reached 1.0.

A further trial of simulations on the concept- 3b model established a twist track defect limit of 45mm that the loaded wagon model could negotiate with the same hard stiffness of 3.38MN/m (cases 8-15) for a design speed of 80km/h. The 45mm twist limit is just below the limit of 48mm corresponding to the P1 limit for the defect band F, but is within the range of defect band F when the P1 limit for the 80km/h speed is in the defect band D. So, the Concept- 3a and Concept- 3b wagon models would require the track quality to be improved by two bands. The datum wagon passed the defect band D in the similar test. So, further work on the suspension is clearly required in order to provide similar twist track defect negotiation capability to the datum wagon. The next step in the development is to consider how the two hypothetical suspensions could be made as a single suspension design, achieving low stiffness when empty and high stiffness when loaded.

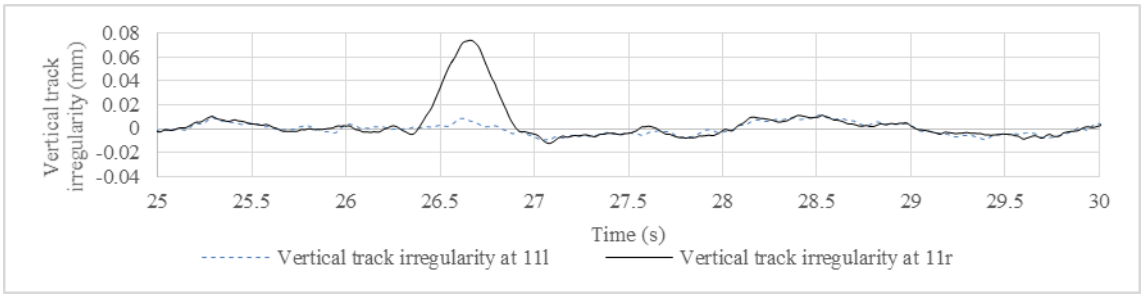

(a) Isolated twist track defect

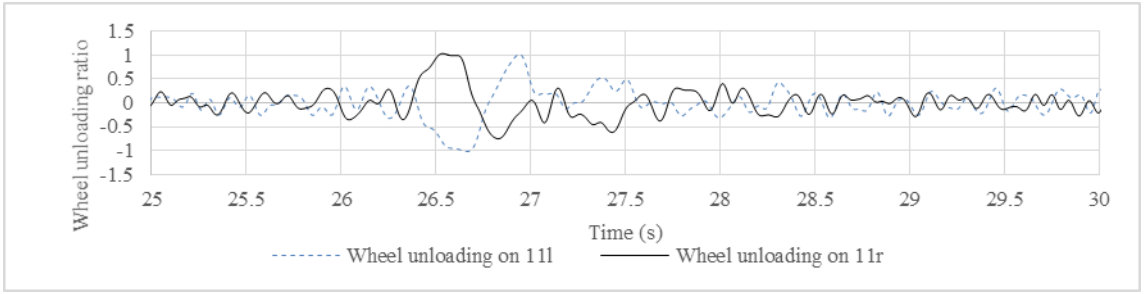

(b) Wheel unloading ratio

(c) Wheel load

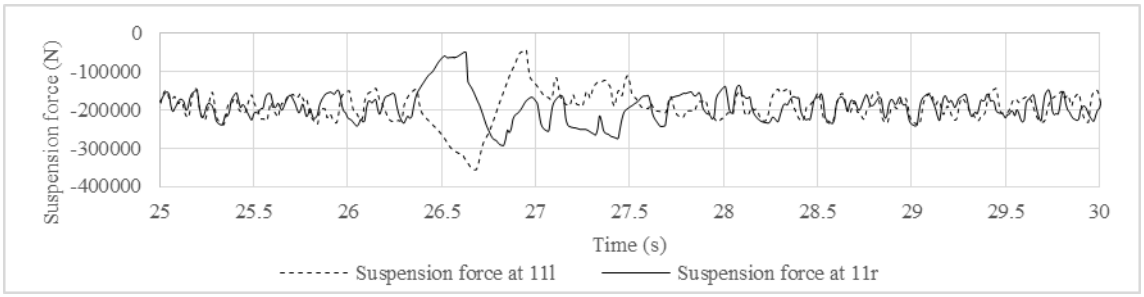

(d) Suspension force

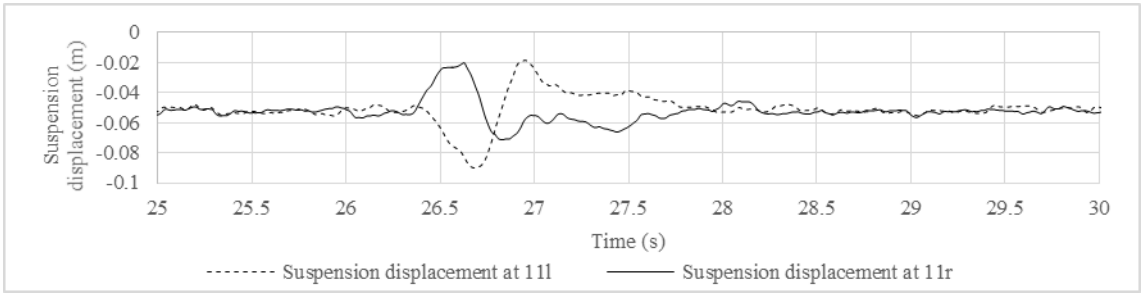

(e) Suspension displacement

Figure 7-21: Application of isolated twist track defect in case 7 of step 5 tests on initial concept wagon (straight track, 88km/h, P1 limit corresponding to 80km/h, loaded condition 78t; wheel load and suspension force act in opposite direction)

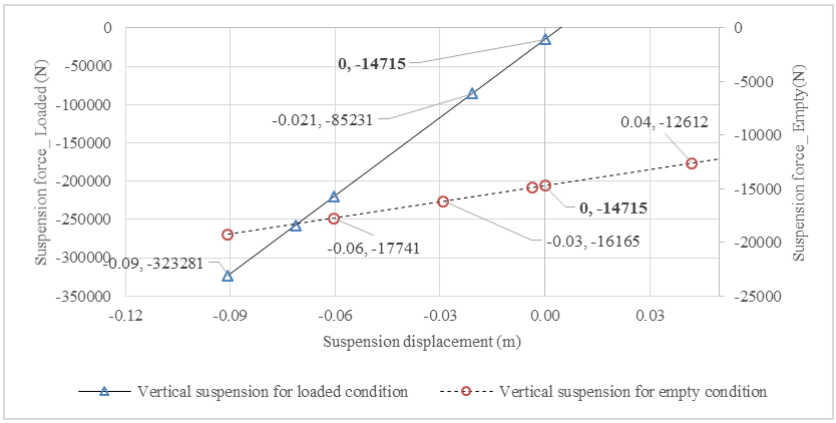

Figure 7-22: Two different vertical suspensions for the empty and loaded conditions as used on the Concept-3a and Concept- 3b wagon models (Empty 6000kg, loaded 78000kg, Empty suspension stiffness 50kN/m, Loaded suspension stiffness 3.38MN/m)

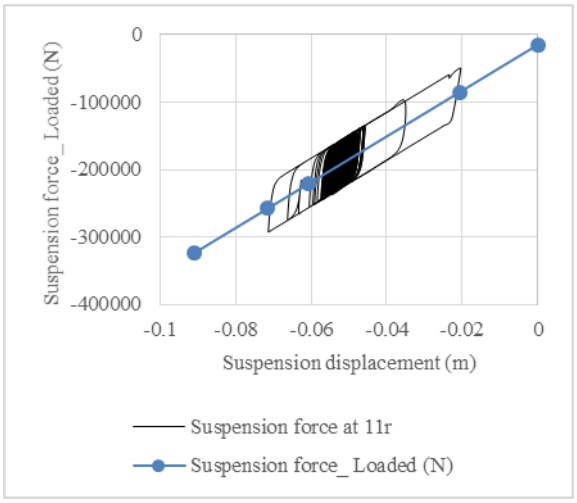

(a) Case 7, isolated twist defect test, loaded, front right rail

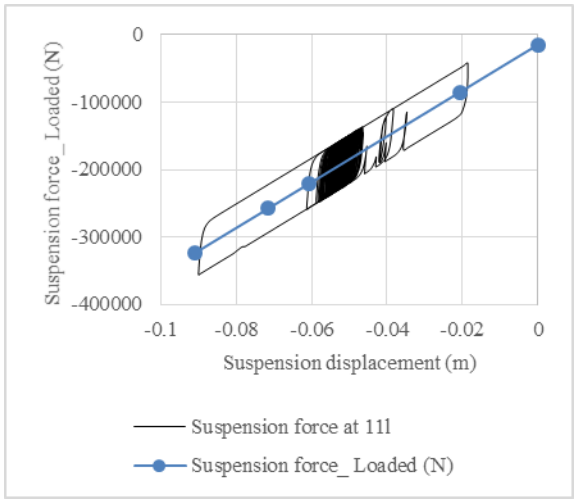

(b) Case 7, isolated twist defect test, loaded, front left rail

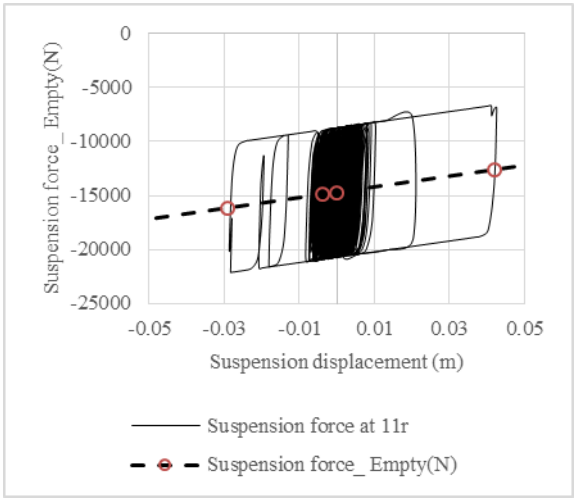

(c) Case 6, isolated twist defect test, empty, front right rail

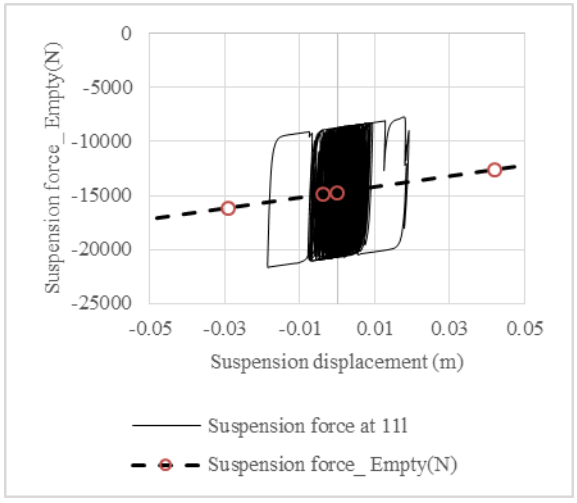

(d) Case 6, isolated twist defect test, empty, front left rail

Figure 7-23: Vertical suspension on front right (11r) and front left (11l) wheels subject to an isolated twist defect of 74mm on right rail (Case 6 and 7, Empty 6000kg, Loaded 78000kg, Empty suspension stiffness 50kN/m, Loaded suspension stiffness 3.38MN/m)

7.8 Practical Consideration of the Suspension Parameters of Concept- 3a and Concept-3b models

At this stage it is important to determine if the suspension parameters obtained from the simulation results of the Concept- 3a and Concept- 3b models in Sections 7.3- 7.7 could be built into a single suspension for practical operation. The vertical stiffness of the Concept-3a and Concept-3b wagon models were 50 kN/m and 3.38 MN/m respectively which gave the static suspension deflection from free length of 294mm in the empty condition and 57mm in the loaded condition on two separate models (considering empty 6000kg, loaded 78000kg). The suspension deflection from free length could be as high as 559mm at 90% wheel overload in the empty condition which is considered as impractical.

The search into existing designs and patents in Chapter 2 revealed that a way to introduce multi-stage stiffness is to add a spring nest. As the development of the concept parameters was obtained starting with a typical UIC link and leaf spring suspension, the possible modification of the UIC link and leaf spring suspension is intended. The concept of the link mechanism with a bar element and coil springs replacing the leaf spring is proposed in a patent [37]. In this thesis, two multi-stage coil springs are proposed to be installed in series with the leaf spring instead of the bar element in the patent [37] to provide the required softness to the suspension at low load conditions (Figure 7-24). The combination presented in this thesis is therefore believed to be new.

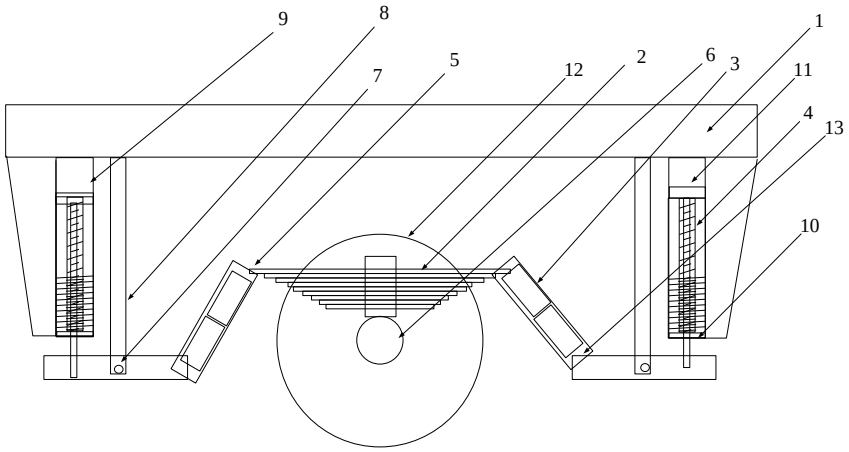

Figure 7-24: Proposed 3 stage suspension [1- Wagon body, 2- Leaf spring, 3- UIC link, 4- Coil spring, 5- Eye of leaf spring, 6- Bearing assembly, 7- Pivot point, 8- Pivot rod, 9- Support block of the coils spring, 10- Seat of coil spring, 11- Fabricated section, 12- Wheel, 13- End bearing]

In the proposed suspension, the end of coil spring 4 is equipped with a hard stop 10 (Figure 7-24). A double-link 3 is used to connect the leaf springs with the coil springs 4 via a pivot point 7. One end of the link is connected to the eye 5 of the leaf spring and the other end is connected to the end bearing 13 in the pivot 7. A fabricated section 11 is installed to support the coil spring 4 along the support block guide 9. The guide 9 can be in the form of a cylinder surrounding the coil spring to constrain the spring movement to just the vertical directions.

A three-stage suspension system has been proposed in this section as a starting point to combine the empty and loaded vertical suspensions (Concept 4). Three stages can be achieved by using two stages on each of the coil springs placed in series with the leaf spring. The coil springs will provide the softness to the suspension in the first two stages. The leaf spring will provide the stiffer third stage. The first stage of suspension needs to be very

soft to provide easy adjustment to twist at low load conditions. As a starting point, a 60mm limit was set at the first stage of suspension. The second and third stages were provided at 60 and 80mm (Figure 7-25). A vertical stop (40MN/m) was provided at a hard limit position of the suspension movement of 180mm. A lift-off element providing no stiffness at the tensile condition was also included.

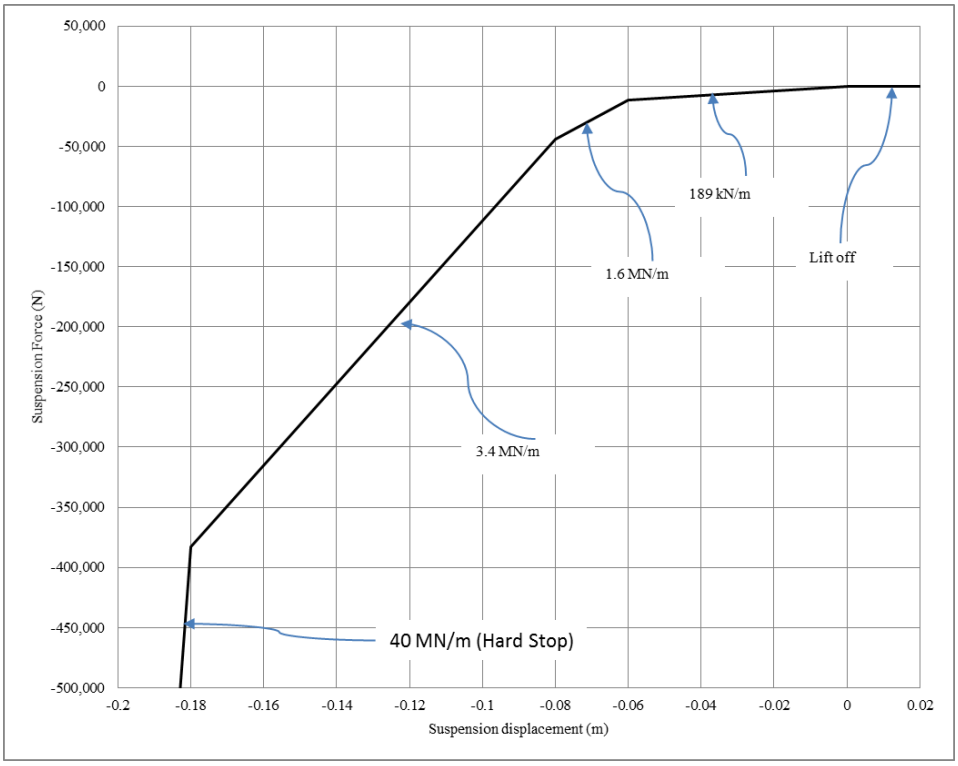

(a) Full vertical suspension

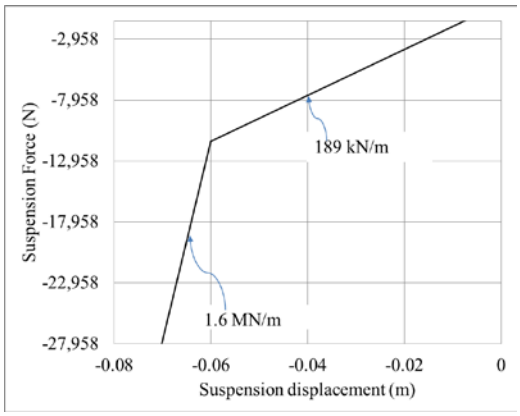

(b) Vertical suspension at ±90% wheel load of empty condition 6000kg

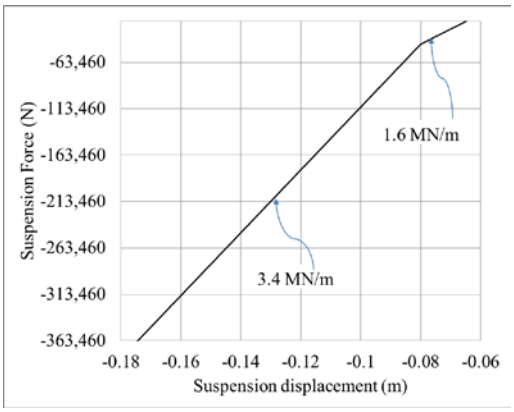

(c) Vertical suspension at ±90% wheel load of loaded condition 78000kg

Figure 7-25: Multi-stage vertical suspension concept

The soft coil springs 4 can deflect to hard limits at higher loads. At a static wheel load of 14.71kN in the empty (6000kg) condition the wagon settles at about 62mm (Figure 7-25b) of suspension movement, and at a static wheel load of 191.3kN in the loaded (78000kg) condition, the wagon settles at about 130mm (Figure 7-25c) of suspension movement which makes a vertical height difference of 58mm in the suspension between the empty and loaded conditions. The placement of different loading ranges from the initial steady positions (62mm and 130mm on the empty and loaded case) showed that the dynamic load situation (within ±90% of the wheel load)

in the empty and loaded conditions stay between stage 1-2 (Figure 7-25b) and stage 2-3 (Figure 7-25c) respectively. The stiffness element then allows total vertical movements of 60mm and 105mm in the empty and loaded conditions respectively in the ±90% of the wheel load range. The softer suspension allows more deflection on the overloading side, reducing unloading on the low load side (better load sharing).

The challenge for the loaded conditions is to limit vertical displacement to practical levels within the suspension unit. A hard limit can create an excessive vertical force on the wheel and generate wheel overloading and severe wagon responses. So, it is necessary to provide sufficient spring travel in the design. The hard limit in the Concept-4 suspension was placed at 180mm which allows more than 90% of wheel overload at the loaded condition of 78t.

7.8.1 Theoretical Stiffness Parameters of the Concept- 4 Suspension

The two coil springs in the Concept- 4 suspension (Figure 7-24) act in a parallel configuration to each other. The coil springs and leaf spring combination acts in series to give different equivalent stiffnesses as per Equation 7-2.

$$k_e = \frac{k_{zc}*(k_{c1}+k_{c2})}{k_{zc}+(k_{c1}+k_{c2})} \qquad \textbf{7-2}$$

where k_e is the equivalent stiffness of the coil and leaf springs (N/m); k_{c1} and k_{c2} are stiffnesses of the coil springs placed in parallel (N/m); k_{ZC} is the stiffness of the leaf spring (N/m)

In order to achieve the equivalent stiffness parameters corresponding to Figure 7-25, the stiffnesses of the coil spring and leaf spring could be chosen as per Table 7-11. As the coil springs have two stages, two more coil spring stiffness elements kc_3 and kc_4 need to be defined. The coil springs are the same on both sides of the axle box, so kc_1 and kc_2 are considered to be the same as are kc_3 and kc_4.

Table 7-11: Vertical suspension parameters of the concept- 4 wagon

Suspension Stages	Coil spring stiffness		Leaf spring stiffness	Equations equivalent stiffness of suspension stages	Equivalent stiffness	Suspension Displacement limits
	kc1= kc2	kc3= kc4	Kzc		ke	
	kN/m	kN/m	kN/m	kN/m	kN/m	mm
1	100	1419	3380	$k_{e1} = \frac{k_{zc} * (k_{c1} + k_{c2})}{k_{zc} + (k_{c1} + k_{c2})}$	189	60
2	100	1419	3380	$k_{e2} = \frac{k_{zc} * (k_{c1} + k_{c2} + k_{c3} + k_{c4})}{k_{zc} + (k_{c1} + k_{c2} + k_{c3} + k_{c4})}$	1600	80
3			3380	$k_{e3} = k_{zc}$	3380	180
4				$k_{e4} = 40 \times 10^6$		

The schematic diagram of the springs in three stages is shown in Figure 7-26. The first stage requires a suspension movement of 60mm on the soft spring of stiffness 100kN/m (Table 7-11). In order to have a soft spring of 60mm movement from the free length position, the spring on the second stage needs to have a free length at least 60mm. The second stage uses a harder coil spring which is allowed 20mm of displacement before hitting the hard stop on the coil spring assembly. The third stage of the suspension (on the leaf spring) activates at a suspension displacement of 80mm (Figure 7-26c).

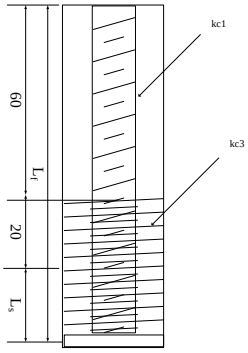

(a) Coil springs in free length condition (includes the first stage, L_f is the free length, L_s is the solid length, kc1 and kc3 are the first and second stage coil spring stiffnesses)

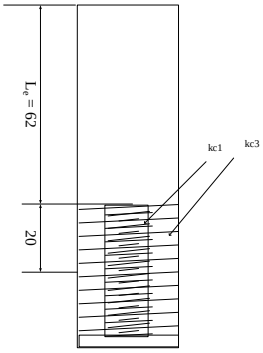

(b) Coil spring in empty settled position (second stage, L_e is the deformation of coil spring in empty condition from free length position)

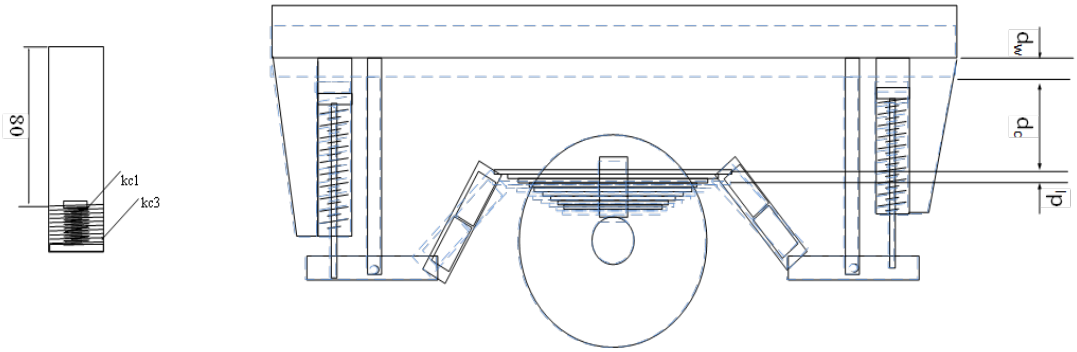

(c) Coil spring and leaf spring in the third stage (blue dotted lines indicate loaded conditions, d_w is the vertical displacement of wagon body due to load, d_c is the displacement on the coil spring from the free length approximation, d_l is the displacement on the leaf spring and link suspension)

Figure 7-26: Schematic diagrams of the Concept- 4 suspension at different stages (all dimensions in mm)

7.8.2 Coil Springs for the Concept- 4 Suspension

A possible nest of AAR springs on the Concept- 4 suspension providing the stiffness parameters in Table 7-11 would be two D3 outer springs and one B354 spring (Table 7-12). The Concept- 4 suspension would have one spring nest on either side of the leaf spring. The spring nest comprising two D3 outer springs and one B354 spring can be arranged in two ways in both longitudinal and lateral orientations (Figure 7-27). The approximate size of the spring nests is evaluated as 400mm X 150mm (Figure 7-28a) and 300mm X 150mm (Figure 7-28b) based on the coil diameter of the coil springs (Table 7-12). If the arrangement of Figure 7-27b is placed along the lateral axis on both sides of the leaf spring, the total length of the Concept- 4 suspension would be increased by at least 300mm to a minimum overall length of 1800mm which would be 100mm longer than the current standard length of 1700mm (considering maximum leaf length of 1400mm) [136]. Both the 300mm and 400mm lateral length orientations are possible as there is no other element under a typical two-wagon chassis at those positions.

Table 7-12: Suitable coil springs from the AAR spring list closely matching the coil springs of the Concept- 4 suspension

Spring name	Coil diameter (mm)	Free Length (m)	Solid Length (m)	Solid Capacity (N)	Stiffness (kN/m)	Number of springs	Total stiffness (kN/m)
D3 outer [137]	140	0.230	0.167	47689	751	2	1500
B 354 [138]	79	0.292	0.167	12700	101	1	101

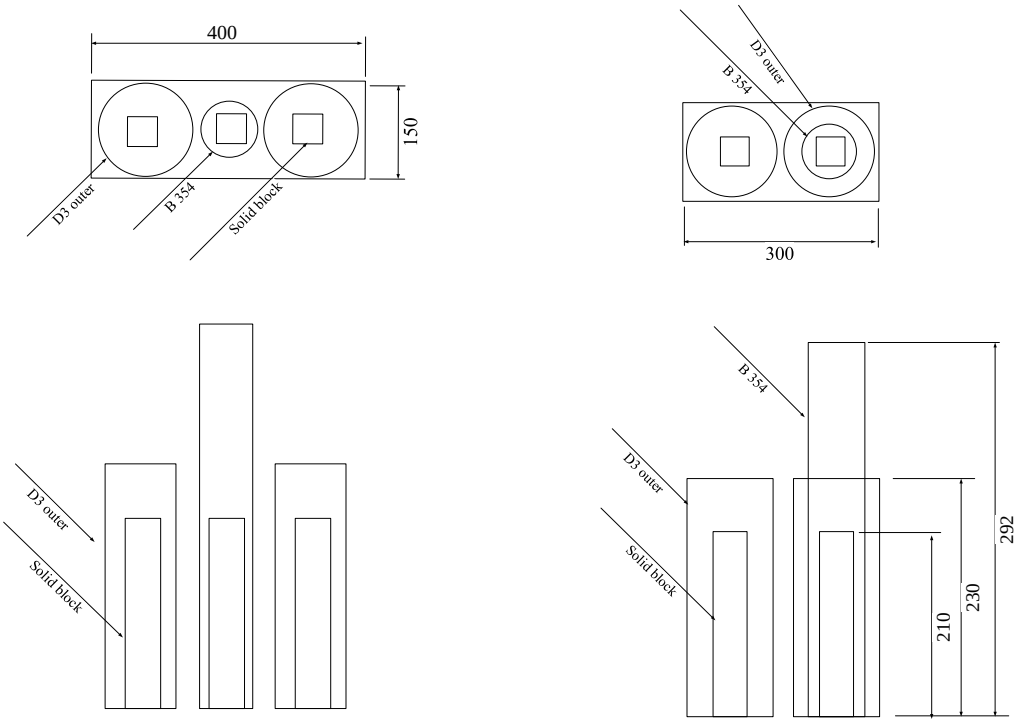

(a) 400mm X 150mm arrangement (b) 300mm X 150mm arrangement

Figure 7-27: Possible coil spring nests on the Concept- 4 suspension

As the empty load (6000kg) condition settles at about 62mm displacement on the vertical suspension, the maximum height of the coil spring suspension would be 230mm considering the maximum free length of 292mm on the B354 springs (Figure 7-27). Based on the current height of the suspension bracket of the UIC link suspension of 340-365mm [136], it is possible to install the coil spring attachment within the standard allowable gap between the wagon body and connection point to the links. As the solid length of the suspension is 167mm, the D3 outer springs would have about 63mm movement which is higher than the intended movement of 20mm on the second stage. So a 210mm high hard stop element (solid block, Figure 7-27) can be attached to the spring mount position to restrict the second stage movement to 20mm.

7.8.3 Leaf Spring for the Concept- 4 Suspension

The leaf spring suspension on the Concept- 4 suspension has almost double the stiffness of the typical UIC link suspensions. So, there is a need to change the leaf parameters to achieve the harder leaf spring for the Concept- 4 suspension. The mean flexibility of the leaf spring can be measured using Equations 7-3 to 7-6 included in the UIC CODE 517 using rectangular cross-section spring leaves and identical thicknesses of leaves [136]. Leaf springs with identical thicknesses are also known as trapezoidal springs [139]. The stiffness of the spring is the inverse of the flexibility term as can be obtained from Equation 7-7. Equations 7-3 and 7-7 show that the stiffness parameter is inversely related to the length of the leaf spring and proportionately related to width, height and number of leaves. The vertical stiffness is also affected by the increased link inclination and elastic deformations on the double-link due to the vertical load [93]. So, it is necessary to use the overall stiffness of the leaf spring and link suspension in the equivalent stiffness term of the Concept- 4 suspension modelling. The stiffness of the

overall suspension of leaf spring and links can be determined considering the camber in the unloaded leaf spring and the diameter of the eye of the leaf spring using Equation 7-8 as included in [93].

$$C_{ar} = \frac{L^3 K_1 K_2}{nbEh^3} \quad \textbf{7-3}$$

$$K_1 = \frac{1}{4}\left\{1 + (1 - \frac{e}{L})^3 \left[3.\frac{\frac{1}{2} - 2v + v^2\left(\frac{3}{2} - \ln v\right)}{(1-v)^3} - 1\right]\right\} \quad \textbf{7-4}$$

$$v = \frac{n'}{n} \quad \textbf{7-5}$$

$$K_2 = \begin{cases} 1 & when\ S_{po} > 0 \\ \sqrt{1 - \frac{16}{3}(\frac{S_{po}}{L})^2}^3 & when\ S_{po} \leq 0 \end{cases} \quad \textbf{7-6}$$

$$k_{ar} = \frac{1}{C_{ar}} \quad \textbf{7-7}$$

$$k_{zc} = \frac{k_{ar}}{1 + 0.0019 * (p - \frac{d_i}{2})} \quad \textbf{7-8}$$

where C_{ar} is the mean flexibility of the leaf spring (mm/kN), L is the length of the main leaf measured between the centres of the rolled eyes with the leaf assumed to be straight (mm), n is the total number of leaves, b is the leaf width (mm), E is the Young's modulus (kN/mm^2), h is the thickness of the leaves (mm), K_1 is a coefficient depending on width of spring bracket and number of leaves, e is the width of the spring bracket (mm), n' is the number of leaves with length L, S_{po} is the deflection of the first spring leaf without load (mm), K_2 is a second coefficient, k_{ar} is the stiffness of the leaf spring (kN/mm), C_{zr} is the overall mean flexibility of the leaf spring and link suspension (mm/kN), p is the camber of unloaded spring (mm), d_i is the diameter of the leaf spring eye (mm), K_{zc} is the overall stiffness of leaf spring and link suspension (kN/mm).

A standard leaf spring suspension with the length of 1200mm has been used to evaluate the change of lengths on stiffness parameters (Table 7-13). A typical leaf spring of the UIC two-axle wagon produces a stiffness of 1.42kN/mm (MN/m) using the parameters in Table 7-13. Both the leaf spring stiffness and overall stiffness parameters of the vertical suspension increases with the decrease of the length of leaf springs (Figure 7-28) as calculated by Equations 7-3 to 7-8 using the parameters of Table 7-13.

The overall stiffness parameters (leaf springs and links) are lower than the leaf spring parameters alone (Figure 7-28). Reducing the length of the leaf spring to 900m provides the overall stiffness of 3.43 MN/m which is close to the desired stiffness of 3.38 MN/m for the Concept- 4 suspension. However, a leaf length of 900m may not be a good option as the links connected to the leaf may be placed within the diameter of the wheel (example 920mm diameter) which may create an obstacle to lateral link movement. So, the other option is to increase leaf width or leaf thickness. Leaf width of about 280mm or each leaf thickness of 21mm could provide 3.3 and 3.2MN/m stiffness on the standard main leaf length of 1200mm (Figure 7-28b, c). The leaf width of 280mm is 2.5 times the standard width of 120mm which may require further adjustment on the axle box. Increasing the thickness of all leaves to 21mm from 16mm would increase the overall height of the leaf spring assembly by 40mm based on an 8 leaf assembly. Making the leaf spring 40mm higher than the standard design would then require a reduction of the suspension bracket height to 325mm. This would still be suitable to accommodate the Concept- 4 coil springs (maximum free length of 292mm). So, the increase in leaf thickness has been accepted in this thesis as a suitable means to achieve the high third stage stiffness of 3.38MN/m. It is possible to achieve 3.22MN/m stiffness on the

leaf spring and links using the leaf thickness of 21mm (parameters set X, Table 7-13). The thickness can be further increased to 21.35mm to obtain the required 3.38MN/m. A more practical way could be reducing the camber of the unloaded spring to 36mm (parameters set Y, Table 7-13). The fine tuning of hard stiffness is not essential at this stage as it is adequate to know that the leaf spring design could be modified in a practical way to achieve the high stiffness intended for the high payload on the concept suspension.

Table 7-13: Parameters of a leaf spring with varying lengths

Parameters	Symbol	Unit	Parameter values						Possible parameter sets	
									X	Y
Length of leaf spring	L	mm	1200	1100	1000	900	800	700	1200	1200
Width of each leaf	b	mm	120	120	120	120	120	120	120	120
Height of each leaf	h	mm	16	16	16	16	16	16	21	21
Number of leaves	n		8	8	8	8	8	8	8	8
Number of leaves having length of L	n/		2	2	2	2	2	2	2	2
Width of spring bracket	e	mm	100	100	100	100	100	100	100	100
Camber of unloaded spring	p0	mm	64	64	64	64	64	64	64	36
Diameter of spring eye	di	mm	36	36	36	36	36	36	36	36
Young's Modulus	E	kN/mm^2	207	207	207	207	207	207	207	207
K1			0.304	0.303	0.302	0.300	0.297	0.295	0.35	0.3045
K2			1	1	1	1	1	1	1	1.00
Mean flexibility of leaf spring	Car	mm/kN	0.646	0.496	0.370	0.268	0.187	0.124	0.29	0.29
Mean flexibility of leaf spring and links	Czr	mm/kN	0.703	0.456	0.341	0.247	0.172	0.114	0.26	0.28
Stiffness of leaf spring	Kar	kN/mm	1.55	2.02	2.70	3.73	5.35	8.06	3.50	3.50
Stiffness of leaf spring and links	Kzc	kN/mm	1.42	1.86	2.48	3.43	4.92	7.41	3.22	3.38

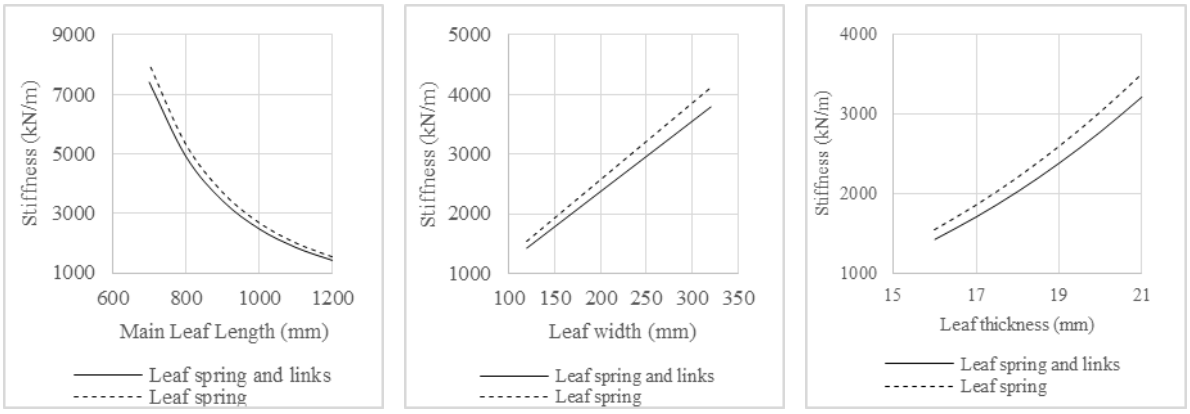

(a) Effect of leaf length (Leaf width 120mm and leaf thickness 16mm)

(b) Effect of leaf width (Main leaf length of 1200mm)

(c) Effect of leaf thickness (Main leaf length of 1200mm)

Figure 7-28: Effect of leaf spring length, width, and thickness on vertical stiffness on trapezoidal leaf springs (using leaf spring parameters presented in Table 7-13)

7.9 Summary

A typical UIC two-axle wagon with leaf spring and link suspensions was used to obtain the parameters of a concept wagon. The principle of vehicle acceptance procedure by simulation (VAPS) was used as a means to evaluate possible concept wagons with the desired capacity and performance. The length parameters (BCD and Overhang), and suspension parameters were changed at different stages to achieve a suitable concept- 2. Practical considerations of buildability and operation revealed that a three-stage suspension would be necessary in order to give the concept wagon satisfactory dynamic performance. A concept suspension using leaf spring, UIC links, and coil springs has been proposed (Concept- 4). It is possible to create a spring nest of the coil springs using existing AAR springs. The thickness (modified to 21mm from the typical 16mm) and camber of the unloaded leaf spring (reduced to 36mm) can be modified on the existing leaf spring and UIC link suspension to achieve the high stiffness (3.38MN/m) requirement in the third stage of the Concept- 4 suspension.

Chapter 8
Evaluating Modelling Parameters of the Concept-4 Wagon Model

8.1 Introduction

The vertical suspension parameters for the concept- 4 wagon developed in Chapter 7 are required to be tested in a model along with other wagon parameters. In this Chapter, a simplified wagon mass model comprising load, suspension, and ground elements (Figure 8-1) has been used to evaluate force-displacement characteristics, modelling methods, damping characteristics and natural frequency of the proposed suspension. The simple wagon mass model provides a simplified platform for examining the suspension without dynamic effects from the connections in a full wagon model. The four suspension elements were placed at the four corners of a rectangular beam representing the wagon body (Figure 8-1).

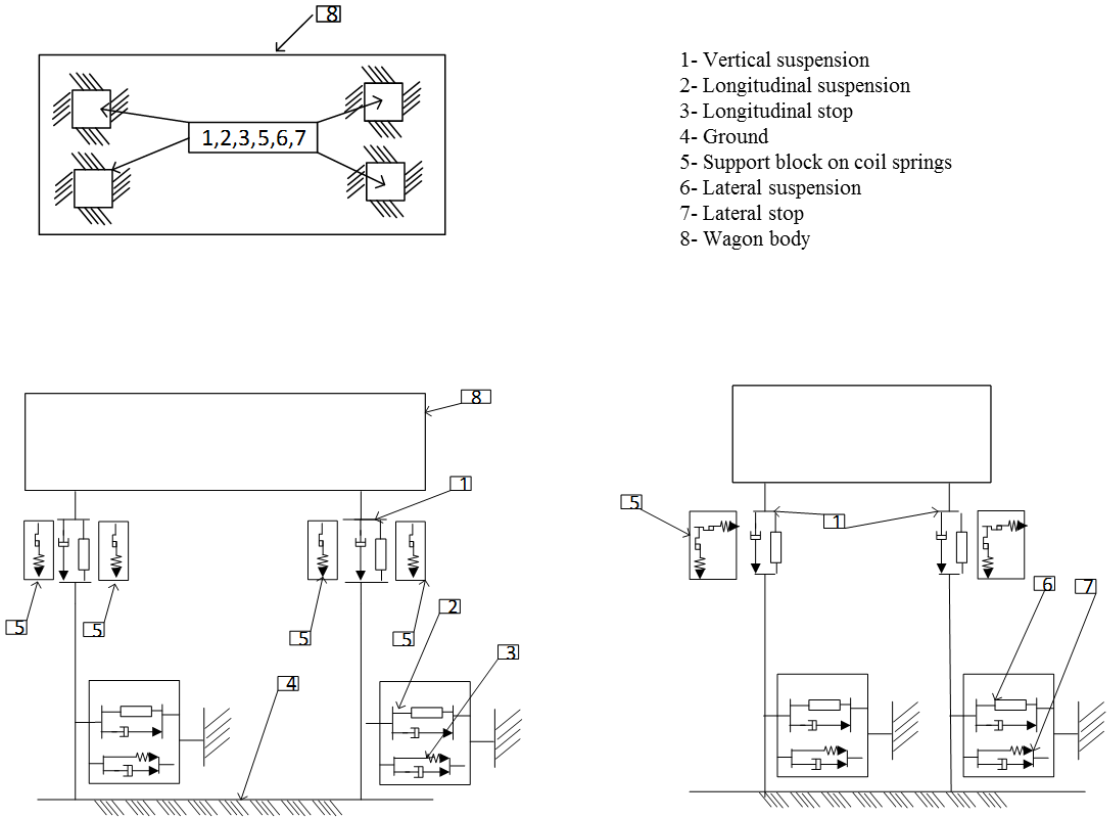

Figure 8-1: Simplified wagon mass model

8.2 Evaluating Vertical Suspension Parameters and Modelling

The Concept- 4 suspension contains a leaf spring, double-links, and coil springs. The leaf spring and UIC double-links arrangement are similar to that used in a typical leaf spring and UIC double-link suspension. As there is no other frictional element in the Concept- 4 wagon model, it is assumed that the friction damping that occurs in the Concept-4 wagon model is similar to that of the typical leaf spring and UIC link suspensions. The characteristic

friction damping property of the Concept- 4 suspension is therefore estimated from the empirical data of the UIC link and leaf spring suspension.

8.2.1 Estimation of Vertical Suspension Characteristic of the Concept- 4 Wagon

The vertical suspension in a typical leaf spring UIC double-link suspension generates a hysteresis loop due to the friction in the suspension as shown in Figure 8-2 [93]. The hysteresis increases with displacement due to higher normal forces and hence higher friction forces. In some cases, a second stage leaf spring is present (Kz_{ed}). As a starting point, the single stage leaf spring (kz_e) DCBA hysteresis loop in Figure 8-2 is considered for estimation as the leaf spring in the Concept- 4 suspension.

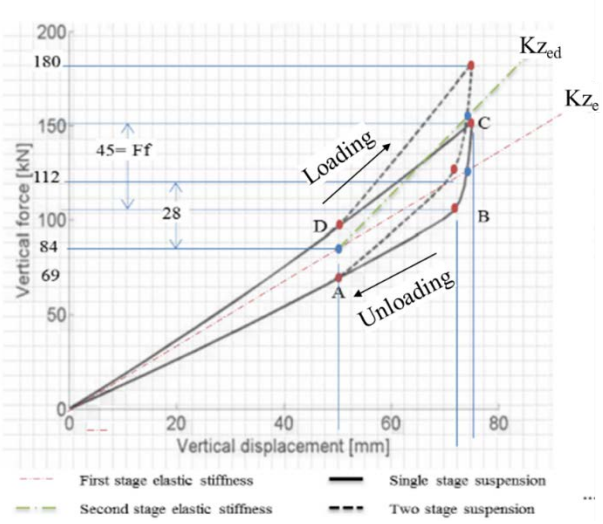

Figure 8-2: Vertical characteristic of a typical UIC leaf spring suspension system [93] (Ff is the friction force)

The loading (DC) and the unloading (BA) cycles in the hysteresis loop possess different stiffnesses in the empirical plot (Figure 8-2). In the modelling, the stiffness parameters in the loading and unloading cycles have been considered to be the same for simplification. The empirical plot has been simplified to form the DCEA loop (Figure 8-3). In the simplified approach in this chapter, the friction damping is considered constant which creates a parallelogram hysteresis (DCEA) instead of the empirical DCBA hysteresis loop (Figure 8-3).

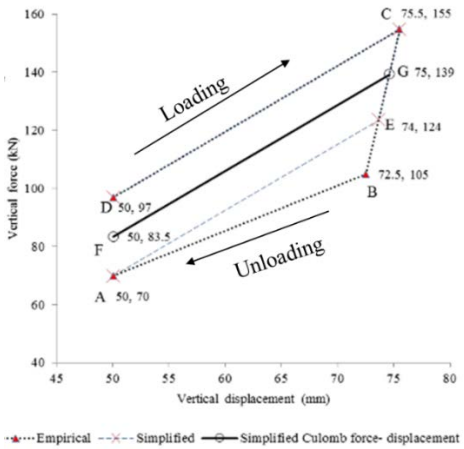

Figure 8-3: Estimated values of leaf spring suspension obtained in this thesis using the plot of Figure 8-2

The following simplifications have been used in the modelling of a simplified vertical Concept-4 suspension in this thesis:

- The stiffnesses in the loading (DC) and unloading (EA) cycles are the same, which creates the DCEA hysteresis loop shown in Figure 8-3
- The elastic stiffness (FG in Figure 8-3) bisects the hysteresis loop (DCEA) equally
- Friction damping is the same at the start of the loading (AD) and the unloading cycle (CE)
- Force changes exponentially with displacement at the terminal points of loading (C) and unloading (A).
- Two different friction damping values are used for the low load (example, empty condition) and high load (example, loaded condition) conditions.

The friction damping has been estimated as ±2.5kN for low vertical load and ±25kN for high vertical load conditions (Figure 8-3). The estimated friction damping represents ±17% and ±13% of the empty and loaded vertical axle box loads respectively (14.7kN for the empty mass of 6000kg, 191.3kN for the loaded mass of 78000kg). The friction damping per axle-box load on the Concept-4 vertical suspension (±13% - ±17%) is higher than for conventional new leaf springs (±4 - 8% [32]) and close to that obtained for reconditioned leaf springs (±13 - ±15% [32]). In this chapter, the friction damping was modelled for static vertical loads (a simplified approach) as used in the tutorial model in Chapter 7. A list of simplified parameters from Figure 8-3 is shown in Table 8-1.

Table 8-1: Estimated values of vertical suspension parameters (Concept- 4) from simplified plots (Figure 8-3) of empirical data

Suspension parameters	Value	Unit	Relevant sections in Figure 8-3
Maximum vertical friction force when moving in positive direction (High vertical load)	24.82	kN	FD
Maximum vertical friction force when moving in negative direction (High vertical load)	24.82	kN	FA
Maximum vertical friction force when moving in positive direction (Low vertical load)	2.5	kN	FD
Maximum vertical friction force when moving in negative direction (Low vertical load)	2.5	kN	FA
Friction damper series stiffness	13.6	MN/m	AD, CE
Elastic vertical stiffness stages	189, 1600, 3380	kN/m	FG

8.2.2 Comparison between the Simplified (Concept- 4) and Empirical Vertical Suspension Parameters

The simplified vertical suspension (Figure 8-3) has been compared with the empirical estimation (Figure 8-2) based on possible wheel unloading ratio characteristics in the hysteresis loop. The effect of fixed friction damping properties for the empty and loaded conditions can be explained as per Figure 8-4. At a suspension displacement of 21mm, empirical estimation gives about -3.2kN of suspension force on the unloading path compared to -1.47kN (on empty unloading path) in the simplified approach (Figure 8-4b). Based on a wheel load of 14.7kN in the empty condition, the wheel unloading ratio will be higher based on the simplified approach compared to the empirical estimation (0.9 and 0.78 in the simplified and empirical approach respectively considering static load condition, Table 8-2).

On the other hand, the suspension force is lower based on the simplified approach than that on the empirical approximation in the loading cycle of the hysteresis loop, and that results in a higher wheel unloading ratio in the empirical approach (0.9) than in the simplified approach (0.75) at a suspension displacement of 6mm (Figure 8-4b,

Table 8-2). In the case of an empty load of 6000kg, the point of changing the hysteresis from the unloading cycle to the loading cycle occurs at about 21mm of vertical displacement corresponding to 90% wheel unloading (Figure 8-4b). At a 21mm displacement in the loading cycle of the hysteresis loop, the empirical and simplified approaches would result in wheel unloading ratios of 0.67 and 0.52 respectively (Table 8-2). So, in the loading cycle, the simplified approach would not provide a strict condition. However, the wheel unloading ratio in the loading cycle is not critical as the maximum wheel unloading ratio would occur on the unloading cycle. The wheel unloading ratio on the loading cycle would be even less considering an exponential type transition between the loading and unloading cycles as is the case for a typical leaf spring. So, the loading cycle generally provides lower wheel unloading ratios than occur on the unloading cycle of the suspension and it is therefore important to evaluate the higher wheel unloading ratio on the unloading cycle of the suspension. As the simplified approach gave higher wheel unloading ratios on the unloading cycle, it is considered as a stricter approach compared to the empirical approach.

The choice of a fixed friction damping property for the empty and loaded conditions in the simplified approach has resulted in a situation of higher suspension force for the low dynamic load situation in the loaded conditions. As an example, a loaded wagon will move the Concept-4 vertical suspension displacement to nearly 80mm on the unloading cycle (Figure 8-4d) where low damping of ±2.5kN is expected as per the empirical approximation. However, in the simplified approach, a damping force of ±25kN has been used throughout the suspension path in the loaded case. The consideration of higher vertical friction damping will give a higher wheel unloading ratio on the unloading cycle in the simplified approximation compared to the empirical approximation (wheel unloading ratios of 0.9 and 0.77 at a suspension displacement of 80mm, Figure 8-4d, Table 8-2). The loading and unloading cycles in the simplified approach become close to the empirical data at higher dynamic load conditions (Figure 8-4c, Figure 8-4e).

Based on the analysis of vertical suspension in this section, it can be seen that the simplified approach used in the simulation study in this thesis gives higher wheel unloading ratios in the unloading cycle of the suspension compared to the empirical estimates.

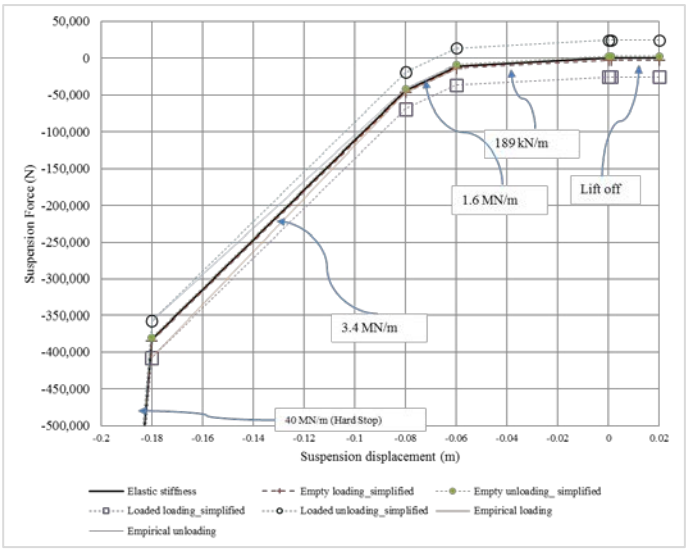

(a) Friction damping in the vertical stiffness element

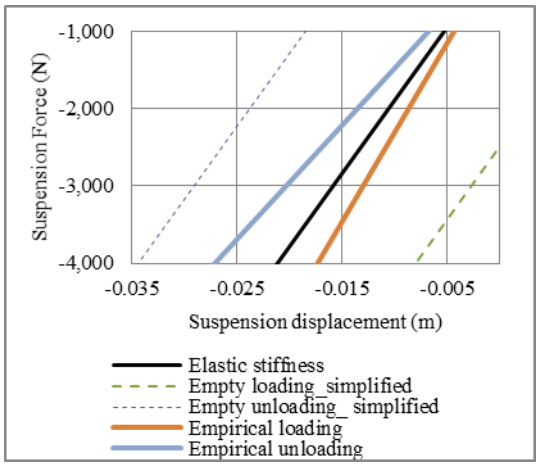

(b) Friction damping near 90% unloading in the empty condition

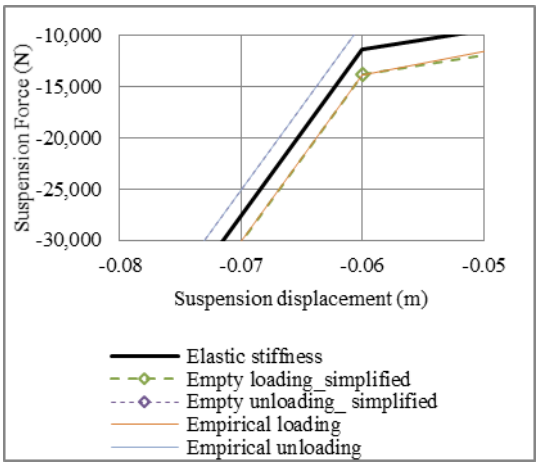

(c) Friction damping near 90% overloading in the empty condition

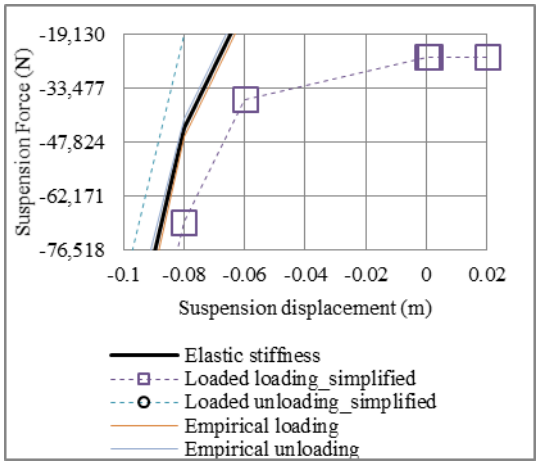

(d) Friction damping near 90% unloading in the loaded condition

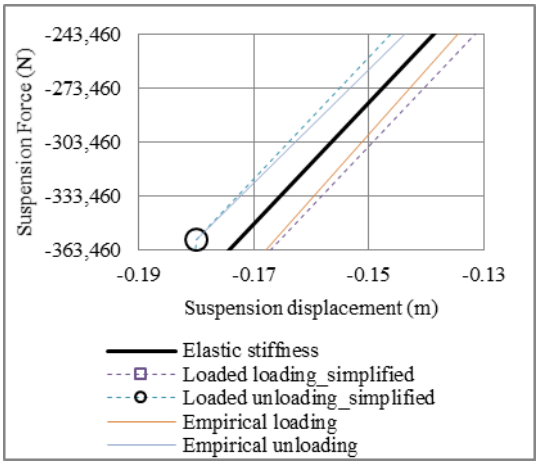

(e) Friction damping near 90% overloading in the loaded condition

Figure 8-4: Approximate friction damping in the empty (6000kg) and loaded (78000kg) conditions on the Concept- 4 suspension [negative suspension force refers to downward force on suspension and reduction in negative force on suspension refers to wheel unloading conditions]

Table 8-2: Some characteristic points in the hysteresis loop of a vertical suspension for comparison of the empirical and simplified (Concept- 4) modelling approach (Empty mass- 6000kg, Loaded mass- 78000kg)

Load	Cycle in the hysteresis loop	Suspension displacement (m)	Suspension force (N)		Wheel unloading ratio		Reference Figure
			Empirical	Simplified	Empirical	Simplified	
Empty	Unloading	-0.021	-3200	-1471	0.78	0.90	Figure 8-4b
Empty	Unloading	-0.006	-1400	-3700	0.90	0.75	Figure 8-4b
Empty	Loading	-0.021	-4800	-7000	0.67	0.52	Figure 8-4b
Loaded	Unloading	-0.08	-44000	-19291	0.77	0.90	Figure 8-4d

Note: Wheel load= mass*9.81/4, Empty wheel load= 14715N, Loaded wheel load= 191295N

8.2.3 Modelling of the Concept- 4 Vertical Suspension

The Concept- 4 suspension (Figure 7-24) contains two elements in the vertical directions- the equivalent stiffness of the leaf spring, links and coil springs. The stiffness and friction damping property was approximated by a force-displacement characteristic that provides hysteresis with an exponential type transition between the loading and unloading cycles. A function (kf_exp2 [140]) in Gensys simulation software was used to represent the vertical suspension characteristics. The elastic stiffness was modelled as the equivalent stiffness of the leaf spring and coil spring combinations (189kN/m, 1.6MN/m and 3.38MN/m at 60, 80 and 180mm of suspension displacement respectively of the Concept- 4 suspension presented in Table 7-11). The friction damping in the vertical suspension was modelled as a friction element with series stiffness (Figure 8-5). The friction damping element contains a friction force element (±2.5kN empty, ±25kN loaded based on static load) and a series stiffness property (13.6MN/m as per Table 8-1) when changing between unloading and loading cycles. A small viscous damping element is provided with the vertical suspension similar to that included in the concept- 1 model.

An additional friction damping element (support block, Figure 8-5) was modelled on each suspension to help settle the suspension. The working principle of the support block element is similar to the friction buffer element in the tutorial model (Section 7.2.3, Equation 7-1). The support blocks were installed between wagon body and axle box. In the support block element, the friction damping element in the lateral and vertical planes were modelled as friction force elements with lateral and vertical friction forces of 600N and a hard stop modelled as 20MN/m.

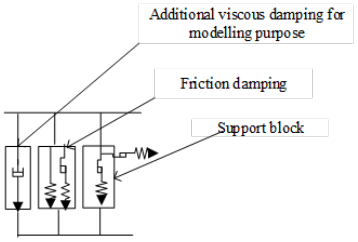

Figure 8-5: Modelling of the Concept- 4 vertical suspension elements

8.2.4 Damping in the Concept- 4 Vertical Suspension

Three conditions were tested on the Concept- 4 wagon suspension on the simplified wagon mass model (Figure 8-1) to evaluate the effect of damping on the Concept- 4 vertical suspension, namely no damping, only viscous damping, and viscous and friction damping.

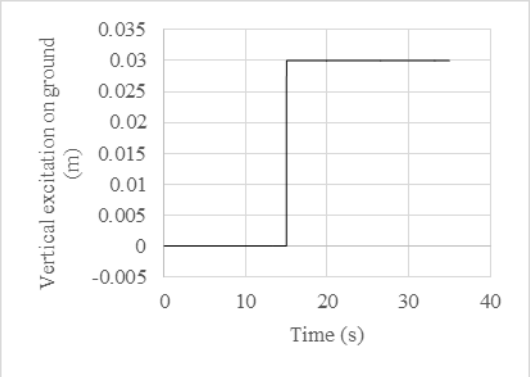

(a) Ground excitation in empty condition

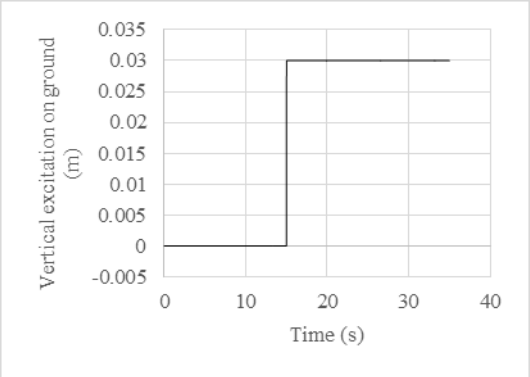

(b) Ground excitation in the loaded condition

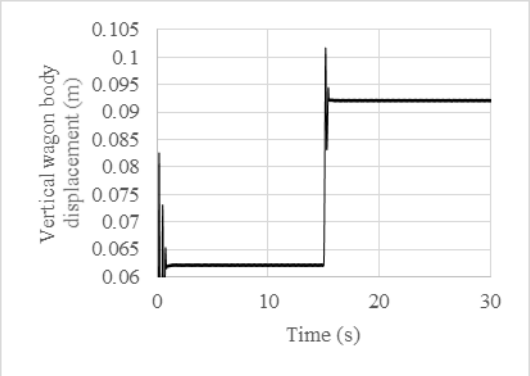

(c) No damping (Empty)

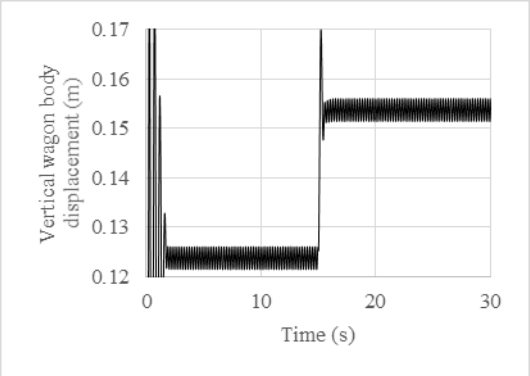

(d) No damping (Loaded)

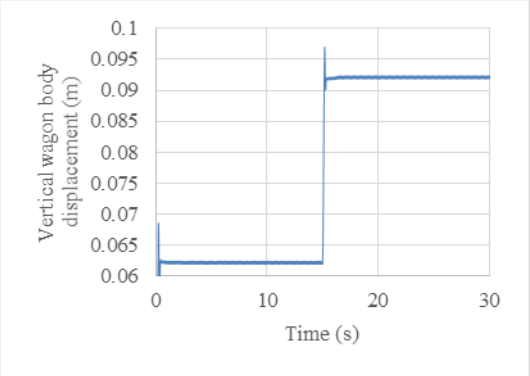

(e) Small viscous damping (Empty)

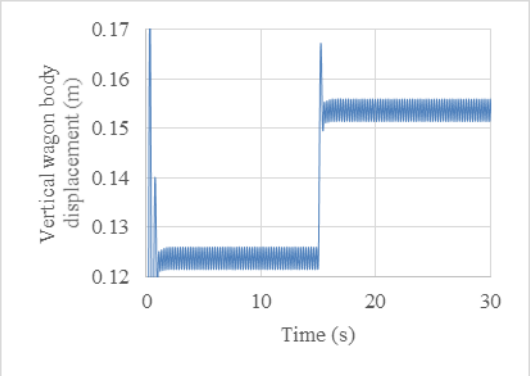

(f) Small viscous damping (Loaded)

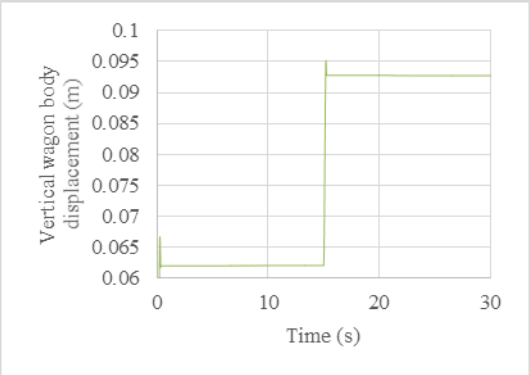

(g) Small viscous and friction damping (Empty)

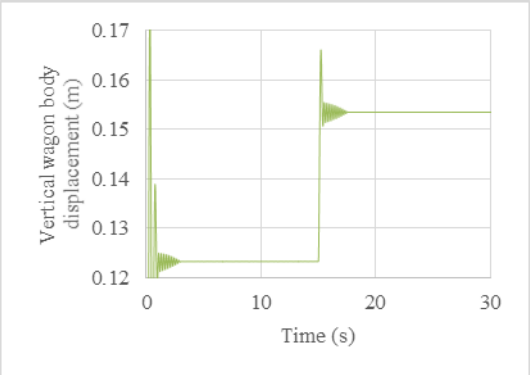

(h) Small viscous and friction damping (Loaded)

Figure 8-6: Damping on vertical suspension (Simplified wagon mass model, Empty- 6000kg, Loaded- 78000 kg)

The ground in the simplified wagon mass model (Figure 8-1) was excited by a step input (Figure 8-6a, b). In both the empty and loaded conditions, the vertical suspension element showed a continued oscillation when no damping was used (Figure 8-6c, d; Figure 8-7a, b). There was also no observable reduction with only the small viscous damping elements (7 kNs/m and 25.7 kNs/m in the empty load condition of 6000kg and the loaded condition of 78000kg respectively, both the empty and loaded condition settled at the third stage of suspension) being used (Figure 8-6e, f; Figure 8-7c, d). The oscillation was greatly reduced when the friction damping element (support block) was added to the suspension (Figure 8-6g, h). The damping on the support block reduced the oscillation almost immediately in the empty condition (damping ratio of 0.65 using the log-dec method). In the loaded case the oscillation was reduced to 0 in about 2s which corresponds to an underdamped situation (damping ratio of 0.28 using the log-dec method). The low break-out force (600N) on the support block provides friction damping at a low vertical displacement which helped to settle the vibration at an early stage.

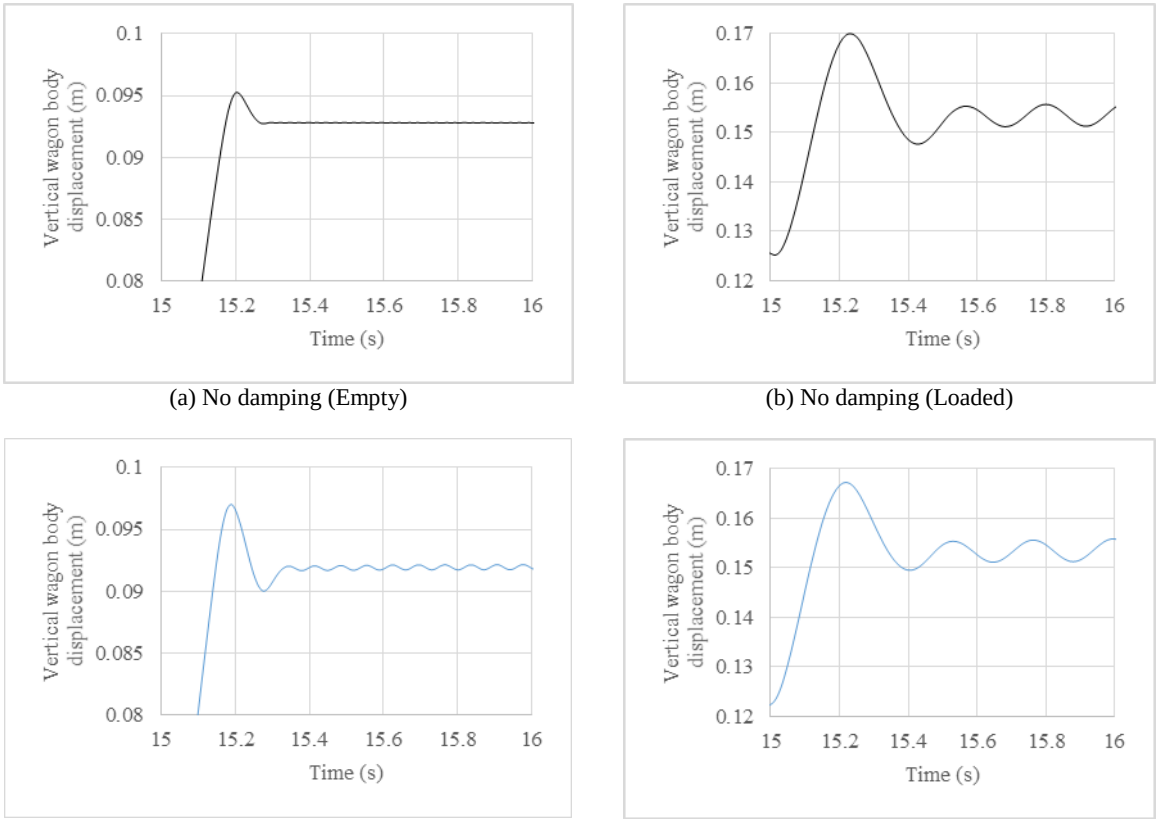

(a) No damping (Empty)

(b) No damping (Loaded)

(c) Small viscous damping (Empty)

(d) Small viscous damping (Loaded)

Figure 8-7: Damping on vertical suspension (Simplified wagon mass model, Empty- 6000kg, Loaded- 78000 kg)

8.3 Evaluating and Modelling of Longitudinal and Lateral Suspension Parameters of Concept- 4 Wagon

The Concept-4 suspension has the same links as used in a typical UIC link and leaf spring suspension. As the coil springs added into the Concept- 4 suspension are constrained in the longitudinal and lateral directions, the Concept- 4 suspension can be assumed to provide similar longitudinal and lateral characteristics to that of the typical UIC link and leaf spring suspension.

The longitudinal stiffness of a UIC link suspension depends on link displacement in the longitudinal direction. The increased vertical load increases inclination from the vertical axis only slightly due to the flattened leaf spring

which affects the longitudinal stiffness of the suspension. Lateral stiffness is achieved by the swinging of the links. The lateral stiffness depends on the geometry of the links and thereby also provides a lateral stiffness depending on the vertical load. In the lateral direction, the link rolls in the end bearing until sliding begins [13]. It is possible to provide one dimensional (lateral) friction in the links and end bearings for the lateral movement and hence make the sliding velocity independent of the axes of the rolling/ sliding elements and achieve a dynamically uncoupled longitudinal and lateral suspension as mentioned in [141]. The same assumption of dynamically uncoupled longitudinal and lateral suspension is used in this thesis which allows modelling of the normalised empirical longitudinal and lateral suspension parameters to represent the Concept- 4 suspension for a higher payload.

The longitudinal and lateral stiffness values were normalised as a function of the vertical load on an axlebox (Fbox) from different studies in [93] (Table 8-3). Cases 1, 3 and 5 represent minimum, average and maximum hysteresis loops respectively which also represent the suspension condition (Table 8-3). The longitudinal and lateral suspensions in the new condition represent the maximum (case 5) and the minimum (case 1) hysteresis conditions respectively. In this thesis, the medium worn (case 3) conditions were used for both the longitudinal and lateral suspensions.

The normalised longitudinal and lateral stiffness values were extrapolated in the Concept- 4 suspension concept design to obtain the required stiffness for the intended maximum payload of 72 tonnes. The extrapolated force and deflection parameters of the longitudinal and lateral suspension parameters corresponding to the maximum payload of 72 tonnes are shown in Figure 8-8 and Figure 8-9 respectively. The empirical data indicates that the friction damping property (F_D and k_2) in the longitudinal and lateral suspensions change linearly with the axle box load (F_{box}) which is different to the non-linear change of friction damping property in the vertical suspension. The variation of the friction damping property in the longitudinal and lateral suspension occurs due to the wear level on the suspension friction elements.

Table 8-3: Typical parameters representing the hysteresis loops observed in experimental and modelling measurements [93]

Cases of hysteresis loop as per [93]	Longitudinal stiffness/ load, kx (1/m)				Lateral stiffness/ load, ky (1/m)			
	$(k_{1x}+k_{2x})$/ Fbox	k_{1x}/ Fbox	F_{Dx}/ Fbox	Condition	$(k_{1y}+k_{2y})$/ Fbox	k_{1y}/ Fbox	F_{Dy}/ Fbox	Condition
1	7	6	0.04	Severely Worn	20	3	0.08	New
2	10	6	0.05	Worn	27	3	0.09	Near new
3	20	6	0.06	Medium worn	35	3	0.1	Medium worn
4	30	6	0.08	Near new	45	3	0.1	Worn
5	40	6	0.1	New	55	3	0.11	Severely Worn

Note: k_1- stiffness in the spring part, k_2- stiffness in the series spring of the friction damper, F_D- breakout force, k_1+k_2 - Equivalent stiffness of the spring element and friction damper (a friction guide block in series with a stiffness element) positioned parallel, Fbox- vertical load per axlebox= mc*9.81/4, where mc is the wagon body mass

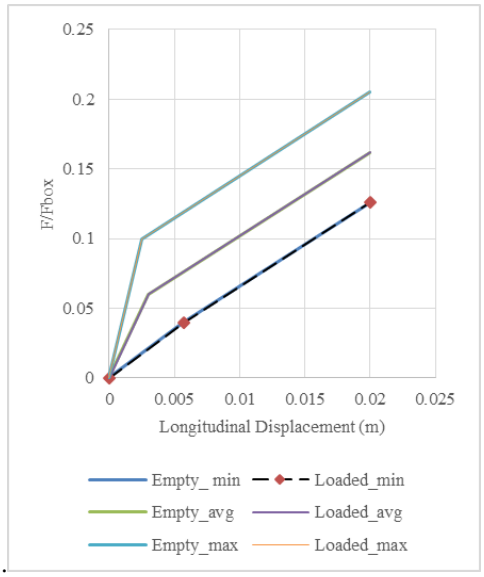

(a) Longitudinal force on suspension/vertical axle box load versus longitudinal displacement

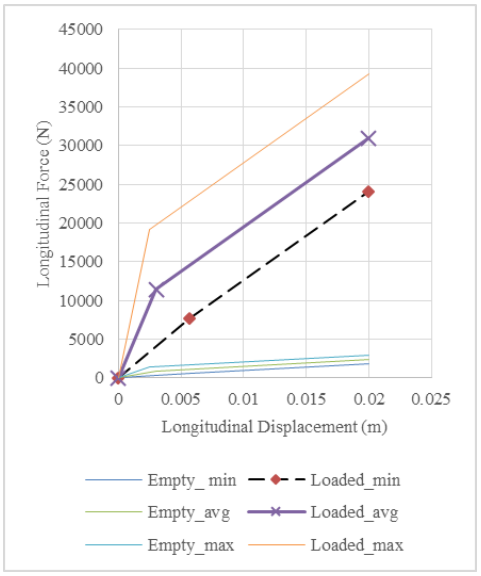

(b) Longitudinal force on suspension versus longitudinal displacement

Figure 8-8: Longitudinal suspension in minimum, average and maximum hysteresis conditions

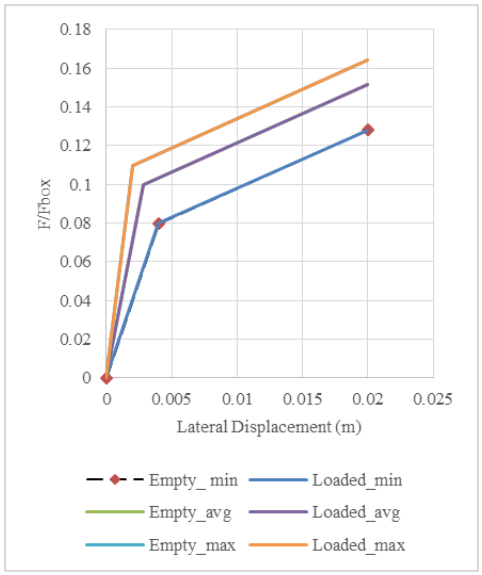

(a) Lateral force on suspension/vertical axle box load versus lateral displacement

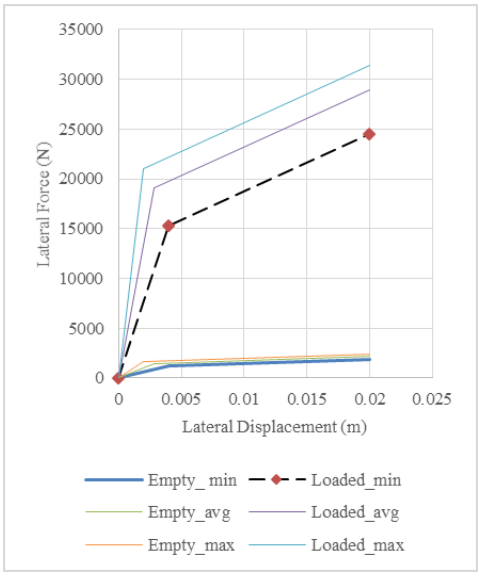

(b) Lateral force on suspension versus lateral displacement

Figure 8-9: Lateral suspension in the minimum, average and maximum hysteresis conditions

Both the longitudinal and lateral suspension parameters of the leaf spring suspension system were modelled using a connection (coupling) element (kf_exp1 [142]) in the Gensys simulation software. The coupling element kf_exp1 is a spring-damper connection with spring and dampers acting in a parallel combination (Figure 8-10). The damper in the kf_exp1 incorporates a stiffness. The kf_exp1 element provides a hysteresis loop force-displacement characteristic of the suspension. The elastic stiffness in the coupling was modified based on the extrapolated data for the load condition for the Concept- 4 suspension. A small viscous damping element was also implemented following the practice of the tutorial model in Chapter 7. Both the longitudinal and lateral suspensions were constrained by bump stops similar to those in the tutorial model. The lateral property of the

Concept- 4 suspension was further affected by the presence of a support block friction element (Figure 8-10b) in the lateral planes.

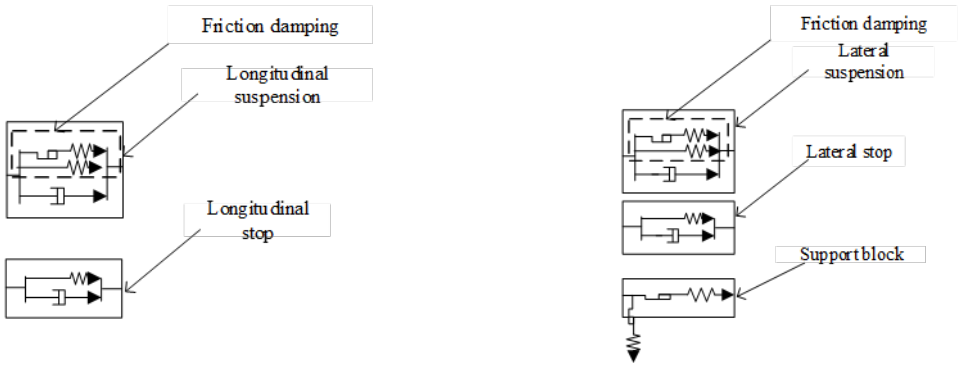

(a) Modelling of longitudinal suspension elements (b) Modelling of lateral suspension elements

Figure 8-10: Modelling of longitudinal and lateral suspension elements (Concept- 4)

The typical hysteresis characteristic of a friction damper and a stiffness element acting in parallel (discussed in section 7.2.1) showed that the hysteresis can change directions sharply when changing from unloading to loading cycles in the hysteresis loop (at points B and C, Figure 8-11). However, the presence of damping behaviour in a practical situation usually provides a smooth transition when moving between the loading and unloading cycles which is approximated as an exponential type smoothing in many studies based on a test on leaf springs in [135]. The smoothing action near the edge of changing direction (example point C at the start of loading cycle) increases area of the hysteresis loop compared to the theoretical assumption (Figure 8-11).

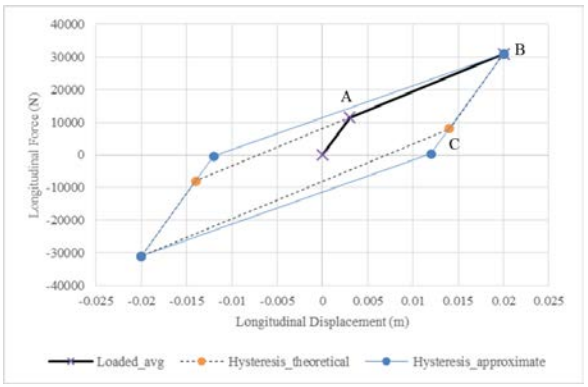

Figure 8-11: Hysteresis loops based on theoretical estimates (Loaded case 78000kg, Average hysteresis criteria of longitudinal suspension as per Table 8-3)

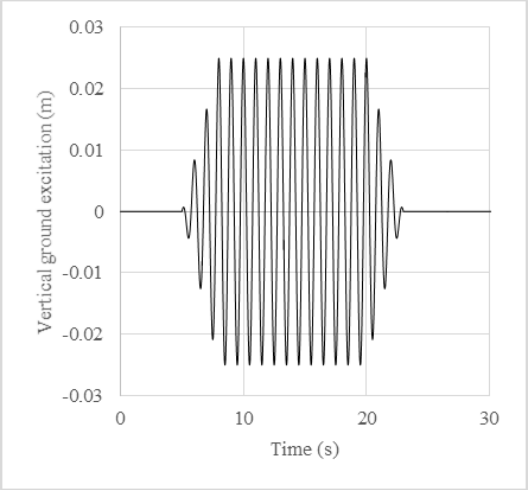

(a) Ground excitation

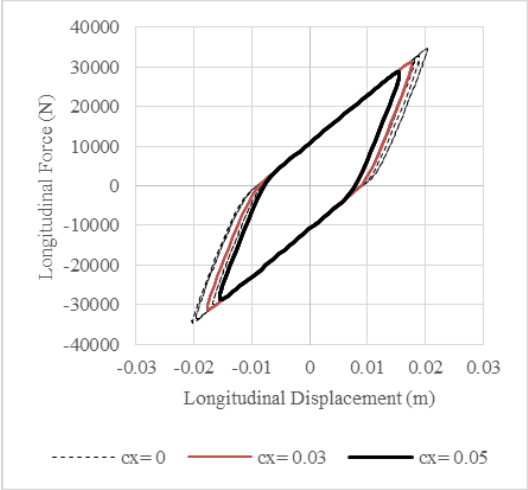

(b) Simulated hysteresis loop on various damping ratio

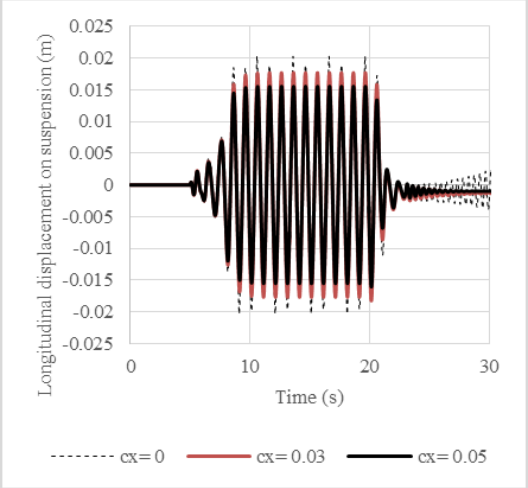

(c) Longitudinal displacement on various damping ratio

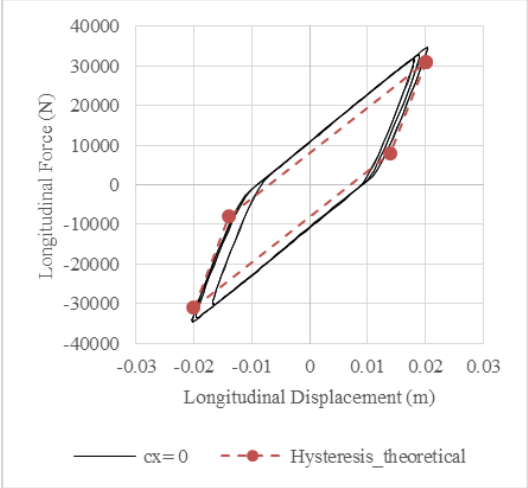

(d) Simulated and theoretical hysteresis loop without damping

Figure 8-12: Hysteresis loop on longitudinal suspension (Loaded 78000kg, excitation ±25mm, frequency of excitation 1.0 Hz)

While the friction damping affected the force component in the hysteresis loop, the additional viscous damping reduced the displacement on the suspension as can be seen in Figure 8-12c. Simulated responses from the simple wagon mass model showed that the addition of viscous damping reduced the longitudinal movement of the suspension (Figure 8-12c) and thus reduced the size of the hysteresis loops (Figure 8-12b). The zero viscous damping was then compared with the theoretical hysteresis obtained in Figure 8-11 and differences in suspension force components due to the smoothing approximation in the simulation were evident (Figure 8-12d).

The size of hysteresis also depends on amplitude and frequency of excitation (Figure 8-13). The response displacement of the longitudinal suspension was found to be increasing with both the increase of excitation frequency (Figure 8-13a) and amplitude (Figure 8-13b).

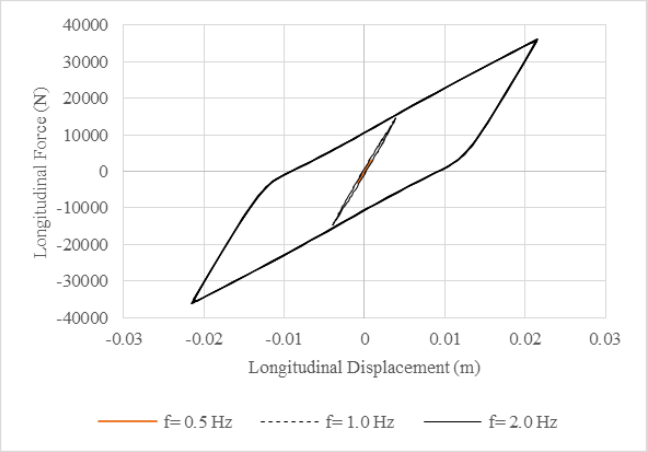

(a) Longitudinal excitation of ±15mm [f- frequency]

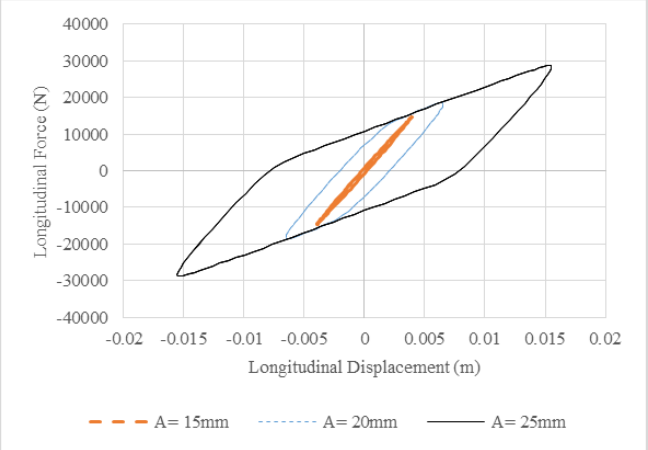

(b) Longitudinal excitation frequency of 1.0 Hz [A- amplitude of excitation]

Figure 8-13: Effect of excitation frequency and amplitude on the hysteresis of longitudinal suspension (Loaded 78000kg, Average hysteresis condition, damping ratio 0.05)

8.3.1 Damping in Longitudinal and Lateral Suspension Elements

The small viscous damping element used in the modelling of Concept- 4 wagon is hardly a significant damping in suspension terms, but it does help settle the model. As an example, the small viscous damping element in the longitudinal and lateral suspension elements reduced the duration of oscillation as obtained on the simplified wagon mass model (Figure 8-14 and Figure 8-15). The presence of friction damping in the support block further reduced the duration of oscillation in the lateral suspension (Figure 8-15g, Figure 8-15h).

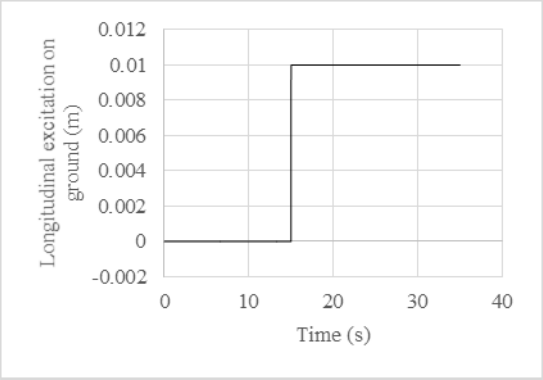

(a) Ground excitation in empty condition

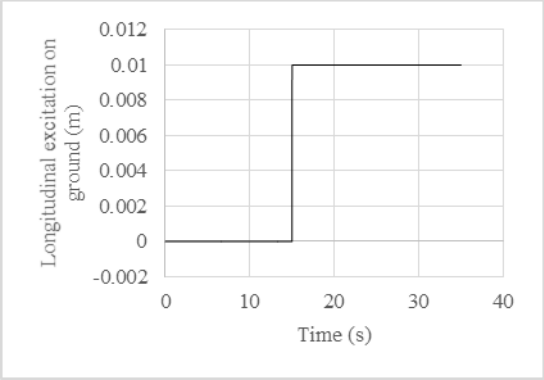

(b) Ground excitation in the loaded condition

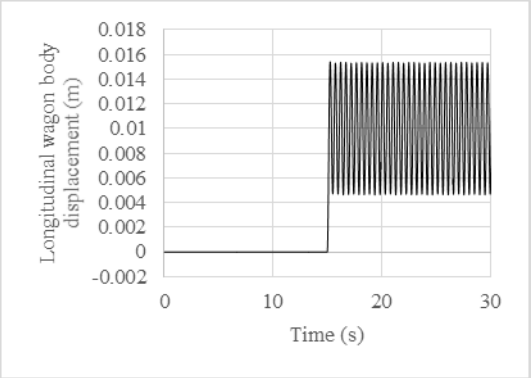

(c) No damping (Empty)

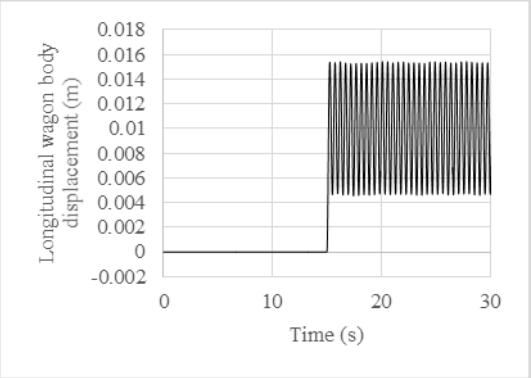

(d) No damping (Loaded)

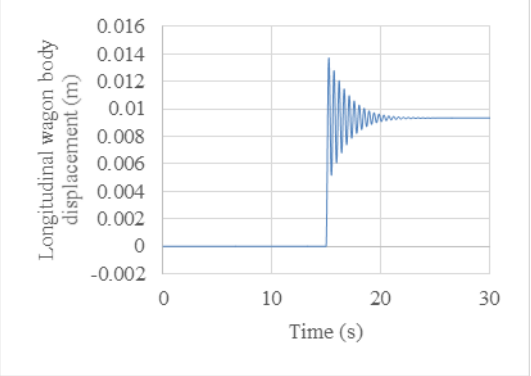

(e) Only small viscous damping (Empty)

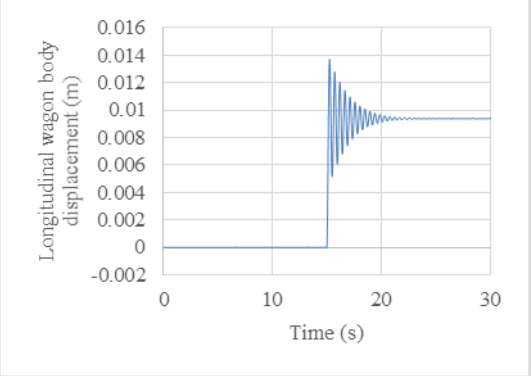

(f) Only small viscous damping (Loaded)

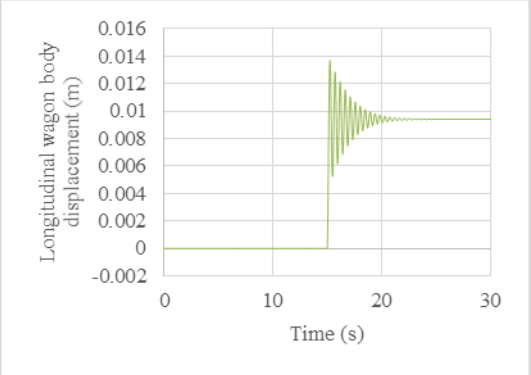

(g) Small viscous and friction damping (Empty)

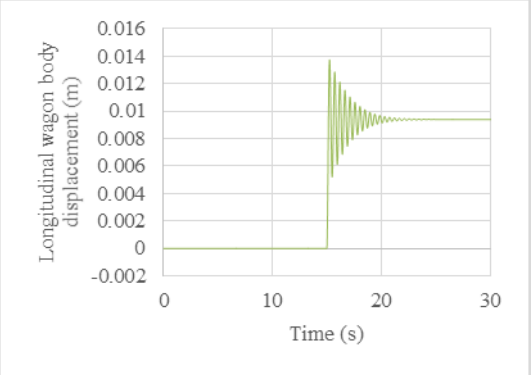

(h) Small viscous and friction damping (Loaded)

Figure 8-14: Damping on longitudinal suspension (Average hysteresis, Simplified wagon mass model, Empty- 6000kg, Loaded- 78000 kg)

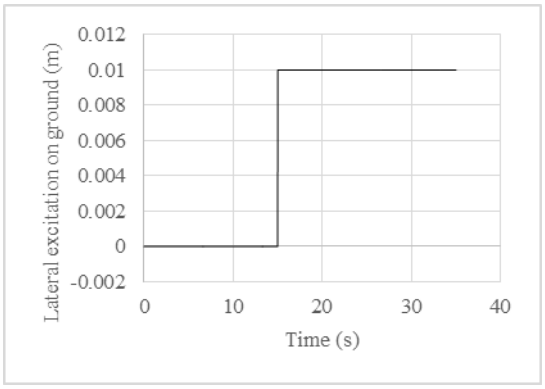

(a) Ground excitation in empty condition

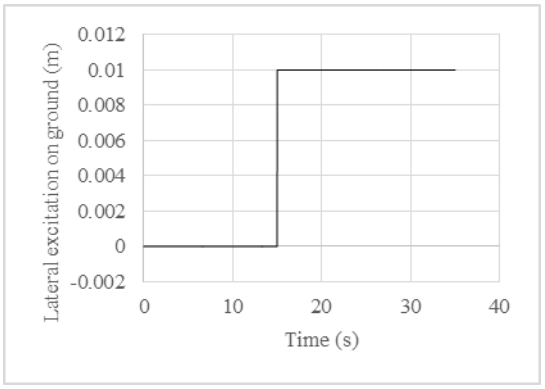

(b) Ground excitation in the loaded condition

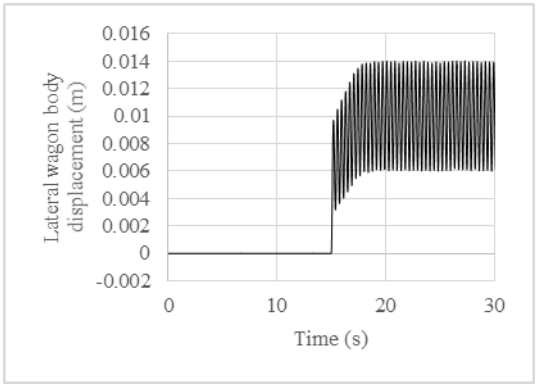

(c) No damping (Empty)

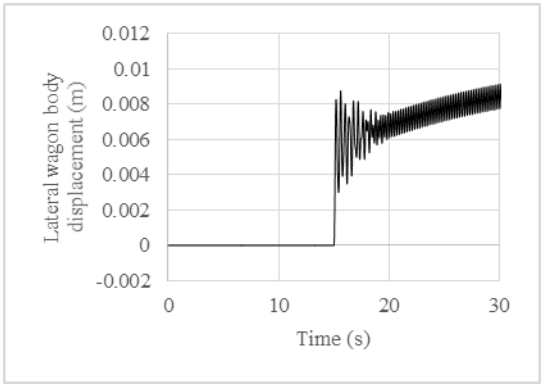

(d) No damping (Loaded)

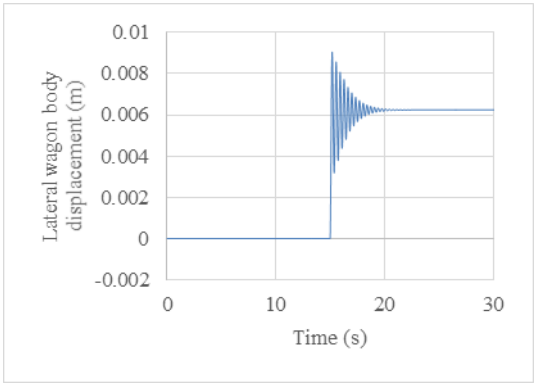

(e) Only small viscous damping (Empty)

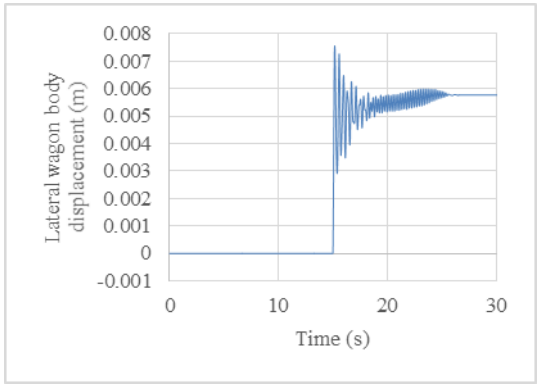

(f) Only small viscous damping (Loaded)

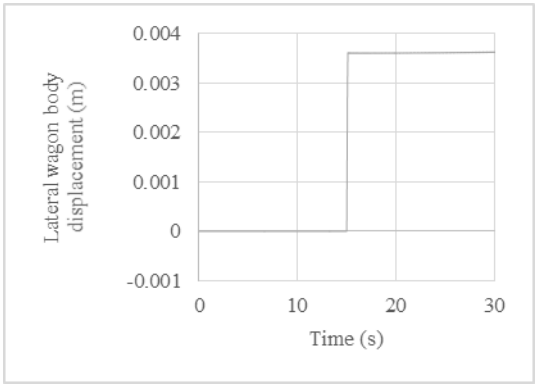

(g) Small viscous and friction damping (Empty)

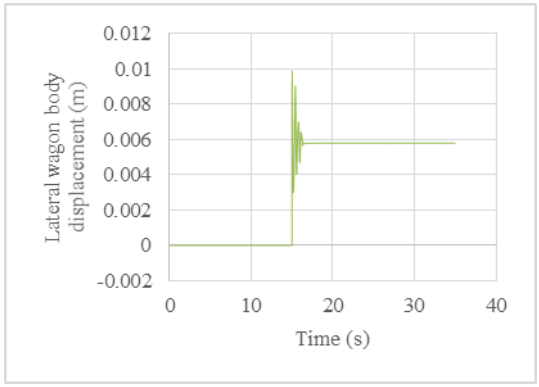

(h) Small viscous and friction damping (Loaded)

Figure 8-15: Damping on lateral suspension (Average hysteresis, Simplified wagon mass model, Empty- 6000kg, Loaded- 78000 kg)

8.3.2 Variation in Longitudinal UIC-Link Suspension Parameters

A simplified approach was considered to investigate the change of stiffness due to longitudinal movement of the links. In the simplified approach, the friction between the end bearing and housing was not considered, the only variable affecting the stiffness parameter then becoming the geometry of the links.

The basic relationship between the link inclination and longitudinal displacement on the axlebox can be obtained from the geometry of the link suspension (Figure 8-16 and Figure 8-17) using Equations 8-1 to 8-4 [93]. Longitudinal stiffness due to change of inclination angles on links on both ends of the leaf spring can be estimated using Equations 8-5 and 8-6. Assuming uniform distribution of the vertical load on both the front and rear links, meaning that $F_{z1} = F_{z1} = F_z/2$, allows Equation 8-7 to be developed.

$$L_k \cos\alpha_1 - L_k \cos\alpha_2 = L \sin\phi \quad \text{8-1}$$

$$x + \frac{L_u}{2} = L_k \sin\alpha_2 + \frac{L\cos\phi}{2} + (h_0 + p)\sin\phi \quad \text{8-2}$$

$$x + \frac{L_k \sin\alpha_1 + L_k \sin\alpha_2 + L\cos\phi}{2} = L_k \sin\alpha_2 + \frac{L\cos\phi}{2} + (h_0 + p)\sin\phi \quad \text{8-3}$$

$$x = \frac{-L_k \sin\alpha_1 + L_k \sin\alpha_2}{2} + (h_0 + p)\sin\phi \quad \text{8-4}$$

$$F_x = F_{x2} - F_{x1} \quad \text{8-5}$$

$$xk_x = F_{z2}\tan\alpha_2 - F_{z1}\tan\alpha_1 \quad \text{8-6}$$

$$k_x = \frac{F_z}{2x}(\tan\alpha_2 - \tan\alpha_1) \quad \text{8-7}$$

here L_k is the length of the link (m), α_1 and α_2 are the link inclination angles (rad), L is the length of the leaf spring (m), ϕ is the inclination of the leaf spring (rad), x is the longitudinal displacement on the axlebox (m), L_u is the overall length of the leaf spring and UIC links (m), h_o is the thickness of the leaf spring (m), p is the camber of the leaf spring under load (m), F_{x1} and F_{x2} are the longitudinal loads on the links (N), F_x is the longitudinal load on the axlebox (N), k_x is the longitudinal stiffness of the leaf spring and UIC link suspension (N/m), F_z is the vertical load on the axlebox (N).

The inclination angles α_1 and α_2 can be estimated from the position of the links (AP and CQ, Figure 8-16c). The parameters X_{1Link}, X_{2Link}, Z_{1Link}, Z_{2Link} can be used to evaluate α_1 and α_2. Both the vertical and longitudinal movements of the links affect α_1 and α_2. The overall change of inclination angles due to vertical and longitudinal displacement of the links and leaf spring can be estimated using a triangular estimation of the leaf spring assembly (Figure 8-17b). The parabolic shape of leaf spring assembly abc (Figure 8-17a) can be assumed triangular to form the triangle 'BGC' in the empty load condition (Figure 8-17b). The length BG is considered as the camber (P_0) at empty load condition. As the load is applied on the link, the resultant vertical force reduces camber on the leaf spring to P (represented by EH in Figure 8-17b) at the loaded condition. As the connection points between the leaf spring eye and links remain (points C and F in Figure 8-17b) unconstrained, the reduction of camber due to vertical load will move the longitudinal position of the connection point C to F and the length of BC and EF will be the same. The triangles due to the empty and loaded conditions can then be used to evaluate parameters X_{1Leaf} and X_{2Leaf} (Figure 8-17c). The resultant longitudinal movement on the link (X_{1Link}, X_{2Link}) can then be evaluated considering both the vertical load and longitudinal displacement on the axlebox (Figure 8-17d).

The geometric displacement and angle parameters of the link suspension and leaf spring can be estimated using Equations 8-8 to 8-18.

$$\boldsymbol{X_{1\,Leaf} = X_{2\,Leaf} = \sqrt{\left(\left(\frac{L}{2}\right)^2 + {P_0}^2 - P^2\right)} - \frac{L}{2}} \quad \textbf{8-8}$$

$$\boldsymbol{X_{1\,Link} = X_{0Link} - X - X_{1\,Leaf}} \quad \textbf{8-9}$$

$$\boldsymbol{X_{2\,Link} = X_{0Link} + X - X_{2\,Leaf}} \quad \textbf{8-10}$$

where $X_{1\,Leaf}$ and $X_{2\,Leaf}$ are the longitudinal movement of the connection point between the leaf spring and UIC links (m), P_0 is the camber at no load condition (m), P is the camber at loaded condition (m), X_{0Link} is the initial (no load or displacement) spread of the UIC links along the longitudinal direction (m), $X_{1\,Link}$ and $X_{2\,Link}$ are the longitudinal spread of the UIC links due to load and displacement of the axlebox (m)

The vertical movement of the connection points between the leaf spring and links can be obtained using Figure 8-16b.

$$\boldsymbol{Z_{0\,Leaf} = \sqrt{{L_k}^2 - {X_0}^2} - P} \quad \textbf{8-11}$$

$$\boldsymbol{\sin\alpha_0 = \frac{X_{0Link}}{L_k}} \quad \textbf{8-12}$$

$$\boldsymbol{P = P_0 - \frac{F_z}{K_z}} \quad \textbf{8-13}$$

$$\boldsymbol{Z_{0Link} = \sqrt{{L_k}^2 - {X_{0Link}}^2}} \quad \textbf{8-14}$$

$$\boldsymbol{Z_{1Link} = Z_{0Link} \mp \frac{L}{2}\sin\phi} \quad \textbf{8-15}$$

$$\boldsymbol{Z_{2Link} = Z_{0Link} \pm \frac{L}{2}\sin\phi} \quad \textbf{8-16}$$

$$\boldsymbol{\tan\alpha_1 = \frac{X_{1Link}}{Z_{1Link}}} \quad \textbf{8-17}$$

$$\boldsymbol{\tan\alpha_2 = \frac{X_{2Link}}{Z_{2Link}}} \quad \textbf{8-18}$$

where k_z is the vertical stiffness of the leaf spring (N/m), Z_{0Link} is the height of the front and rear links at zero longitudinal displacement (m), Z_{1Link} is the height of the front link at α_1 inclination (m), Z_{2Link} is the height of the front link at α_2 inclination (m)

Equations 8-4 and 8-7 were used to obtain longitudinal stiffness parameters with respect to longitudinal displacement on the axlebox. A typical dimension of the UIC links and leaf spring suspension (Table 8-4) has been used in this section to evaluate longitudinal stiffness parameters. The vertical stiffness of the leaf spring was considered as being the same as that of the Concept- 4 suspension (3.38 MN/m). In the forward movement of the axlebox, the link inclination angles (Equations 8-17 and 8-18) on the front and rear links decrease (Figure 8-18a) and increase (Figure 8-18b) respectively which clearly indicates the geometrical feature of the link suspension (Figure 8-16c). So, the equations (8-1 – 8-18) developed in this section generally represent the geometry of the link suspension.

The longitudinal stiffness normalised with the vertical load (Equation 8-7) was estimated with the change of axlebox movement (x) in the longitudinal direction (Equation 8-4). As the longitudinal movement due to the

vertical load only does not move the axlebox, a movement on the axlebox was applied at 1, ±10 and ±20mm to evaluate the longitudinal suspension properties due to vertical load and steering effect. The longitudinal stiffness increases with both the forward and rearward movement of the axlebox (Figure 8-19) in the empty and loaded conditions. The normalised longitudinal stiffness in different axlebox steering positions increases by 0.04 kN/m when the steering position of the axlebox changes by 20mm in both the empty (4.58- 4.62 kN/m per kN) and loaded (4.71- 4.75 kN/m per kN) conditions (Figure 8-19a). The effect of an increase in longitudinal stiffness due to variation in steering positions is, therefore, more in the loaded condition than the empty condition (for example, 7.8kN/m for the 80t loaded wagon, Figure 8-19c and 0.59kN/m for the 6t empty wagon, Figure 8-19b). It thus follows that the increase in longitudinal stiffness due to higher steering force (as could occur due to a high vertical track defect) in the loaded condition would be higher than that in the empty condition.

The longitudinal stiffness is minimum near the centre of the axle centre positions. The longitudinal movement of the axlebox in the loaded condition is only slightly less than that for the empty condition, having been found as 1.2mm lower for the 80t load compared to that for the 6t load when the axlebox movement of ±20mm was applied (Figure 8-19d).

A further investigation was carried out to observe the effect of a change in longitudinal movement of links from the initial position of leaf spring eyes ($X_{1\ leaf,}$ Figure 8-17a). The longitudinal stiffness was found to increase with the increase in longitudinal displacement of the links ($X_{1\ leaf,}$ Figure 8-19a). The displacement on the links was provided by using different loads (Figure 8-19a, Equation 8-9) and different axlebox steering positions (x being 1, ±10 and ±20) to obtain the static measurement as per equations 8-1 to 8-18. The longitudinal displacement of the leaf spring eye ($X_{1\ leaf}$) increases with the increase of load (Figure 8-20a). The maximum longitudinal movement ($X_{1\ leaf}$) was found to be 3.3mm for the 80t load (Figure 8-20a)

The combination of vertical load and applied steering on the link suspension obtained from Equations 8-1 to 8-7 showed that the stiffness is high at higher longitudinal movements and load conditions (Figure 8-20b). The normalised stiffness thus varies between 4.58 kN/m per kN and 4.75 kN/m per kN when load condition varies between 6t and 80t, and the longitudinal movement of the axlebox (x) is up to 20mm. In practice, the longitudinal movement of the axlebox is restricted to 22.5mm in the UIC link suspension, and the normalised longitudinal stiffness is therefore expected to be less than 4.75 kN/m per kN based on the simplified theoretical analysis in this section.

In the empty condition, the longitudinal stiffness does not change significantly which justifies the constant longitudinal stiffness for empty condition tests such as the hunting tests that have been widely implemented in literature. The assumption of constant stiffness in the loaded condition may not be a suitable approximation when a large vertical track defect is present. The effect of vertical track irregularities on the position of axlebox is not further evaluated in this thesis, realising that the concept wagon would require a better track with a high axle load capacity that would eliminate the possibility of large track defects. So, the constant longitudinal stiffness for all load and steering positions is adopted in the modelling in this thesis.

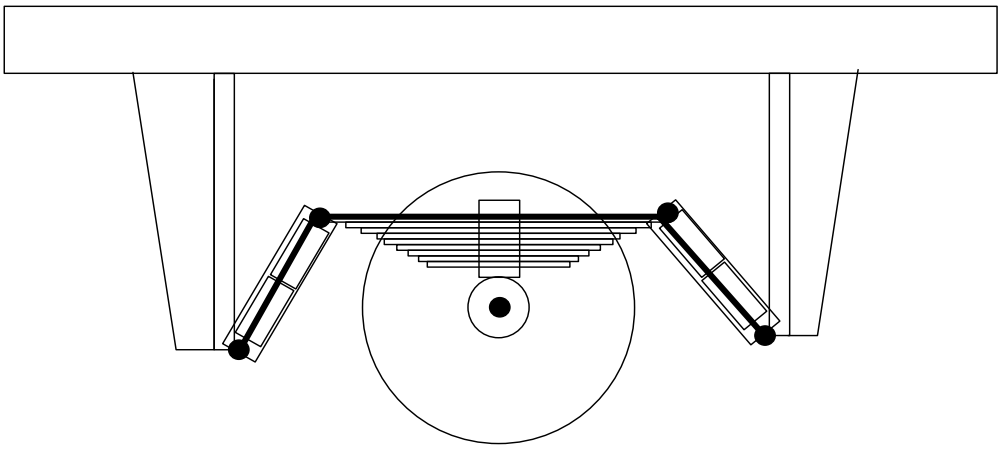

(a) Schematic diagram of the UIC link and leaf spring suspension

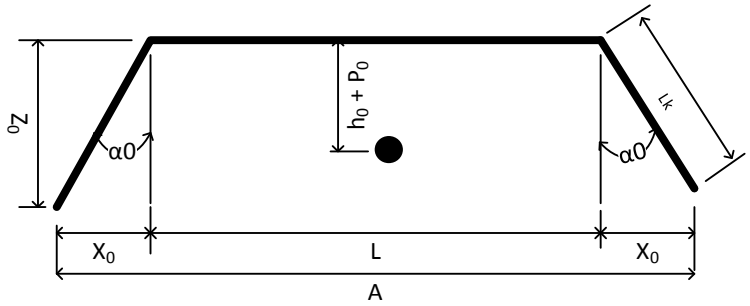

(b) Line diagram of the UIC link and leaf spring suspension without any load or longitudinal movement

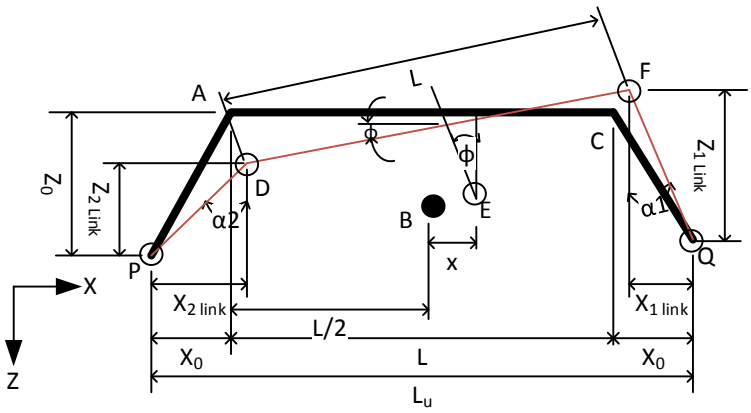

(c) UIC link and leaf spring suspension during an operating situation of longitudinal and vertical movement of the axlebox

Figure 8-16: UIC link and leaf spring suspension

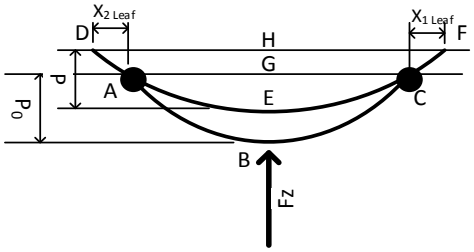

(a) Parabolic shape of leaf spring under vertical load

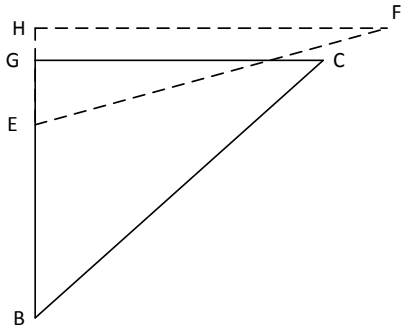

(b) Assumed triangular geometry of the leaf spring under vertical load

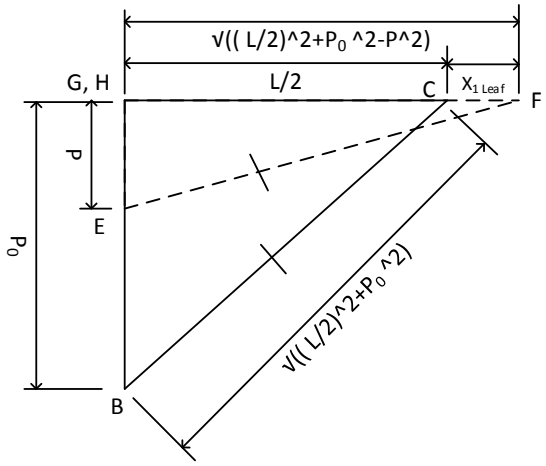

(c) Quantified parameters of the assumed triangular shape of the leaf spring suspension

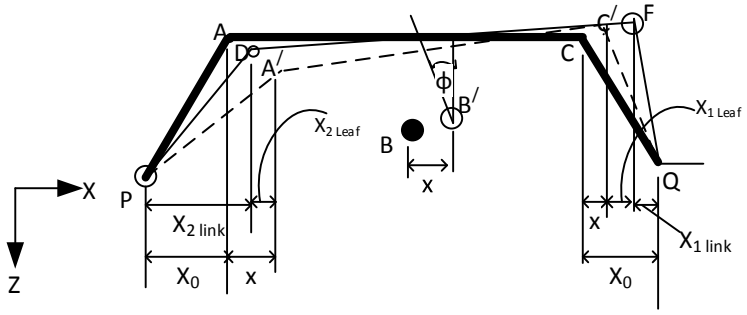

(d) UIC link and leaf spring suspension under vertical load and longitudinal displacement

Figure 8-17: UIC link and leaf spring suspensions under vertical and longitudinal displacement

Table 8-4: Parameters used to obtain the longitudinal stiffness parameters in this section

Parameters	Value	Unit
x0 link	0.15	m
Vertical stiffness of the leaf spring, kz	3.38	MN/m
Empty Load	6000	kg
Loaded	80000	kg
Number of leaves	9	
Leaf thickness	0.016	m
h0	0.144	m
Camber at no load, P0	0.064	m
Length of the link, Lk	0.289	m
Length of the leaf spring, L	1.2	m
Longitudinal length between the connection points of a link with leaf spring and wagon body, A	1.5	m

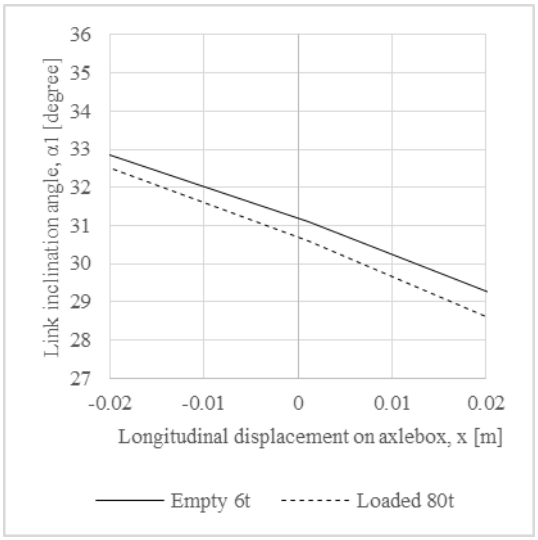

(a) Front link

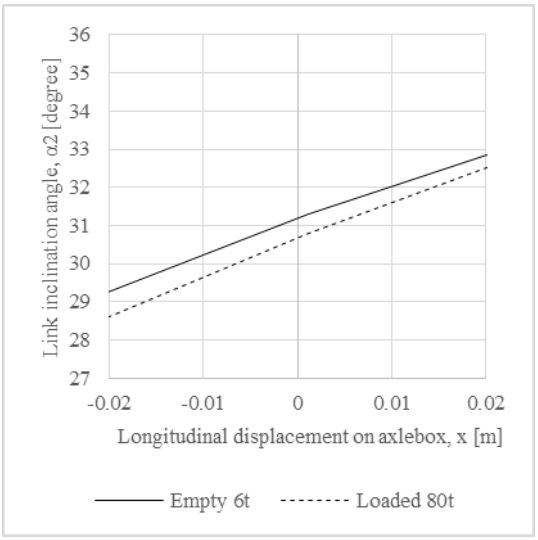

(b) Rear link

Figure 8-18: Variation of link inclination angles using Equations 8-4, 8-17, 8-18

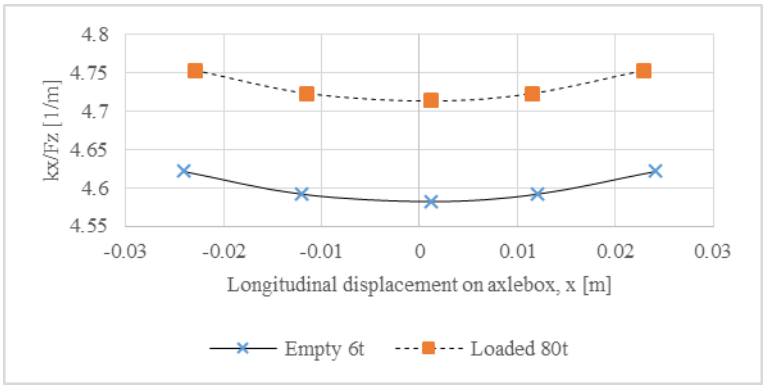

(a) Normalised longitudinal suspension parameters for empty and loaded conditions

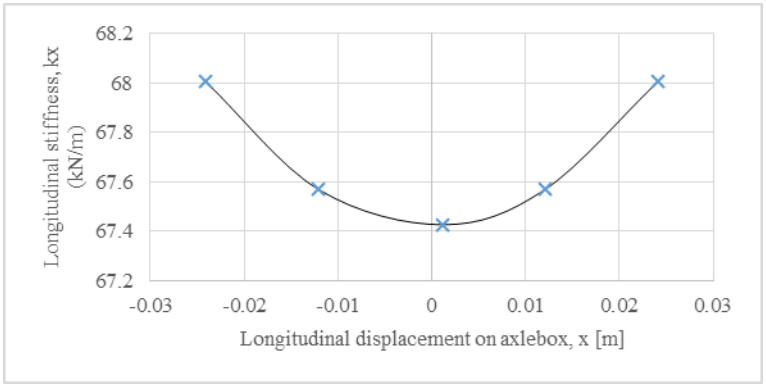

(b) Longitudinal stiffness change along the longitudinal displacement on axle box (Empty condition)

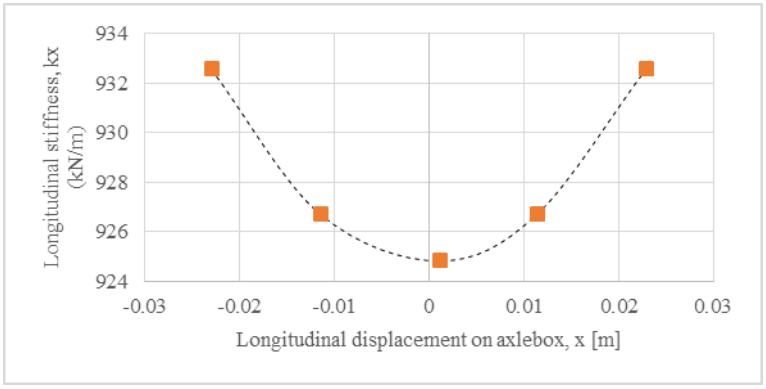

(c) Longitudinal stiffness change along the longitudinal displacement on axle box (Loaded condition)

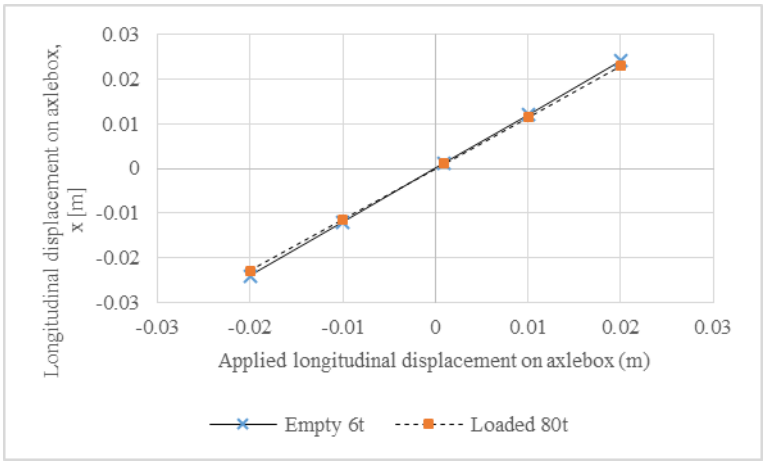

(d) Variation of longitudinal displacement due to vertical load and steering

Figure 8-19: Longitudinal stiffness of the UIC link and leaf spring suspension based on Equations 8-4, 8-6

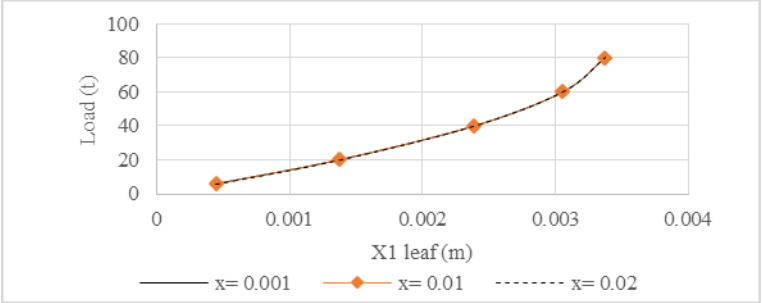

(a) Variation of leaf eye movement with load at different axlebox steering positions (x) (Equation 8-8)

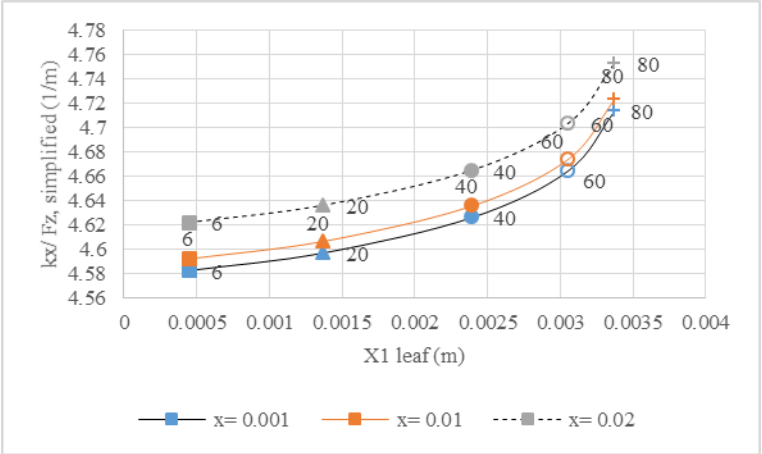

(b) Normalised kx at different axlebox steering positions (x), data points refer to loads in tonnes

Figure 8-20: Variation in longitudinal stiffness with longitudinal displacement on the link due to various load conditions

8.3.3 Variation in the Lateral UIC Link Suspension Parameters

The force on the links (F) on the vertical and longitudinal plane can be calculated using vertical load and longitudinal geometry of the links (Figure 8-21a). The link is then rotated in the lateral (Y) direction by angle β (Figure 8-21b). At a displacement of Y from the initial zero position, Equations 8-19 to 8-23 can be obtained. As the front and rear links are placed in parallel connection between the leaf spring and wagon body, the equivalent stiffness (normalised with vertical load) can be calculated using Equation 8-24. Assuming similar geometry of the front and rear links on a leaf spring, the lateral displacement of the suspension is considered as the average lateral displacement of the front and rear links.

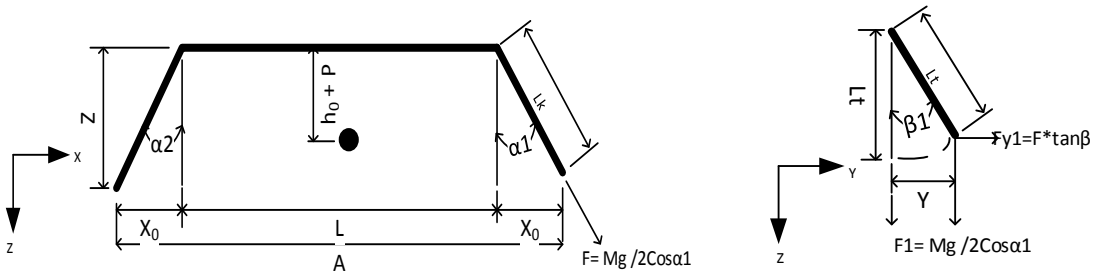

(a) Longitudinal link

(b) Lateral link

Figure 8-21: Lateral behaviour of UIC link suspension

$$Y1 = L_{t1} \sin \beta_1 \quad \textbf{8-19}$$

$$F_{y1} = F_1 \tan \beta_1 \quad \textbf{8-20}$$

$$F_{y1} = \frac{Mg \tan \beta 1}{2Cos\alpha 1} \quad \textbf{8-21}$$

$$K_{y1} = \frac{Mg \tan \beta 1}{2yCos\alpha 1} \quad \textbf{8-22}$$

$$\frac{K_{y1}}{Mg} = \frac{\tan \beta 1}{2y1Cos\alpha 1} \quad \textbf{8-23}$$

$$\frac{K_y}{Mg} = \frac{K_{y1}}{Mg} + \frac{K_{y2}}{Mg} \quad \textbf{8-24}$$

where Y is the lateral displacement of the link from the leaf spring eyes (m), L_t is the height of the links (m), β_1 is the lateral inclination angle on the front link (rad), F_{y1} is the lateral force at the hanging part of the links (N), F_1 is the force on the longitudinal and vertical plane (N), M is the mass per axlebox (kg), α_1 is the link inclination angle on the front link (rad), K_{y1} and K_{y2} are the lateral stiffness of the front and rear links (N/m), K_y is the equivalent lateral stiffness of the front and rear links.

The lateral stiffness due to movement of the links in the lateral direction was found to be increasing with the increase of lateral displacement as can be obtained by Equation 8-24 assuming the lateral inclination angles β_1 and β_2 are the same on the front and rear links (Figure 8-22). The longitudinal inclination varies due to load and longitudinal displacement of the axlebox. The change in longitudinal position of links due to load was then plotted with two different load conditions (6t and 80t) and a similar trend of increasing lateral stiffness with lateral displacement of links was obtained (Figure 8-22). The variation of the normalised stiffness in the empty (6t) and loaded conditions (80t) are 0.00823 kN/m per kN and 0.00844 kN/m per kN respectively which is equivalent to 0.121kN/m and 1.6kN/m respectively. Due to the small variation in normalised lateral stiffness with the change of lateral displacement of the links, it is adequate to consider the normalised lateral stiffness parameter independent of lateral movement of the links. The assumption of constant stiffness along the lateral length is justified based on the simplified geometric analysis of the links.

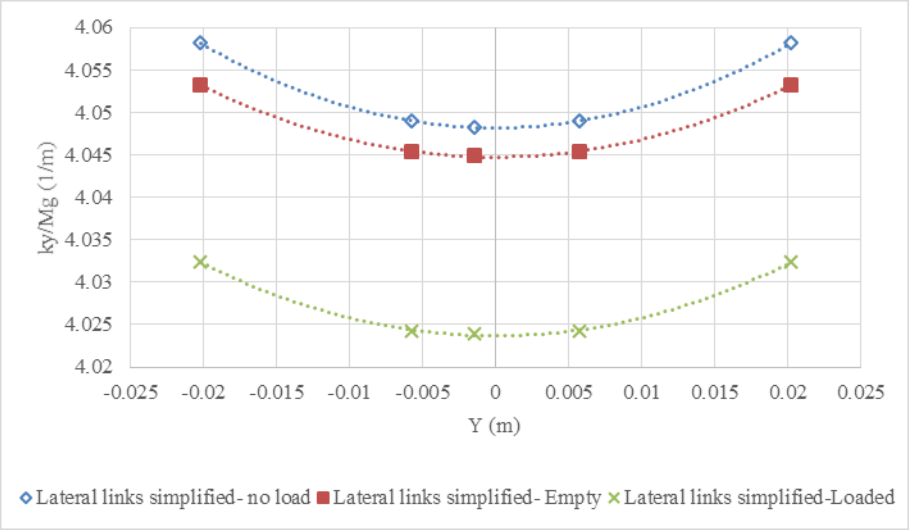

Figure 8-22: Variation of normalised lateral stiffness with the lateral displacement of links from leaf spring eyes

Experimental data establishes a normalised parameter of 3kN/m per kN (k_{1y}/Fbox in Table 8-3) for the lateral suspension characteristics of links which are significantly less than that obtained by simplified theoretical analysis in this section. The empirical data has been further used in this thesis, realising that the change in normalised stiffness due to lateral movement of the links is negligible.

8.4 Damping in the Concept- 4 Suspension

The damping property of the Concept-4 was evaluated using step responses in sections 8.2.4 and 8.3.1. The damping characteristics of the Concept-4 suspension in the vertical-empty, vertical-loaded and lateral-empty conditions were found to be underdamped (Figure 8-6g, Figure 8-6h and Figure 8-15g). The damping properties of all other conditions were found to be very low damping, as can be seen from the damping ratios calculated using the log-dec method from the step responses on the Concept- 4 suspension (Table 8-5). The vertical friction damping on the support block is similar for all load conditions which increases the damping ratio for the empty load condition (Figure 8-6g). The viscous damping for the loaded condition is higher than for the empty load condition as the damping was provided as a damping ratio in the modelling, but the amplitude of oscillation remains large due to the high vertical force in the loaded condition (Figure 8-6h). The vertical damping in the loaded condition provided a lower damping ratio (0.28) than that of the empty condition (0.65).

In the longitudinal direction, the friction damping property is dependent on the load only and is assumed as a viscous damping property for modelling purpose which provides similar damping ratios on the empty (0.06) and loaded (0.05) conditions.

In the lateral suspension, the damping was made higher by the application of lateral friction damping on the support blocks in the Concept- 4 suspension. The fixed lateral friction damping element on the support blocks damped the oscillation in the empty condition almost instantly, representing an underdamped case (damping ratio measured as 0.34, Figure 8-15g). The lateral suspension in the loaded condition provides a very low damping ratio (0.1).

Table 8-5: Damping ratio of the Concept- 4 suspension on a simplified model (obtained by logarithmic decrement method)

Case	Figure	Damping ratio	Comment
Vertical- empty	Figure 8-6g	0.65	Underdamped
Vertical- loaded	Figure 8-6h	0.28	Underdamped
Longitudinal- empty	Figure 8-14g	0.06	Very low damping
Longitudinal - loaded	Figure 8-14h	0.05	Very low damping
Lateral- empty	Figure 8-15g	0.34	Underdamped
Lateral- loaded	Figure 8-15h	0.1	Very low damping

8.5 Natural Frequency in the Bounce, Pitch, and Roll Directions

Bounce (vertical), pitch and roll are three important modes of vibration of a vehicle. Hence, it is important to know the resonance parameters in the bounce, pitch, and roll modes for the dynamic stability of the rail vehicle. As there are three different stiffnesses at three vertical displacement values, it is possible to have different natural frequencies in the different stiffness regions which will correspond to different loading masses. Suspension initially settles at a point depending on the load and suspension parameters. The external excitation then moves

the suspension. Depending on the frequency of excitation, the suspension may show resonance response. However, the presence of damping may restrict the resonance response and a high damping will make resonance response impossible to detect. One way to increase the visibility of possible resonance response is to reduce damping in the model. Reduced damping increases response sensitivity which could also allow the suspension to move to a different stiffness stage of the suspension and a different natural frequency would result due to a different average stiffness. However, low damping requires a long time to settle a wagon mass model. So, a suitable damping needs to be selected to find resonance in the design

As a starting point to provide low damping, the vertical friction damping in the leaf spring of the Concept-4 wagon model was reduced to $1e^{-5}$ N in both the empty and loaded conditions. The support blocks were removed. The viscous damping element was changed corresponding to different damping ratios (0.001, 0.01, 0.03, and 0.05) of the stiffness elements. The modified wagon model with low damping characteristics for the analysis of the natural frequency is termed as the Concept-5 wagon model.

An excitation event was designed to test the resonance characteristic of the suspension. The excitation amplitude was increased gradually to 40mm to avoid a step at the start and then uniform excitation was provided for 12s before gradually decreasing to zero (Figure 8-23). If damping is too low, the vibration may continue for a long time which affects the next excitation event. To obtain the approximate resonance frequency within a reasonable time of simulation, the excitation was set to zero for 2s between two excitation events (example 123-125s, Figure 8-23). In order to test the effect of damping on evaluating the resonance response, the ground was excited at 0-40mm using different frequencies (Figure 8-24a). Suspension displacement was found to be higher in the case of lower damping (0.001, 0.01) compared to those of the higher damping ratios (0.03, 0.05) in the Concept-5 wagon model. The maximum deflection was found to be about 2.2- 2.4 Hz for all damping ratios (Figure 8-24a, Figure 8-24b).

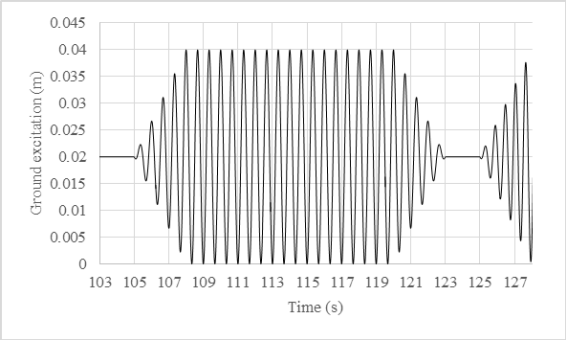

Figure 8-23: Ground excitation example to evaluate natural frequency of the suspension

As the Concept- 4 vertical suspension contains non-linear stiffness parameters, it is also necessary to investigate the resonance characteristic based on non-linear approximation. In a non-linear system, instability can occur in a wide range of frequencies due to non-linear stiffness [143]. The theoretical frequency response of a system with a hardening stiffness indicates that location of peak response varies for increasing and decreasing frequencies (Figure 8-25). If the frequency is slowly increased from zero, the peak response occurs at point 2 after which a sudden drop in response to point 4 occurs. In the case of decreasing excitation frequency, the steady state response suddenly jumps from point 3 to point 1. The region between point 1 and point 4 is known as the unstable region [143] where peak response can vary depending on whether the excitation frequency is increasing or decreasing.

The Concept-5 wagon model with the damping ratio of 0.03 in the simplified wagon mass model has been further used to observe the effect of change of excitation amplitude and frequency. As the Concept- 5 suspension system is non-linear, the frequency of excitation was increased and decreased according to the theory presented in Figure 8-25. The peak amplitudes on each set of vertical excitation amplitudes (20, 30, 50mm in empty and 20, 40, 80mm in loaded conditions) corresponding to different frequencies were determined. The response factor and the maximum amplitude responses of both the empty (Figure 8-26a, Figure 8-26b) and loaded conditions (Figure 8-26c, Figure 8-26d) were then plotted against the frequency of excitation.

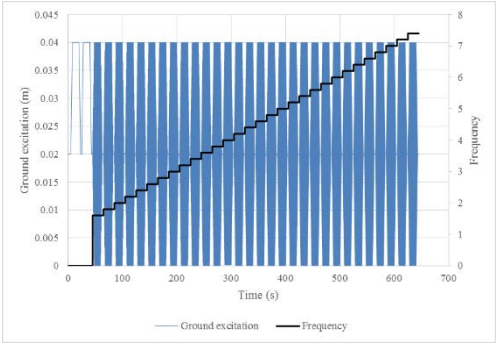

(a) Ground excitation and frequency

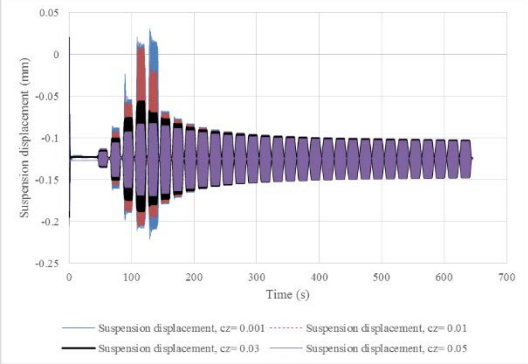

(b) Response on suspension at different damping ratios

Figure 8-24: Effect of damping on investigation of resonance (Loaded, with ground excitation of 0-40mm, increasing frequency mode) [Note: negative value on vertical suspension refers to compression of suspension, i.e. downward movement of wagon body]

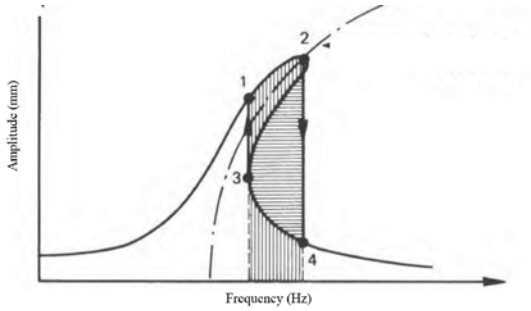

Figure 8-25: Frequency response of a non-linear hardening type resonant system [143]

In the empty condition of the Concept-5 wagon model, the frequency range 6-7Hz contains the highest vertical response factors (Zout/ Zin, 0.8 to 1) (Figure 8-26a). In the cases of loaded condition of the Concept-5 wagon model, the vertical response factors become high (0.8 to 1.1) in the frequency range of 2-2.5Hz (Figure 8-26c). In both the empty and loaded conditions, the response factors (output/ input) were high when the suspension

displacements crossed the limit values of the setpoint stages (the second stage in an empty condition and third stage in a loaded condition). As the suspension moves towards the stiffer stages, it is likely that the resonance frequency will also increase. It is, therefore, important to identify a range of resonance frequency for the Concept-5 suspension system instead of a single resonance frequency. Based on the high response factor, the range of bounce resonance frequencies are 6 to 7Hz in the empty condition and 2 to 2.5Hz in the loaded condition of the Concept- 5 suspension.

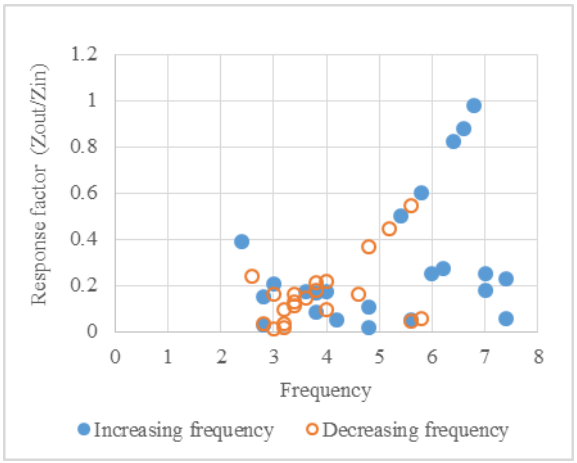

(a) Response factor in Empty condition

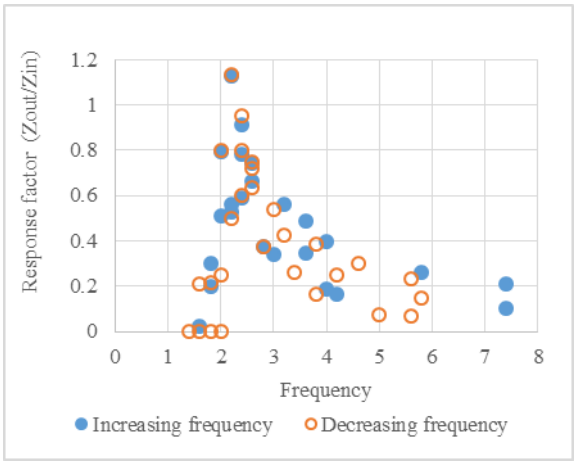

(c) Response factor in Loaded condition

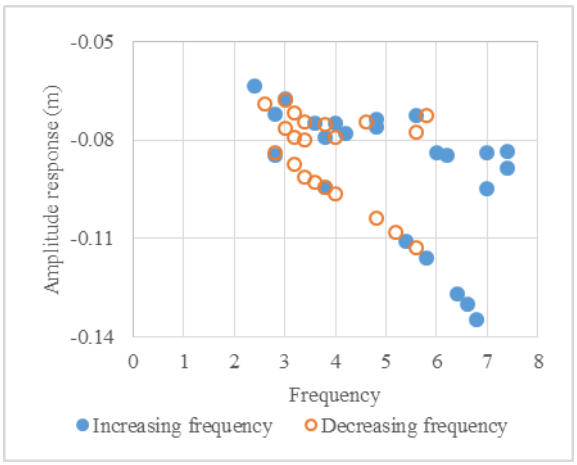

(b) Vertical Amplitude response in Empty condition

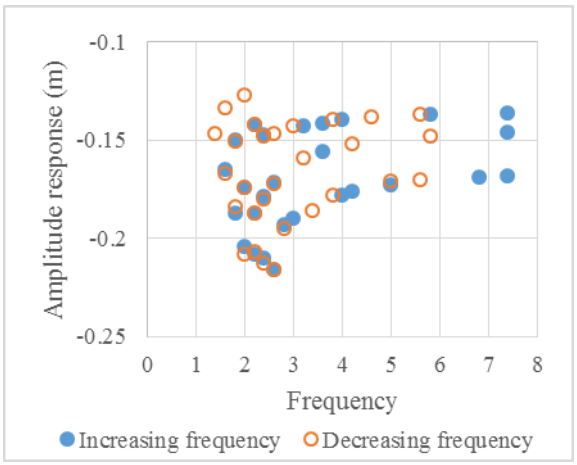

(d) Vertical Amplitude response in Loaded condition

Figure 8-26: Response factor and amplitude versus frequency of Concept- 5 wagon [Note: negative value on vertical suspension refers to compression of suspension, i.e. wagon body is moving downward, 3% damping]

Similarly, sinusoidal excitations were provided in the pitch and roll directions (Concept-5 wagon model) to determine resonant frequencies in the pitch and roll modes. The natural frequencies of pitch and roll modes were determined using a similar approach to Figure 8-26 and the results are shown in Figure 8-27. The increasing and decreasing frequency approach picked some of the high responses which would be undetected if only an increasing or decreasing frequency were used. As an example, the roll resonance frequency of 3.2 Hz (gave response factor fout/fin of 0.87) was detected by the decreasing frequency method but was undetected with the increasing frequency approach (Figure 8-27).

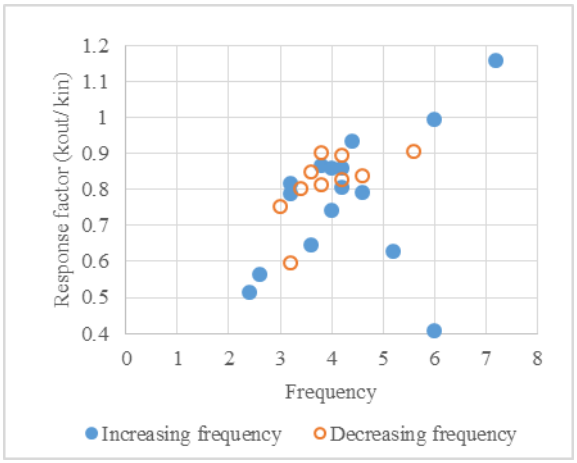

(a) Pitch Empty

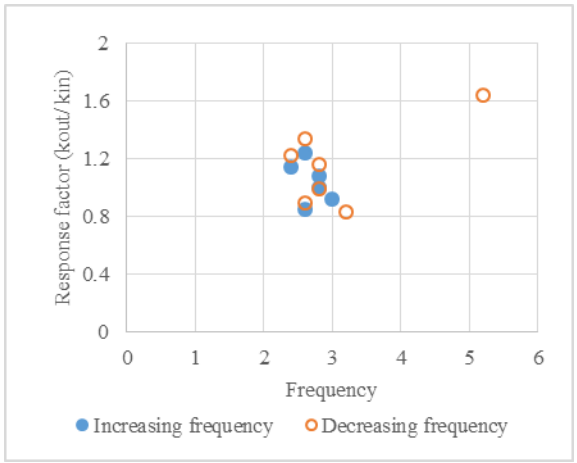

(b) Pitch loaded

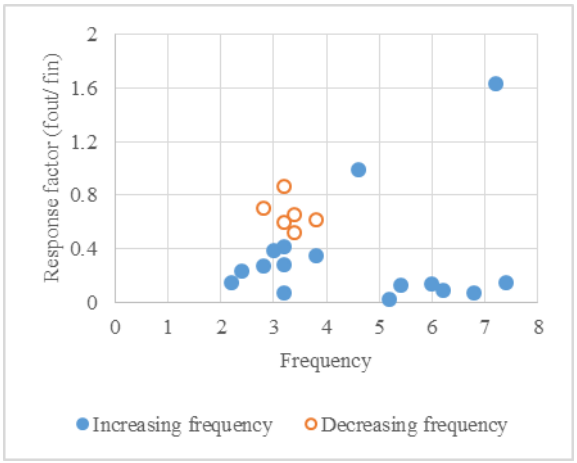

(c) Roll empty

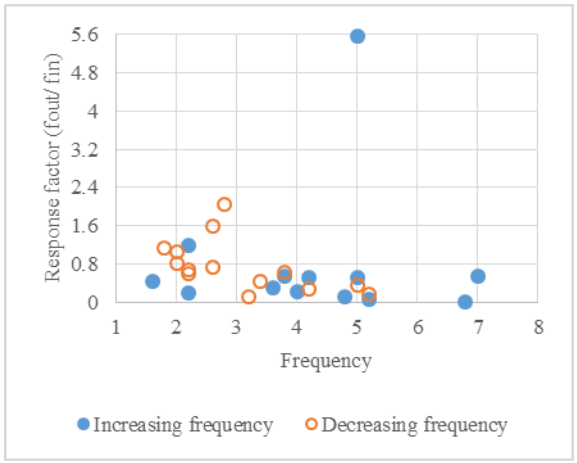

(d) Roll loaded

Figure 8-27: Response versus frequency in pitch and roll modes (Concept- 5)

The estimated non-linear resonant frequency ranges (Table 8-6) differed from those obtained by theoretical calculations (Equations 5-4 to 5-7) using linear approximation (Table 8-7). Considering a higher damping ratio of 0.05 in the Concept- 4 suspension model compared to the tested damping ratio of 0.03 in the Concept-5 model, the resonance response could be further controlled. A practical way to look into the suspension properties of a non-linear suspension is to consider the range of resonance frequency from both the simulation results (Table 8-6) and theoretical approximations (Table 8-7). The lower limit of resonant frequency obtained by simulation was higher than the theoretical resonance frequency at the low stiffness stages in the Concept- 5 suspension. The higher range of the simulated resonant frequency showed a better match with the 3rd stage stiffness of the Concept- 5 suspension. The higher resonant frequencies obtained in the Concept-5 wagon model (Table 8-6) are unlikely to occur within the design speed in this thesis. As an example, the vertical resonance frequency needs to lower than 1.6Hz to provide resonance within 80km/h when BCD is 13.81m. The theoretical calculations for resonance frequency at different suspension stages and load conditions can also be used as those values are likely to produce resonance frequency within the typical freight speed (empty condition 1.79 Hz on the first stage, loaded condition 1.44 Hz on the second stage of the Concept- 5 suspension, Table 8-7).

Table 8-6: Natural frequencies of the Concept- 5 vertical suspension observed in the non-linear model (simulated results, Empty- 6000kg, Loaded- 78000kg)

Mode	Empty	Loaded
Bounce	6- 7	2- 2.5
Pitch	3 - 7	2.5 - 5
Roll	3 - 7	2 - 5

Table 8-7: Natural frequencies of the Concept- 5 vertical suspension by linear approximation (Theoretical calculation, simplified chassis approximation, empty 6000kg, and loaded 78000kg)

Suspension Stage	Equivalent stiffness (ke)	Natural frequency (Hz)					
		Bounce		Pitch		Roll	
	kN/m	Empty	Loaded	Empty	Loaded	Empty	Loaded
1	189	1.79	0.50	2.16	0.59	2.02	0.40
2	1600	5.20	1.44	6.27	1.72	5.89	1.17
3	3380	7.55	2.10	9.12	2.50	8.55	1.70

8.6 Discussion

The parameters of the Concept- 4 suspension and relevant modelling approach have been developed in this Chapter. The suspension characteristics were evaluated on a simplified wagon mass model and compared with available normalised data in published materials. The Concept- 4 suspension incorporated two additional spring nests (with variable stiffness and lengths) with a UIC link and leaf spring suspension. The coil springs, due to the design of the Concept- 4 suspension, do not affect longitudinal and lateral suspension properties which then allows using extrapolated suspension parameters for the longitudinal and lateral suspension from normalised measurement data in various studies [93, 144]. The longitudinal and lateral suspension properties are subject to wear and friction which changes the hysteresis of the force-displacement characteristics. In this thesis, the medium worn condition (corresponding to average hysteresis) is chosen for further investigations.

The modelling was performed to represent the evaluated properties of the Concept- 4 suspension. Some of the assumptions and approximations were included in the modelling to reduce complexity in the modelling as discussed in sections 8.2 and 8.3.

The vertical friction damping due to leaf springs was also made constant for all the dynamic load situations which gave higher damping at the low load conditions compared to the smaller damping corresponding to the low load condition due to the load dependent characteristics of the friction damper. Thus, in the simplified low load situation, the vertical suspension force in decompressed mode (on the unloading cycle of suspension) creates a higher wheel unloading ratio compared to that of empirical approximation. At a high dynamic load situation, the approximation of the friction damping becomes close to the empirical values. So, the assumption of constant vertical friction damping in the modelling provides a higher wheel unloading ratio at low dynamic load and similar wheel unloading ratio at high dynamic loads compared to the empirical values.

The other assumption of providing vertical friction damping based on static loads (empty or loaded) creates a higher wheel unloading ratio on the low dynamic load situation compared to empirical load dependent friction damping. In reality, a very low dynamic load situation of the loaded condition, the friction damping could be as

low as that of the empty load situation. But, in the modelling of the loaded condition, the same high friction damping was used at the low dynamic load situation that resulted in high wheel unloading ratio in the modelling compared to empirical case.

At high dynamic load conditions, during loading of the suspension, the constant friction damping assumption will give a higher wheel unloading ratio than the actual case. However, the wheel unloading ratio in the loading cycle is less than the wheel unloading ratio on the unloading cycle. So, it is justified to use constant friction damping in both the loading and unloading cycles of the suspension in the modelling.

The longitudinal and lateral suspension properties of the UIC link and leaf spring suspensions were found to change slightly with the change of link geometry. The assumption of constant longitudinal and lateral suspension properties was justified considering the low steering movement of the axlebox in a typical operation (straight track, and track with larger track radius). It follows that the critical speed test and large curve negotiation test would normally give a similar result for both the constant and variable longitudinal and lateral suspension stiffness parameters. It is anticipated that a big track defect would provide a larger steering movement on the axlebox and higher longitudinal and lateral stiffnesses would be active based on the different steering positions of the axlebox. However, the size of the track defects to initiate larger axlebox movement was not quantified in this thesis as the Concept- 4 wagon is expected to run on a better quality track maintained to avoid large track defects as needed to meet the expectation of a high axle load. The longitudinal and lateral stiffnesses were therefore considered constant for all the steering positions of the axleboxes in the modelling.

Finally, the overall damping of the Concept- 4 suspension and the resonance frequency of the Concept- 4 suspension were evaluated on a simple wagon mass model. The Concept- 4 suspension generally has an underdamped and/ or very low damping property in the longitudinal, lateral and vertical suspension properties. Three important modes of vibration of bounce, pitch and roll modes were evaluated to obtain the resonance frequency. The damping of concept- 4 wagon was reduced to detect any possible resonance. The concept-4 with low damping was termed as concept- 5. As the vertical suspension has multiple stages, a non-linear approach was taken to evaluate the resonance frequency range. The resonance frequency range found by non-linear approximation was higher than the theoretical resonance frequency at different stages of the suspension.

Chapter 9
Model Validation and Verification

9.1 Introduction

In this Chapter, firstly, the modelling approach used in the concept- 4 suspension was validated. Secondly, a model verification was performed to check outputs of the simulation of the concept suspension. Thirdly, detailed modelling parameters of the proposed suspension has been presented.

9.2 Model Validation

As the concept-4 wagon was at the hypothetical design stage, it was not possible to obtain physical test results to validate the model. An alternative validation approach was taken in this thesis to compare simulation results of the concept- 4 model with other reference studies using the same input parameters. A similar validation approach was also performed in [93]. Two reference studies of the Technical University of Denmark (DTU) [94] and Royal Institute of Technology, Sweden (KTH) [93] have been used in this Chapter for model validation.

9.2.1 Comparison with Simulation Results of a DTU Model

The difference between the DTU model [94] and the concept- 4 model in this thesis lies in the modelling techniques including the vertical suspension element, the degree of freedom of elements, contact modelling, rail-track and track-ground connection elements. The DTU model was implemented in programming languages C++, Java, and Matlab using the derived equations of different elements of a freight wagon [94]. The concept- 4 model is implemented in Gensys simulation software. The dataset for the model validation (Table 9-1) was chosen for that used for a kbps wagon in [94]. The concept – 4 model was modified (and now referred to as the Concept- 6 model) to represent some similar parameters of the DTU model as presented in Table 9-1 and discussed in this section. It was not possible to replicate all the data of the DTU model due to differences in modelling technique in the software and lack of full data.

The longitudinal and lateral suspension elements were modelled as a linear spring in parallel with a friction damper (elastic elements with dry friction) in the DTU model [94]. In the concept- 6 model, an equivalent element providing the similar hysteresis loop of the parallel combination of a linear spring and friction damper is used. The longitudinal guidance was set at 20mm for the kbps wagon in both the DTU and concept- 6 wagon models. The longitudinal axle guidance was modelled using Newton's impact law with a coefficient of restitution in the DTU model. In the concept- 6 model, the longitudinal stop element was modelled as a dead band spring model with a high stiffness value (4MN/m).

The lateral stop element was modelled as dead band elements in both the DTU and concept- 6 model. In the DTU model, two stages of the lateral stop were used at 10mm and 20mm between the UIC links and suspension bracket. The stiffness of lateral stop at the axle guidance was set to 1.5MN/m at 20mm clearance in both the DTU and concept- 6 model. However, the stiffness at 10mm lateral displacement was not mentioned in the DTU model [94]. So, in the concept- 6 model, the stiffness at 10mm of lateral axle displacement was assumed as 900kN/m. The

stiffness of 900kN/m is active between the 10-20mm lateral position of the axlebox and, after 20mm, the higher stiffness of 1.5MN/m is active.

The vertical suspension was modelled following Fancher's study [135] on the hysteresis loop of the leaf spring in the DTU model. In the concept- 6 model, a function of Gensys was used to provide a similar hysteresis loop to that obtained by a modified Fancher's approximation with a difference near the endpoints of the changing of direction between loading and unloading stages in the hysteresis loop to form a closed loop as also used in [93]. In the DTU model, the friction force was modelled based on the dynamic load on the suspension which allows a low friction damping at empty or low load conditions. In the concept- 6 model, a fixed damping is used based on the static load condition. The fixed friction damping allows higher damping in the low load condition compared to that obtained in empirical approximation (Figure 8-2, Figure 8-3). The maximum friction damping in the vertical suspension was modelled as 13% of the static vertical load (±2.7kN for the empty kbps wagon) in the concept- 6 model based on the data in [93].

There are differences in the degrees of freedom of various elements between the DTU and concept- 6 models (Table 9-2). In the DTU model [94], the detailed track modelling was not included, the wheelsets were connected to rigid rails. In the concept- 6 model, the track components were connected to ground by stiffness and damping elements. In the DTU model, the wagon body did not have a degree of freedom in the longitudinal direction. In order to compare the two models, the DOF of the wagon body was constrained in the longitudinal direction and track ground connections were constrained in all 6 directions (Table 9-2).

In the DTU model, the wheel-rail contact was modelled using the RSGEO program based on the theory by Shen-Hedrick-Elkins which differs from the FASTSIM method and this was indicated as an important parameter to cause the difference between the two models compared in [93]. The wheel profile (S1002), rail profile (UIC60), Poisson's ratio (0.27) and Young's modulus of elasticity (210 GPa) in the concept- 6 model were set to the same values as in the DTU model to minimise the differences in contact parameters. An initial excitation was provided on the wagon body (lateral velocity 0.15m/s, yaw velocity 0.15rad/s) to create oscillation.

Both the DTU and concept- 6 models of the kbps wagon showed some oscillation throughout the time simulation (Figure 9-1). So, it was not possible to determine a critical hunting speed based on the decreasing speed method. A similarity exists between the lateral behaviour of the front wheelset and wagon body of the DTU and concept- 6 model. The oscillation becomes low at about 31.4m/s (113km/h) on the concept- 6 model (Figure 9-1a) compared to about 35m/s (126km/h) on the DTU model (Figure 9-1b) when rail inclination of 1 in 40 was used. The wagon body movement was found to be generating a resonance pattern at about 40s (corresponding to 16m/s) on both the concept- 6 and DTU models (Figure 9-1). The lateral wheelset movement became low in a shorter time on the concept- 6 model compared to the DTU model which indicated that the concept- 6 model had a higher damping ratio in lateral suspension compared to that of the DTU model.

In the case of a rail inclination of 1 in 30 on both the concept- 6 and DTU models, the oscillation of wheelsets continued till a very low speed of 5m/s (Figure 9-2). There are differences in the amplitude of oscillation between the two models. Three different oscillation patterns were visible on the DTU model near 4, 30 and 46s (Figure 9-2b). On the DTU model (Figure 9-2b) at 4s, the lateral movement of the front wheelset became about ±2mm.

Table 9-1: Model parameters of the DTU model [94] and concept- 6 model (kbps wagon)

Parameters	Unit	DTU model	Concept- 6 model
		Value	
Mass of wheelset	kg	1420	1420
Mass moment of inertia of wheels set, roll	kgm^2	1040	1040
Mass moment of inertia of wheels set, pitch	kgm^2	154	154
Mass moment of inertia of wheels set, yaw	kgm^2	1040	1040
Mass of wagon body	kg	8610	8610
Mass moment of inertia of wheels set, roll	kgm^2	25000	25000
Mass moment of inertia of wheels set, pitch	kgm^2	121400	121400
Mass moment of inertia of wheels set, yaw	kgm^2	127700	127700
Radius of wheelset	m	0.46	0.46
Lateral equilibrium position of the centre of mass	m	0	0
Vertical equilibrium position of the centre of mass	m	0.46	0.46
Lateral equilibrium position of the centre of mass	m	0	0
Vertical equilibrium position of the centre of mass	m	1.2	1.2
Longitudinal clearance between axle box and axle guidance	m	0.02	0.02
Lateral clearance between suspension UIC links and suspension bracket	m	0.01	0.01
Lateral clearance between axle box and axle guidance	m	0.02	0.02
Lateral stop stiffness between suspension UIC links and suspension bracket	kN/m		900
Lateral stop stiffness between axle box and axle guidance	MN/m	1.5	1.5
Wheel base	m	8	8
Centre of mass (COM) height	m	1.2	1.2
Longitudinal and lateral suspension parameters from DTU model			
$k_{1x}+k_{2x}$	1/m	29.5	29.5
k_{1x}	1/m	4.5	4.5
Fdx		0.08	0.08
$k_{1y}+k_{2y}$	1/m	24.9	24.9
k_{1y}	1/m	4.9	4.9
Fdy		0.1	0.1
Vertical suspension in the DTU model			
Stiffness, k_{1z}	MN/m	1.1	1.1
Decay constant	mm	2	
$k_{1z}+k_{2z}$ (1)	MN/m	6	
Fdz (1)		0.13	
Wheel-rail contact			
Wheel profile		S1002	S1002
Rail profile		UIC 60	UIC 60
Rail inclination		1/40, 1/30	1/40, 1/30
Friction coefficient		0.3	0.3
Poisson's ratio		0.27	0.27
Young's modulus	GPa	210	210
Contact Stiffness normal to the surface, knwr	MN/m		600
Rail track			
Vertical Stiffness, kzrt	MN/m		230
Lateral Stiffness, kyrt	MN/m		17
Vertical rail track damping, czrt	kNs/m		50
Lateral rail track damping, cyrt	kNs/m		10
Track- ground			
Vertical contact stiffness, kztg	MN/m		220
Lateral contact stiffness, kytg	MN/m		40
Vertical track ground damping ratio, ζ			0.36
Lateral track ground damping ratio, ζ			0.55

Note: (1) Value taken from [93], as the DTU model did not use the same modelling approach

At about 18s, the lateral movement of the front wheelset started to increase gradually and became higher than ±5mm at about 30s (Figure 9-2b). The lowering of displacement of the front wheelset at about 4s on the DTU model was not visible in the concept- 6 model (Figure 9-2b). In the concept- 6 model, the oscillation pattern of the front wheelset (bogie hunting) was similar to that on the DTU model between 25s and 30s (Figure 9-2a). The oscillation patterns of wagon body lateral movement (body hunting) on the concept- 6 and DTU models were also found to be similar between 25 and 45s (Figure 9-2). The body hunting on the concept- 6 model showed lower lateral amplitude of oscillation compared to that of the DTU model between 0s and 25s. In the concept- 6 model, bogie hunting occurred out of phase (Figure 9-3a) and in phase (Figure 9-3b) to the body hunting mode from 0-25s and 25-45s respectively which decreased amplitude of wagon body oscillation from 0-25s and increased amplitude of wagon body oscillation from 25-45s (Figure 9-2a). While the out of phase bogie and body hunting detected on the concept- 6 model was not detectable in the DTU model, the DTU model showed an increase in lateral wagon body displacement after about 25s (corresponding to speeds of 35m/s and lower).

Table 9-2: Degrees of Freedom on the DTU [94] and concept- 6 model

DOF	Wagon body		Front wheelset		Rear wheelset	
	DTU [94]	Concept- 6	DTU [94]	Concept- 6	DTU [94]	Concept- 6
Longitudinal, X			√	√	√	√
Lateral, Y	√	√	√	√	√	√
Vertical, Z	√	√	√	√	√	√
Roll, f	√	√	√	√	√	√
Pitch, k	√	√		√, k=0, initial vk= Vo/ro		√, k=0, initial vk= Vo/ro
Yaw, p	√	√	√	√	√	√
Spin			√ (1)	√ (2)	√ (1)	√ (2)

Note: Shaded cells indicate no DOF is allowed in that direction, (1) Spin perturbation refers to difference between the nominal and actual spin of the wheelset around its axis of revolution, the nominal spin is V/r0, where r0 is the nominal rolling radius, (2) calculates spin Creepage

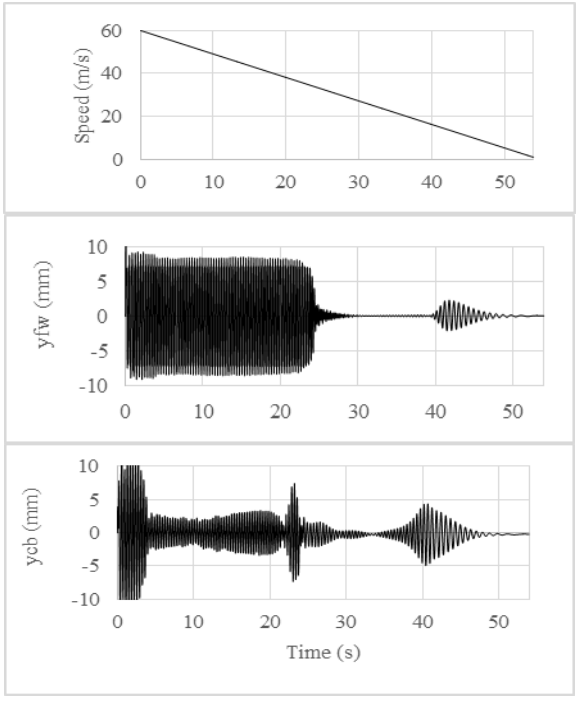

(a) Simulation results on concept- 6 model

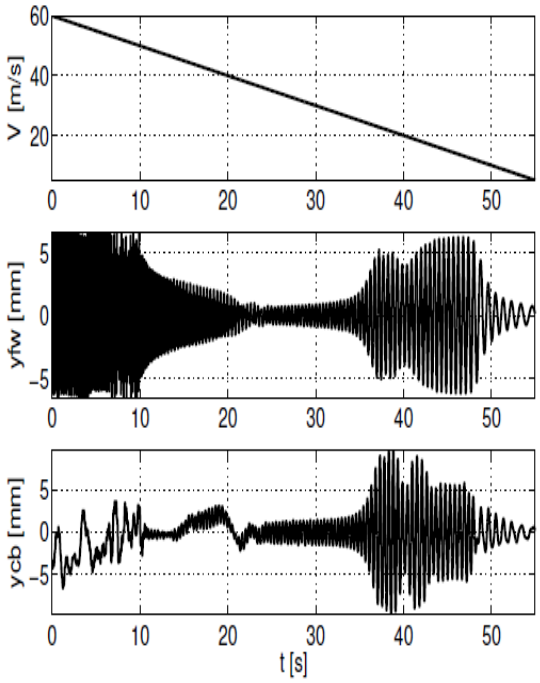

(b) Results from DTU model [94]

Figure 9-1: Kbps wagon, empty, rail inclination 1/40 (Wheel profile S1002, Rail profile UIC60, ycb- lateral wagon body displacement, yfw- lateral front wheelset displacement)

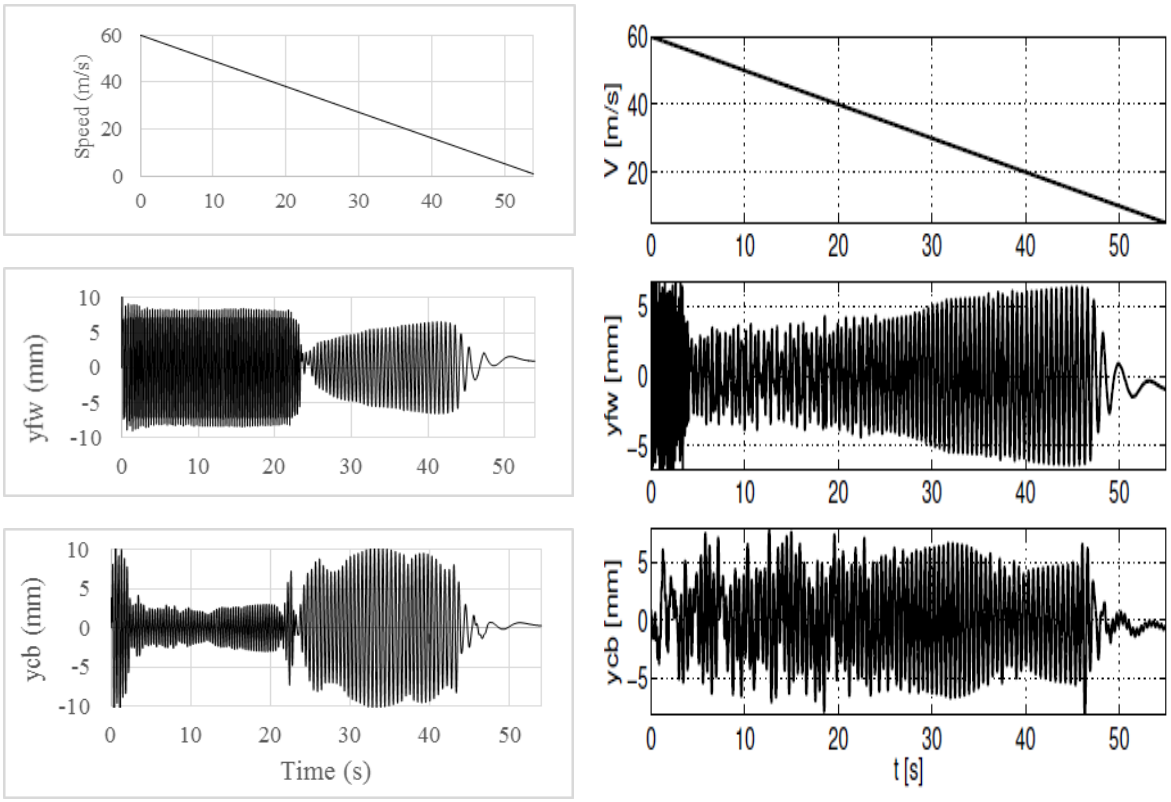

(a) Simulation results on concept- 6 model (b) Results from DTU model [94]

Figure 9-2: Kbps wagon, empty, rail inclination 1/30 (Wheel profile S1002, Rail profile UIC60, ycb- lateral wagon body displacement, yfw- lateral front wheelset displacement, yrw- lateral rear wheelset displacement)

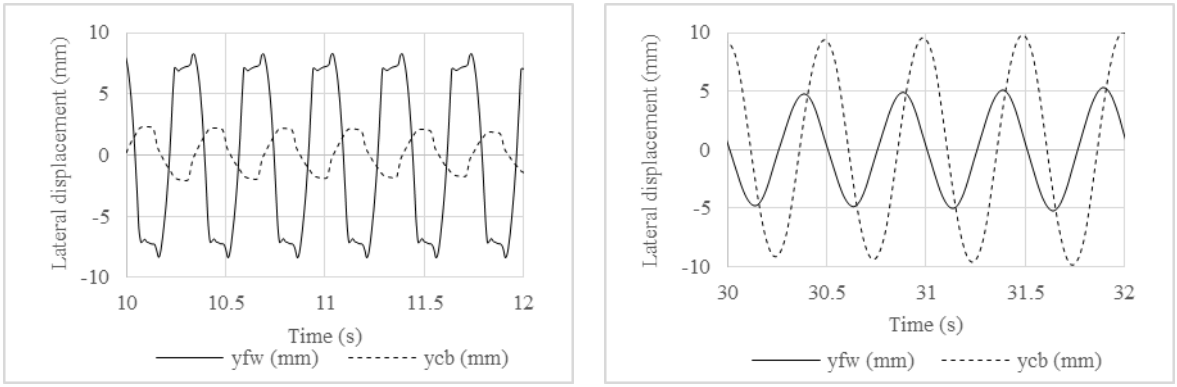

(a) Out-of-phase (b) In-phase

Figure 9-3: In and out-of-phase bogie and body hunting in the concept- 6 wagon model (empty, rail inclination 1/30, Wheel profile S1002, Rail profile UIC60, ycb- lateral wagon body displacement, yfw- lateral front wheelset displacement, yrw- lateral rear wheelset displacement)

9.2.2 Comparison with Simulation Results of a KTH Model

A two-axle covered wagon (Hbbills311, operated in the DB network, Germany) was modelled in the Gensys simulation environment in [93]. As the concept- 4 model was also developed in Gensys simulation software, it is possible to model the wagon in a similar way. The mass and inertia parameters of the concept- 4 model were modified to the data of the Hbbills311 wagon and is now termed as the concept- 7 model. The full dataset of the Hbbills311 wagon model was not available in [93]. Some of the data was therefore provided in the concept- 7 model from the DTU model (Table 9-3). The DOFs in the concept- 7 model were set as per Table 9-2.

Table 9-3: Model parameters for the Hbbills wagon in the KTH model and concept- 7 model

Parameters	Units	KTH model	Concept-7 model
		Values	
Mass of wheelset [1]	Kg		1490
Mass moment of inertia of wheels set, roll [1]	kgm^2		988
Mass moment of inertia of wheels set, pitch [1]	kgm^2		90
Mass moment of inertia of wheels set, yaw [1]	kgm^2		988
Mass of wagon body	Kg	15176	15176
Mass moment of inertia of wheels set, roll	kgm^2	32675	32675
Mass moment of inertia of wheels set, pitch	kgm^2	422084	422084
Mass moment of inertia of wheels set, yaw	kgm^2	413250	413250
Radius of wheelset [1]	M		0.46
Longitudinal clearance between axle box and axle guidance [3]	M		0.0225
Lateral clearance between axle box and axle guidance [3]	M		0.02
Wheelbase	M	10	10
Centre of mass (COM) height	M	1.57	1.57
Longitudinal and lateral suspension from another study			
$k_{1x}+k_{2x}$	1/m	13.18	13.18
k_{1x}	1/m	5.51	5.51
Fdx		0.059	0.059
$k_{1y}+k_{2y}$	1/m	13.79	13.79
k_{1y}	1/m	3.41	3.41
Fdy		0.08	0.08
Vertical suspension in the other study [2]			
$k_{1z}+k_{2z}$	MN/m	6	6
k_{1z}	MN/m	1.1	1.1
Fdz		0.13	0.13
Wheel-rail contact			
Wheel profile		S1002	S1002
Rail profile		UIC 60	UIC 60
Rail inclination		1 in 30	1 in 30
Friction coefficient [1]			0.3
Poisson's ratio [1]			0.27
Young's modulus [1]			2.10E+11
Contact Stiffness normal to the surface, knwr [3]	MN/m		600
Rail track			
Vertical Stiffness, kzrt	MN/m		230
Lateral Stiffness, kyrt	MN/m		17
Vertical rail track damping, czrt	kNs/m		50
Lateral rail track damping, cyrt	kNs/m		10
Track- ground			
Vertical contact stiffness, kztg	MN/m		220
Lateral contact stiffness, kytg	MN/m		40
Vertical track ground damping ratio, ζ			0.36
Lateral track ground damping ratio, ζ			0.55

Note: [1] Parameters not mentioned in the KTH model, indicative from the DTU model has been used in the current model, [2] Modelled as a single stage compared to two stage in the DTU model, [3] Parameters not mentioned in the comparative analysis in the KTH model, taken from Gensys tutorial manual and UIC standards

The simulation tests were performed at constant speeds (30-150km/h at 5km/h intervals) to generate a bifurcation diagram for the concept- 7 model (Figure 9-4). An initial excitation similar to that applied in section 9.2.1 was provided on the wagon body (lateral velocity 0.15m/s, yaw velocity 0.15rad/s). The concept- 7 model provides a higher lateral oscillation amplitude of the wheelset compared to those on the KTH model (example: 6mm on the concept- 7 model compared to about 5.4mm on the KTH model at about 12m/s, Figure 9-4). The trends of the concept- 7 bifurcation diagram generally agrees well with the KTH model (Figure 9-4).

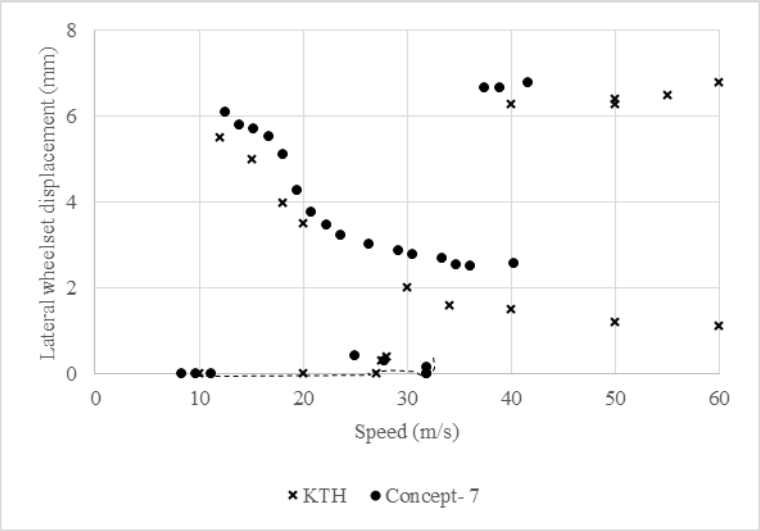

Figure 9-4: Validation of the concept- 7 model with a KTH model [93] using bifurcation diagram (Hbbills310 wagon, rail inclination 1 in 30)

9.3 Model Verification of the Proposed Suspension

Some preliminary tests on the concept- 4 wagon model were performed in this section to verify the suspension characteristics in the modelling based on applied input parameters. This was to confirm that the applied modelling approach replicated the intended behaviour of the concept- 4 suspension.

9.3.1 Hysteresis Loop of the Vertical Concept Suspension

The hysteresis loops of the concept- 4 suspension were obtained by sinusoidal excitations. The vertical amplitude of the sinusoidal excitation provided on the ground was 0-40mm in the empty and the loaded conditions. The frequencies of these vertical excitations were chosen as 3.6 and 2.1Hz which are near the resonance frequencies in the non-linear approximation of suspension characteristics evaluated in Chapter 8. The resonance frequencies are expected to provide higher displacements on the suspension which would allow observing the hysteresis over a longer displacement regime and allow a greater understanding of damping to be gained.

The empty load of 6000kg settled at about 62mm on the concept- 4 suspension in the simulation (Figure 9-5a). The excitation by the ground (0-40mm) at the resonant frequency gave vertical displacements corresponding to 10mm compression (overloading) and 50mm unloading from the initial steady level position (Figure 9-5b). The displacements due to dynamic overload remained at the same stage of the suspension (stage 2), but the displacement corresponding to unloading returned to the softer first stage (Figure 9-5b). The difference between loading and unloading force curves representing the total friction force was about 5kN (Figure 9-5b). Exponential smoothing was added near the transition points between the unloading and loading cycles.

The responses of the vertical suspension for the loaded mass corresponded to 60mm overloading and 80mm unloading from the initial static deflection at 130mm (Figure 9-5c). The unloading stage on the vertical suspension in the loaded condition moved the suspension to the second stage from the third stage. However, the displacement from the further dynamic overload hit the hard stop limit at the end of stage 3. The hysteresis loop in the loaded condition is indicative of a total friction force of 50kN in the concept- 4 vertical suspension (Figure 9-5d). The higher friction force in the loaded condition was due to the load dependent nature of friction in the leaf spring

(Figure 8-2). The low dynamic load in the loaded condition did not, however, provide a corresponding low damping in the model which was due to the simplified approximation of the constant friction damping based on static load only as included in Section 8.2.1 and Table 8-1. The parameters in Figure 9-5 agreed with the approximations in Table 8-1 which indicated that the vertical suspension was modelled accordingly.

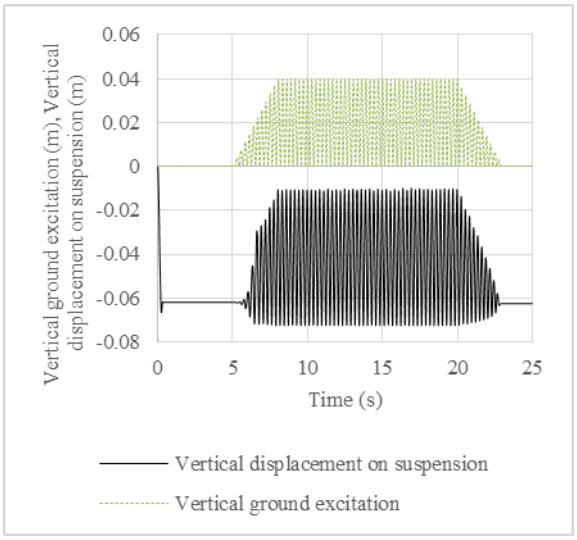

(a) Ground excitation and vertical suspension displacement in empty condition

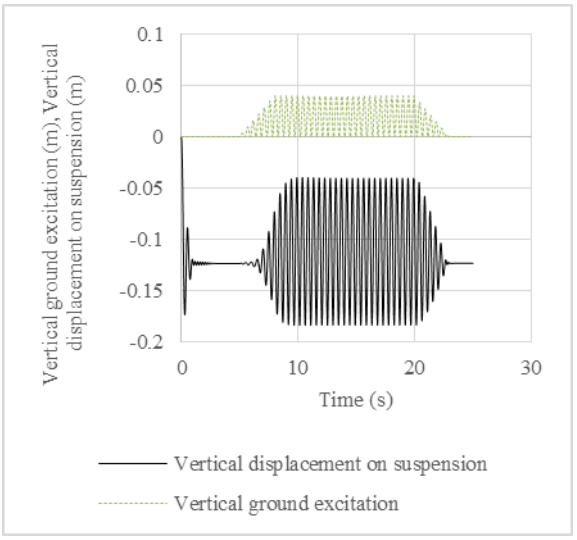

(c) Ground excitation and vertical suspension displacement in loaded condition

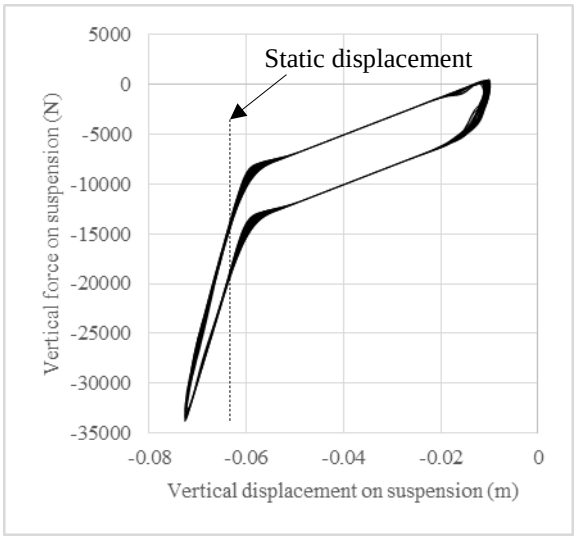

(b) Force versus displacement in empty condition

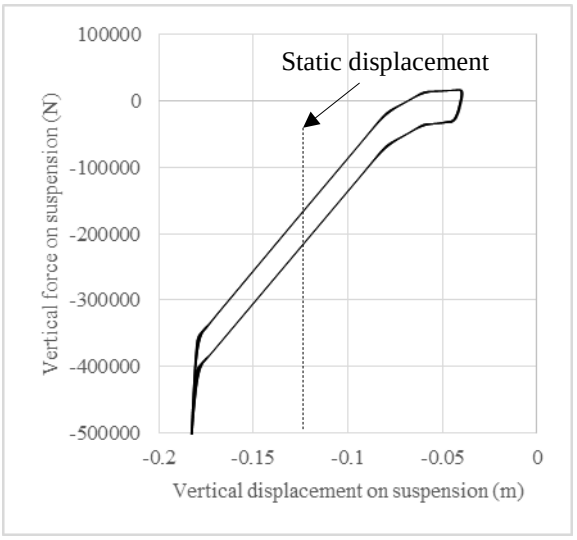

(d) Force versus displacement in loaded condition

Figure 9-5: Hysteresis loop on the concept- 4 vertical suspension

9.3.2 Comparing Longitudinal Suspension of the Concept- 4 with Experimental Data

The concept-4 wagon model was given longitudinal excitations of ±30mm (Figure 9-6a, Figure 9-6c). The suspension was displaced to about ±20mm until the motion was restricted by the longitudinal stops placed at 20mm on the front and rear of each axle box. A hysteresis loop was examined with suspension displacements slightly less than these limits. The empty (6000kg) and loaded (78000kg) cases showed approximate friction damping of ±0.83 ($0.056F_{box}$) and ±10.65kN ($0.056F_{box}$) respectively which was close to the estimated breakout force ($0.06F_{box}$) for the average (medium worn) hysteresis condition used in simulation as per Table 8-3 as used in the simulation. The friction damping property in the modelling thus followed the intended characteristics.

The longitudinal parameters of the concept- 4 wagon model have been further tested under different vertical loads (Figure 9-7b). The force-displacement characteristic in the longitudinal direction on the concept- 4 suspension showed a similar trend to that reported in a laboratory testing (Figure 9-7a) [144]. Both the laboratory measurements in [144] and the simulated results of the proposed suspension system showed a higher friction damping force for a higher vertical load which validated that the longitudinal stiffness was modelled as a load dependent parameter.

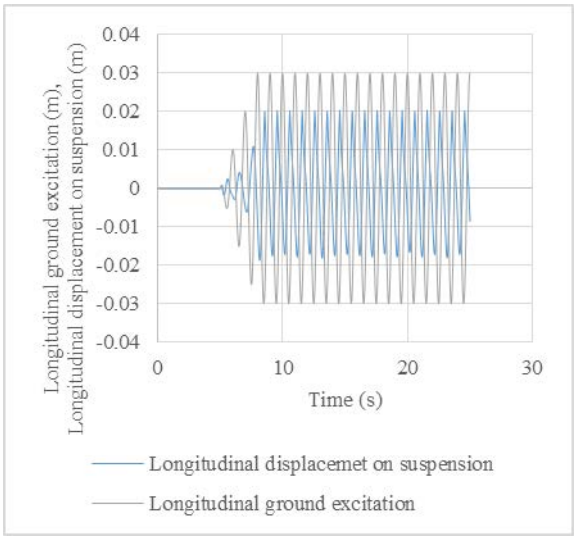

(a) Ground excitation and longitudinal suspension displacement in TARE mass condition

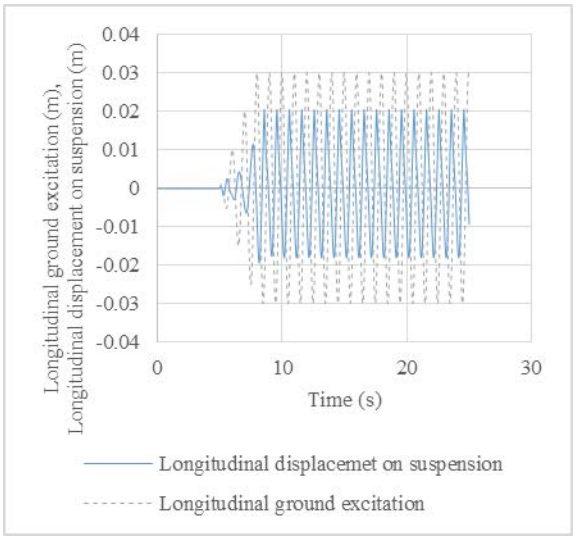

(c) Ground excitation and longitudinal suspension displacement in loaded mass condition

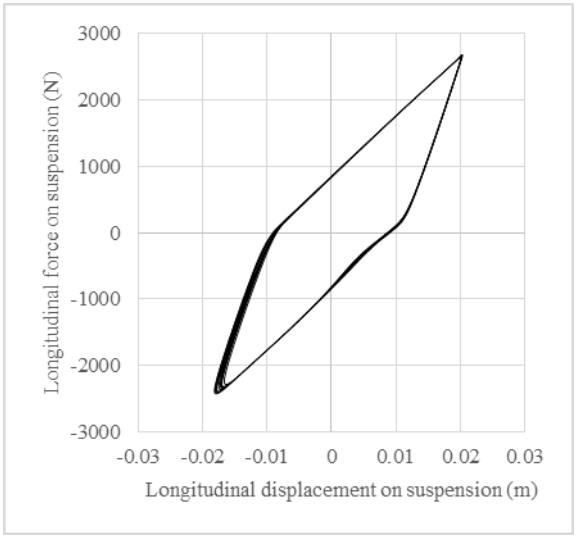

(b) Force versus displacement in TARE condition

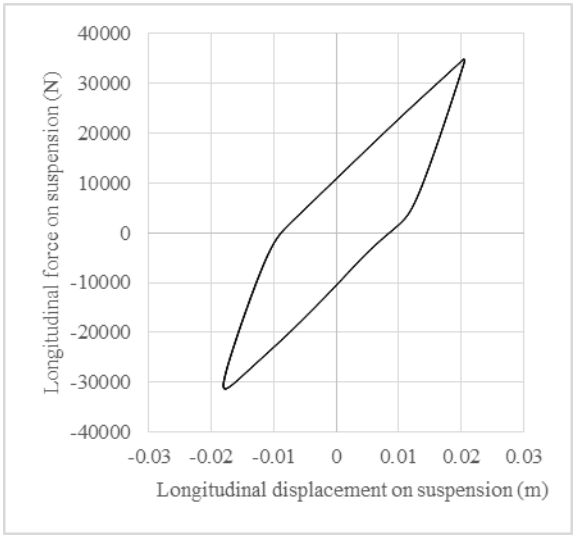

(d) Force versus displacement in loaded condition

Figure 9-6: Hysteresis loop on the longitudinal suspension

The longitudinal friction damping used in the laboratory tests in [144] was higher than was used in the concept-4 wagon model using the average hysteresis condition (medium worn longitudinal suspension parameters). The laboratory test data showed about 37-50% higher friction damping compared to the average hysteresis approximation (medium worn) (Table 9-4). The maximum hysteresis approximation (new longitudinal suspension, Figure 9-7c) provided a better match (-7% to 16% variation) to the laboratory test data in [144] (Table 9-4). While the suspension conditions of the laboratory tests were not published, it was anticipated that the property of the suspension used in the laboratory measurement contained new longitudinal suspension.

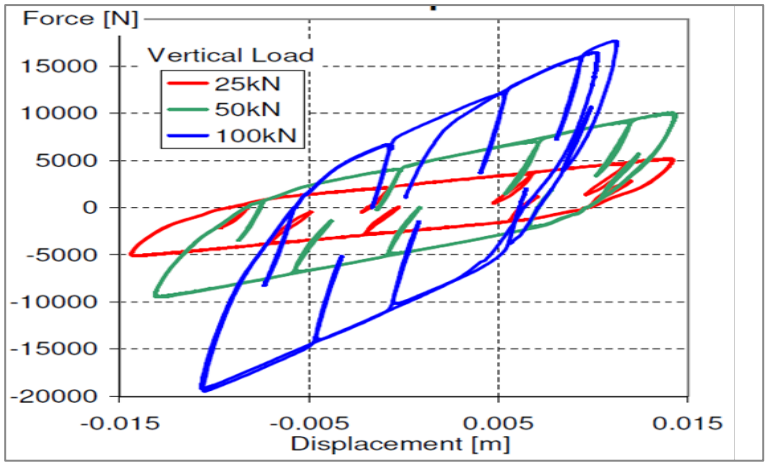

(a) Experimental data on a leaf spring with chain links observed in [144]

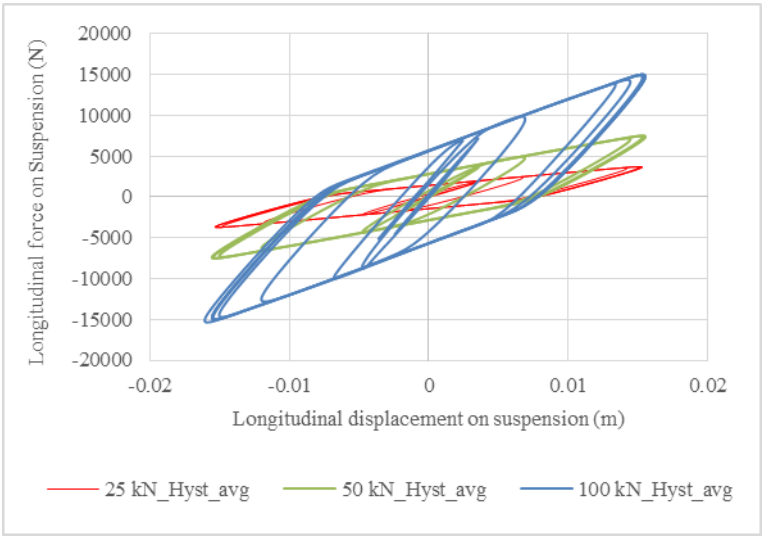

(b) Average hysteresis (Frequency of excitation 1.0Hz, Amplitude of excitation ±25Hz, Hyst_avg- average hysteresis)

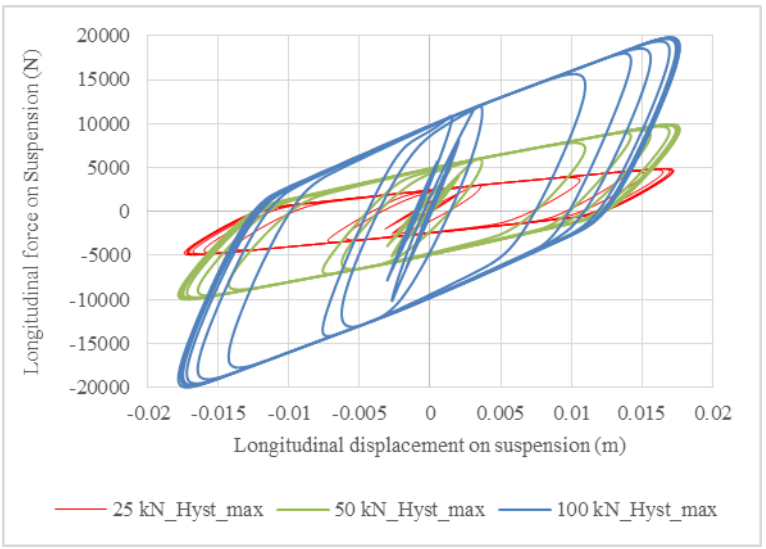

(c) Maximum hysteresis (Frequency of excitation 1.2Hz, Amplitude of excitation ±25Hz, Hyst_max- maximum hysteresis)

Figure 9-7: Longitudinal suspension characteristics under vertical loads of 25kN, 50kN and 100kN

Table 9-4: Comparison of longitudinal friction damping between concept- 4 and a laboratory measurement

Vertical load (kN)	Friction damping (kN)			% Difference in friction damping of the proposed suspension from laboratory test data	
	laboratory test [144] Figure 9-7a	Concept- 4 model (Medium worn suspension) Figure 9-7b	Concept- 4 model (New suspension) Figure 9-7c	Concept- 4 model (Medium worn suspension)	Concept- 4 model (New suspension)
25	5.8	2.9	4.9	50%	16%
50	9.9	5.7	9.6	42%	3%
100	17.9	11.3	19.2	37%	-7%

Note: Friction damping measured from Figure 9-7, Positive % difference means experimental data is higher than that from the concept-4 suspension model

9.3.3 Comparing Lateral Suspension Property of the Concept- 4 Suspension with Available Data in Literature

The concept- 4 wagon model was excited by a displacement of ±50mm in the lateral direction at 1Hz frequency. The lateral response was restricted to ±20mm by lateral stops at a ±20mm distance from the axle box in the lateral direction (Figure 9-8a, Figure 9-8c). The lateral suspension parameters gave about +/-1.45 kN ($0.096F_{box}$) friction force (damping) in the empty condition and about +/-18.5 kN ($0.096F_{box}$) friction force (damping) in the loaded condition (Figure 9-8b, Figure 9-8d) which were close to the breakout force estimations for the lateral suspension corresponding to medium worn suspension ($0.1F_{box}$, Table 8-3).

The suspension properties of the concept- 4 wagon model were normalised with vertical axle box load as a useful comparison is possible with published values from a UIC suspension [93]. The trend of lateral suspension characteristics of the concept- 4 wagon model (Figure 9-9a) generally matches with the measured data of a UIC link suspension system (Figure 9-9b). Generally, the maximum suspension forces per vertical load (0.17, point B) and breakout force ratio (0.1, point A) on the concept- 4 wagon model was less than that (about 0.18 and 0.12) of the UIC link suspension system (Figure 9-9b).

In the case of starting a lateral movement on a suspension from the zero position, the force first reached to the breakout force (point A, Figure 9-9b) and then moved along the hysteresis loop. As the hysteresis loop depends on the amplitude and frequency of excitation, it was not possible to compare the simulated data (Figure 9-9a) with the measured data (Figure 9-9b) in [144]. The series stiffness (OA), pendulum stiffness (AB) and friction break-out force (A) obtained were close to the input (theoretical hysteresis) for the medium worn suspension parameters (Figure 9-9a). The small differences on the simulated hysteresis loop are due to the smoothing effect applied at the change of direction between loading and unloading cycles in the simulation.

The segments representing OA and point A in the concept- 4 model (Figure 9-9a) were within the data range obtained experimentally in [144] (Figure 9-9b). The segment AB representing the pendulum stiffness were also within the stiffness envelope of the experimental data. The stiffness showed by BC (friction series stiffness) on the concept- 4 wagon model was within typical experimental data (Figure 9-9b). As the depth and width of the force-displacement hysteresis loop is dependent on the frequency and amplitude of input excitation, the variation in positioning of point B is not uncommon. The difference between the concept- 4 and typical data lies in the positioning of points B and C. The points B and C settled at about 22mm and 16mm (Figure 9-9a) of lateral displacement which is more than the experimental data (at about 14mm and 9mm) (Figure 9-9b). The agreement in stiffness and friction damping properties of the lateral suspension of the concept 4 model with typical experimental data was expected to be sufficient represent a typical lateral suspension behaviour of a UIC link suspension.

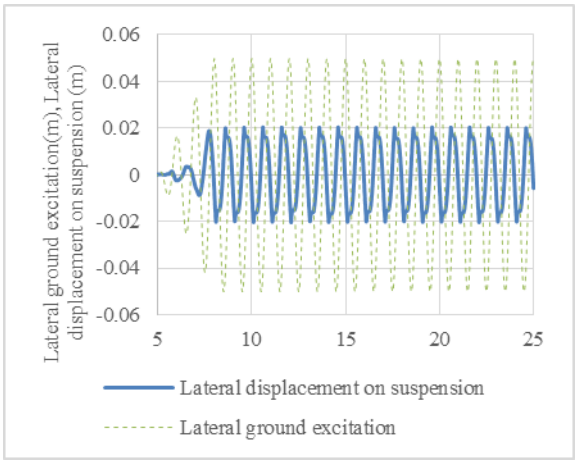

(a) Ground excitation and lateral suspension displacement in empty condition

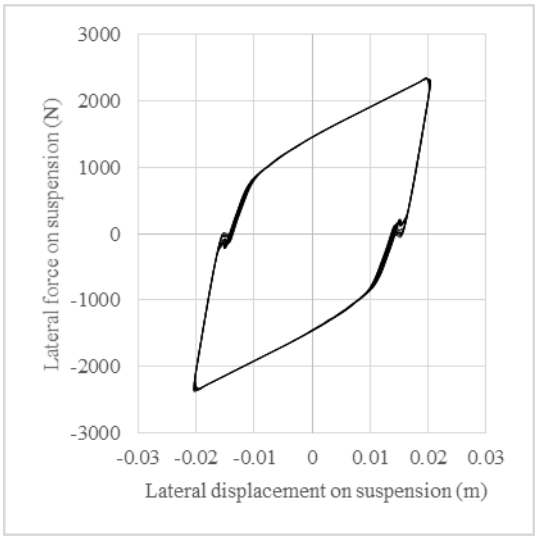

(b) Force versus displacement in empty condition

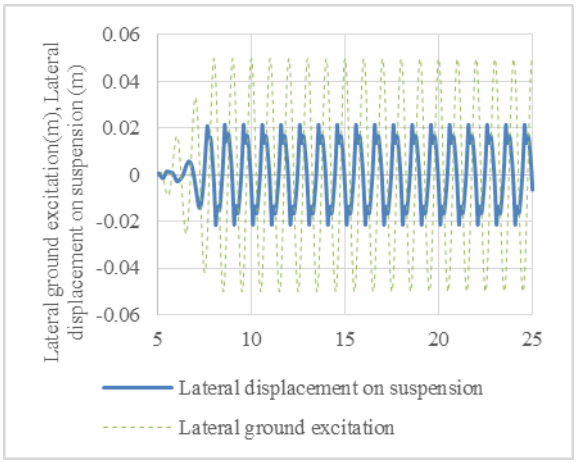

(c) Ground excitation and lateral suspension displacement in loaded condition

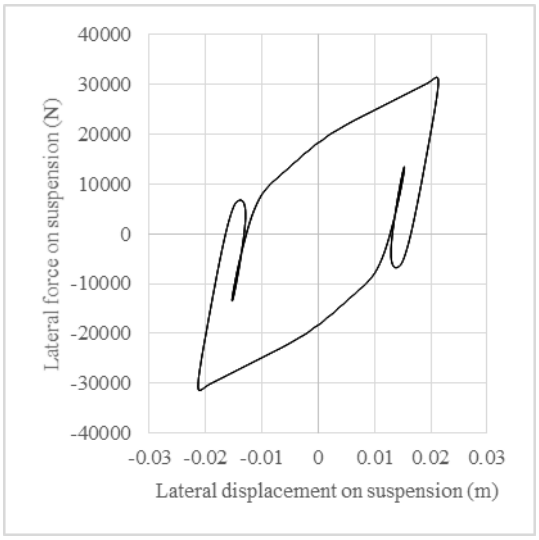

(d) Force versus displacement in loaded condition

Figure 9-8: Hysteresis loop on the lateral suspension

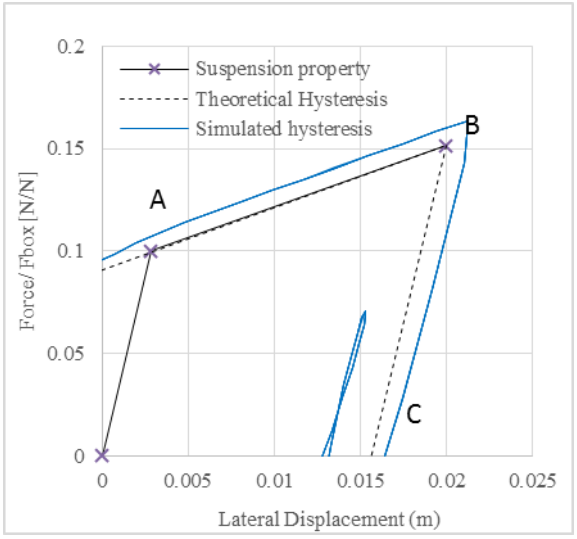

(a) Normalised output from the simple model

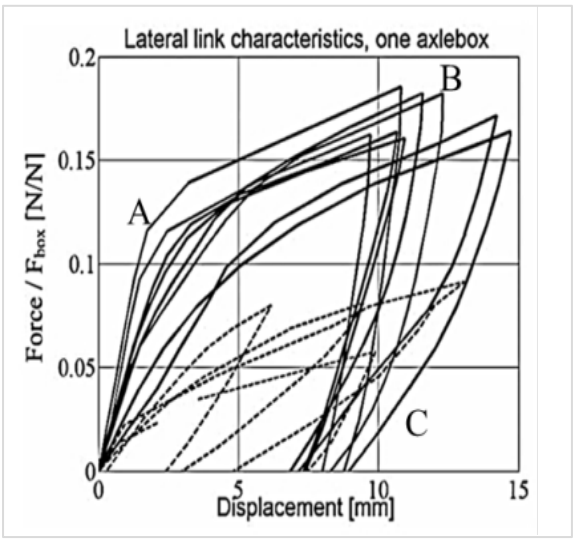

(b) Measured data in [144]

Figure 9-9: Lateral link characteristics

9.3.4 Summary of the Modelling Parameters of the Concept- 4 Wagon Model

The modelling approach of the concept- 4 wagon model was validated with two different studies in DTU and KTH. Further verification and comparison of concept- 4 modelling parameters in a simplified wagon mass model indicated that it was possible to model the suspension properties.

The suspension parameters of the concept- 4 wagon model evaluated on a simplified wagon mass model are now required to be further tested on a full wagon model (concept -8). The full wagon model (concept – 8) consists of wheel-rail contact, track and ground modelling which were considered as similar to that of the tutorial model in Gensys software described in section 7.2. The modelling approach of the vertical, longitudinal and lateral suspension elements of the concept -8 model are similar to that of concept- 4 model and is included in sections 8.2.2 and 8.3. The parameters of the concept- 8 wagon model are shown in Figure 9-10 and Table 9-5.

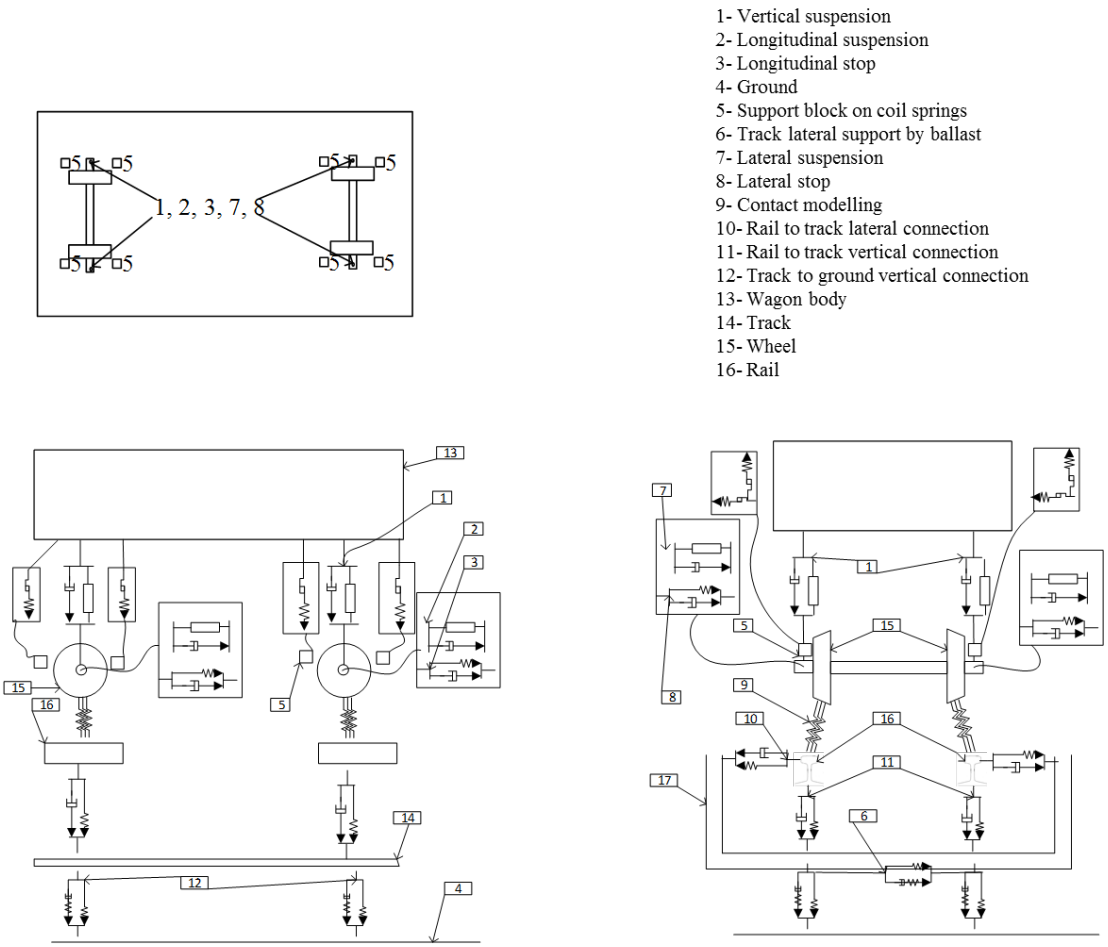

Figure 9-10: Schematic diagram of the full wagon model (concept- 8)

Table 9-5: Model parameters of the tutorial model and the concept- 8 wagon

Parameter	Unit	Tutorial model in Gensys		Concept- 8	
		Empty	Loaded	Empty	Loaded
Wagon body					
Wagon body mass	Kg	6000	43000	6000	78000
Axle centre distance	M	12	12	13.82	13.82
Overhang on each end of the wagon	M	1	1	3	3
Total wagon length	M	14	14	19.82	19.82
Centre of gravity [1]	M	1	2.03	0.9	2.1
Vertical Suspension Parameters on the tutorial model [2]					
Vertical Stiffness, kz	MN/m	1.6	1.6		
Friction force (Damping) [4]	kN	±6	± 21.2		
Stiffness at changing direction [4]	MN/m	64	96		
Vertical damping ratio, ζ		0.05			
Proposed Vertical Suspension Parameters (Calculated combined stiffness parameters) [3]					
Lift off				0	0
Stage 1 stiffness	kN/m			189	189
Stage 2 stiffness	MN/m			1.6	1.6
Stage 3 stiffness	MN/m			3.4	3.4
Hard limit	MN/m			40	40
Damping ratio				0.05	0.05
Friction force at low displacement [4]	kN			2.5	25
Friction force at high displacement [4]	kN			2.5	25
Changing stiffness from static to friction	MN/m			13.6	13.6
Proposed Vertical Suspension Parameters (Stiffness values of springs) [3]					
Stage 1 Coil spring stiffness	kN/m			100	100
Stage 2 Coil spring stiffness	MN/m			1.5	1.5
Leaf spring stiffness	MN/m			3.38	3.38
Longitudinal Suspension Parameters					
Longitudinal Stiffness, kx [4]	kN/m	78	500	88.29	1148
Stiffness at changing direction [4]	kN/m	585	3750	294	3826
Friction force (Damping) [4]	kN	4	22	0.9	11.4
Longitudinal damping ratio, ζ		0.05	0.05	0.05	0.05
Longitudinal stop position	Mm	± 20	± 20	± 20	± 20
Longitudinal stop damping ratio, ζ		0.05	0.05	0.05	0.05
Lateral Suspension Parameters					
Lateral Stiffness, ky [4]	kN/m	123	500	44	574
Stiffness at changing direction [4]	kN/m	3075	12500	515	6695
Friction force (Damping) [4]	kN	4.9	24.4	1.5	19
Lateral damping ratio, ζ		0.05	0.05	0.05	0.05
Lateral stop position	mm	20	20	20	20
Lateral stop damping ratio, ζ		0.05	0.05	0.05	0.05
Friction buffer at both end of wagon [2]					
Friction force in lateral and vertical plane	N	700	700		
Series stiffness with the friction blocks	MN/m	20	20		
Support block on coil spring [3]					
Friction force in lateral and vertical plane	N			600	600

Parameter	Unit	Tutorial model in Gensys		Concept- 8	
		Empty	Loaded	Empty	Loaded
Series stiffness with the friction blocks	MN/m			40	40
Wheel-rail contact					
Wheel profile		S1002	S1002	WPR2000	WPR2000
Rail profile		UIC 60	UIC 60	AS60	AS60
Rail inclination		1 in 40	1 in 40	1 in 20	1 in 20
Friction coefficient at wheel-rail contact, μ		0.5	0.5	0.4	0.4
Contact Stiffness normal to the surface, knwr	MN/m	2400	2400	2400	2400
Creepage reduction factor for rail contamination		0.6	0.6	0.6	0.6
Rail track					
Vertical Stiffness, kzrt	MN/m	230	230	230	230
Lateral Stiffness, kyrt	MN/m	17	17	17	17
Vertical rail track damping, czrt	kNs/m	50	50	50	50
Lateral rail track damping, cyrt	kNs/m	10	10	10	10
Track- ground					
Vertical contact stiffness, kztg	MN/m	220	220	220	220
Lateral contact stiffness, kytg	MN/m	40	40	40	40
Vertical track ground damping ratio, ζ		0.36	0.36	0.36	0.36
Lateral track ground damping ratio, ζ		0.55	0.55	0.55	0.55

Note: [1] calculated value based on loads and centre of gravity of loads [2] The proposed suspension uses a multi-stage suspension, so, the vertical suspension parameters of the concept-8 model is provided separately in this Table, [3] Does not exist on the tutorial model, [4] Load dependent variable

9.4 Summary

Validation for the proposed concept- 4 model was performed by comparing the simulation data with those of DTU and KTH models. A modelling parameter set was established for a fully detailed wagon (concept- 8) in this Chapter based on some preliminary tests on a simple wagon mass model. The modelling parameters developed in this Chapter will be further tested by the VAPS method in Chapter 10.

Chapter 10
The Concept Wagon- Precise Modelling of Final Design

10.1 Introduction

In this chapter, the concept- 8 wagon suspension parameters evaluated in Chapters 8 and 9 have been simulated in a fully detailed wagon model using Gensys. The simulation tests follow the VAPS method. The mass moment of inertia was chosen as that for a realistic chassis approximation (Table 4-3).

10.2 Step 1- Critical Speed Test on the Concept-8 Wagon

The critical speed of the concept- 8 suspension system was obtained as about 20km/h using the decreasing velocity method (Figure 10-1). Clearly, this would be unacceptable for any commercially viable design. The critical hunting speed can be increased by increasing longitudinal stiffness of the suspension as found in [46]. The longitudinal stiffness can be increased by reducing the length of the links as mentioned in [84] or adding additional longitudinal stiffness between the axlebox and wagon body. Reducing the length of the links would change the normalised longitudinal stiffness parameters which may not be representative of the UIC link estimation used in this thesis. It will also be difficult to obtain a constant longitudinal stiffness as the connection points on the axlebox and wagon body will not be aligned to longitudinal direction due to movement of axlebox and wagon body.

At the concept development stage a fixed value of longitudinal stiffness was provided for preliminary assessment in sections 10.2 and 10.3 which was further evaluated for practicality in section 10.4.

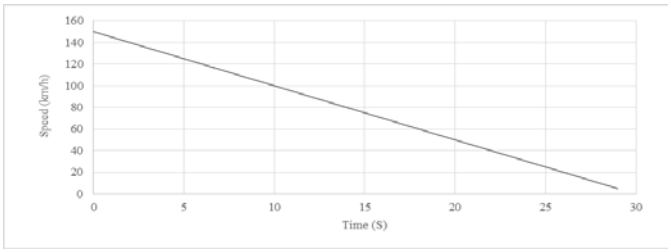

(a) Decreasing velocity for critical hunting speed test

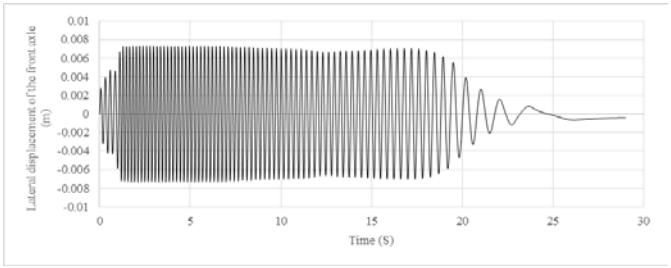

(b) Lateral front axle displacement

Figure 10-1: Measuring critical speed using decreasing velocity on the concept- 8 wagon (empty wagon body mass 6000kg, half axle centre distance 6.906m, Overhang 3m)

The required property of the additional element to achieve a desired critical speed (greater than 80km/h) was obtained by adding longitudinal stiffness of fixed value (independent of load) to the existing longitudinal suspension. As a trial, the existing longitudinal stiffness parameters were increased. The combined stiffness (k_c), pendulum stiffness (k_p) and breakout force (F_D) of the longitudinal suspension in the empty condition were tested

with values of 700kN/m, 150kN/m and 900N respectively (Table 10-1). These modifications if used would result in low values of longitudinal stiffness parameters (k_c, k_p and F_D are 700kN/m, 150kN/m and 900N respectively) for the maximum loaded conditions (k_c, k_p and F_D of the 78000 kg load on a medium worn UIC link suspension is 3826kN/m, 1147kN/m and 11478 N respectively). So, the possible additional element has been separated and added in parallel to the existing load-dependent longitudinal stiffness term in the concept- 9 model (example: $k_c = 20*F_{box}+405.7$). The resultant characteristic data showed that the additional element increased longitudinal combined stiffness (k_c) by 138% and longitudinal pendulum stiffness (k_p) by 70% in the empty condition (Table 10-1). The additional element affects the loaded suspension less significantly as only 11% and 5% increases were obtained in the combined stiffness and pendulum stiffness parameters. The breakout force was increased by 17N only as a trial which corresponds to 2% and 0.1% increases in the empty and the loaded conditions respectively. The additional stiffness element can therefore be considered to mainly affect empty and part-loaded conditions.

Table 10-1: Modification in the longitudinal suspension (Empty- 6000kg, Loaded- 78000kg)

Longitudinal suspension properties	Indicative values for wagon loads		Property of additional longitudinal element	Equivalent values of properties of the concept- 8 and the added longitudinal element (concept- 9)		% increase in parameter in concept- 9 compared to that in concept- 8	
	Empty	Loaded		Empty	Loaded	Empty	Loaded
Combined stiffness (k_c), k1 + k2, kN/m	294	3826	405.7	700	4231.6	138	11
Pendulum stiffness(k_p), k1, kN/m	88	1147	61.7	150	1209.4	70	5
Breakout force, Fd, N	883	11478	17	900	11495	2	0.1

Note: Fbox is the axlebox load= mc*9.81/4, where mc is the wagon body mass including any load

The force-displacement characteristics of the longitudinal suspension with (concept- 9) and without (concept- 8) the additional longitudinal stiffness-damper in the empty condition showed that the added longitudinal stiffness-damper can provide force-displacement characteristics to be within the hysteresis loop of the suspension properties of the new condition (empty_max) parameters for longitudinal movement up to 8mm (Figure 10-2a). However, the longitudinal force at a displacement greater than 8mm in the empty condition on the concept- 9 suspension was higher than that available for the suspension properties in new condition (empty_max).

The modified longitudinal suspension (concept- 9) with the added separate longitudinal stiffness-damper was further tested on a simplified model as used in Chapter 8 to compare hysteresis loops. The characteristic changed significantly in the empty condition (Figure 10-2c) and remained almost unaffected in the loaded condition (Figure 10-2d). So, based on the parameters chosen in Table 10-1 for further tests, it was anticipated that the UIC-links and leaf spring alone cannot achieve the desired suspension properties and these needed to be achieved by additional elements. For simulation purpose, this was considered a reasonable approach to determine a practical suspension design that could achieve the desired dynamic outcome.

It was shown that the existing UIC link and leaf spring suspension with the additional longitudinal stiffness element (additional k_c, k_p and F_D of 405.7kN/m, 61.7kN/m and 17N respectively) increased critical hunting speed to about 100km/h (Figure 10-3).

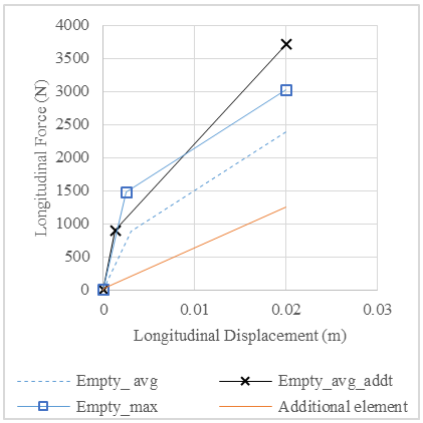

(a) Model parameters in the empty condition

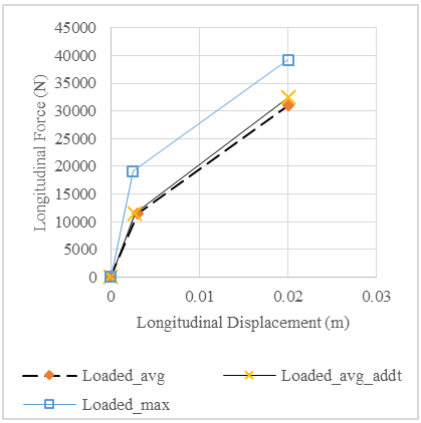

(b) Model parameters in the loaded condition

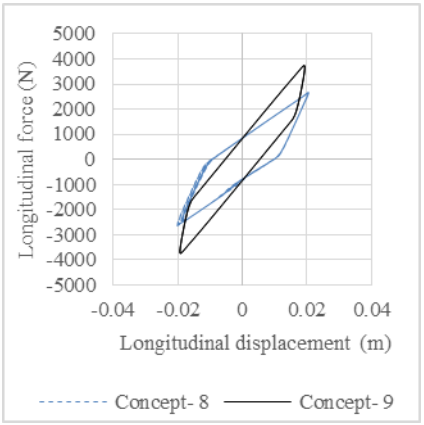

(c) Force-displacement in the empty condition

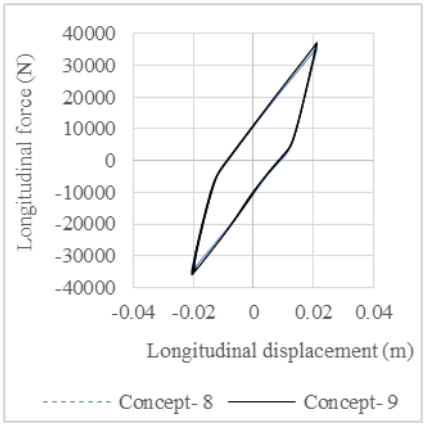

(d) Force-displacement in the loaded condition

Figure 10-2: Modification in the longitudinal suspension to achieve a higher critical hunting speed (Empty_avg- corresponding to medium worn longitudinal suspension, Empty_max- corresponding to new longitudinal suspension, Empty_avg_addt- corresponding to medium worn longitudinal suspension with the additional element, Empty 6000kg, loaded 78000kg)

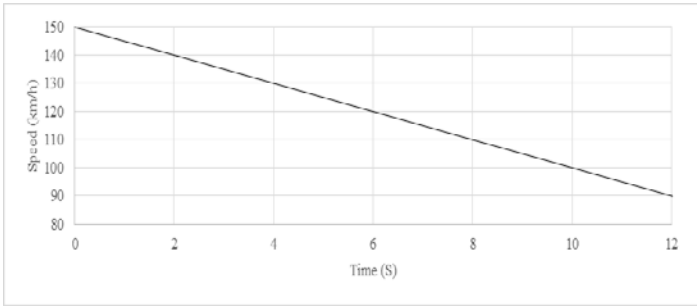

(a) Decreasing velocity to measure critical hunting speed

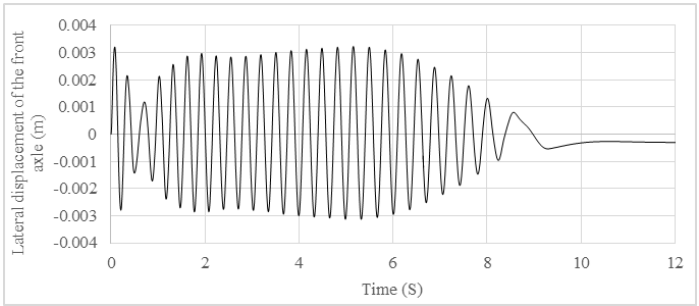

(b) Lateral front axle displacement

Figure 10-3: Step 1 tests on the concept- 9 suspension

10.3 Step 2 – Curve Negotiation Test on the Concept- 9 Wagon

The concept- 9 wagon did not pass the step 2 tests at the exit transition on wheel L/V ratio on the front wheel on the high rail (#11l, Figure 10-4b). The wheel L/V ratio was 1.2 at about 23.4s, the lateral load was about 11.43kN while vertical load reduced to 8.5kN at wheel #11l (Figure 10-4e). In the transition section a combination of geometry and a defect occurs which further affect wheel load distributions on the wagon body. As a softer suspension reduced the wheel unloading ratio at the curve transition during the concept development stage (concept- 1 to concept- 4), it was decided to soften the vertical suspension further in low load conditions. As a starting point, the first two stages of the vertical suspension were moved to 80 and 100mm compared to an initial approximation of 60 and 80mm for concept- 9 (Figure 10-5b). This new suspension design is designated as concept- 10. The concept- 10 suspension allowed the empty load (14.7kN for wagon body mass of 6000kg, 20.049kN for wagon tare mass of 8175kg) condition to settle at about 78mm which is within the displacement range of the first stage of concept- 10 suspension (0-80mm) instead of 62mm which is on the second stage of the suspension (60- 80mm) on the concept- 9 suspension (Figure 10-5b). The concept- 9 suspension moved to the harder second stage when suspension force reached 11335N (the simulated wheel unloading ratio of 0.43) at vertical suspension displacement of 60mm (Figure 10-5b). The harder stage provided a faster increase in suspension force that further increased the wheel unloading ratio. The concept- 10 suspension did not go to the second stage until the suspension force reached 15115N (the simulated wheel unloading ratio of 0.25) at vertical suspension displacement of 80mm (Figure 10-5b).

The vertical load in the loaded condition (80175kg) settled at about 142mm on the concept- 10 vertical suspension compared to about 124mm on the concept- 9 vertical suspension. So, the suspension movement between the empty and loaded conditions remained similar on both the concept- 9 (62mm) and concept- 10 vertical suspensions (64mm). The modification of the suspension in the concept-10 vertical suspension reached hard stop earlier. In the loaded condition, the concept-10 suspension hit the hard stop at suspension force of about 313kN (corresponding wheel overloading of 60%) at suspension displacement of 180mm (Figure 10-5d). The concept-9 vertical suspension allowed more overload (382kN, corresponding wheel overloading of 95%) before hitting the hard stop.

The modified position of the vertical suspension stages (concept – 10) in the step 2 test increased the minimum vertical wheel load to 12kN and reduced the lateral wheel load to 10kN which then reduced the wheel L/V ratio to 0.8 at 23.4s (Figure 10-6b). The concept- 10 vertical suspension was further tested on empty and loaded conditions at various speed conditions. No unacceptable derailment parameters were found in the tested four cases on a 300m radius track (Table 10-2). As the vertical parameters were changed at step 2, a further critical speed test was performed on the concept- 10 vertical suspension parameters. The concept- 10 vertical suspension did not change the critical hunting speed of 100km/h obtained in the first step in section 10.3. The lateral axle movement was found as about ±3mm and started to decrease at about 7s and reached zero at about 10s corresponding to the speed of 100km/h (Figure 10-7).

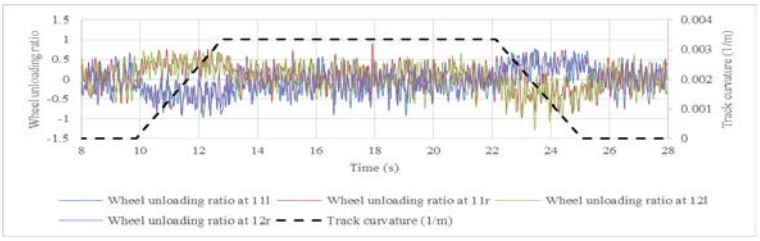

(a) Wheel unloading ratio

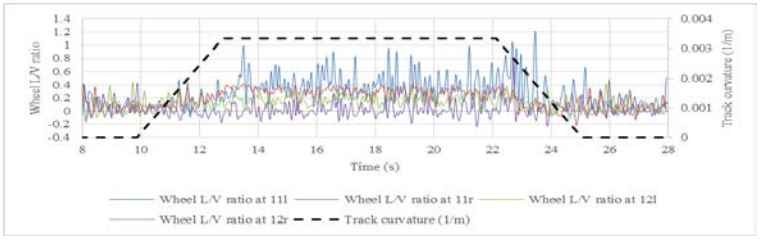

(b) Wheel L/V ratio

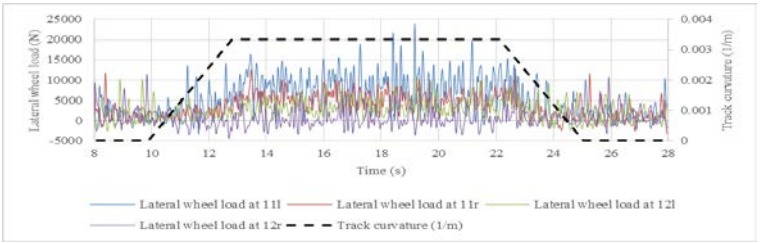

(c) Lateral wheel load

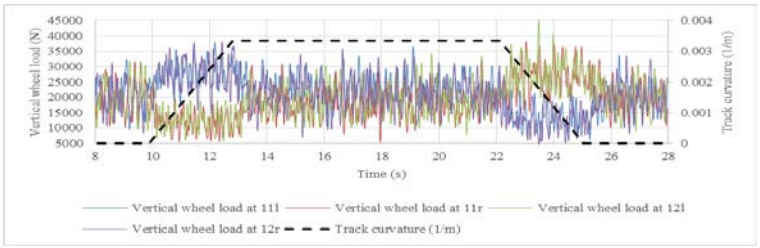

(d) Vertical wheel load

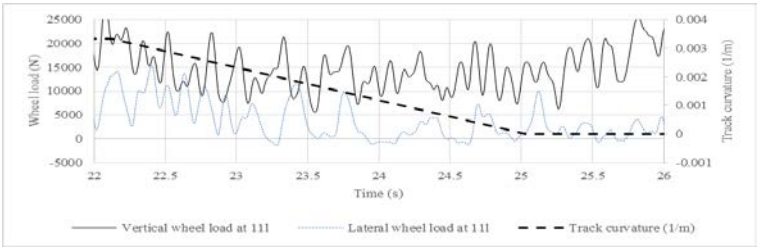

(e) Vertical and lateral wheel loads near exit transition

Figure 10-4: Step 2 tests on the concept- 9 wagon (empty condition, track radius 300m, cant 125mm, cant deficiency 110mm, FRA track class 4)

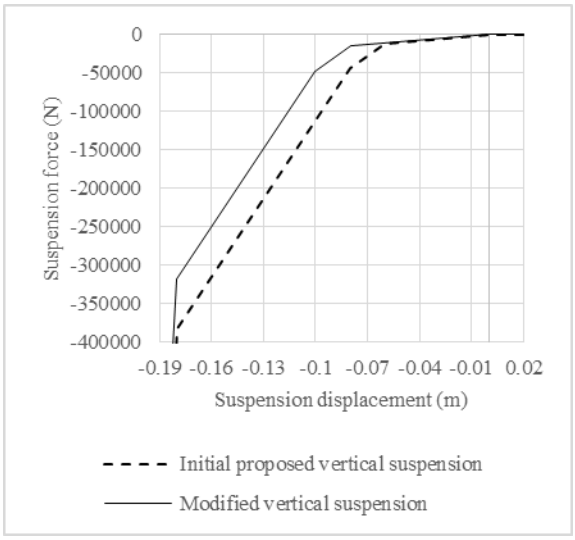

(a) Full vertical suspension

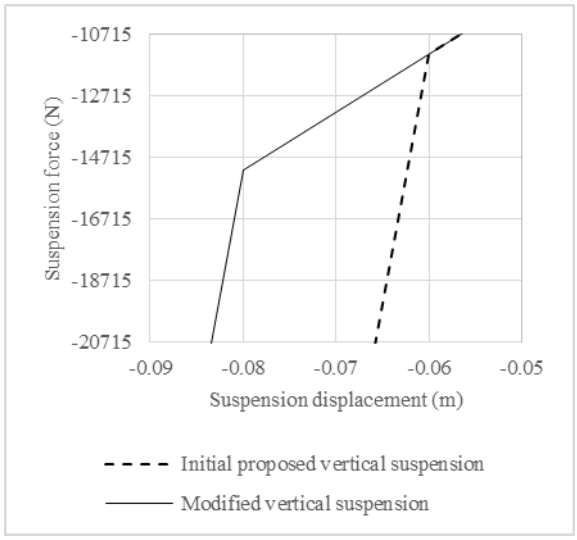

(b) Example plot of static load in low load condition

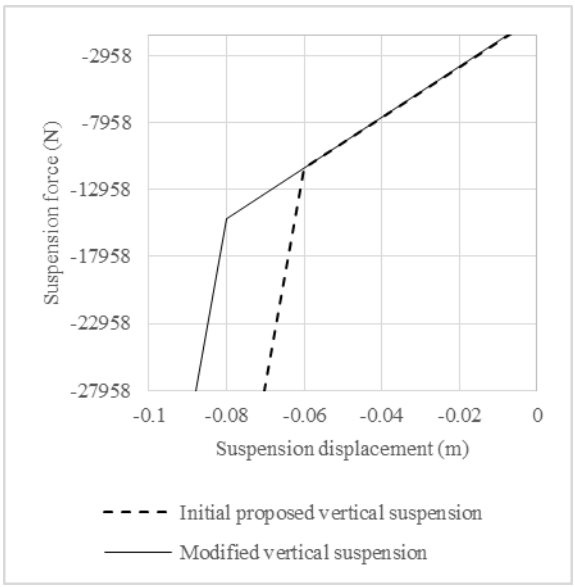

(c) ±90% of the static wheel load of empty condition 6000kg

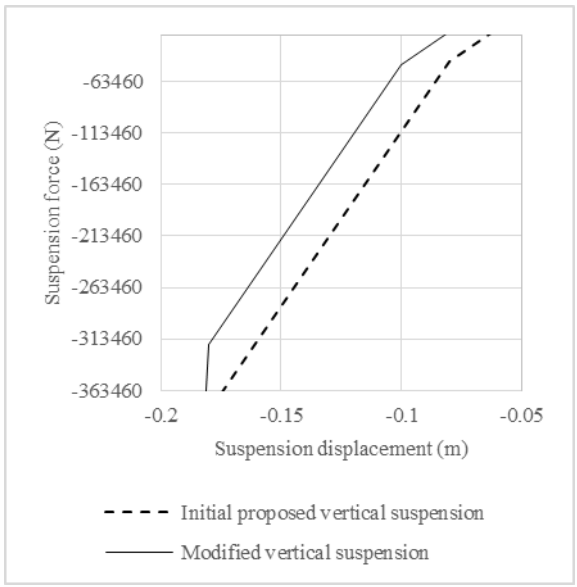

(d) ±90% of static wheel load of loaded condition 78000kg

Figure 10-5: Modification in the vertical suspension stages (Note: Initial proposed vertical suspension is the concept-9 model, modified vertical suspension is the concept- 10 model)

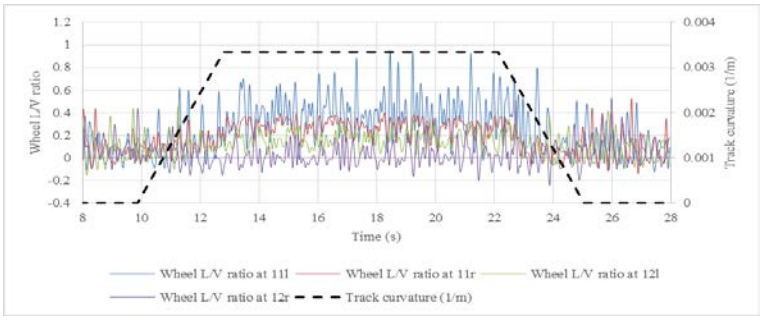

(a) Wheel L/V ratio and track curvature

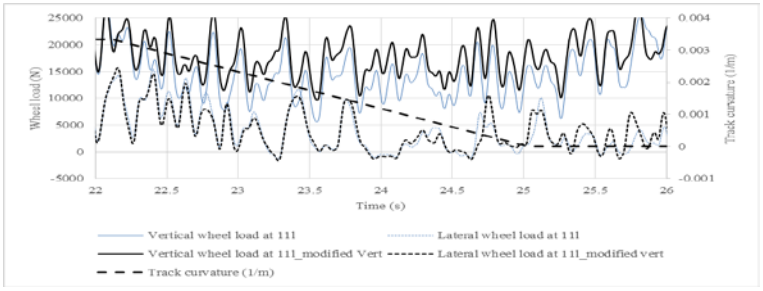

(b) Wheel load in concept-9 and concept-10 wagon (modified vert)

Figure 10-6: Step 2 tests on the concept- 10 wagon (empty condition, track radius 300m, cant 125mm, cant deficiency 110mm, FRA track class 4)

Table 10-2: Derailment parameters of the step 2 tests on the concept- 10 wagon (Empty 6000kg, loaded 78000kg, Track radius 300m, applied cant 125mm)

Case	Load	Cant deficiency	Maximum L/V wheel ratio				Maximum L/V axle ratio		Maximum Wheel unloading ratio			
		mm	11l	11r	12l	12r	11	12	U11l	U11r	U12l	U12r
1	Empty	110	0.95	0.53	0.52	0.53	1.31	0.78	0.67	0.62	0.56	0.59
2	Loaded	110	0.6	0.41	0.29	0.37	1.01	0.5	0.87	0.87	0.87	0.87
3	Empty	-75	0.78	0.46	0.81	0.74	1.18	1.17	0.65	0.56	0.66	0.56
4	Loaded	-75	0.88	0.44	0.26	0.39	1.28	0.55	0.87	0.87	0.87	0.87

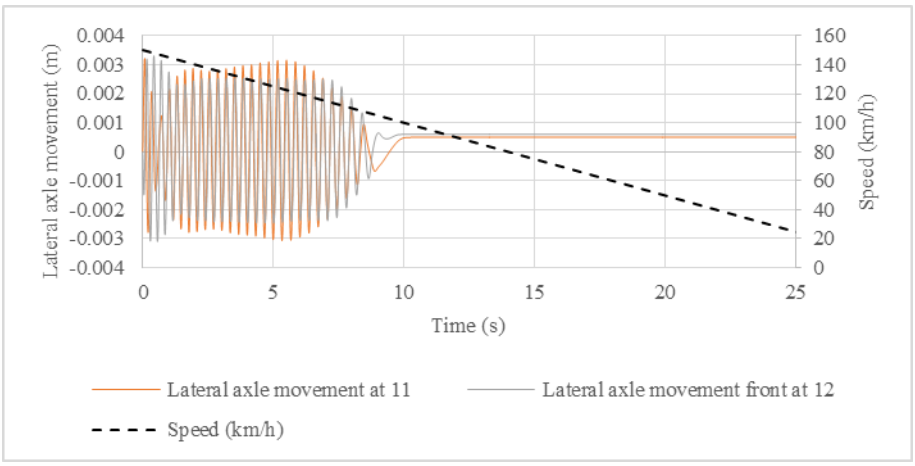

Figure 10-7: Critical speed test on the modified vertical suspension concept- 10

10.4 Practicality of the Additional Longitudinal Element

A practical way to provide the longitudinal stiffness is to provide a spring damper component connecting the axlebox to the wagon body (part no 14, Figure 10-8). The connection point on the wagon body was placed on the pivot mounting (part no 8, Figure 10-8) which is located at a distance of 0.8m from the axlebox (Figure 10-9). The additional element is termed as the 'Yaw link' element.

The change of stiffness of the yaw link element due to the vertical movement of the suspension is expected to be low given the large distance of 0.8m between the two connection points of the yaw link element. As an example, at a vertical displacement of 80mm on the vertical suspension would create an angle of 5.71^0 on the yaw link element. The angle on the yaw link element would reduce the longitudinal stiffness of the yaw link elements by 0.5% and provide an additional vertical stiffness of 10% of the stiffness of the yaw link element. Considering, the yaw link stiffness of 1.71MN/m the modified longitudinal stiffness will be 1.701MN/m and change in vertical stiffness would be 170kN/m. The additional vertical stiffness of 170kN/m due to the yaw link element is considered small comparing the vertical stiffness of 1.6 and 3.38MN/m in the second and third stages of the concept-11 vertical suspension. The added vertical stiffness due to the yaw links would add stiffness to the soft first stage. The first stage would affect the low load, in particular empty load situations. The change of vertical stiffness due to the yaw link element was not included in most of the tests except the isolated twist track defect test realising that the small change in vertical stiffness may increase wheel unloading ratio when subject to a twist track defect.

The additional vertical stiffness due to the yaw link element in the first stage of suspension would be less than the calculated maximum value of 170kN/m. The vertical movement of suspension in the empty conditions (8175kg) would be 40mm at 90% wheel unloading situations which would increase the vertical stiffness by 85kN/m. So, the first stage of suspension would face less change of vertical stiffness due to yaw link element compared to second and third stages of suspension.

As a trial, four yaw link stiffness elements were placed between the wagon body and the axleboxes (Concept- 11, Figure 10-9). The stiffness properties were set to act along the direction between the connection points of the yaw link elements.

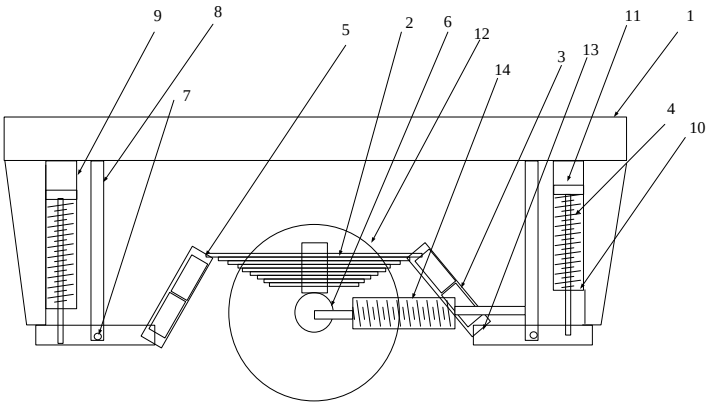

Figure 10-8: Concept- 11 suspension with the yaw link element [1- wagon body, 2- leaf spring, 3- UIC link, 4- Coil spring, 5- Eye of leaf spring, 6- Bearing assembly, 7- Pivot point, 8- Pivot rod, 9- support block of the coils spring, 10- seat of coil spring, 11- fabricated section, 12- Wheel, 13- End bearing, 14- yaw link element]

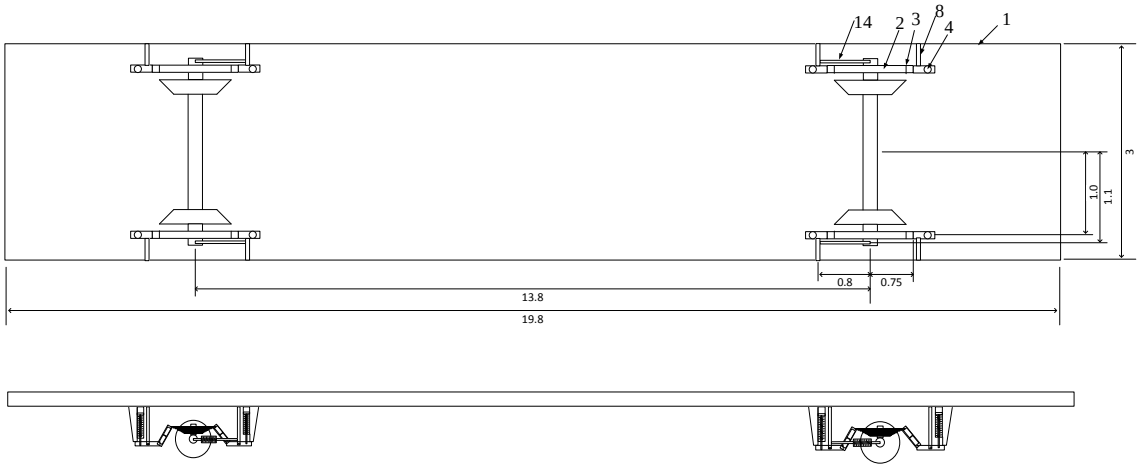

Figure 10-9: Schematic diagram of the positions of the yaw link element on the concept- 11 wagon [1- wagon body, 2- leaf spring, 3- UIC link, 4- Coil spring, 8- Pivot rod, 14- yaw link element]

10.5 Modified Inertia Parameters Including Suspension Mass Elements

The leaf spring mass elements were not included in the simulation cases in the early concept development stages (concept- 1 to concept- 10) for simplification (Chapters 7-10). In this section, the concept- 10 wagon was further modified to include the inertia parameters of the leaf spring suspension. The leaf spring inertia parameters were included with the wheelset inertia parameters as per Equations 10-1 to 10-4 [94].

$$\boldsymbol{m_{wl} = m_w + m_l} \quad \textbf{10-1}$$

$$\boldsymbol{I_{x\_ws} = I_{x\_w} + m_l * r_x^{\,2}} \quad \textbf{10-2}$$

$$\boldsymbol{I_{y\_ws} = I_{y\_w} + m_l * r_y^{\,2}} \quad \textbf{10-3}$$

$$\boldsymbol{I_{z\_ws} = I_{z\_w} + m_l * r_z^{\,2}} \quad \textbf{10-4}$$

where m_{wl} is the mass of the wheelset and leaf spring suspension (kg), m_w is the mass of the wheelset (kg), m_l is the mass of the leaf spring suspension per wheelset (kg), I_{x_ws}, I_{y_ws}, I_{z_ws} are the moments of inertia of the wheelset and leaf spring suspension (kgm^2), I_{x_w}, I_{y_w}, I_{z_w} are the moments of inertia of the wheelset (kgm^2), r_x, r_y, r_z are the distances of the suspension elements from the wheelset centre (m), The distance parameters of the suspension

elements along the x and z axes are 1m (r_x= r_z= 1) and in the y direction the suspension coincides with the wheelset (r_y= 0).

The concept-10 wagon with the modified inertia parameters (Table 10-3) is termed as concept- 11 wagon. The wheelset inertia and mass parameters in Equations 10-1 to 10-4 were replaced by conventional wheelset and UIC link suspension inertia parameters (Table 10-3) used in the modelling of a kbps wagon in a DTU study [94]. The additional mass of the modified leaf springs was then added with the conventional parameters in [94] to obtain the required wheelset and suspension inertias.

Table 10-3: Modified wheelset and chassis mass and inertia parameters including mass of suspension elements (concept- 11)

Parameters		Unit	Conventional UIC link and leaf spring suspension	Concept- 11 suspension
Leaf spring per suspension	Length	m	1.2	1.2
	Width	m	0.12	0.12
	Height	m	0.016	0.021
	Number		8	8
	Total mass	kg	147.6	194
	Volume of leaf spring	m^3	0.0184	0.0242
	Density	kg/m^3	8008	8008
	Additional mass of the modified leaves	Kg		46
Wheelsets and suspension inertia	Mass of wheelset and suspension, mw	Kg	1420	1512
	Ix	kgm^2	1040	1132
	Iy	kgm^2	154	154
	Iz	kgm^2	1040	1132
Tare load	Target tare	kg	8175	8175
Chassis	Wagon body mass, mc	kg	5335	5151
	Mass of rectangular beam, mbr	kg	1888	1888
	Mass of triangular beam, mbt	kg	302	302
	Modified mass of deck to meet target TARE md_mod	kg	2843	2659

The conventional UIC suspension with a parabolic leaf spring used in the kbps wagon model in [94] weighs 147.6kg, which is increased to 193.7kg in the concept-11 suspension (considering leaf thickness of 21mm as established in Chapter 7).

The additional mass of the wheelset due to consideration of the leaf spring increases the tare of the wagon. In order to limit the total wagon tare mass to the target tare of 8175kg, the mass of the deck elements was lowered to 2658kg (Table 10-3).

10.6 Load Dependent Lateral and Longitudinal Stiffness (Modelling)

The longitudinal and lateral suspension of a UIC link suspension with leaf spring were modelled as dependent only on the vertical static load (so a constant stiffness throughout the simulation) in the early stages of concept development (concept- 1 to concept- 10) in Chapters 7-10. In this section, the longitudinal and lateral suspension stiffnesses were changed at every time step on the concept -11 model taking into account of the link angles to give the vertical suspension stiffnesses and forces as expressed by Equations 10-5 to 10-7.

$$\boldsymbol{k_{cijk} = c_j * F_{zik}} \quad \textbf{10-5}$$

$$\boldsymbol{k_{pijk} = p_j * F_{zik}} \quad \textbf{10-6}$$

$$\boldsymbol{F_{dijk} = d_j * F_{zik}} \quad \textbf{10-7}$$

where, k_{cijk}, k_{pijk} and F_{dijk} are the combined stiffness (N/m), the pendulum stiffness (N/m) and the breakout force (N) respectively, c_j, p_j and d_j are the normalisation factors of the combined stiffness (N/m per N), pendulum stiffness (N/m per N) and breakout force (N per N) parameters, F_{zik} is the vertical suspension force (N), i is the suspension positon (#11l, #11r etc.), *j* is the suspension type (longitudinal, lateral), *k* is the time step (s).

10.7 Additional Yaw Force (Modelling) on the Wheelsets

In the earlier concept suspensions (concept- 1 to concept- 10), the additional yaw forces due to the positioning of the UIC links were not added. As the direction of the stiffness elements in the modelling was chosen based on suspension properties in translational directions (vertical, longitudinal and lateral), this gives an improvement in the modelling by considering the steering forces. These forces are then reacted by the wheelsets due to the longitudinal and lateral forces on the pivot points between wheelsets and leaf springs; and wagon body and links. The relevant equations (Equations 10-8 to 10-41) can be obtained using Figure 10-10.

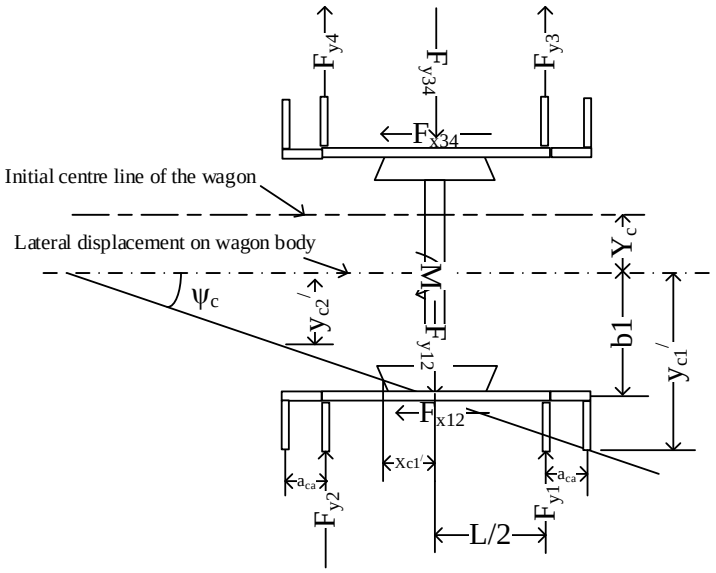

Figure 10-10: Schematic diagram of the kinematics of a wheelset on a UIC link and leaf spring suspension (L is the length of the leaf spring, a_{ca} is the distance between the leaf spring eye and pivot connection point between the links and wagon body, Fx and Fy are the suspension forces on the wheelset, b1 is the lateral semi-distance between the wagon body centre and suspension elements, ψ_c is the yaw angle of the wagon body, M is the yaw moment on the wheelset)

Equations 10-8 to 10-27 have been used in [93] in order to develop kinematic equations of a typical UIC link and leaf spring suspension assuming the static (dependent on the static vertical load of a wagon) stiffness parameters for all the suspension. In this thesis, the variation in stiffness of each suspension element due to dynamic load condition has been developed by using different stiffness parameters for each suspension element (Equations 10-28 to 10-33).

Assuming a rigid connection between the leaf spring seat and the axlebox, the yaw deflection on the leaf spring suspension relative to the wheelset is considered as zero (Equation 10-34). The lateral stiffness on both links on both sides of a leaf spring is assumed to be the same (Equations 10-35, 10-37). The lateral stiffness on the front and rear links of a leaf spring constitute the equivalent lateral stiffness of the suspension (Equations 10-36, 10-38). The longitudinal suspension stiffness element on wheel 12 was considered as the left longitudinal stiffness (Equation 10-39) and on wheel 34 was considered as the right longitudinal stiffness (Equation 10-40).

The yaw moment on the wheelset (Equation 10-14) was then modified (Equation 10-41) to include the kinematic equations of the wheelset and wagon body using several assumptions as set out in Equations 10-34 to 10-40. The modified yaw moment equation (Equation 10-41) developed in this thesis provides the yaw moment based on the "Load dependent lateral and longitudinal stiffness (modelling)" parameters discussed in section 10.6.

The force and moment components between the wheelsets and leaf springs:

$$\boldsymbol{F_{y12} = F_{y1} + F_{y2}} \quad \textbf{10-8}$$

$$\boldsymbol{F_{y34} = F_{y3} + F_{y4}} \quad \textbf{10-9}$$

$$\boldsymbol{M_{ls12} = \frac{F_{y1} - F_{y2}}{L/2}} \quad \textbf{10-10}$$

$$\boldsymbol{M_{ls34} = \frac{F_{y3} - F_{y4}}{L/2}} \quad \textbf{10-11}$$

Force and moments on the wheelsets:

$$\boldsymbol{F_x = F_{x12} + F_{x34}} \quad \textbf{10-12}$$

$$\boldsymbol{F_y = F_{y12} + F_{y34}} \quad \textbf{10-13}$$

$$\boldsymbol{M = M_{ls12} + M_{ls34} + F_{x12} \cdot b_1 - F_{x34} \cdot b_1} \quad \textbf{10-14}$$

Kinematics on a wheelset:

$$\boldsymbol{x_{ws12} = x_{ws} - b_1 \psi_{ws}} \quad \textbf{10-15}$$

$$\boldsymbol{x_{ws34} = x_{ws} + b_1 \psi_{ws}} \quad \textbf{10-16}$$

$$\boldsymbol{y_{ws1} = y_{ws} + \left(\frac{L}{2}\right)\psi_{ws} + \left(\frac{L}{2}\right)\psi_{ls12}} \quad \textbf{10-17}$$

$$\boldsymbol{y_{ws2} = y_{ws} - \left(\frac{L}{2}\right)\psi_{ws} - \left(\frac{L}{2}\right)\psi_{ls12}} \quad \textbf{10-18}$$

$$\boldsymbol{y_{ws3} = y_{ws} + \left(\frac{L}{2}\right)\psi_{ws} + \left(\frac{L}{2}\right)\psi_{ls34}} \quad \textbf{10-19}$$

$$\boldsymbol{y_{ws4} = y_{ws} - \left(\frac{L}{2}\right)\psi_{ws} - \left(\frac{L}{2}\right)\psi_{ls34}} \quad \textbf{10-20}$$

Wagon body displacement at any point:

$$x_{c1}{}' = b_1 \tan\psi_c = b_1\psi_c \quad \textbf{10-21}$$

Wagon body kinematics:

$$x_{c12} = x_c - b_1\psi_c \quad \textbf{10-22}$$

$$x_{c34} = x_c + b_1\psi_c \quad \textbf{10-23}$$

$$y_{c1} = y_c + \left(a_{ca} + \frac{L}{2}\right)\psi_c \quad \textbf{10-24}$$

$$y_{c2} = y_c + \left(a_{ca} - \frac{L}{2}\right)\psi_c \quad \textbf{10-25}$$

$$y_{c3} = y_c - \left(a_{ca} + \frac{L}{2}\right)\psi_c \quad \textbf{10-26}$$

$$y_{c4} = y_c - \left(a_{ca} - \frac{L}{2}\right)\psi_c \quad \textbf{10-27}$$

Forces between the wheelsets and wagon body:

$$F_{y1} = k_{y1}\left(y_{ws1} - y_{c1}\right) \quad \textbf{10-28}$$

$$F_{y2} = k_{y2}\left(y_{ws2} - y_{c2}\right) \quad \textbf{10-29}$$

$$F_{y3} = k_{y3}\left(y_{ws3} - y_{c3}\right) \quad \textbf{10-30}$$

$$F_{y4} = k_{y4}\left(y_{ws4} - y_{c4}\right) \quad \textbf{10-31}$$

$$F_{x12} = k_{x12}\left(x_{ws12} - x_{c12}\right) \quad \textbf{10-32}$$

$$F_{x12} = k_{x34}\left(x_{ws34} - x_{c34}\right) \quad \textbf{10-33}$$

Assumptions:

$$\psi_{ls12} = \psi_{ls34} = 0 \quad \textbf{10-34}$$

$$k_{y1} = k_{y2} \quad \textbf{10-35}$$

$$k_{y1} + k_{y2} = k_{yl} \quad \textbf{10-36}$$

$$k_{y3} = k_{y4} \quad \textbf{10-37}$$

$$k_{y3} + k_{y4} = k_{yr} \quad \textbf{10-38}$$

$$k_{x12} = k_{xl} \quad \textbf{10-39}$$

$$k_{x34} = k_{xr} \quad \textbf{10-40}$$

Yaw moment on the wheelset considering “Load dependent lateral and longitudinal stiffness (modelling)” elements:

$$M_i = k_{yli}(\psi_{wsi} - \psi_c)\left(\frac{L}{2}\right)^2 + k_{yri}(\psi_{wsi} + \psi_c)\left(\frac{L}{2}\right)^2 + k_{xli}(x_{wsi} - b_1\,\psi_{wsi} - x_c + b_1\psi_c)b_1 - k_{xri}(x_{wsi} + b_1\,\psi_{wsi} - x_c - b_1\psi_c) \quad \textbf{10-41}$$

where k_{yli} and k_{yri} are the lateral suspension stiffness on left and right axleboxes on the i-th wheelset (N/m), k_{xli} and k_{xri} are the longitudinal suspension stiffness on left and right axleboxes on the i-th wheelset (N/m), ψ_{wsi} is

the yaw movement on the i-th wheelset (rad), ψ_c is the yaw movement on the wagon body at the centre of the wagon body (rad), L is the length of the leaf spring (m), b_1 is the lateral distance between the suspension on the axlebox and centre of the axle (m).

Equation 10-41 provides yaw moment resulting on a typical UIC-link suspension. Equation 10-41 does not have the a_{ca} component representing the longitudinal distance between the leaf spring eye and the pivot connection points between the links and wagon body (Figure 10-10) which means that the yaw moment of a wheelset is independent of the connection points of the UIC links to the wagon body. The concept- 11 suspension, having a different pivot point connection to the wagon body compared to the UIC link suspension, is therefore believed to provide a similar yaw moment to that obtained using the typical UIC link suspension approximation (Equation 10-41) in this section.

In the modelling of yaw movement of the wheelsets, only the pendulum stiffness (k_1, Figure 7-4b) components of the longitudinal and lateral suspensions were considered. It is assumed that sliding occurs in the friction dampers of the links to provide the yaw damping on the wheelset (i.e. k_2 becomes inactive, Figure 7-4b). This assumption would reduce the damping in the steering force. So, a higher steering force is modelled in the concept-11 wagon model than may occur in practice which can improve curve negotiability but reduce critical hunting speed. As the yaw force component on the wheelset was small compared to overall vehicle dynamics, such a change would affect the result less significantly as can be seen from some of the preliminary tests in the next section 10.8.

10.8 Step 1 Test on the Concept- 11 Wagon

Step 1 tests on the concept- 11 wagon with the yaw link elements were performed to find a suitable stiffness parameter of the yaw link elements. The stiffness (kadd) of each yaw link element was set to 751, 1052 and 1710kN/m as an initial trial. Both the “Load dependent lateral and longitudinal stiffness (modelling)” as defined in section 10.6 and “Additional yaw force (modelling)” was applied on the concept- 11 wagon model. The critical speed was found to increase with the increase of stiffness of the yaw link elements in the concept- 11 wagon (Figure 10-11, Figure 10-12).

The critical speed was found to be 20km/h when no yaw link stiffness was added (Figure 10-11a). The critical speed was increased to about 72km/h when the stiffness of the yaw link element was chosen as 522kN/m (Figure 10-11b). Critical speed was found as high as 204km/h when a high yaw link stiffness of 1.7MN/m was added in the concept-11 wagon model.

The yaw link stiffness of 1.7MN/m was further used to evaluate the effect of the “Load dependent lateral and longitudinal stiffness (modelling)” as defined in section 10.6 and “Additional yaw force (modelling)” as defined in section 10.7 (Figure 10-13). Three different models were evaluated- concept- 12 wagon without the consideration of load dependent stiffness and additional yaw force, concept- 13 model with only the “Load dependent lateral and longitudinal stiffness (modelling)” and the concept- 14 model with both the “Load dependent lateral and longitudinal stiffness (modelling)” and “Additional yaw force (modelling)” elements.

The concept- 13 model increased critical speed significantly (195km/h, Figure 10-13b) compared to the concept-12 model (120km/h, Figure 10-13c). The concept- 14 model further improved critical speed to 204km/h (Figure

10-13a). The lateral axle movement and the yaw displacement of the wheelset (Figure 10-13e) in the concept-13 model were settled quicker than that of the concept- 12 model (Figure 10-13f). The concept- 14 model reduced the yaw displacement further compared to the concept- 12 wagon model (Figure 10-13d). The vertical suspension forces in the concept- 13 and 14 models were lower than those in the concept-12 model (Figure 10-14) which affected the reduced longitudinal and lateral suspension stiffness and helped the concepts- 13 and 14 models settle in a quicker time. The stiffness of 1.7MN/m was chosen (concepts- 12, 13, 14) to perform the remaining tests of the VAPS method.

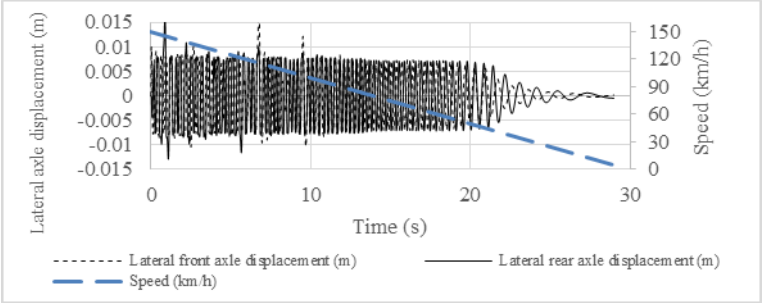

(a) No additional element

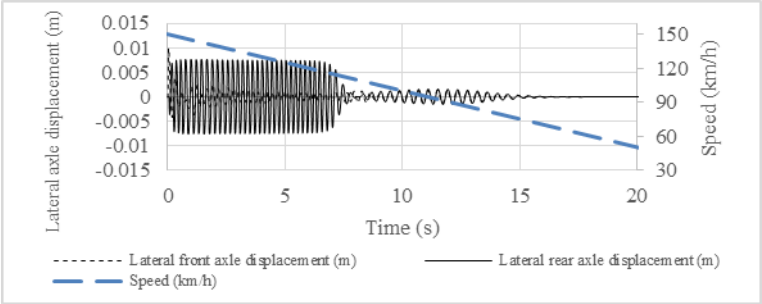

(b) Additional yaw link stiffness, kadd= 522kN/m

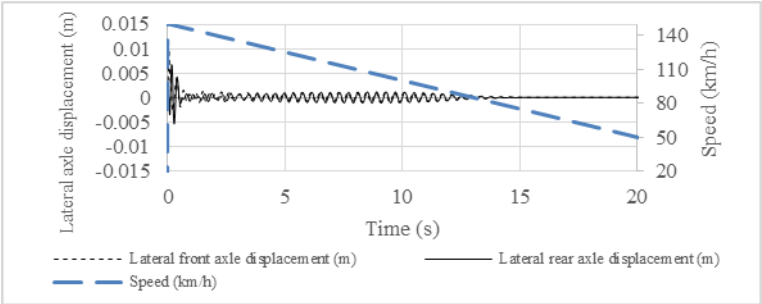

(c) Additional yaw link stiffness, kadd= 751 kN/m

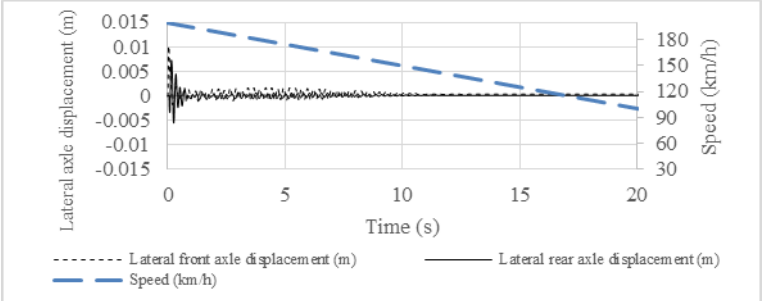

(d) Additional yaw link stiffness, kadd= 1052 kN/m

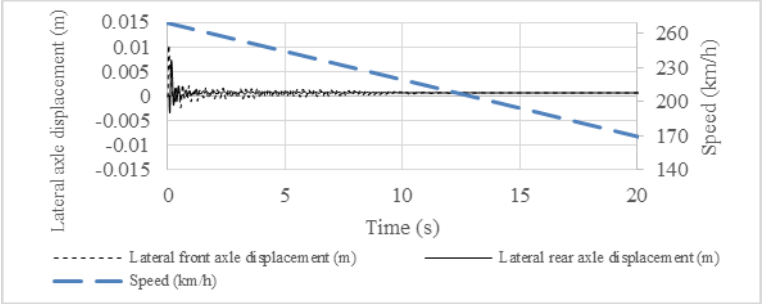

(e) Additional yaw link stiffness, kadd= 1710 kN/m

Figure 10-11: Critical speed test on the concept- 11 wagon with yaw link stiffness, kadd

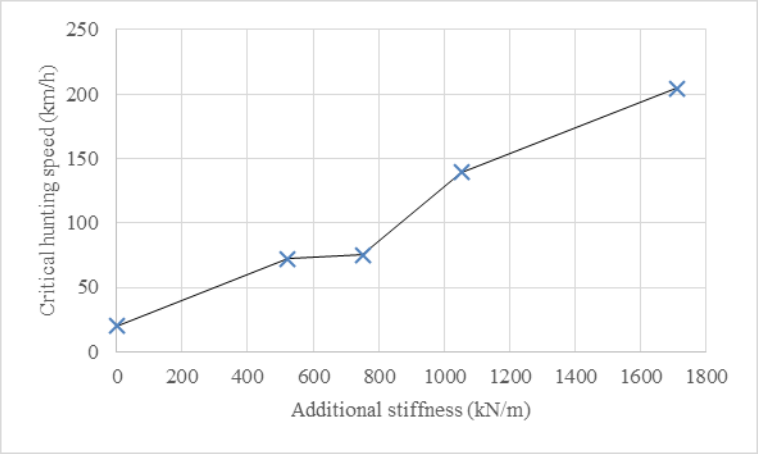

Figure 10-12: Change of critical hunting speed on the concept- 11 wagon model due to change of stiffness of the yaw link element (kadd)

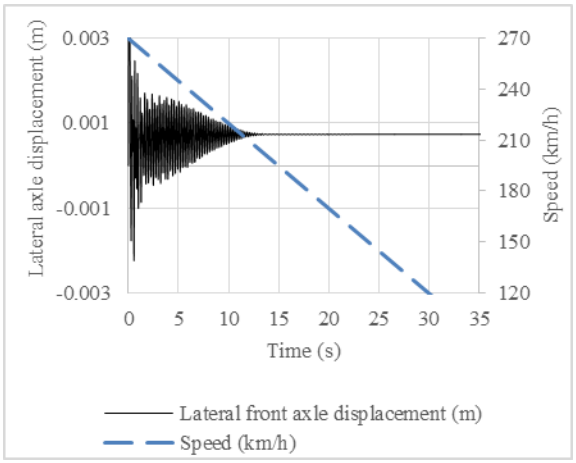

(a) Lateral front axle displacement (Concept- 14 model)

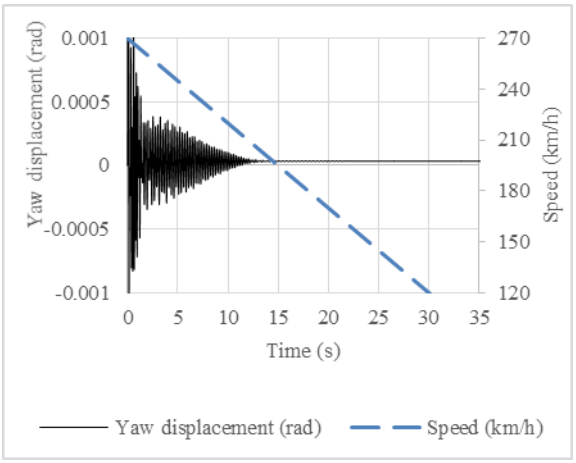

(d) Front axle yaw displacement (Concept- 14 model)

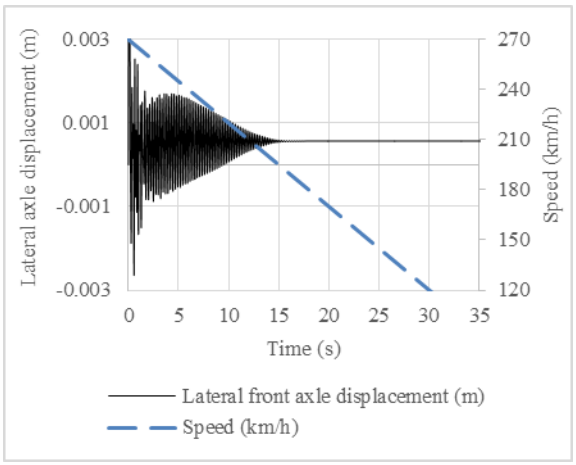

(b) Lateral front axle displacement (Concept- 13 model)

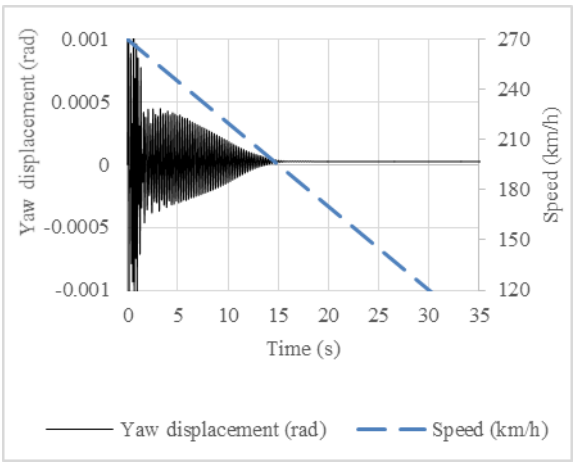

(e) Front axle Yaw displacement (Concept- 13 model)

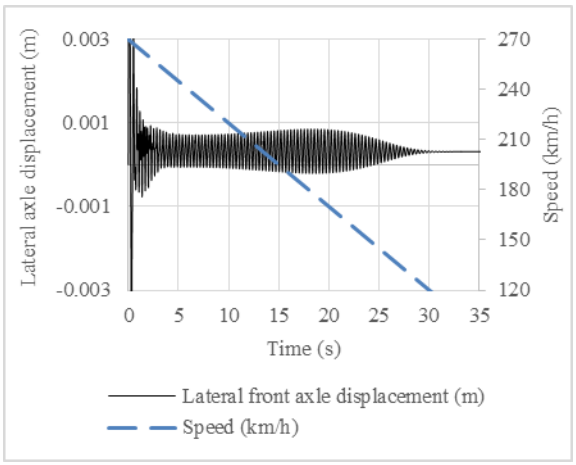

(c) Lateral front axle displacement (Concept- 12 model)

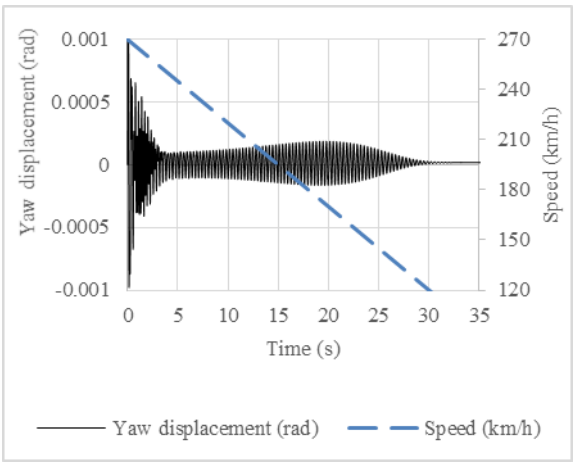

(f) Front axle yaw displacement (Concept- 12 model)

Figure 10-13: Critical speed of the concept- 12, 13 and 14 wagon models (yaw link stiffness of 1.7MN/m)

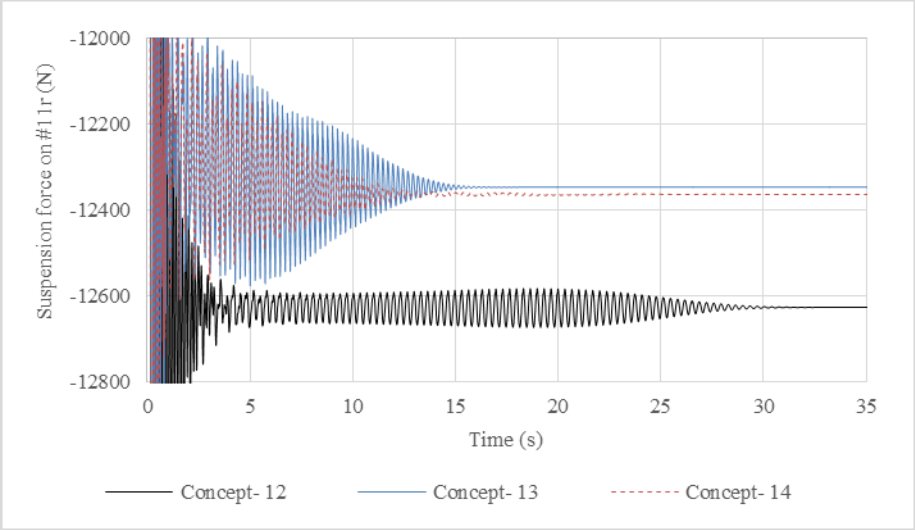

Figure 10-14: Change of suspension force on the concept- 12, 13 and 14 wagon models

10.9 Step 2 Test on the Concept- 14 Wagon

The concept- 14 wagon was tested using datum test conditions (Cases 1-4, Table 10-4). The concept- 14 wagon in the empty condition failed on wheel L/V ratio (#11l) in the datum case 1 in cant deficient condition but passed the cant excess condition (case 3, Table 10-4). The concept- 14 wagon in the loaded condition passed the datum condition for the 110mm cant deficient speed on FRA Class 4 track (case 2) but failed in the cant excess condition (case 4).

A series of simulation tests were then performed (cases 5-17) to determine curve conditions where the concept- 14 wagon would pass the acceptance criteria. The empty concept- 14 wagon showed a high wheel L/V ratio on the front left wheel (#11l on the high rail) in cant deficient conditions (cases 1, 5, 9, 13, 15, 16, 17; Table 10-4). At cant deficient conditions, it is typical that the wheel on the high rail would face higher lateral load due to centrifugal action which thus creates a higher wheel L/V ratio. The concept- 14 wagon provided a pass condition in case 17 (cant deficiency 65mm, FRA Class 6 track; Table 10-4). The speed corresponding to 65mm on a 300m radius track is 69.4km/h which is about 10km/h less compared to that corresponding to 110mm cant deficiency. So, the applicability of concept-14 wagon would require comparison of benefits between the savings on fuel per payload in the context of operating speed.

The loaded conditions in cant excess conditions showed an irregular pattern of outcomes when different track irregularities were applied (cases 4, 8, 12, 14). The concept- 14 wagon passed the cant excess condition when FRA Class 5 track (case 8) was provided, but failed when FRA Class 6 track (case 12) was provided. The FRA Class 6 track (case 12) being smoother than the FRA Class 5 track (case 8) was expected to provide a better dynamic outcome. The variation in the results of these two track classes (cases 8, 12) indicates that the positioning of track irregularities affects the outcome. In the search for a pass condition, the cant excess was increased (70mm in case 14) on the FRA Class 6 track which provided a pass condition for the loaded wagon in cant excess conditions.

Based on the analysis in this section, a pass condition for the concept- 14 was evaluated as 65mm cant deficiency and 70mm cant excess situations on FRA Class 6 track.

Table 10-4: Derailment parameters of the step 2 tests on the concept- 14 wagon (Empty 6000kg, loaded 78000kg, Track radius 300m, applied cant 125mm)

Case	Load	Cant deficiency (mm)	Speed (km/h)	FRA track class	Maximum L/V wheel ratio				Maximum L/V axle ratio		Maximum Wheel unloading ratio			
					11l	11r	12l	12r	11	12	U11l	U11r	U12l	U12r
1	Empty	110	77.2	4	1.36	0.44	0.45	1.05	1.78	1.47	0.69	0.77	0.81	0.92
2	Loaded	110	77.2	4	0.66	0.42	0.41	0.72	1.07	1.09	0.84	0.89	0.84	0.89
3	Empty	-75	35.6	3	0.90	0.47	0.52	0.78	1.34	1.17	0.49	0.47	0.61	0.41
4	Loaded	-75	35.6	3	1.11	0.44	0.39	0.65	1.53	0.90	0.87	0.86	0.87	0.87
5	Empty	110	77.2	5	1.13	0.44	0.44	0.64	1.55	1.06	0.53	0.50	0.62	0.45
6	Loaded	110	77.2	5	0.62	0.42	0.40	0.77	1.01	1.11	0.84	0.89	0.85	0.89
7	Empty	-75	35.6	5	0.81	0.45	0.42	0.75	1.24	1.15	0.40	0.40	0.50	0.30
8	Loaded	-75	35.6	5	0.95	0.43	0.34	0.52	1.36	0.76	0.89	0.84	0.89	0.84
9	Empty	110	77.2	6	1.05	0.44	0.43	0.58	1.47	0.99	0.41	0.38	0.46	0.36
10	Loaded	110	77.2	6	0.60	0.41	0.39	0.77	0.99	1.09	0.87	0.86	0.87	0.87
11	Empty	-75	35.6	6	0.76	0.45	0.42	0.71	1.19	1.11	0.35	0.34	0.46	0.26
12	Loaded	-75	35.6	6	1.01	0.43	0.33	0.48	1.42	0.72	0.87	0.87	0.87	0.86
13	Empty	100	75.6	6	1.06	0.44	0.43	0.58	1.48	1.00	0.41	0.42	0.44	0.37
14	Loaded	-70	37.4	6	0.96	0.43	0.33	0.50	1.37	0.75	0.84	0.89	0.84	0.89
15	Empty	80	72.1	6	1.05	0.44	0.43	0.62	1.47	1.03	0.38	0.45	0.48	0.33
16	Empty	75	71.2	6	1.04	0.44	0.43	0.63	1.46	1.04	0.37	0.43	0.49	0.34
17	Empty	65	69.4	6	0.98	0.44	0.43	0.63	1.40	1.04	0.38	0.43	0.49	0.31
17_concept 13	Empty	65	69.4	6	1.00	0.44	0.43	0.63	1.42	1.04	0.39	0.45	0.48	0.32
17_concept 12	Empty	65	69.4	6	1.05	0.44	0.42	0.60	1.46	1.00	0.35	0.39	0.46	0.30

Case 17 of the step 2 test (Table 10-4) was further used to investigate the effects of "Load dependent lateral and longitudinal stiffness (modelling)" and "Additional yaw force (modelling)". The concept- 14 wagon gave different wheel L/V ratio compared to the concept- 13 wagon model (Figure 10-15c). Case 17 on concept 12 wagon model generated unacceptable wheel L/V ratio of 1.04 at 25.49s compared to 0.96 on concept- 14 wagon (Figure 10-15c). However, the concept- 14 wagon did not always provides a lower wheel L/V ratio than that on concept- 12 wagon model as evident from the wheel L/V ratio at 25.71s on concept- 14 wagon (0.83) and concept- 12 (0.78) wagon (Figure 10-15c).

In the concept- 14 wagon the hysteresis of the longitudinal and lateral suspensions becomes larger compared to those of the concept- 12 wagon (Figure 10-16). The longitudinal suspension of the concept- 14 wagon on the front left wheels on the high rail of a right hand curve (#11l) experienced more force towards the front of the wheelset (termed positive suspension force) compared to that on the low rail (#11r) which would improve steering capability compared to the concept- 12 wagon. On the rear wheels of the concept- 14 wagon, the suspension on the high rail (#12l) experienced force towards the rear and the suspension the low rail (#12r) experienced force towards the front of the wheelset compared to those on concept- 12 wagon which also means a variation in steering occurs on the rear wheelset of concept- 14 wagon.

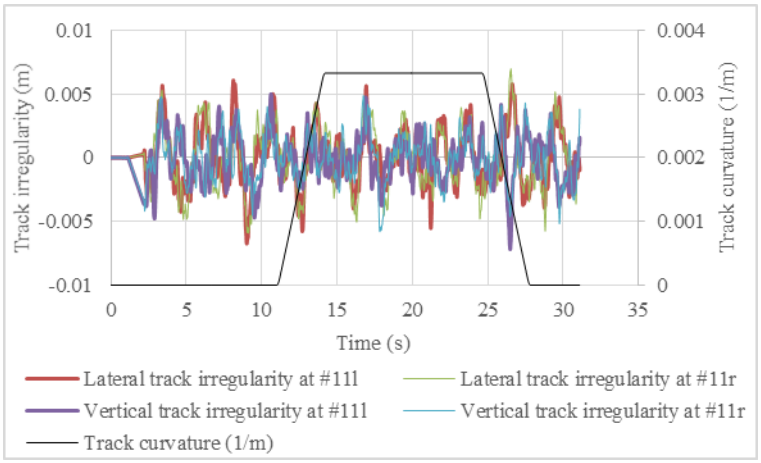

(a) Track defect and geometry

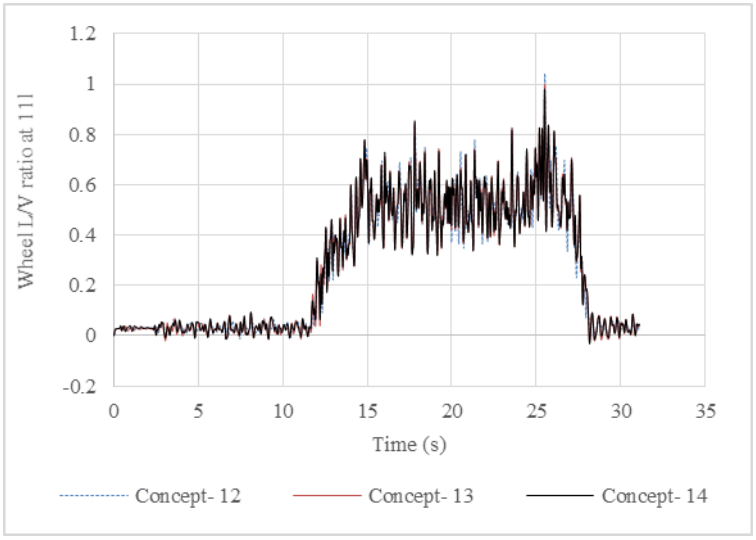

(b) Wheel L/V ratio at #11l

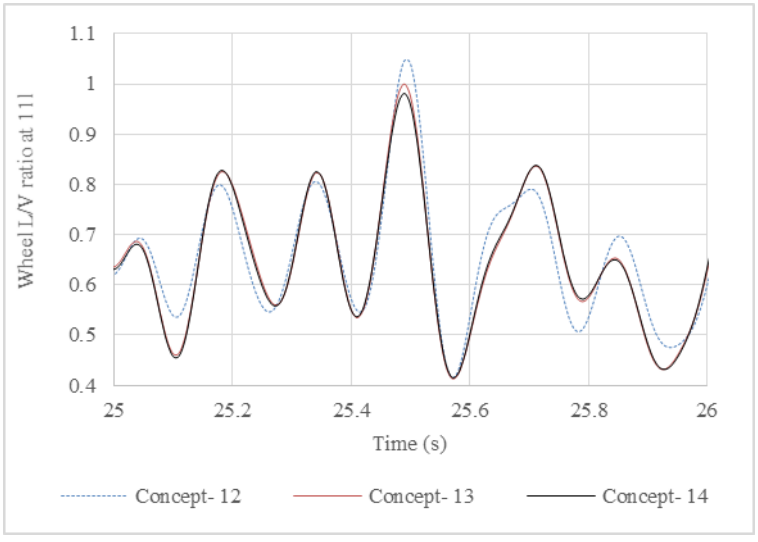

(c) Wheel L/V ratio at #11l near exit of curve

Figure 10-15: Wheel L/V ratio variation due to applied on concept- 12, 13 and 14 wagon models during a curve negotiation test (case 17, Track radius 300m)

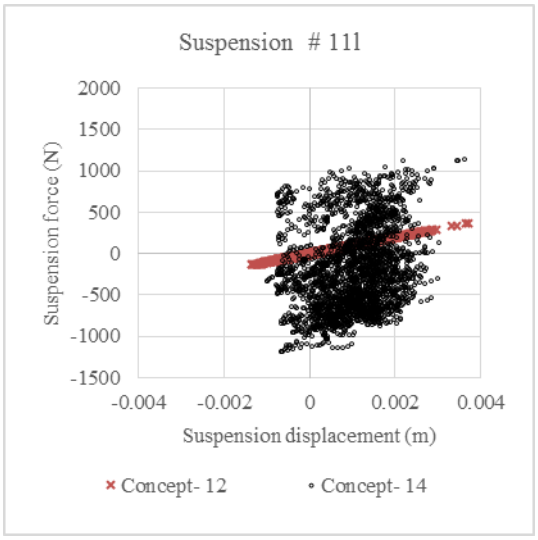

(a) Suspension force and displacement at #11l

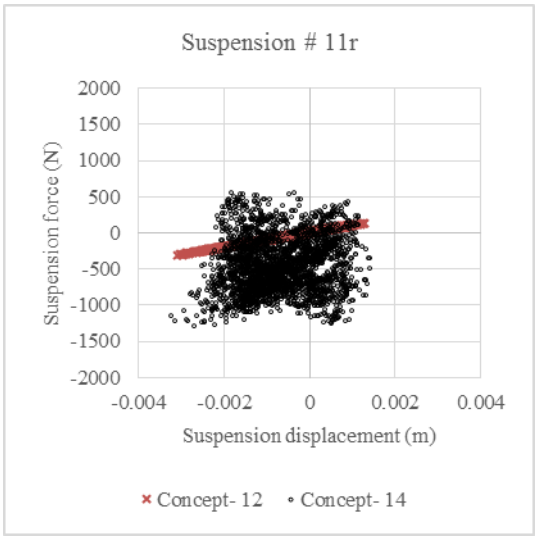

(b) Suspension force and displacement at #11r

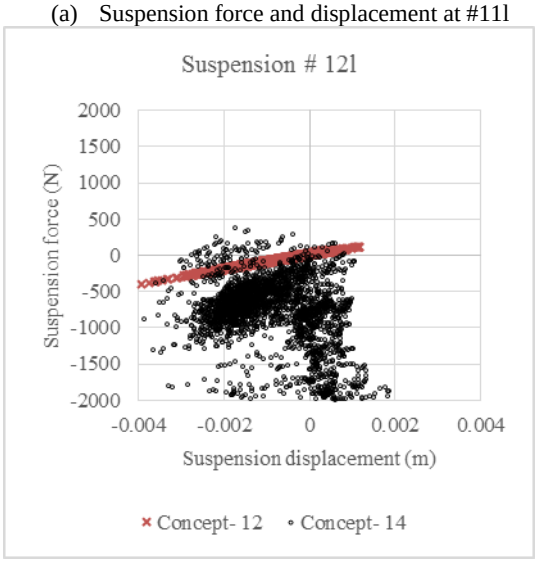

(c) Suspension force and displacement at #12l

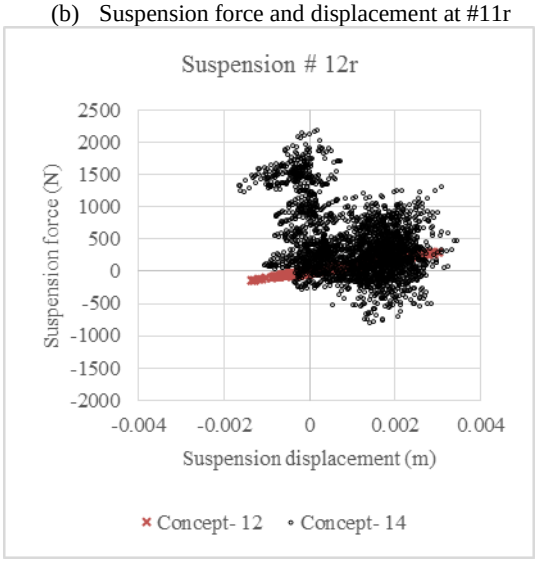

(d) Suspension force and displacement at #12r

Figure 10-16: Longitudinal Suspension force and displacement characteristics on concept- 12 and 14 wagon models (case 17, Track radius 300m, positive suspension force and displacement refers to the forward directions)

10.10 Step 3 –Alternate Hunting Test on the concept- 14 wagon

The concept- 14 wagon model was further tested on a long straight track at a constant speed to check for wagon body hunting (step 3). The wagon was tested at five different speeds of 88km/h (case 1) on FRA Class 4 track; 122km/h (case 2) and 110km/h (case 3) on FRA Class 5 track; and 170km/h (case 4) and 150km/h (case 5) on FRA Class 6 track (Table 10-5). Cases 1 and 2 showed unacceptable wheel unloading ratios and hence are considered as unsuitable for the concept- 14 wagon.

Cases 3, 4, 5 showed acceptable wheel L/V, L/V axle sum and wheel unloading ratios. The average value of the peak acceleration values (cases 3-5) measured over 5s were also found to be within the acceptable limit of 0.35g ($3.4335 m/s^2$) as per AS 7509. Based on the analysis in this section, a maximum operational speed limit on the concept- 14 wagon can then be considered as 150km/h on FRA Class 6 track (considering the AS7509 requirement of a test speed being 10% higher than the design speed).

Table 10-5: Results of the step 3 tests on the concept-14 wagon

Case	FRA track class	Speed (km/h)	Maximum L/V wheel ratio				Maximum L/V axle ratio		Maximum Wheel unloading ratio				Average Lateral acceleration over 5s (m/s^2)	
			11l	11r	12l	12r	11	12	U11l	U11r	U12l	U12r	ay1_avg	ay2_avg
1	4	88	0.63	0.60	0.63	0.47	0.90	0.82	0.80	0.93	0.79	0.85	Unacceptable wheel unloading ratio	
2	5	122	0.46	0.42	0.39	0.32	0.61	0.45	1.00	1.27	0.82	0.94	Unacceptable wheel unloading ratio	
3	5	110	0.36	0.43	0.24	0.24	0.63	0.37	0.67	0.86	0.67	0.66	1.32	1.42
4	6	170	0.49	0.24	0.19	0.18	0.37	0.14	0.84	0.89	0.77	0.84	1.43	1.73
5	6	150	0.29	0.20	0.15	0.17	0.26	0.16	0.52	0.64	0.53	0.61	1.07	1.54

10.11 Step 4- Cyclic Track Defect Tests on the Concept- 14 Wagon

The resonance responses of the concept- 4 (similar vertical stiffness property of the concept- 14) suspension at various frequencies are shown in section 8.5. Resonances can occur at different frequencies due to the 3 stage suspension. The presence of damping may hide any resonance if damping is adequate. As a conservative approach, it is necessary to identify the frequencies in the operational range which may induce resonance. It is obvious that the suspension with loss of damping is susceptible to such situations. The fundamental natural frequency (Equations 5-4 to 5-7) being the lowest possible value corresponding to resonance within the operating service speed.

The empty (6000kg) and loaded (78000kg) conditions operate on stages 1-2 and 2-3 respectively on the concept-14 vertical suspension in the ±90% of the wheel load conditions. The fundamental natural frequencies have been determined for the realistic chassis approximation on the first, second and third stages of suspension for the empty and loaded conditions (Table 10-6). The maximum test speed was set as 165km/h (corresponding to 10% higher than the 150km/h obtained in step 3 test). So, where the resonant frequencies correspond to speeds above the 165km/h the simulation tests were performed at 165km/h (Table 10-7).

Table 10-6: Natural frequencies and corresponding speed of the concept- 14 vertical suspension by simulated approximation and fundamental natural frequency calculation (empty mass 6000kg, loaded mass 78000kg)

Parameters	Mode	Simulated approximation					Fundamental frequency (Equations 5-4 to 5-7)			
		Empty		Loaded			Empty		Loaded	
		Minimum	Maximum	Minimum	Maximum		1st Stage	2nd Stage	2nd Stage	3rd stage
Natural frequencies (Hz)	Bounce	6	7	2	2.5		1.79	5.2	1.44	2.1
	Pitch	3	7	2.5	5		3.31	9.65	1.97	2.86
	Roll	3	7	2	5		2.7	7.87	1.39	2.03
Velocities (km/h)	Bounce	299	348	100	124		89	259	72	104
	Pitch	149	348	124	249		165	480	98	142
	Roll	149	348	100	249		134	392	69	101

Notes: Shaded cells are above 165km/h, Empty condition do not move to the 3rd stage and loaded condition rarely could go to the first stage, so 3rd and 1st stage calculation in the empty and loaded conditions were not considered

The type D track defect (cyclic track defect corresponding to wagon parameters) as developed per the VAPS in Chapter 5, have been used to test the concept- 14 wagon model. The concept- 14 wagon passed all the cyclic track defect tests (Table 10-7, Table 10-8) as per the VAPS. Of the 18 cases, the highest derailment (wheel unloading

ratio of 0.62 on #11l, #11r; case 6, Table 10-8) and vertical acceleration (5.4m/s^2) parameters were found in the bounce motion in the loaded condition at 124km/h (case 6, Figure 10-17).

In case 6, the wheel load on the front left wheel reduced to about 76kN (corresponding to a wheel unloading ratio of about 0.62 considering a static load of 191kN on 78000kg load) when the vertical suspension moved to 115mm from the initial steady position of 140mm (Figure 10-17). The applied cyclic vertical track defect of 19.2mm created a suspension displacement of 27mm which was about 40% higher than the applied vertical cyclic track defect. A resonance pattern of vertical displacement of suspension is visible in Figure 10-17. However, the wheel load and suspension movement became zero when the applied cyclic track defect was removed and the derailment parameters were within the AS 7509 requirement. The wheel load and suspension forces showed an increasing trend till the last applied track defect which may impose resonance if subject to further cycles of track defect. However, the vehicle acceptance test standard AS 7509 does not require to test more than 4 cycles of track defect and the concept- 14 wagon was considered acceptable based on the AS 7509 requirement.

Table 10-7: Input parameters for the cyclic track defect tests (step 4) tests on the concept- 14 wagon

Case	Load (kg)	Mode of tests	Speed (km/h)				Track defect amplitude (mm)			
			a	b	c	d	a	b	c	d
1, 2	0	Bounce	89	165			24.8	19.2		
2- 6	72000	Bounce	72	100	104	124	26.8	21.2	21.2	19.2
7- 8	0	Pitch	149	165			29.6	29.6		
9- 12	72000	Pitch	98	124	142	165	38.4	29.6	29.6	29.6
13- 15	0	Roll	134	149	165		19.2	19.2	19.2	
16- 18	72000	Roll	69	101	165		26.8	21.2	19.2	

Table 10-8: Results of the cyclic track defect tests (step 4) for the concept- 14 wagon

Case	Maximum Wheel L/V ratio				Maximum L/V axle		Maximum Wheel unloading ratio				Maximum Lateral acceleration (m/s^2)		Maximum Vertical acceleration (m/s^2)	
	11l	11r	12l	12r	11	12	U11l	U11r	U12l	U12r	ay1	ay2	az1	az2
1	0.09	0.08	0.08	0.09	0.17	0.16	0.16	0.17	0.17	0.16	0.17	0.27	1.4	1.6
2	0.08	0.08	0.07	0.09	0.14	0.13	0.3	0.32	0.32	0.29	0.52	0.52	3.6	3.5
3	0.06	0.06	0.04	0.06	0.11	0.10	0.2	0.14	0.16	0.2	0.16	0.15	2	1.66
4	0.04	0.05	0.06	0.05	0.10	0.10	0.26	0.29	0.27	0.31	0.33	0.2	2.8	2.6
5	0.06	0.06	0.04	0.06	0.10	0.09	0.4	0.38	0.44	0.41	0.44	0.23	3.94	4.13
6	0.055	0.04	0.04	0.04	0.09	0.08	0.6	0.62	0.62	0.58	0.71	0.22	5.4	5.4
7	0.05	0.06	0.06	0.06	0.12	0.12	0.13	0.14	0.09	0.13	0.24	0.34	1.3	1.2
8	0.06	0.07	0.07	0.07	0.12	0.12	0.15	0.15	0.13	0.14	0.21	0.34	1.78	1.68
9	0.04	0.046	0.045	0.046	0.09	0.09	0.1	0.11	0.11	0.12	0.1	0.08	1.4	1.2
10	0.04	0.04	0.04	0.042	0.09	0.09	0.15	0.15	0.11	0.14	0.08	0.07	1.85	2.04
11	0.04	0.047	0.043	0.045	0.09	0.09	0.17	0.15	0.14	0.16	0.05	0.1	1.46	2.04
12	0.046	0.047	0.046	0.046	0.09	0.09	0.2	0.2	0.21	0.21	0.22	0.17	1	2.53
13	0.33	0.29	0.18	0.16	0.35	0.16	0.35	0.16	0.40	0.39	2.56	2.47	0.9	1.68
14	0.47	0.44	0.22	0.14	0.53	0.25	0.53	0.25	0.46	0.46	2.99	4.45	0.73	1.97
15	0.63	0.54	0.23	0.17	0.69	0.30	0.69	0.30	0.50	0.50	3.28	5.20	1.36	1.97
16	0.15	0.15	0.16	0.15	0.08	0.09	0.56	0.52	0.56	0.52	2.54	2.28	1	1.58
17	0.14	0.13	0.13	0.13	0.08	0.08	0.43	0.42	0.45	0.45	2.02	1.76	1.58	1.19
18	0.16	0.16	0.15	0.16	0.09	0.09	0.32	0.46	0.38	0.35	4.06	3.47	1.96	2.53

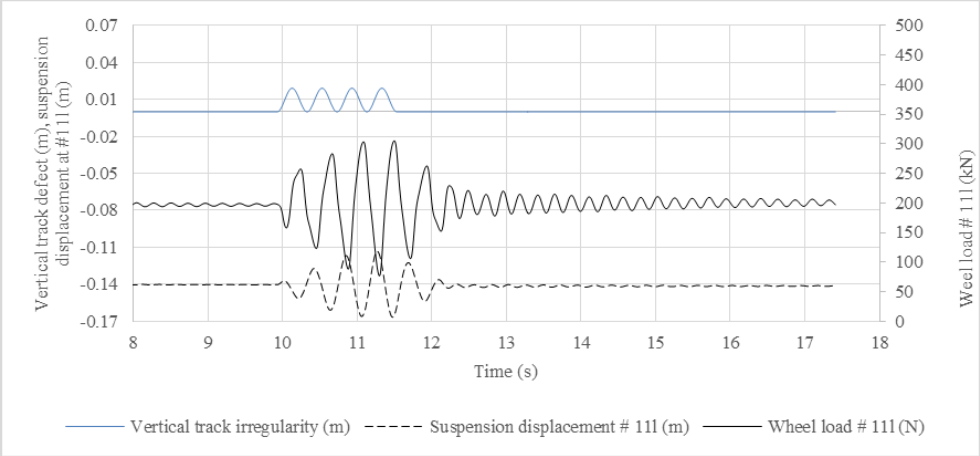

Figure 10-17: Wheel load and vertical displacement on suspension due to cyclic bounce track defect in a cyclic bounce track defect tests on the concept-14 wagon (case 6, load 78000kg)

10.12 Step 5a- Isolated Lateral and Vertical Track Defect Test on the Concept- 14 Wagon

The concept- 14 wagon was tested as per the step 5 tests of the VAPS using datum conditions (cases 1-4, Table 10-9). The concept- 14 wagon in loaded conditions (cases 2 and 4, Table 10-10) passed the datum tests but failed in empty conditions on wheel L/V ratio and lateral wagon body accelerations (cases 1, 3, Table 10-10). The highest wheel L/V ratio in case 1 (1.13 on #11l) and case 3 (1.08 on #11r) occurred on the high rail on both the flattening (case 1) and sharpening (case 3) type lateral defects (Table 10-10).

The speed was reduced in cases 5-9 to achieve a pass condition. Reducing the speed to 72.2 km/h (corresponding to 80mm cant deficiency on 300m radius track with 125mm cant) in cases 5 and 6 (Table 10-9) reduced the maximum wheel L/V ratio (example, maximum wheel L/V ratio on #11l becomes 1.02 in case 5 compared to that of 1.13 in case 1, Table 10-10) and lateral acceleration values (Table 10-10), but were still outside the acceptable limits as per AS7509.

Table 10-9: Simulation cases of the isolated lateral and vertical track defects on concept- 14 wagon (Track radius 300m, applied cant 125mm)

Case	Load (kg)	Track Radius (m)	Speed (km/h)	Track irregularity (FRA track class)	P1 limits corresponding to Speed board limit (km/h)	Amplitudes of track fault (mm)	Track defect band	Variation in defect band from the design
1, 2	0, 72000	300	77.23	5	115	61.2, 21.8, 25	F	-3
3, 4	0, 72000	-300	77.23	5	115	61.2, 21.8, 25	F	-3
5, 6	0	300, -300	72.2	5	115	61.2, 21.8, 25	F	-3
7, 8	0	300, -300	72.2	6 (smoothing near defects)	115	61.2, 21.8, 25	F	-3
9	0	-300	71.2	6 (smoothing near defects)	115	61.2, 21.8, 25	F	-3

The superimposed isolated track defects of the various FRA track classes created situations where combination of track defects added more dynamics to the wagon on curved sections of track. If the isolated track defect occurs over a sharp track irregularity on the track, it may generate a worse condition for wagon dynamics. In cases 7 and 8, the isolated track defects were applied on a smooth section (without any track irregularity) of a curved track (Example case 7 in Figure 10-18) to reduce the effect of a combination of track defects on wagon dynamics (Table

10-9). The smooth entry and exit to the isolated track defects reduced the possibility of any sharp change of track position in the simulation. The smoothing action reduced wheel L/V ratio and lateral wagon body acceleration in case 7 (Figure 10-19e, f) compared to case 5 (Figure 10-19b, c).

However, the added smoothing of the track defect in case 8 (lateral sharpening track defect on the curved section) was not adequate to reduce lateral wagon body acceleration within the acceptable limit (5.14m/s^2, Table 10-10). The speed was then further reduced to 71.2 km/h (case 9, Table 10-10) which reduced the lateral wagon body acceleration within the acceptable limit as per AS 7509 (Table 10-10).

Table 10-10: Results of the step 5a tests (isolated lateral and vertical track defects) on the concept-14 wagon

Case	Maximum L/V wheel				Maximum L/V axle		Maximum Wheel unloading ratio				Maximum Lateral acceleration (m/s^2)		Maximum Vertical acceleration (m/s^2)	
	11l	11r	12l	12r	11	12	U11l	U11r	U12l	U12r	ay1	ay2	az1	az2
1	1.13	0.44	0.44	0.52	1.55	0.93	0.71	0.58	0.66	0.63	8.75	10.44	6.87	5.73
2	0.61	0.42	0.41	0.65	1.01	1.01	0.47	0.68	0.48	0.55	3.23	3.70	4.63	5.39
3	0.45	1.08	0.71	0.43	1.51	1.11	0.72	0.66	*0.93*	0.66	10.09	6.27	6.87	5.73
4	0.42	0.67	0.73	0.43	1.05	1.07	0.73	0.31	0.62	0.49	3.30	3.03	4.53	5.30
5	1.02	0.44	0.44	0.55	1.45	0.92	0.73	0.54	0.67	0.87	6.00	4.77	6.87	5.55
6	0.44	0.98	0.71	0.44	1.42	1.11	0.60	0.55	0.64	0.63	6.89	5.06	6.87	5.55
7	0.84	0.44	0.43	0.56	1.27	0.98	0.55	0.56	0.56	0.53	4.70	3.68	6.87	6.30
8	0.44	0.84	0.61	0.43	1.27	1.02	0.55	0.56	0.56	0.53	5.14	4.58	6.87	6.30
9	0.44	0.85	0.52	0.43	1.28	0.92	0.55	0.55	0.57	0.56	4.37	3.36	6.87	6.10

Note: Values in the shaded cell do not meet the acceptance criteria described in Chapter 5

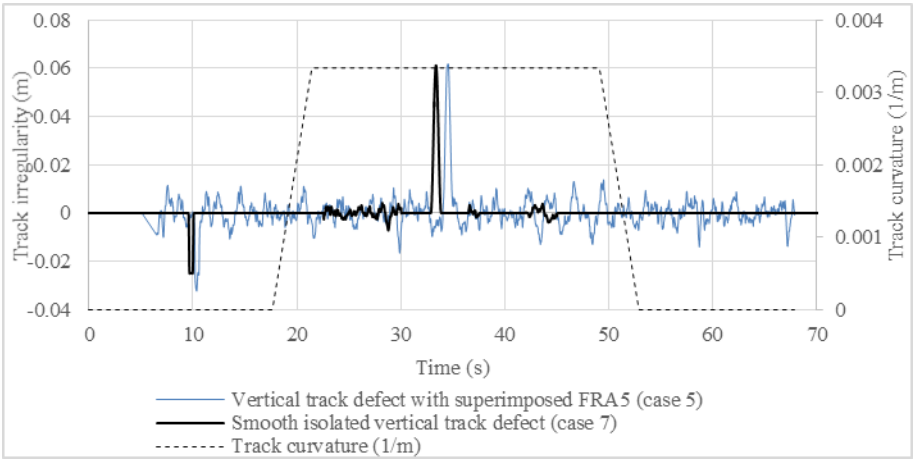

Figure 10-18: Smoothing of an isolated track defect

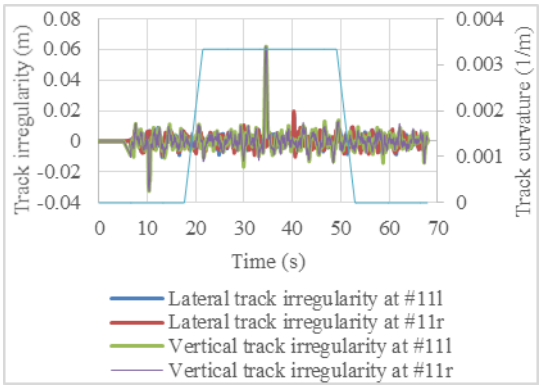

(a) Track defect superimposed with FRA Class 5 track irregularity (case 5)

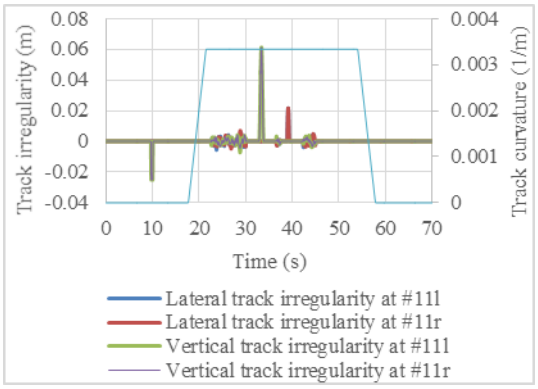

(d) Track defect without any superimposed irregularity (case 7)

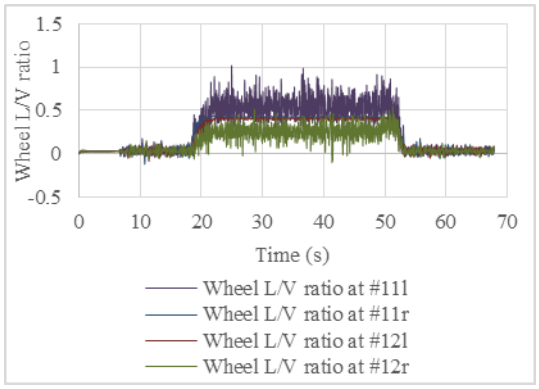

(b) Wheel L/V ratio (case 5)

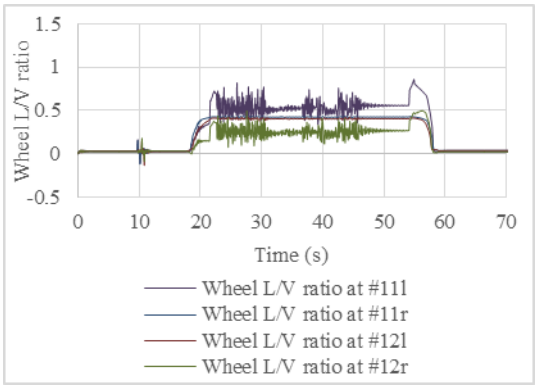

(e) Wheel L/V ratio (case 7)

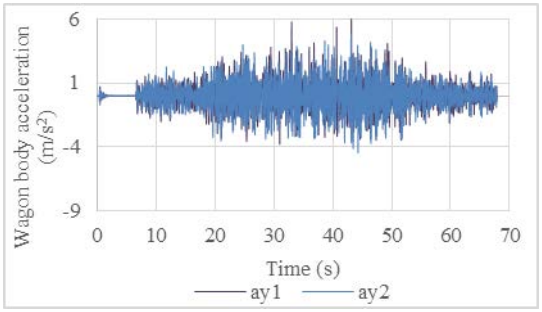

(c) Lateral wagon body acceleration (case 5)

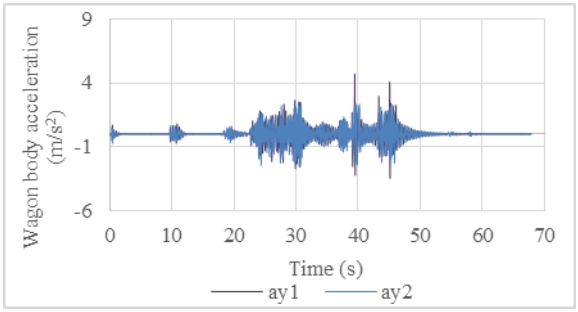

(f) Lateral wagon body acceleration (case 7)

Figure 10-19: Smoothing of track near the applied isolated track defect (Concept- 14 wagon, Empty condition, Track radius 300m, cases 5 and 7)

10.13 Step 5b- Isolated Twist Track Defect on concept- 14 wagon

Isolated twist track defect tests on the concept- 14 wagon were performed on a straight track as per the datum conditions (case 1, 2; Table 10-11). The concept- 14 wagon model in the empty condition failed in wheel unloading ratio on the rear right wheel (#12r, case 1, Table 10-12). The isolated twist track defect was then applied using the smoothing of the applied track defect following the process described in section 10.12. The smoothing of track defects, in this case, make the situation worse as the amplitude of the short twist track defect was increased to a standard value 14.4mm (case 3) compared to 12mm in the datum (case 1, 2) condition (Table 10-11). Case 3 also failed in wheel unloading ratio on #12r. In case 4, the amplitude of the short twist track defect was reduced to 10mm over a 2m wavelength which provided a pass condition for the concept- 14 wagon. The reduced amplitude of the short twist track defect in case 4 (10mm) was smaller than the smoothest track defect band G (design short twist limit 12mm) as per the ARTC track network standard.

The case 4 was further evaluated with an additional vertical stiffness of 85kN/m as could be increased due to the influence of the additional yaw link elements. The additional vertical stiffness of 85kN/m was modelled as a stiffness element between each wheelset and wagon body. As the derailment parameters were not significantly affected due to the added vertical stiffness of 85kN/m (case 4- additional yaw kz, Table 10-12) the small change in vertical stiffness due to the yaw link element is considered negligible when considering the tests as per the VAPS.

Table 10-11: Simulation cases of the isolated twist track defects on concept- 14 wagon (Straight track)

Case	Load (kg)	Speed (km/h)	Track irregularity (FRA track class)	P1 limits corresponding to Speed board limit (km/h)	Amplitudes of twist test track defect (mm)	Track defect band	Variation in defect band from the design limit
1, 2	0, 72000	88	6	115	51.48, 12	F	-1
3	0	88	6 (smoothing near defect)	115	48, 14.4	F	-1
4	0	88	6 (smoothing near defect)	115	48, 10	F	-1

Table 10-12: Results of the step 5b- twist track defect tests on the concept-14 wagon

Case	Maximum L/V wheel				Maximum L/V axle		Maximum Wheel unloading ratio				Maximum Lateral acceleration (m/s^2)		Maximum Vertical acceleration (m/s^2)	
	11l	11r	12l	12r	11	12	U11l	U11r	U12l	U12r	ay1	ay2	az1	az2
1	0.29	0.19	0.36	0.18	0.38	0.47	0.72	0.76	0.63	1.14	3.22	3.04	6.87	3.77
2	0.13	0.15	0.14	0.16	0.11	0.10	0.89	0.84	0.89	0.84	1.48	1.87	4.06	4.23
3	0.31	0.20	0.22	0.19	0.39	0.36	0.75	0.77	0.40	0.96	3.25	3.21	6.87	3.93
4	0.14	0.20	0.14	0.14	0.28	0.25	0.62	0.59	0.38	0.76	2.65	2.27	3.23	3.91
4_additional yaw kz	0.15	0.23	0.15	0.15	0.31	0.24	0.53	0.58	0.47	0.74	2.01	2.09	7.45	3.58

Note: Values in the shaded cell do not meet the acceptance criteria described in Chapter 5

10.14 Effect of Wheel-Rail Profiles on Critical Hunting Speed of the Concept- 14 Wagon

The new WPR2000 wheel profile and new AS60 rail profile (trace A in Figure 10-20) have been used in all simulation cases carried out so far for concept- 1 to concept- 14. In this section, two other combinations (B and C in Figure 10-20) of wheel and rail profiles were tested on the concept- 14 wagon. The 'B' and 'C' combinations were obtained by using one measured worn WPR2000 wheel profile (supplied by a rail company in Australia) coupled with two different worn AS60 rail profiles (Figure 10-20). The worn wheel-rail combinations (B and C) gave higher equivalent conicity until 7mm of lateral wheelset displacement is reached (Figure 10-20).

The new wheel new rail combination (A) gave flange contact at about 8mm lateral displacement of the wheelset on a 1435mm gauge track which created a sudden increase of equivalent conicity at 8mm of wheelset lateral movement (Figure 10-20). In the case of worn wheel-rail combinations B and C, flange contact did not occur until 10mm lateral displacement, so the equivalent conicities in B and C were lower than that of A at the lateral wheelset movement of 8mm. The equivalent conicities calculated at 3mm using the recommended method in the EN15302 [105] standard were 0.148, 0.267 and 0.249 for the three combinations A, B, and C respectively. The new wheel

and new rail combination (A) was further simulated at different track gauges (cases 4-6, Table 10-13) to provide different equivalent conicity conditions for simulation purpose.

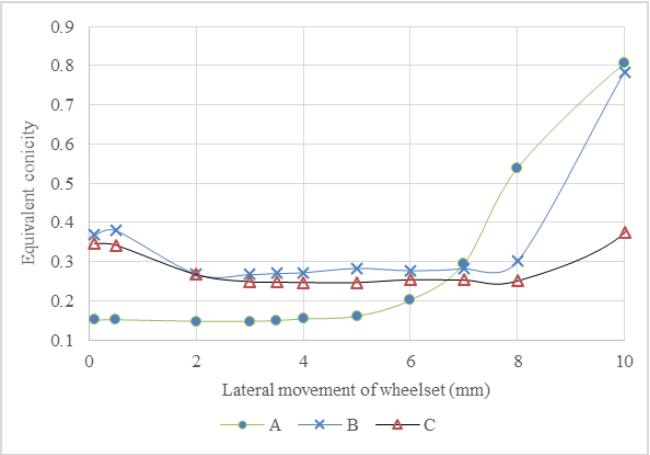

Figure 10-20: Equivalent conicities of different wheel and rail combinations on a standard gauge (1435mm) track

Table 10-13: Critical hunting speed of the concept- 14 wagon on different wheel and rail profiles

Case	Wheel	Rail	Track gauge (mm)	Equivalent conicity at 3mm using the recommended method in EN15302 [105]	Critical hunting speed (km/h)
1	New WPR2000	New AS60	1435	0.148	204
2	Worn WPR2000	Worn 1 AS60	1435	0.267	99.3
3	Worn WPR2000	Worn 2 AS60	1435	0.249	112.5
4	New WPR2000	New AS60	1433	0.186	160
5	New WPR2000	New AS60	1431	0.229	139.2
6	New WPR2000	New AS60	1429	0.372	100

The new WPR2000 wheel and new AS60 rail (case 1) gave a critical hunting speed of 175km/h (Figure 10-21a). The worn WPR2000 wheel and worn 1 AS60 rail (case 2) produced a higher equivalent conicity (0.267) compared to that on the new wheel with new rail combination (0.148) and gave a lower critical hunting speed of 99km/h than did the new wheel and new rail combination (Figure 10-21b). The other worn wheel with worn rail combination (case 3) generated lower equivalent conicity (0.249) compared to the first worn wheel with worn rail combination (case 2) and generated a higher critical speed of 112km/h than did case 2.

The inverse relationship between the equivalent conicity and critical hunting speed was further confirmed by using different track gauges (cases 4-6, Figure 10-21d, e, f, Figure 10-22). Simulations in this section confirm that the concept- 14 wagon could operate at a speed as high as 90km/h under an equivalent conicity condition of 0.372.

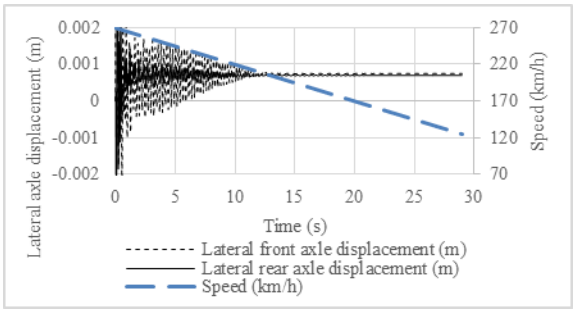

(a) New WPR2000, New AS60, Case 1

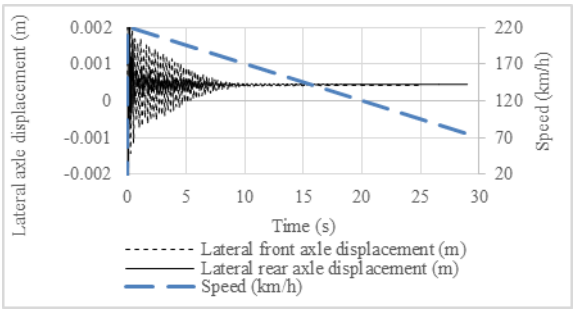

(d) New WPR2000, New AS60, Track gauge 1433, case 4

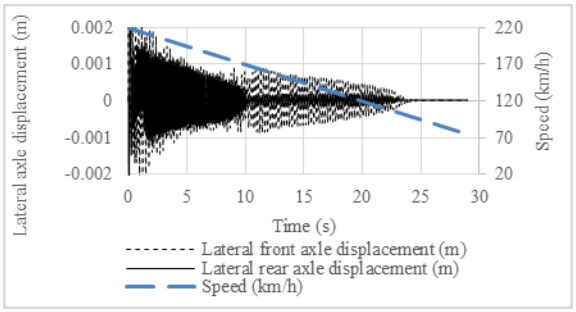

(b) Worn WPR2000, Worn 1 AS60, Case 2

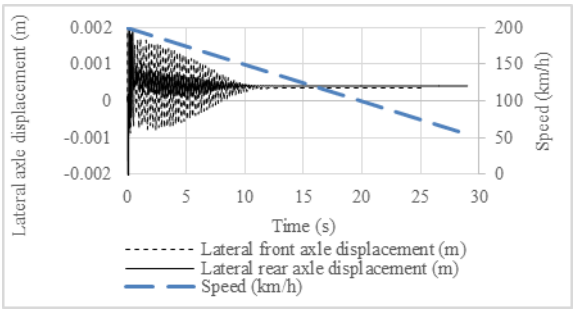

(e) New WPR2000, New AS60, Track gauge 1431, case 5

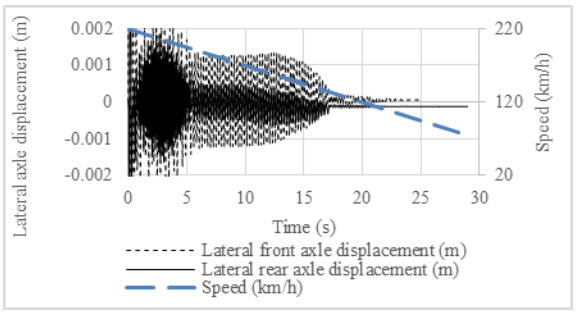

(c) Worn WPR2000, Worn 2 AS60, case 3

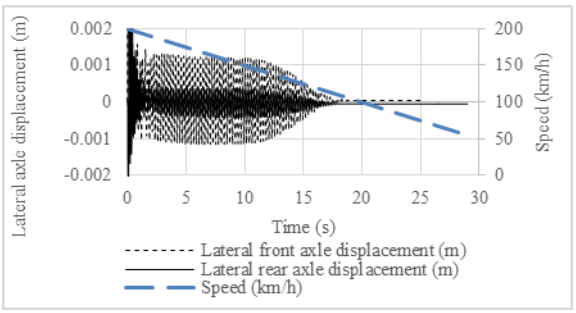

(f) New WPR2000, New AS60, Track gauge 1429, case 6

Figure 10-21: Effect of high equivalent conicity on concept- 14 wagon

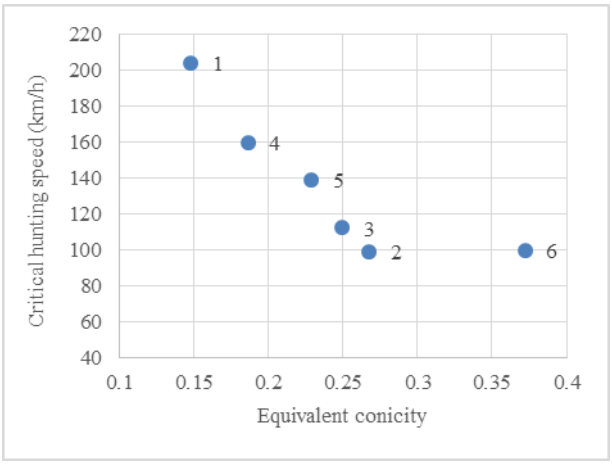

Figure 10-22: Critical hunting speed with equivalent conicity on the concept- 14 wagon

10.15 Summary of Operational and Wagon Parameters of the Final Concept- 14 Wagon

The operational limits and parameters of the concept-14 wagon (final concept) as developed in this chapter are presented in Table 10-14 and Table 10-15.

Table 10-14: Operational parameters of the concept- 14 wagon (final concept)

Parameters	Value
Critical hunting speed, km/h	204
Minimum curve radius, m	300
Maximum cant deficiency on a 300m radius curve, mm	65
Maximum cant excess on a 300m radius curve, mm	70
Maximum design speed considering permitted isolated twist track defect band F for isolated lateral, vertical and twist track defect; allowable short twist track defect of 8mm which is smaller than allowed on defect band G, km/h	80
Track irregularity, FRA class	6

Table 10-15: Concept- 14 (final concept) wagon and suspension parameters

Model parameters	Value	Unit
Wagon parameters		
Length of the deck	19.8	m
Axle centre distance	13.8	m
Overhang	3	m
Empty wagon body mass	6	Tonne
Loaded wagon body mass, tonne	78	Tonne
Maximum Payload	72	Tonne
Tare mass	8.175	Tonne
Gross mass	80.175	Tonne
Tonne axle load	40.87	Tonne
Vertical Suspension Parameters (Calculated combined stiffness parameters)		
Lift off element		
Stage 1 stiffness	189	kN/m
Stage 2 stiffness	1.6	MN/m
Stage 3 stiffness	3.4	MN/m
Hard stop	40	MN/m
Damping ratio	0.05	
Friction force at low displacement	2.5	kN
Friction force at high displacement	25	kN
Changing stiffness from static to friction	13.6	MN/m
Vertical Suspension Parameters (Stiffness values of springs)		
Stage 1 Coil spring stiffness	100	kN/m
Stage 2 Coil spring stiffness	1.5	MN/m
Leaf spring stiffness	3.38	MN/m
Limit positions of vertical suspension stages (1)		
First stage	80	mm
Second stage	100	mm
Third stage	180	mm
Longitudinal Suspension Parameters		
Combined stiffness, k_{cx} (k1x+k2x)	$\boldsymbol{c_x} * \boldsymbol{F_{zik}}$	N/m per N
Pendulum stiffness, k_{px} (k1x)	$\boldsymbol{p_x} * \boldsymbol{F_{zik}}$	N/m per N
Breakout force, FDx	$\boldsymbol{d_x} * \boldsymbol{F_{zik}}$	N per N
Damping	$2*0.05 * \sqrt{k_{cx} * m}$	Ns/m
Longitudinal stop		
Allowable longitudinal movement	±20	mm
Stiffness of longitudinal stop	4	MN/m
Lateral Suspension Parameters		
Combined stiffness, k_{cy} (k1y+k2y)	$\boldsymbol{c_y} * \boldsymbol{F_{zik}}$	N/m per N
Pendulum stiffness, k_{py} k1y	$\boldsymbol{p_y} * \boldsymbol{F_{zik}}$	N/m per N
Breakout force, FDy	$\boldsymbol{d_y} * \boldsymbol{F_{zik}}$	N per N
Damping ratio	$2*0.05 * \sqrt{k_{cy} * m}$	Ns/m
Lateral stop		
Position of lateral stop	±20	mm
Stiffness of lateral stop	1.5	MN/m
Additional yaw link **elements**		
Additional yaw link stiffness between axlebox and wagon body	1.7	MN/m
Length of the yaw link stiffness element	0.8	M

Note: $\boldsymbol{c_x}$, $\boldsymbol{p_x}$, $\boldsymbol{d_x}$ are normalised longitudinal stiffness parameters; $\boldsymbol{c_y}$, $\boldsymbol{p_y}$, $\boldsymbol{d_y}$ are normalised lateral stiffness parameters; m is the wagon body supported by one suspension elements, assuming equal mass distribution over four suspensions (N)

10.16 Comparison of the Final Concept (Concept- 14) Wagon with the RQTY Wagon

The final concept wagon allows higher design speed (150km/h) than the RQTY wagon (77km/h) on a straight track as can be seen from the outcome of three tests (step 1, 3, 4) of the VAPS (Table 10-16). The critical hunting speed of the final concept wagon (204km/h) is higher than that of the RQTY wagon (85km/h). The higher critical speed on the final concept wagon allows a higher design speed of 170km/h. However, a smoother track with FRA Class 6 track irregularities was required for the final concept wagon to run safely at 170km/h. The final concept wagon failed to operate safely on a rougher FRA Class 4 track irregularity at the datum (88km/h) conditions. The alternate hunting speed test also showed that the final concept wagon could only pass the test at 110km/h on a rougher FRA Class 5 track.

The higher speed operation on a straight track for the final concept wagon was also restricted by the presence of isolated twist track defects, in particular the short twist track defect. A quantification showed that the concept-14 wagon could negotiate a band F isolated twist track defect at the datum test speed of 88km/h.

The long twist track defect negotiability of the final concept wagon (band F defects) is worse than that of the RQTY wagon (band D defects). The concept-14 wagon would also require an improved quality of track with smaller short twist track defect (8mm, design defect amplitude being 20% higher than 8mm, i.e. about 10mm) than the smoothest defect band (G, having short twist limit of 10mm) currently available in the ARTC network.

Table 10-16: Comparison of performance of the final concept wagon with the RQTY wagon

Steps of VAPS	Performance parameters	Final concept	RQTY	Qualitative Performance	
				Final concept	RQTY
1- Critical hunting speed test	Critical hunting speed	204	85	√	
2- Curve negotiation (applied cant 125mm)	Track radius (m)	300	300	√	√
	Cant deficiency (mm)	65	110		√
	Cant excess (mm)	70	75		√
	FRA track class	6	4		√
3- Alternate hunting speed test	Test speed of FRA4 track (km/h)		88		√
	Test speed on FRA5 track (km/h)	110		√	
	Test speed on FRA6 track (km/h)	170		√	
4- Cyclic track defect test	Maximum test speed (km/h)	165	88	√	
	Type of track defect	D	D	√	√
5a- Isolated lateral and vertical track defects on curved track (applied cant 125mm)	Track radius (m)	300	300	√	√
	Cant deficiency (mm)	75	110		√
	Type of track defect	A	A	√	√
	Track class	6 with smoothing	5		√
	Defect band	F	F	√	√
5b- Isolated twist track defect on straight track	Speed (km/h)	88	88	√	√
	Type of track defect	A	A	√	√
	Track class	6 with smoothing	6		√
	Defect band for long twist	F	D		√
	Defect band for short twist	H	D		
	Design long twist defect (mm)	48	62.4		√
	Design short twist defect (mm)	10	19.2		√

Notes: √ indicates better performance of the two wagons, -with smoothing refers to the removal of irregularity over the applied track defects

The final concept wagon showed worse curving performance compared to the RQTY wagon. The high speed (cant deficiency of 65 and 110mm on final concept and RQTY wagon respectively) was needed to be reduced (69km/h) and low speed (cant excess of 70 and 75mm on final concept and RQTY wagon respectively) was needed to be increased (37km/h) for the final concept compared to the RQTY wagon (77km/h and 35km/h on high and low speed situations respectively) to provide a pass condition. Furthermore, a smoother track (FRA Class 6 track) was required compared to that allowable for the RQTY wagon (FRA Class 4 track).

The presence of isolated track defects on a curved track established a smoother track requirement (FRA Class 6 track with further smoothing near the track defect) for the final concept wagon compared to a rougher track (FRA Class 5 track) for the RQTY wagon. The smoothing (reduce combination of track defect and curvature) of the track irregularity on the curved section for the concept-14 wagon in step 5 tests allowed an increased speed of 71km/h (corresponding to cant deficiency of 75mm on 300m radius curve) compared to that obtained in step 2 tests (cant deficiency of 65mm) for the final concept wagon.

10.17 Discussion

Two design ideas- softening of the vertical suspension stages (concepts 4 through 14, improves curving) and increasing longitudinal suspension stiffness (concepts 9 through 14, increases critical speed) generally improved the performance of the concept wagons. A careful choice of softness and allowable suspension movement on the softer first and second stages of the vertical suspension element improved curve negotiability of the concept wagons (example: concepts 4 and 9) compared to a fixed vertical suspension stiffness in a typical UIC link and leaf spring suspension.

The curve negotiability of the final concept wagon was still worse than a similar capacity bogied wagon such as the RQTY wagon. The final concept wagon also allowed a smaller short twist track defect (8mm) than the smoothest defect band G (short twist of 10mm). The final concept wagon did allow a rougher track (band F) for the isolated lateral, vertical and long twist compared to the short twist track defect. However, the concept wagon wagon would require smoother track compared to that (band D) required for the RQTY wagon. The possible benefit of the final concept wagon can, therefore, be realised when straight track sections dominate a track network and track is expected to be of high quality.

The consideration of load dependent lateral and longitudinal stiffness modelling (concepts-13 and 14) showed an improved steering characteristic of the wheelsets during curving. At low vertical dynamic load, the longitudinal stiffness was lowered which allowed the wheelset to achieve a better steering position. The more accurate model reported a better performance than that obtained on a model with the constant longitudinal and lateral stiffnesses.

The simulation study performed in this thesis is based on some conservative assumptions including rigid body approximations and the fixed friction damping property of the vertical suspension for both high and low loads. Future improvement in the modelling includes modification in the vertical friction damping property to allow for change of friction damping property with the dynamic vertical load. By providing a load dependent vertical friction damping property, it will be possible to have low suspension force at low dynamic load (such as during an unloading stage in the empty condition) that could help reduce wheel unloading ratio during negotiating a twist track defect.

The reduced dynamic performance on a curved track and improved track quality requirement for the final concept wagon create a challenge for implementing such a concept design on a network unless the saving in energy consumption due to low tare is significant enough to compensate the cost of maintaining a high quality track. An initial assessment of energy consumption under different operational situations is investigated in Chapter 11.

Chapter 11
Train Simulation to Evaluate Energy Consumption and Payload Productivity

11.1 Introduction

Train simulations are necessary to evaluate the energy consumption and payload productivity of train designs. In this chapter, the final concept wagon and some other existing wagons were simulated in train configurations to investigate the advantages of the final concept wagon over the existing wagons. Before doing the comparison based on the train simulation, it is necessary to define the train, test track, train control and speed for the desired operation.

11.2 Train Benchmarks

In this study, a freight train of 50 wagons has been selected as the targeted train operation which is a typical freight intermodal service. Two locomotives were provided with each trainset to allow reasonable performance on grades and allow grade and curving to be studied where larger tractive effort is necessary.

A list of wagons for comparison with the concept wagon has been identified (Table 11-1). The list includes some heavy haul mineral wagons (example Pilbara, Hunter Valley) as these designs are considered to be highly optimised and are therefore useful to consider in performance comparisons. The double stack container arrangement gets special attention when considering intermodal transportation. Four different combinations of double stack arrangements depending on the size of containers are listed (Table 11-1).

The payload/ tare ratio is a good indicator of a wagon's productivity potential. So, the top 8 wagons having the higher Payload/ Tare ratio (shaded cells) have been considered for the comparison of energy consumption.

Table 11-1: Characteristic of some wagons chosen for initial estimates of energy consumption by train simulation

Wagon type	Tare (tonne)	Payload (tonne)	Gross (tonne)	Payload/ Tare	BCD (m)	Total length over couplers (m)	Coupler length (m)	Overhang (m)	Number of axles	Tonne axle load (tonne)
Hunter Valley	22.4	98	120.4	4.38	11.97	14.94	0.45	1.03	1.50	8.06
Articulated	20	86	106	4.30	16.8	17.7	0.8	0.05	1.13	5.99
UIC-link	8	37	45	4.63	12	16	0.8	1.2	***0.50***	***2.81***
Pilbara	21	121.4	142.4	5.78	5.2	8.2	0.45	1.05	2.56	17.37
Concept	8.175	72	80.175	8.81	13.812	20.7	0.44	3	***0.39***	***3.87***
RQTY	18	72	90	4.00	14.94	20.09	0.44	2.13	0.90	4.48
sgns60	20	72	92	3.60	14.2	19.74	0.62	2.15	1.01	4.66
sgnss	17	72	89	4.24	14.2	20	0.62	2.28	***0.85***	4.45
DS1	22	96	118	4.36	*15*	*19.59*	*0.45*	*1.85*	1.12	6.02
DS2	22	78.48	100.48	***3.57***	*15*	*19.59*	*0.45*	*1.85*	1.12	5.13
DS3	22	60.96	82.96	***2.77***	*15*	*19.59*	*0.45*	*1.85*	1.12	***4.23***
DS4	22	60.96	82.96	***2.77***	*15*	*19.59*	*0.45*	*1.85*	1.12	***4.23***

Notes: Bold italic fonts are the minimum three values of the column, shaded cells are the maximum eight/ three values of the Payload/Tare and Tonne axle load columns; DS- Double stack, the container arrangements for the DS1, DS2, DS3 and DS4 wagons are 4x 20′, 1x40′ +2x 20′, 2x 53′, 2x 40′ respectively. Tare is the mass of the wagon without containers. The payload includes the mass of the container and load within it.

11.3 Test Track

A typical inner-city track on the ARTC network [145] containing curves and gradients was considered for the investigation (Figure 11-1). The track section considered was 40km long. The track consists of an increase in elevation of about 20m across the route and the smallest curve radius is 210m. The track has 31 curves. The relevant 40km track section was converted for use in the train simulation as shown in Figure 11-2.

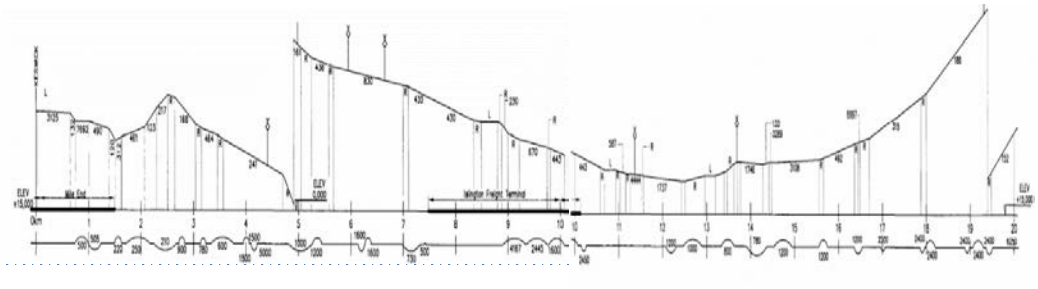

Figure 11-1: A section of the test track [145]

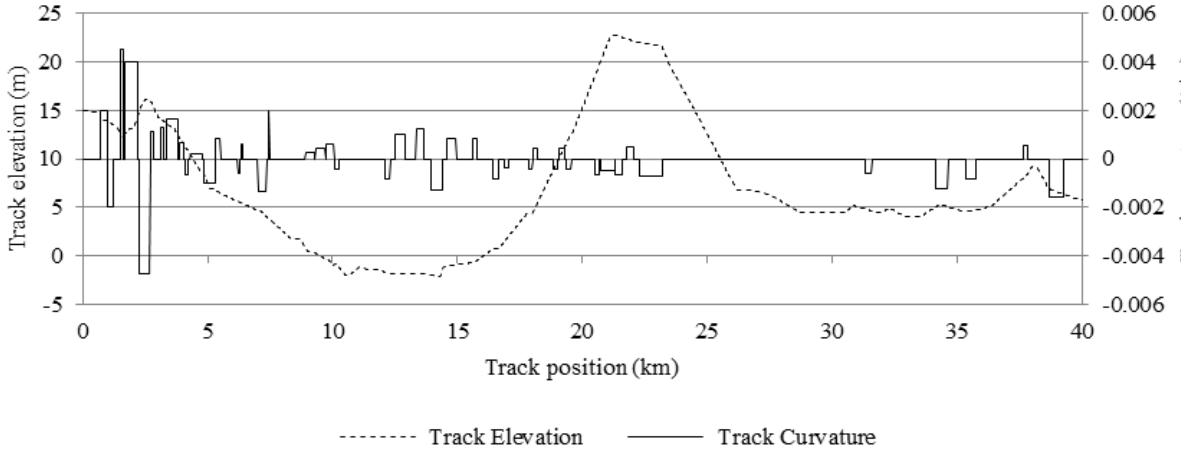

Figure 11-2: Track profile used in train simulations

11.4 Train Control and Speed

Two train operations of start-stop and continuous running modes were used in this Chapter for the evaluation of energy consumption. A total of 4 stops (at 3.8, 15.7, 21.5 and 30.972 km) were used to replicate the 4 stations spread over the 40km section of the track (Figure 11-3a). In this train simulation approach, both the air and dynamic braking principles were used to stop the trains. Depending on the ratio of train mass to dynamic brake (DB) capability of the trains (as the locomotives were the same in each case), the application level of the dynamic braking is varied to allow the train to stop at the desired points (Figure 11-3c). So, the heavier and higher speed train requires more dynamic braking than the lighter or slower speed train (Figure 11-3c). As an example, the heavier Hunter Valley (HV) and Pilbara (PB) trains require more dynamic braking distance than the other lighter trains such as the UIC train. Due to this variation in dynamic braking requirement, it was not possible to compare the trains based on the exactly the same braking (or driving) conditions.

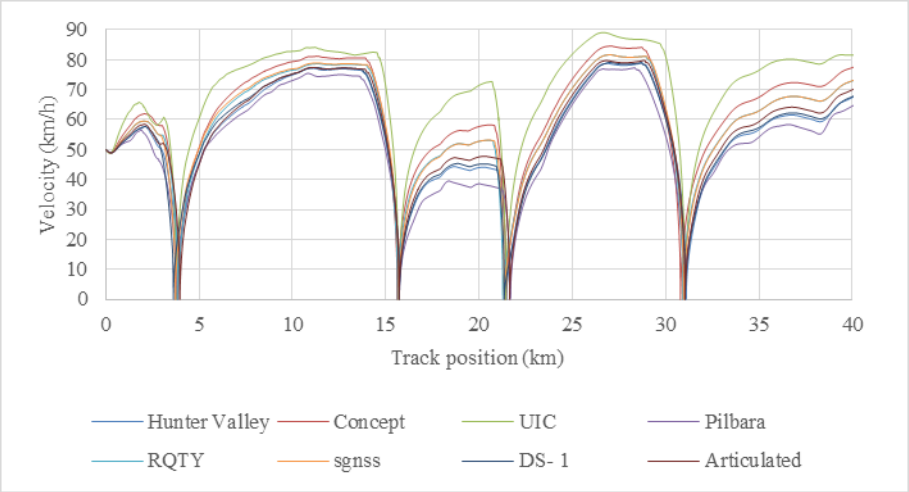

(a) Velocity profile over the 40km track section

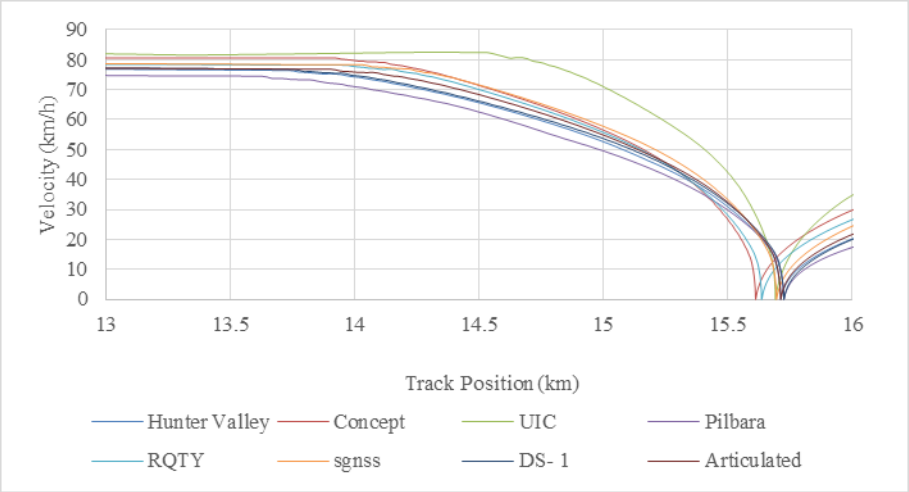

(b) Velocity profile near a stopping point (15.7km)

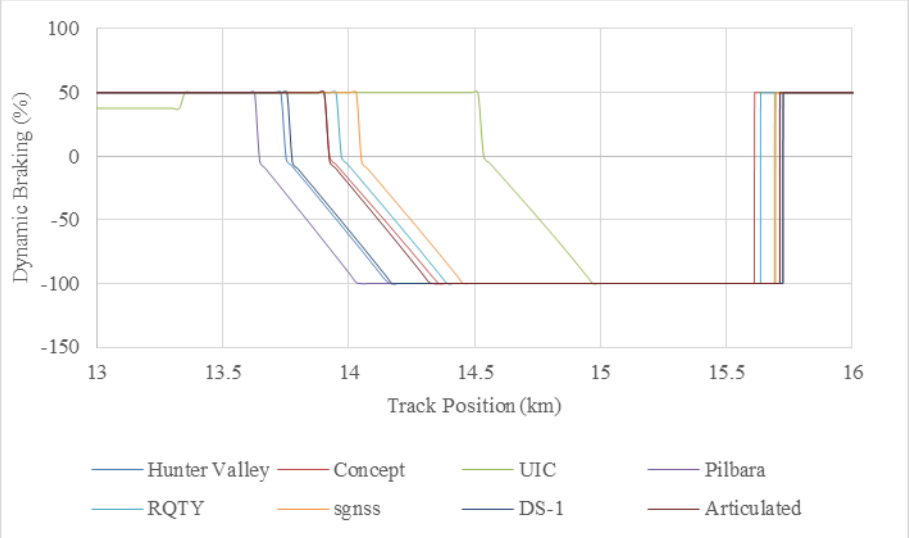

(c) Dynamic braking near a stopping point (15.7km)

Figure 11-3: Velocity and dynamic braking on the start-stop mode operation (fully loaded based on maximum payload on each wagon)

11.5 Energy Consumption and Productivity

It is necessary to normalise the 'energy consumption' term in order to better compare the payload productivity of the trains. The normalisation can be done in two steps. Firstly the energy consumption must be calculated based on the input energy and wasted energy for the trip. As train masses and routes are often different, energy results are usually normalised for both tonnes hauled and kilometres travelled.

The energy mix can be divided into the input energy such as the traction energy and gains from lowering elevation (downhill) and the output energy such as the produced or lost energy by the gain or loss of speed, elevation, and braking. The energy used to gain elevation and speed can be partially recovered by coasting, however, the energy used for any braking is generally wasted unless using the regenerative dynamic braking principle.

In reality, some use of air brakes is always required as dynamic braking as dynamic braking effort is low in certain speed ranges [146]. The air brake energy consumption is considered as non-recoverable as the application of the brakes on the wagon wheels results in train kinetic energy being dissipated as heat.

The duration of application of air brakes can be significantly less than that of the dynamic braking as can be seen from a sample plot of the simulation study for the train consisting of concept wagons (Figure 11-4). The air brake was applied during the very low speed of less than 20km/h in an example case and was applied for a distance of about 50m (Track position 3849-3888m). On the other hand, the dynamic braking was applied for 750m (Track position 3035-3888m) at a higher speed (about 58km/h) at a deceleration rate of 0.06m/s^2.

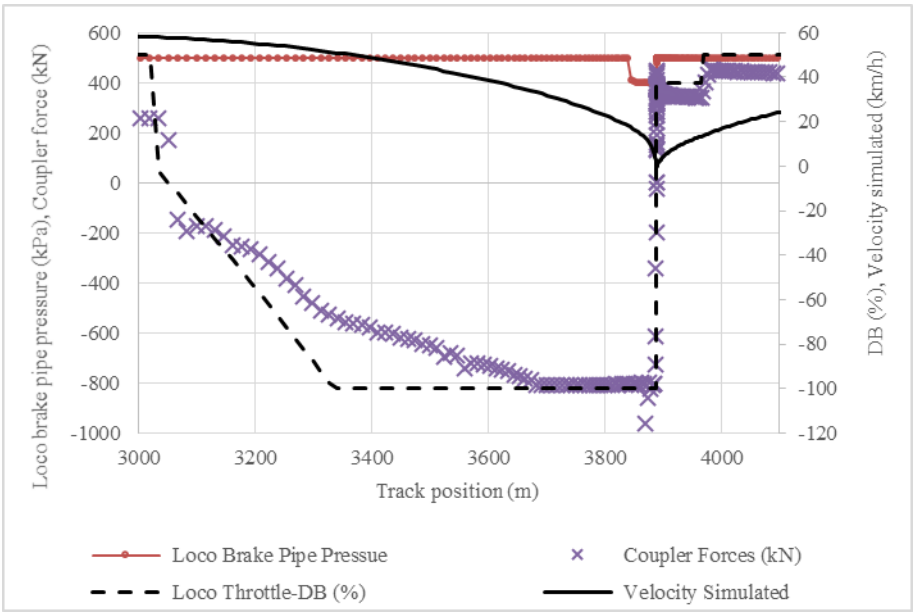

Figure 11-4: Application of air brake and dynamic brake using train consisting of the final concept wagon

The traction energy (Energy In) was calculated using equation 11-1. The energy consumptions to achieve the speed (kinetic energy) and elevation (potential energy) were calculated using equations 11-2 and 11-3. The energy consumptions due to dynamic and air braking were calculated using equations 11-4, and 11-5.

A residual energy (E_r) term has been introduced here which indicates the amount of energy that is retained in gains of elevation and speed (Equation 11-6). The residual energy is the energy consumed by the wagons

(excluding braking) only. In order to compare the energy consumption of all train simulations at the same datum points, the energy available at the end-point of the trip, the residual energy, and braking energy have been deducted from the 'Energy In' term (Equation 11-7). The energy consumption due to air braking is not reusable and hence is included as a contribution to the energy consumption (Equation 11-7). The term energy consumption used in this chapter refers to that obtained by Equation 11-7.

$$E_{In} = \sum_{i=i}^{i=f} F_{i-1} V_{i-1} \Delta t/3600 \quad \textbf{11-1}$$

$$E_k = 0.5 * m_t * (v_2^2 - v_1^2)/3600000 \quad \textbf{11-2}$$

$$E_p = m_t g (h_2 - h_1)/3600000 \quad \textbf{11-3}$$

$$E_d = \sum_{i=di}^{i=df} F_{di-1} V_{di-1} \Delta t/3600 \quad \textbf{11-4}$$

$$E_a = \sum_{i=ai}^{i=af} F_{ai-1} V_{ai-1} \Delta t/3600 \quad \textbf{11-5}$$

$$E_r = E_k + E_p \quad \textbf{11-6}$$

$$E = E_{In} - E_r - E_d - E_a \quad \textbf{11-7}$$

where, E_{In} is the traction energy consumption (kWhr), F is the longitudinal coupler force at the rear of the last connected locomotive (kN), V is the simulated velocity (m/s), Δt is the trip time (hrs), E_k is the residual kinetic energy at the end of the trip (kWhr), m_t is the total train mass (kg), v_2 is the speed at the end of the trip (m/s), v_1 is the speed at the start of the trip (m/s), E_p is the residual potential energy at the end of the trip (kWhr), g is the gravitational acceleration (m/s^2), h_2 is the elevation at the end of the trip (m), h_1 is the elevation at the start of the trip (m), E_d is the recoverable energy consumption as can be stored in battery or supplied to the grid by the regenerative braking elements using dynamic braking principle (kWhr), E_r is the residual energy (kWhr), E_a is the energy consumption due to air braking (kWhr), E is the energy consumption excluding residual energy (kWhr), *i* is the initial time (s), *f* is the final time (s), *di* is the initial time for application of DB (s), *df* is the end time for application of DB (s), *ai* is the initial time for application of air brake (s), *af* is the end time for application of air brake (s).

11.5.1 Energy Consumption under Fully Loaded Conditions and Start-Stop Operation

The 8 wagon types with the higher payload/ tare ratio obtained from Table 11-1 were simulated in fully loaded conditions to compare energy consumption on the selected intermodal route of 40km length and with 4 station stops (Figure 11-2).

The final concept wagon consumed less energy per tonne per km than did the wagons of a similar application, length and type, i.e. the RQTY wagon and the UIC two-axle wagon (Figure 11-5). However, the final concept wagon consumed more energy per unit mass compared to heavy haul trains, i.e. the Pilbara and Hunter Valley wagons and other heavily loaded trains such the double stack (DS-1) and articulated configuration.

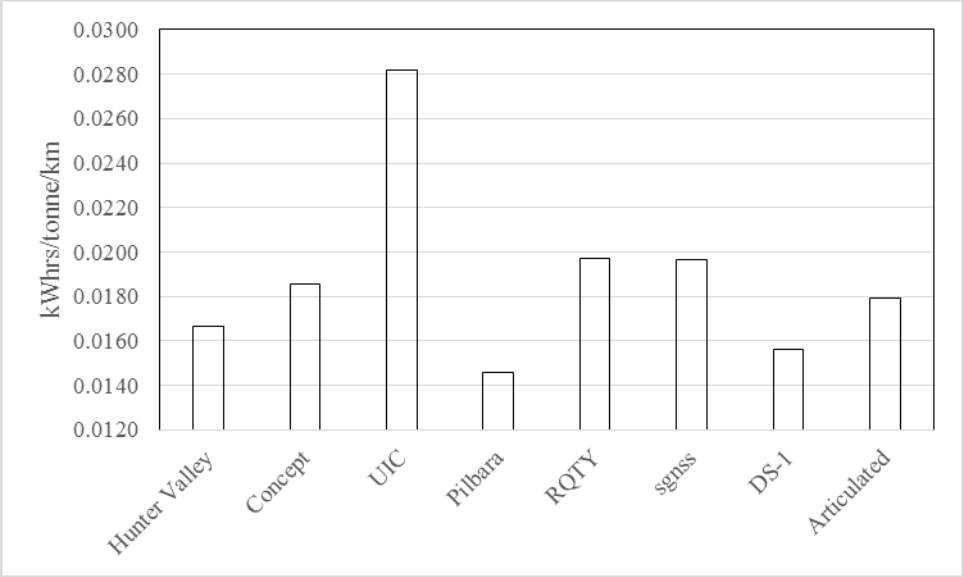

Figure 11-5: Energy consumption per payload per km on various trains using 4 stops and same DB control, fully loaded condition one-way trip

11.5.2 Energy Consumption under Empty Conditions and Start-Stop Operation

The heavy haul trains usually return empty to the loading point after unloading which reduces payload productivity when a full round trip is considered. These heavy haul wagons have relatively high tare due to the strength requirements and so also will have relatively high energy consumption to carry the tare load only. Five of the wagon types were further evaluated for the empty return path on the same track starting at 40km and travelling towards 0km with stops at the four stations (Figure 11-2). The low tare wagons (Concept and UIC wagons) consumed less energy compared to higher tare wagons (Figure 11-6) as expected.

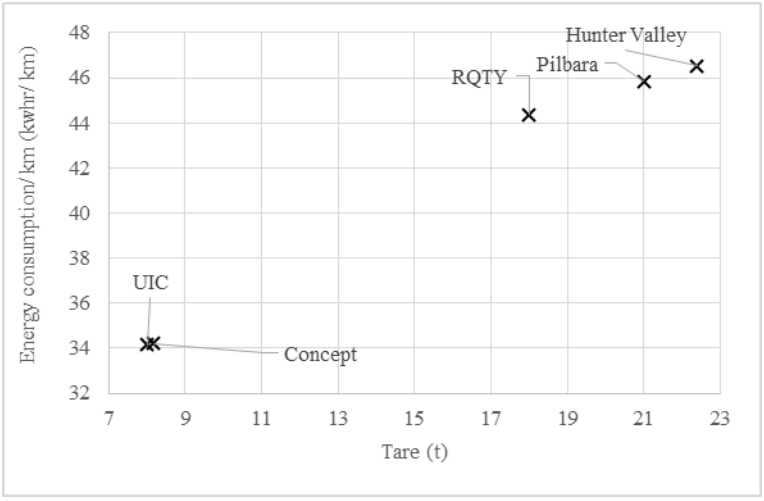

Figure 11-6: Energy consumption per km on various empty trains on return trip using 4 stops and same DB control

11.5.3 Energy Consumption for the Full Trip with Start-Stop Operations

The heavy haul operation usually carries no payload on the return trip to the loading point. But, the intermodal operation usually carries a payload in both directions. Comparison of the heavy haul operation with the intermodal operation needs to consider the full round trip situation. Two situations were considered in this section, namely return empty on all trains as per the heavy haul operation and return loaded on intermodal trains only, and all trains stopped at the four stations.

In the first operation scenario (all trains return empty), the payload productivity of the full trip was still dominated by the payload capacity of the wagons. The heavy haul wagons, being able to carry a significantly larger payload (121t on Pilbara wagons) compared to typical intermodal wagons (example 72t on RQTY), maintain a lower normalised energy consumption (energy consumption/ payload) compared to that on the lower tare wagons. As an example, the energy consumptions per payload on the full trip (80km, loaded one way, empty on the return path) in the Hunter Valley and Pilbara wagons were 1.045 and 0.885 kWhr/payload compared to 1.123 kWhr/payload for the concept wagon (Figure 11-6). So, the concept wagon on a typical heavy haul operation scenario did not provide higher payload productivity than the existing heavy haul wagons.

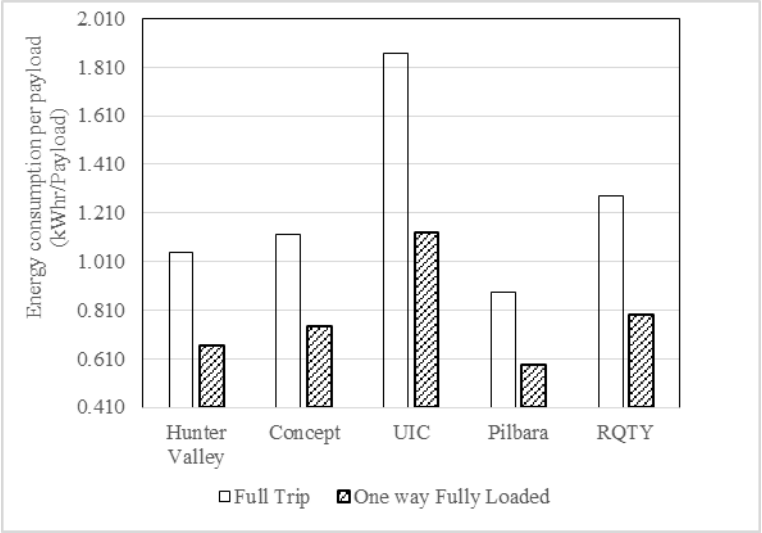

Figure 11-7: Energy consumption per payload on various trains using 4 stops and same DB control, empty condition on a return trip

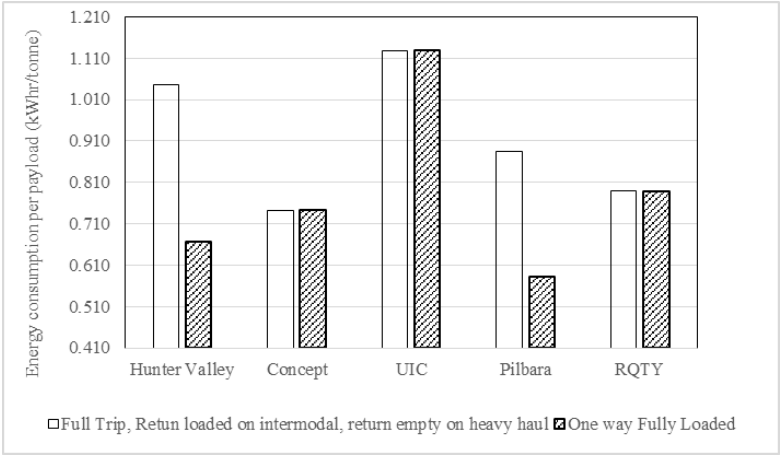

Figure 11-8: Energy consumption per payload on various trains using 4 stops and same DB control, empty condition on a return trip for heavy haul trains (Hunter Valley, Pilbara), Loaded condition on the return trip for intermodal trains (Concept, UIC, RQTY)

In the second operation scenario, the intermodal trains were run in the fully loaded condition and the heavy haul trains were run in the empty condition on the return trip. The energy consumption for the loaded condition of intermodal trains on the return path was taken as similar to that obtained in section 11.5.1. There would be some variation due to change of direction and driving principles on the intermodal wagon. However, the variation is expected to be negligible as the train mass, track geometry and number of stops are the same. The energy

consumption per payload on the full trip based on typical heavy haul and intermodal applications reveals that energy consumption per payload on the concept wagon (0.74 kWhr/tonne) and RQTY wagon (0.79 kWhr/tonne) was lower than that of the Hunter Valley (1.04 kWhr/tonne) and the Pilbara (0.89 kWhr/tonne) heavy haul trains on the full trip (Figure 11-8). The lower capacity intermodal wagon, the UIC wagon (1.13 kWhr/tonne), was unable to provide the low energy consumption per payload for the full trip.

11.5.4 Partial Loading in Intermodal Operations

The intermodal operation could consist of frequent loading and unloading which could leave the trains partially loaded for part of the full trip. The chosen single independent wagon for a target payload productivity established in Chapter 4 is about 65′ which can accommodate three 20′ containers to provide the maximum payload of 72 tonnes on each wagon. Of the 8 wagons, the RQTY, the sgnss, the concept and the double stack (example DS-1) wagons have the capability to carry three 20′ containers. So, these four wagons have been considered for a normalised intermodal operation comparison.

Three cases were considered, namely a fully loaded train and two partially loaded trains. In the partially loaded trains, 90% and 70% of the wagons in the train (i.e. 45 and 35 out of the 50 wagons) were loaded with the maximum payload of 72t and the remaining wagons were empty. The stops remained the same as used in section 11.4.

The concept wagon has the lowest tare of the four wagons and consumed the least energy per payload per km as expected (Figure 11-9). The energy consumption per payload per km increased with the decrease of loading on the trains. The increase in normalised energy consumption is more severe when the proportion of payload is decreased. As an example, the rate of increase in energy consumption is higher when the load is decreased from 90% to 70% loaded condition compared to when the load is decreased from 100 to 90% (Figure 11-9).

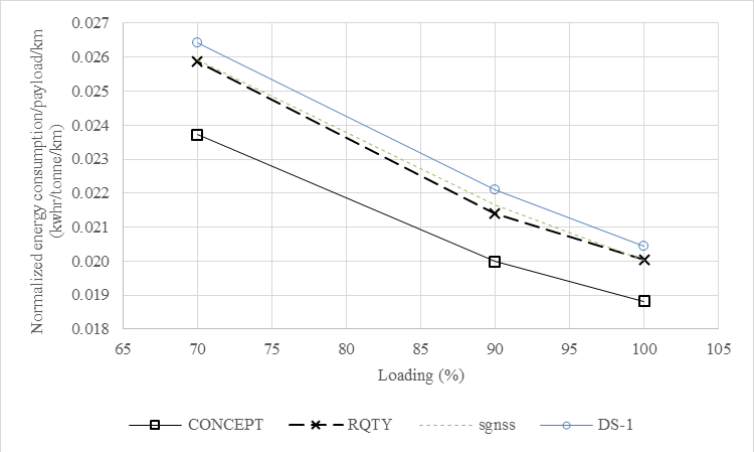

Figure 11-9: Normalised energy consumption on partially loading situations (payload 72t on all loaded wagons)

The RQTY, sgnss and DS-1 wagons under fully loaded conditions consumed about 6.5, 6.4 and 8.7% higher energy compared to the concept wagon (Table 11-2). The concept wagon performed even better in terms of energy consumption per payload per km when even more empty wagons were considered. As an example, the RQTY, sgnss and DS-1 wagons consumed about 9.1, 9.3 and 11.4% more energy compared to the concept wagon when 30% of wagons in the train were considered empty (Table 11-2). So, savings in the concept wagon are higher for the typical container transportation where loading and unloading of containers may leave some of the wagons

empty. Overall, the savings in energy consumption on the concept wagon compared to that on the available similar capacity wagons ranged from 6 to 11% for 100% and 70% loaded conditions respectively as obtained for a start-stop operation analysis performed in this section.

Table 11-2: Comparison of the concept wagon in terms of lower energy consumption percentage with some existing wagon normalised to a maximum payload of 72 tonnes for each wagon

Payload on train (%)	Empty wagon (%)	Energy consumption/payload/km (kWhr/tonne/km)				% increase in energy consumption/ payload/ km compared to the concept wagon		
		Concept	RQTY	sgnss	DS-1	RQTY	sgnss	DS-1
100	0	0.0188	0.0200	0.0200	0.0205	6.5	6.4	8.7
90	10	0.0200	0.0214	0.0217	0.0221	7.1	8.3	10.5
70	30	0.0237	0.0259	0.0259	0.0264	9.1	9.3	11.4

11.5.5 Continuous Running in Fully Loaded Condition

The continuous running mode simulation with all wagons fully loaded was carried out to compare possible savings on operations when there are the least possible number of stops, in particular on a long haul freight route. The four stoppages of the 40km track section used in the previous section 11.4 were removed in the tests for the continuous running operations. The concept wagon was found to be superior in terms of payload productivity (Table 11-3). The other three wagons performed close to each other, but consumed about 12% more energy (corresponding to about 11% less energy consumption on the concept wagon) than the concept wagon in the fully loaded condition in continuous running.

Table 11-3: Comparison of Energy consumption/payload/km for continuous running fully loaded

Wagon type	Energy consumption/payload/km	% increase in energy consumption compared to the concept
Concept	0.0113	-
RQTY	0.0126	12.1
sgnss	0.0126	11.9
DS-1	0.0126	11.9

The normalised energy consumption in the continuous running operation was about 58-67% less than for the start-stop mode of operation when fully loaded conditions were tested (Table 11-4). The train using concept wagons provides the largest decrease in energy consumption (67%) on continuous operation compared to start-stop operation. For both start-stop and continuous running, the normalised energy consumption increased with the increase of gross mass of wagons (Figure 11-10) as found on the four wagons considered for the continuous running operation.

Table 11-4: Comparison of normalised energy consumption between continuous operation and start-stop operation (payload 72t, track length 40km)

Wagon type	Gross mass (tonne)	Energy consumption/payload/km		% decrease of energy consumption on continuous operation
		Continuous operation	start-stop	
Concept	80.175	0.01127	0.01882	67.00
RQTY	90.0	0.01264	0.02004	58.63
sgnss	89.4	0.01261	0.02003	58.85
DS	94.0	0.01262	0.02045	62.13

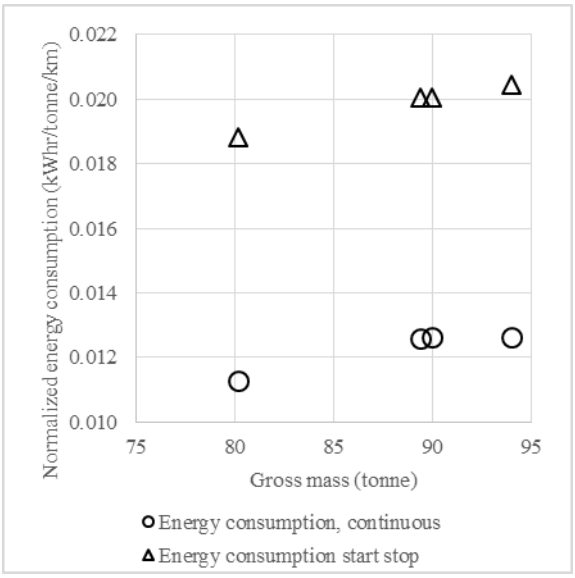

Figure 11-10: Effect of wagon mass on normalised energy consumption

11.6 Discussion

The concept wagon along with a selection of existing wagons have been tested using train simulations to compare energy consumption. Three operation conditions were compared, namely fully loaded and completely empty trains in the start-stop mode of operation, partially loaded trains in start-stop mode operation and fully loaded trains in a continuous running mode of operation.

The low tare on the concept wagon gave reduced energy consumption in the empty condition. The advantage of the low tare option was greater on intermodal operation than the heavy haul operation. The high payload requirement of the heavy haul operation (as high as 121t on Pilbara trains) generally provided higher payload productivity on the heavy haul operation compared to an intermodal operation based on the empty return trip on all trains considered in this Chapter. However, in the consideration of a loaded return trip on the intermodal operation, the intermodal wagons with higher payload capacity could produce better payload productivity (about 30% less energy consumption per unit payload) than the heavy-haul trains as indicated in the simulation results in this Chapter.

In the intermodal operation, high payloads similar to the heavy haul operation are not required as the goods and products are less dense. The intended intermodal operation in this thesis was carrying standard containers which limited the payload to 72t on a 65’ wagon. The payloads on all other intermodal wagons were set to 72t for comparison in this Chapter. The fully loaded condition on the concept wagon consumed 6 to 8% less energy per payload per km compared to other similar capacity intermodal wagons, i.e. RQTY, sgnss, and DS-1. The payload (72t) being the same in all the wagons, the saving in energy was due to the low tare of the concept wagons. The fully loaded condition in a continuous running operation showed a greater saving on the concept wagon compared to the start-stop mode. The concept wagon consumed about 11% less energy compared to RQTY, sgnss and DS-1 wagons when a continuous running operation was carried out in the fully loaded condition on a 40km test track.

The advantage on the concept wagon was found to be even greater when partial loading was considered. The energy consumption on the concept wagon was found to be about 10% less than the nearest competitor in the

intermodal operation (RQTY, sgnss and DS-1 wagon) when about 30% of the train was empty in a start-stop mode operation. A quantified approach showed that a train made up of concept wagons at the 90% loaded condition provided more payload productivity than its nearest competitors (RQTY, and sgnss wagons) at the 100% loaded condition of transportation. Partial loading is a common situation in container transportation by rail, hence the contribution of the concept wagon in intermodal transportation operation will be significantly higher than the existing similar wagons as the comparison shows in this chapter.

The saving with the concept wagon compared to that of the other wagons in continuous running operation is higher than for the start-stop mode operation. The continuous mode of operation with the concept wagon consumed less energy (58-67% less as per simulation in this Chapter) than that for the start-stop mode. The higher percentage of energy saving (67%) on the continuous running mode operation compared to the start-stop mode also indicates a possible higher saving with the concept wagon on a long haul freight operation.

The analysis performed in this chapter is based on a typical inner-city freight route of 40km. The number of start-stop positions could be different on a long haul freight route as compared to the four stops used on the 40km track. The saving in energy consumption terms, therefore, represents an inner-city freight transportation situation.

The length of a train in a general freight transportation operation other than heavy haul transportation is restricted by the infrastructure requirements, a typical limit being 700m in the European network [54]. The 700m length would allow 31 concept wagons in a train based on two locomotives (22m long) in a train. The same length of 700m would allow a train of 41 UIC link wagons. So, the length limitation would impose a further restriction on payload productivity of a train. A further normalisation on train length could be performed if the payload productivity of two different trains appears a close match.

Chapter 12
Conclusion

The following conclusions were drawn in this thesis:

- It will be possible to build a very low tare wagon of ~8 tonnes with the capacity of either three 20' containers or a 40' and a 20' or a 65' container in single stack configuration.
- Research and innovations contributed by this thesis allowed the development of a suitable suspension design for axle loads up to 41 tonnes and allowing payloads of 72t over a deck length of 65' (19.8m).
- The ratio of payload to tare of the concept wagon developed is 8.8 which is significantly higher than some of the current heavy haul wagons (e.g. Pilbara iron ore wagon of 5.78) and high performance container wagons (e.g. UIC link two-axle wagon of 4.63).
- After an iterative process of design and simulation, innovations in the design of a very low tare concept wagon included the following:
    - Two multistage suspension elements comprising leaf and vertical coil springs. The vertical coil springs provide the required softness to the suspension to reduce the wheel unloading ratio for large track top defects and twists.
    - An additional longitudinal stiffness element to improve critical hunting speed.
- The resulting concept wagon suspension gave dynamic stability (hunting) up to a speed of 204 km/h but the long distance between the axles imposes some restrictions on operation. Assuming track and defect standards typical of the current ARTC and RISSB standards the speed of such a wagon on a curved section would be limited to 70 km/h and operation would not be possible on curves tighter than 300m radius. The track would have to be maintained to a defect band F or better for the isolated lateral (18mm over 10m), vertical (51mm over 20m) and long twist (40mm over 14m) track defects. The permissible track defect for the isolated short twist track defect must be less than 8mm over 2m which is smaller than that allowed by the smoothest defect band G of the ARTC track geometry standard.
- The resulting suspension design utilised conventional components to ensure that the concept wagon was something that could be considered as a design option for manufacture.
- The concept wagon gave energy savings in the range of 6 to 12 % when compared with current RQTY, sgnss and DS-1 wagons. The specific comparisons were:
    - Fully loaded with stop start, the concept wagon consumed 6-8% less energy compared to that on the similar capacity intermodal wagons.
    - Partially loaded with stop start, the concept wagon gave greater energy savings up to 10%.
    - In continuous running operation, the energy saving on the concept wagon could be up to 11-12%
- Although the energy savings are modest and the design imposes greater restrictions on the permitted magnitude of isolated track defects, the design could find greater use on mixed use lines where freight trains share with higher speed trains and hence lower track defect levels.
- A process termed Vehicle Acceptance Procedure by Simulation (VAPS) was used to test the implications of the new design further that would be required using conventional standards. This

approach reveals more about the vehicle capabilities and some parts of this approach could be considered for future vehicle roadworthiness standards.

References

[1] FERRMED. (2012, 06 December). *Ferrmed*. Available: http://www.ferrmed.com/

[2] FERRMED. (2017, 21 April). *FERRMED Wagon Concept*. Available: http://www.ferrmed.com/?q=en/ferrmed-studies

[3] European Commission. (2017, 21 April). *Transport - sustainable surface transport*. Available: http://www.transport-research.info/programme/sustainable-surface-transport-0

[4] WikiPedia. (2013, 12 December). *Flat Wagon*. Available: https://en.wikipedia.org/wiki/Flat_wagon

[5] K. GmbH, "Efficient intermodal wagons " COSMOS Project, Good Practice Manual, 2013, KombiConsult GmbH, www.cosmos-project.eu2013.

[6] ARTC, "Section 10 locomotive and rolling stock data," ed, 2014.

[7] A. C. Zanuy, H. Boysen, J. Mašek, M. Buda, F. Janíèek, and J. Karabin, "VEL Wagon: State of the art and concept drafting," VEL-Wagon2011.

[8] T. Hazeldine, A. Pridmore, D. Nelissen, and J. Hulskotte, "Technical Options to reduce GHG for non-Road Transport Modes. Paper 3 produced as part of contract ENV.C.3/SER/2008/0053 between European Commission Directorate-General Environment and AEA Technology plc; see website www.eutransportghg2050.eu " 2009.

[9] H. Helms and U. Lambrecht, "Energy savings by light-weighing," Institute for Energy and Environmental research (IFEU) on behalf of International Aluminium Institute (IAI), Heidelberg2004.

[10] R. Kimpton, "Productivity Improvement Program for National Rail's Fleet," presented at the Conference on Railway Engineering, 1998.

[11] SSAB News. (2001, 21 April). *High strength steels for higher payload on railway wagons*. Available: https://www.yumpu.com/en/document/view/11500713/high-strength-steels-for-higher-payload-on-railway-wagons-ssab

[12] Rail Safety and Standards Board Limited. (2008, 14 Jun). *Technology Transfer for Reducing Mass*. Available: http://www.rssb.co.uk/Library/research-development-and-innovation/Research-brief-T688.pdf

[13] S. D. Iwnicki, S. Stichel, A. Orlova, and M. Hecht, "Dynamics of railway freight vehicles," *Vehicle System Dynamics*, vol. 53, pp. 995-1033, 2015/07/03 2015.

[14] W. Williams, D. Ferris, and R. Kimpton, "Freight Wagon Design for the 21st Century," presented at the Conference on Railway Engineering, Adelaide, 2000.

[15] G. P. Wolf, "Innovative Engineering Concepts for Unit Train Service: The Slackless Drawbar Train and Continuous Center Sill Trough Train," presented at the The Fourth International Heavy Haul Railway Conference, Brisbane, 1989.

[16] Rail Safety and Standards Board Limited, "Guidance on Gauging," in *Railway Group Guidance Note*, ed. London: Rail Safety and Standards Board, 2004.

[17] D. M. Johnson, "Gauging Issues," in *Handbook of railway vehicle dynamics*, S. Iwnicki, Ed., ed: Taylor & Francis Group: Boca Raton., 2006, pp. 181- 207.

[18] M. W. J. Etwell, "Advances in rail wagon design," *Proceedings of the Institution of Mechanical Engineers, Part F: Journal of Rail and Rapid Transit*, vol. 204, pp. 45-54, 1990.

[19] UIC. (2008, 9 September). *DIOMIS- Assessing new technologies in the wagon field*. Available: http://www.uic.org/diomis/IMG/pdf/Livre_DIOMIS_A10_final_.pdf

[20] Market-up. (2013, 11 November). *Versatile efficient and longer wagons for Intermodal Transport show case*. Available: http://www.transport-research.info/Upload/Documents/201301/20130109_140255_57430_intermodal_vel_wagon_show_case.pdf

[21] C. Cole, "Longitudinal train dynamics," in *Handbook of railway vehicle dynamics*, S. Iwnicki, Ed., ed: Taylor & Francis Group: Boca Raton., 2006, pp. 239-277.

[22] A. GARCIA, "High speed, energy consumption and emissions," International union of railways (UIC), Paris2010.

[23] Y.-C. Lai and C. Barkan, "Options for Improving the Energy Efficiency of Intermodal Freight Trains," *Transportation Research Record: Journal of the Transportation Research Board*, vol. 1916, pp. 47-55, 2005.

[24] C. Cole, M. Spiryagin, Y. Sun, and M. McClanachan, "Investigation of Hybrid Locomotive Options for Mixed Freight and Inter-Modal Trains," presented at the 10th World Congress on Railway Research (WCRR2013), Sydney, 2013.

[25] A. Orlova and Y. Boronenko, "The Anatomy of Railway Vehicle Running Gear," in *Handbook of railway vehicle dynamics*, S. Iwnicki, Ed., ed: Taylor & Francis Group, LLC: Boca Raton., 2006, pp. 39-83.

[26] P.-A. Jonsson, "Freight wagon running gear - a review," Royal Institute of Technology, Sweden2002.

[27] S. S. N. Ahmad, C. Cole, M. Spiryagin, and Y. Sun, "Integrated methodology for investigation of wagon bogie concepts by simulation," in *ASME 2014 12th Biennial Conference on Engineering Systems Design and Analysis (ESDA2014)*, Copenhagen, Denmark, 2014.

[28] Amsted Rail International. (2008) Global rail supply strategies. *Revista Ferroviária*. Available: http://www.revistaferroviaria.com.br/nt2008/palestras/05112008/Steve_Becker/ARX.pdf

[29] Transport Canada. (1988, January- February) Radial Axle Freight Car Trucks Generate Savings. *TR News*. Available: http://onlinepubs.trb.org/onlinepubs/trnews/rpo/rpo.trn134.pdf

[30] B. T. Scales. (1979) Scales-Devine radial bogie: a solution to wheel/rail interaction. *Rail Engineering International*. 43-44.

[31] M. G. Pollard, "The development of cross-braced freight bogies," *Rail International*, pp. 736-758, 09 1979.

[32] S. Stichel and P.-A. Jonsson, "Is there a Future for Freight Wagon with Link Suspension?," in *9th International Heavy Haul Conference*, Shanghai, China, 2009.

[33] S. Iwnicki, Y. Bezin, A. Orlova, P.-A. Johnsson, S. Stichel, and H. Schelle, "The 'SUSTRAIL' high speed freight vehicle: Simulation of novel running gear design," presented at the IAVSD, 2013.

[34] E. C. Slivsgaard, "On the interaction between wheels and rails in railway dynamics," PhD, Institute of Mathematical Modelling, Technical University of Denmark, 1995.

[35] UIC. (2002). *Single-axle bogies*. Available: http://www.railway-energy.org/static/Single_axle_bogies_11.php

[36] Y. Suda, S. Nishimura, A. Matsumoto, and M. S. Y. Sato, "Development of single axle truck for new generation commuter," presented at the World Congress on Railway Research, Germany, 2001.

[37] M. Kibble, "Suspension for Railway Vehicles," United States Patent 4699065, 1987.

[38] N. A. Harwood, "Suspension Arrangements for Four-wheeled Railway Vehicles," 4583464, 1986.

[39] H. W. Mulcahy, "Single Axle Suspension System for Railroad Vehicle," US Patent Number 4561360, 1985.

[40] S. Lin, Y. Suda, and A. Hirai, "Dynamics of three-axle-one-unit vehicles with self-steering single axle," *Vehicle System Dynamics*, vol. 46, pp. 837-847, 2008/09/01 2008.

[41] H. W. Mulcahy and R. P. Radwill, "Single Axle Suspension System for Railway Car Truck," 5001989, 1991.

[42] H. B. Weber, "Single Axle Truck for Large Railroad Cars," US Patent Number 5524552, 1996.

[43] A. H. Briggs, "Railway wagon suspension units " European Patent Number 0011453, 1979.

[44] A. H. Wickens, *Fundamentals of Rail Vehicle Dynamics Guidance and Stability*: Swets and Zeitlinger, Lisse, The Netherlands, 2003.

[45] A. A. Shabana, K. E. ZaaZaa, and H. Sugiyama, *Railroad Vehicle Dynamics: A computational approach*: CRC Press, Taylor and Francis Group, 2008.

[46] D. I. Habil and O. Polach, "Bogie design for better dynamic performance Example of a locomotive bogie," *European Railway Review*, pp. 69-77, 2003.

[47] E. Satou and M. Miyamoto, "Dynamics of a bogie with independently rotating wheels," *Vehicle System Dynamics*, vol. 20, pp. 519-534, 1992/01/01 1992.

[48] S. Stichel, "Limit Cycle Behaviour and Chaotic Motions of Two-Axle Freight Wagons with Friction Damping," *Multibody System Dynamics*, vol. 8, pp. 243-255, 2002.

[49] European Committee for Standardisation, "EN 14363: 2005 (E)," in *Railway applications - Testing for the acceptance of running characteristics of railway vehicles - Testing of running behaviour and stationary tests*, ed, 2006.

[50] H.-M. Hur, J.-H. Park, W.-H. You, and T.-W. Park, "A study on the critical speed of worn wheel profile using a scale model," *Journal of Mechanical Science and Technology*, vol. 23, pp. 2790-2800, 2009/10/01 2009.

[51] S. A. Simson, "Lateral stability performance in uni-directional rollingstock," in *Rail Conference, 2006. Proceedings of the 2006 IEEE/ASME Joint*, 2006, pp. 209-216.

[52] D. Skerman, "Selection of wheel and rail profiles for hunting tests," in *Conference On Railway Engineering*, Wellington, 2010.

[53] G. R. M. Mastinu and M. Gobbi, "On the optimal design of railway passenger vehicles," *Proceedings of the Institution of Mechanical Engineers, Part F: Journal of Rail and Rapid Transit*, vol. 215, pp. 111-124, March 1, 2001 2001.

[54] M. Beth. (2017, 16 October). *Intermodal Freight*. Available: http://www.railway-technical.com/operations/intermodal-freight.html

[55] ARTC, "Section 5: Track Geometry," ed, 2013.

[56] Ettamogah Rail Hub. (2017, 21 April). *Innovation*. Available: http://ettamogah-hub.com.au/innovation-2/

[57] Railway Age. (1991) Iron Highway fills a gap (new railroad freight loading concept could multiply business by ten). *Railway Age*. Available: HighBeam Research. 20 Apr. 2017 <https://www.highbeam.com>.

[58] S. S. N. Ahmad, C. Cole, M. Spiryagin, and Y. Sun, "Integrated methodology for investigation of wagon design concepts by simulations," in *Proceedings of the ASME 2014 International Design Engineering Technical Conferences & Computers and Information in Engineering Conference*, Buffalo, USA, 2014.

[59] C. Cole, M. McClanachan, M. Spiryagin, and Y. Q. Sun, "Wagon instability in long trains," *Vehicle System Dynamics*, vol. 50, pp. 303-317, 2012.

[60] D. Chen, "Derailment Risk Due to Coupler Jack-Knifing under Longitudinal Buff Force," *Proceedings of the Institution of Mechanical Engineers, Part F: Journal of Rail and Rapid Transit*, vol. 224, pp. 483-490, September 1, 2010 2010.

[61] Standards Australia and Rail Industry Safety & Standards Board, "AS 7509.2 Railway Rolling Stock - Dynamic Behaviour - Part 2: Freight Rolling Stock.," ed, 2009.

[62] O. Polach, M. Berg, and S. D. Iwnicki, "Simulation," in *Handbook of railway vehicle dynamics*, S. Iwnicki, Ed., ed: Taylor & Francis Group: Boca Raton., 2006, pp. 359-421.

[63] C. Weidemann, "State-of-the-Art Railway Vehicle Design with Multi-Body Simulation," *Journal of Mechanical Systems for Transportation and Logistics*, vol. 3, pp. 12-26, 2010.

[64] Y. Q. Sun, "A wagon – track system dynamics model for the simulation of heavy haul railway transportation," PhD, Centre for Railway Engineering, Central Queensland University, 2003.

[65] S. Bruno, J. Vinolas, M. Berg, O. Polach, and S. Stichel, "Modelling of Suspension Components in a Rail Vehicle Dynamics Context," *Vehicle System Dynamics*, vol. 49, pp. 1021-1072, 2011.

[66] J. R. Evans, "The modelling of railway passenger vehicles," *Vehicle System Dynamics*, vol. 20, pp. 144-156, 1992/01/01 1992.

[67] AB DEsolver. (2012, 16 May). *The Calc Func manual*. Available: http://www.gensys.se/doc_html/calc.html

[68] K. Knothe, R. Wille, and B. W. Zastrau, "Advanced Contact Mechanics–Road and Rail," *Vehicle System Dynamics*, vol. 35, pp. 361-407, 2001.

[69] J.-B. Ayasse and H. Chollet, "Wheel-Rail Contact," in *Handbook of railway vehicle dynamics*, S. Iwnicki, Ed., ed: Taylor & Francis Group, LLC: Boca Raton., 2006, pp. 85-120.

[70] J. Piotrowski and H. Chollet, "Wheel–rail contact models for vehicle system dynamics including multi-point contact," *Vehicle System Dynamics*, vol. 43, pp. 455-483, 2005.

[71] C. Esveld and L. Gronskov, "MINIPROF wheel and rail measurement," in *Proceedings of 2nd Mini Conference on Contact Mechanics and Wear of Rail/ Wheel Systems*, TU Budapest, 1996, pp. 69-75.

[72] J. A. Elkins, "Prediction of Wheel/Rail Interaction: the State of the Art," in *12th IAVSD Symposium*, Lyon, France, 1991, pp. 1-27.

[73] S. Z. Meymand, A. Keylin, and M. Ahmadian, "A survey of wheel–rail contact models for rail vehicles," *Vehicle System Dynamics*, vol. 54, pp. 386-428, 2016/03/03 2016.

[74] L. H. Ren, G. Shen, and Y. S. Hu, "A test-rig for measuring three-piece bogie dynamic parameters applied to a freight car application," *Vehicle System Dynamics*, vol. 44, pp. 853-861, 2006/01/01 2006.

[75] P. E. Klausur and J. C. McMunn, "Track-worthiness Testing Of Span-bolster Cars," in *Railroad Conference, 1992. Proceedings of the ASME/IEEE Spring Joint*, 1992, pp. 41-50.

[76] F. Braghin, S. Bruni, and F. Resta, "Active yaw damper for the improvement of railway vehicle stability and curving performances: simulations and experimental results," *Vehicle System Dynamics*, vol. 44, pp. 857-869, 2006/11/01 2006.

[77] A. Alonso, J. G. Giménez, and E. Gomez, "Yaw damper modelling and its influence on railway dynamic stability," *Vehicle System Dynamics*, vol. 49, pp. 1367-1387, 2011/09/01 2011.

[78] A. Orlova and Y. Romen, "Refining the wedge friction damper of three-piece freight bogies," *Vehicle System Dynamics*, vol. 46, pp. 445-455, 2008/09/01 2008.

[79] A. B. Kaiser, J. P. Cusumano, and J. F. Gardner, "Modeling and Dynamics of Friction Wedge Dampers in Railroad Freight Trucks," *Vehicle System Dynamics*, vol. 38, pp. 55-82, 2002/07/01 2002.

[80] N. B. Do, A. A. Ferri, and O. A. Bauchau, "Efficient Simulation of a Dynamic System with LuGre Friction," *Journal of Computational and Nonlinear Dynamics*, vol. 2, pp. 281-289, 2007.

[81] S. Iwnicki and J. Stow, "Modelling the behaviour of freight vehicles," The Rail Technology Unit, Manchester2012.

[82] M. Arnold, B. Burgermeister, C. Führer, G. Hippmann, and G. Rill, "Numerical methods in vehicle system dynamics: state of the art and current developments," *Vehicle System Dynamics*, vol. 49, pp. 1159–1207, 2011.

[83] J. G. d. Jalón and E. Bayo, "Numerical Integration of the Equations of Motion," in *Kinematic and Dynamic Simulation of Multibody Systems: The Real-Time challenge* ed: Springer-Verlag, New-York, 1994.

[84] S. Stichel, "How to improve the running behaviour of freight wagons with UIC-Link Suspension," *Vehicle System Dynamics*, vol. Supplement 33, pp. 394- 405, 1999.

[85] Association of American Railroads, "Manual of Standards and Recommended Practices," in *Design, Fabrication, and Construction of Freight Cars*, ed: The Association of American Railroads, 2011.

[86] Rail Safety and Standards Board Limited, "Resistance of Railway Vehicles to Roll-Over in Gales, GM/RT2142," ed: Rail Safety and Standards Board, 2014.

[87] International Union of Railways (UIC), "UIC CODE 518," in *Testing and approval of railway vehicles from the point of view of their dynamic behaviour - Safety - Track fatigue - Ride quality*, ed, 2005.

[88] ATSB, "Derailment of ore train 4413," Australian Transport Safety Bureau ATSB RO-2014-008, 2015.

[89] ATSB, "Derailment of Train 5WX2 near Winton, Victoria," ATSB, Canberra2008.

[90] AB DEsolver. (2017, 16 April). *GENSYS in short*. Available: http://gensys.se/GENSYS_in_short/index.html

[91] M. Spiryagin, A. George, S. S. N. Ahmad, K. Rathakrishnan, Y. Q. Sun, and C. Cole, "Wagon model acceptance procedure using Australian standards," in *Conference on Railway Engineering*, Brisbane, 2012.

[92] AB DEsolver, "GENSYS 1611," in *Tutorial file vehicle_11: 2-axle wagon with UIC-links*, ed, 2016.

[93] P.-A. Jönsson, "Multibody simulation model for freight wagons with UIC link suspension," Doctor of Philosophy, Royal Institute of Technology, Stockholm, Sweden, 2006.

[94] M. Hoffmann, "Dynamics of European two–axle freight wagons," PhD, Informatics and Mathematical Modelling, Technical University of Denmark, Denmark, 2006.

[95] Department of Transport, "Shaping Melbourne's Freight Future Proposals for an intermodal solution to service Melbourne's growing containerised freight task," Department of Transport, Melbourne, 2010.

[96] Rail Safety and Standards Board Limited, "GM/GN2688 Guidance on Designing Rail Freight Wagons for use on the GB Mainline Railway," ed. London: Rail Safety and Standards Board, 2013.

[97] ARTC, "Route Access Standard," ed, 2012.

[98] Hupac Intermodal SA. (2017, 3 December). *60-foot container wagon, ultra-light*.

[99] W. D. Pilkey, "Beams and Columns," in *Formulas for Stress, Strain, and Structural Matrices*, ed: John Wiley & Sons, Inc., 2008, pp. 519-618.

[100] Australian Tube Mills, "Design capacity tables for structural steel hollow sections," 2013.

[101] B. Ellingwood. (1989) Serviceability guidelines for steel structures.

[102] B. Kirke and I. H. Al-Jamel, "Steel Structures Design Manual To AS 4100," 2004.

[103] J. A. Myers, "Handbook of Equations for Mass and Area Properties of Various Geometrical Shapes," U. S. Naval Ordnance Test Station, China Lake, CA, 1962.

[104] N. Wilson, R. Fries, M. Witte, A. Haigermoser, M. Wrang, J. Evans, *et al.*, "Assessment of safety against derailment using simulations and vehicle acceptance tests: a worldwide comparison of state-of-the-art assessment methods," *Vehicle System Dynamics*, vol. 49, pp. 1113-1157, 2011/07/01 2011.

[105] European committee for standardization, "EN 15302:2008A1:2010 (E) Railway applications - Method for determining the equivalent conicity," ed. Brussels, 2010.

[106] L.-O. Jönsson, N. Nilstam, and I. Persson, "Using simulations for approval of railway vehicles: a comparison between measured and simulated track forces," *Vehicle System Dynamics*, vol. 46, pp. 869-881, 2008/09/01 2008.

[107] O. Polach, A. Böttcher, D. Vannucci, J. Sima, H. Schelle, H. Chollet, *et al.*, "Validation of simulation models in the context of railway vehicle acceptance," *Proceedings of the Institution of Mechanical Engineers, Part F: Journal of Rail and Rapid Transit*, vol. 229, pp. 729-754, August 1, 2015 2015.

[108] AB DEsolver. (2011, 16 October). *Debugging a vehicle model*. Available: http://www.gensys.se/doc_html/analyse_check.html#Mainmenu

[109] Standards Australia and Rail Industry Safety & Standards Board, "AS 7508.2 Australian standard-Railway Rolling Stock - Track Forces and Stresses - Part 2: Freight Rolling Stock," ed: RISSB, 2008.

[110] M. Spiryagin, A. George, Y. Q. Sun, and C. R. Cole, "Locomotive model acceptance procedure based on international standards," presented at the 2nd Joint International Conference on Multibody System Dynamics, Stuttgart, Germany, 2012.

[111] AB DEsolver. *Users Manual for Program RUNF_INFO*. Available: http://www.gensys.se/doc_html/misc_runf_info.html

[112] AEA Technology plc, *VAMPIRE (Version 4.32) User Manual*, 2004.

[113] D. W. Skerman, Mark; Boyce, Mark and Hermann, Peter, " Development of Complimentary Track and Rollingstock Performance Standards [online]," presented at the CORE 2004: New Horizons for Rail, Darwin, N.T, 2004.

[114] Y. Q. Sun, M. Spiryagin, C. R. Cole, and D. Nielsen, "Wheel-rail wear investigation on a balloon loop track through simulation of slow speed wagon dynamics," in *Proceedings of the 10th International Contact Mechanics Conference of Wheel/Rail systems*, Colorado Springs, USA, 2015.

[115] Y. Q. Sun, C. R. Cole, M. Spiryagin, and M. Dhanasekar, "Vertical dynamic interaction of trains and rail steel bridges," *Electronic Journal of Structural Engineering (Special Issue)*, vol. 13, pp. 88-097, 2014.

[116] Y. Q. Sun, Q. Wu, M. Spiryagin, and C. R. Cole, "Determination of dynamic characteristics of draft gears of heavy haul train using collision simulations," presented at the International Heavy Haul Association Conference, Perth, 2015.

[117] Y. Q. Sun, M. Spiryagin, C. R. Cole, and S. Simson, "Effect of wheel-rail contacts and track gauge variation on hunting behaviours of Australian three-piece bogie wagon," in *Proceedings of 23rd International Symposium on Dynamics of Vehicle on Roads and Tracks*, Qingdao, China, 2013.

[118] O. Polach and A. Vetter, "Methods for running stability prediction and their sensitivity to wheel rail contact geometry," in *6th International conference on railway bogies and running gears*, Budapest, 2004.

[119] O. Polach, "On non-linear methods of bogie stability assessment using computer simulations," *Proceedings of the Institution of Mechanical Engineers, Part F: Journal of Rail and Rapid Transit*, vol. 220, pp. 13-27, January 1, 2006 2006.

[120] John Holland, "Minimum Operating Requirements for Freight Vehicles," in *Wheel Profiles*, ed, 2011.

[121] AB DEsolver. (December 3). *Users Manual for Program KPF* Available: http://www.gensys.se/doc_html/kpf.html#Mainmenu

[122] Federal Railroad Administration, "Track and Rail and Infrastructure Integrity Compliance Manual, Volume II Track Safety Standards, Chapter 1 Track Safety Standards, Classes 1 through 5," 2007.

[123] Federal Railroad Administration, "Track Safety Standards Classes 6 through 9," ed, 2002.

[124] B. Kufver, "Tracks for tilting trains," European Commission 2005.

[125] B. Kufver, *Mathematical Description of Railway Alignments and Some Preliminary Comparative Studies*: Swedish National Road and Transport Research Institute, 1997.

[126] B. Kufver, "Realigning railways in track renewals linear versus S-shaped superelevation ramps renewals - linear versus S-shaped superelevation ramps," presented at the 2nd International conference Railway Engineering London, 1999.

[127] O. Polach, "Creep forces in simulations of traction vehicles running on adhesion limit," *Wear*, vol. 258, pp. 992-1000, 2005.

[128] E. Andersson, M. Berg, and S. Stichel, *Rail Vehicle Dynamics*. Sweden: Kungliga Tekniska högskolan (KTH), 2007.

[129] H. Harrison, T. McCanney, and J. Cotter, "Recent developments in coefficient of friction measurements at the rail/wheel interface," *Wear*, vol. 253, pp. 114-123, 7// 2002.

[130] G. H. Batchelor, "Paper 3: The Influence of Track Twist on Vehicle Design," *Proceedings of the Institution of Mechanical Engineers, Conference Proceedings*, vol. 180, pp. 86-98, 1965.

[131] F. P. Beer, E. R. Jonhston, and J. T. DeWolf, *Mechanics of Materials* 4ed. New York: McGraw Hill, 2006.

[132] P.-A. Jönsson, "Modelling and Laboratory Investigations on Freight Wagon Link Suspensions with respect to Vehicle-track Dynamic Interaction," Aeronautical and vehicle engineering, Royal Institute of Technology (KTH), Stockhom, 2004.

[133] H. Lange, "Dynamic analysis of a railway freight car with standard UIC single- axle running gear," Master of Science, Department of Vehicle Engineering, Royal Institute of Technology (KTH), Sweden, 1996.

[134] AB DEsolver. (2017, 4 October). *Coupling element kf_exp3*. Available: http://gensys.se/doc_html/calc_coupl.html#jkf_exp3

[135] P. S. Fancher, R. D. Ervin, C. C. MacAdam, and C. B. Winkler, "Measurement and representation of the mechanical properties of truck leaf springs," SAE-800905, 1980.

[136] International Union of Railways (UIC), "UIC Code 517 Wagons- Suspension gear- Standardisation," ed, 2007.

[137] Association of American Railroads, "Trucks and Truck Details," in *Manual of standards and recommended practices, Section D*, ed. Washington, D.C., 2007.

[138] Standard Car Truck Company. (20 May 2017). *Section 3, Springs*. Available: http://www.sctco.com/pdf/Section3.pdf

[139] International Union of Railways (UIC), "UIC CODE 821 Technical Specification for the supply of parallel leaf springs for vehicles," ed, 2003.

[140] AB DEsolver. (2017, 5 October). *Coupling element kf_exp2*. Available: http://gensys.se/doc_html/calc_coupl.html#jkf_exp2

[141] J. Piotrowski, "Model of the UIC link suspension for freight wagons," *Archive of Applied Mechanics*, vol. 73, pp. 517-532, 2003.

[142] AB DEsolver. (2017, 5 October). *Coupling element kf_exp1*. Available: http://gensys.se/doc_html/calc_coupl.html#jkf_exp1

[143] J. T. Broch, *Mechanical Vibration and Shock Measurements*. Copenhagen, Denmark: Bruel & Kjaer, 1980.

[144] M. Stiepel and S. Zeipel, "Freight Wagon Running Gears with Leaf Spring and Ring Suspension," presented at the Simpack User Group Meeting, Eisenach, Germany, 2004.

[145] ARTC, "Code of practice for operations & safeworking," ARTC2006.

[146] BNSF Railway, "Air Brake and Train Handling Rules," 2011.